A PARAMETRIC WIND-WAVE MODEL FOR ARBITRARY WATER DEPTHS

by

HANS CHRISTIAN GRABER

B.E.(CE), The City College of New York
(1977)

S.M., Massachusetts Institute of Technology
(1979)

SUBMITTED IN PARTIAL FULFILLMENT
OF THE REQUIREMENTS FOR THE
DEGREE OF

DOCTOR OF SCIENCE

at the

MASSACHUSETTS INSTITUTE OF TECHNOLOGY
May, 1984

© Massachusetts Institute of Technology, 1984

Signature of Author .....
Department of Civil Engineering
May 11, 1984

Certified by .....
Professor Ole Secher Madsen
Thesis Supervisor

Accepted by .....
Professor François M.M. Morel, Chairman
Departmental Committee on Graduate Students
of the Department of Civil Engineering

ARCHIVES
MASSACHUSETTS INSTITUTE
OF TECHNOLOGY

JUN 2 9 1984

LIBRARIES

A PARAMETRIC WIND-WAVE MODEL FOR ARBITRARY WATER DEPTHS

by

HANS CHRISTIAN GRABER

Submitted to the Department of Civil Engineering
in partial fulfillment of the
requirements for the Degree of Doctor of Science

ABSTRACT

An extension of a deep water hybrid parametric wave model has been developed for arbitrary water depths. The windsea is described by the JONSWAP parameter set and by a directional parameter representing the mean direction of the windsea spectrum. This mean direction has been re-derived based on more general energy flux arguments. The windsea spectrum in finite depth is assumed to have a similarity shape which is related to the deep water energy spectrum by multiplying with a depth dependent transformation factor. This factor affects the spectral shape of the high-frequency part which is proportional to f^{-5} in deep water and to f^{-3} in shallow water. The directional dependence of the spectrum is assumed to be $\cos^2(\theta-\theta_o)$, centered around the mean wave direction. The windsea model explicitly accounts for finite depth effects such as refraction, shoaling and dissipation by bottom friction.

Based on an energy flux transport equation, the full set of prognostic parameters is derived including finite depth effects. The equations of the prognostic variables are solved on a finite difference grid by means of the Lax-Wendroff method. Swell is treated in a decoupled spectral fashion. For simplicity all swell characteristics are considered straight and effects of refraction are disregarded. However, shoaling and dissipation of energy by bottom friction are included.

The model has been applied to a deep water and finite depth case study. The deep water hindcast was performed for an extratropical cyclone in the Gulf of Alaska. Predicted significant wave heights and zero-crossing wave periods are compared with measurements from six stations in the Gulf of Alaska. The finite depth wave conditions are hindcasted for a complex frontal system off the North Carolina coast during ARSLOE. Predicted spectral wave parameters such as significant wave height, spectral peak frequency and mean wave direction are compared with observations from several different measurement techniques. From the same data set, observed wave spectra are compared with hindcasted model spectra. A discussion of the results for both applications is presented.

Thesis Supervisor: Ole Secher Madsen

Title: Professor of Civil Engineering

TO MY LOVING WIFE
ELAINE

O GLÜCKLICH, WER NOCH HOFFEN KANN,
AUS DIESEM MEER DES IRRTUMS AUFZUTAUCHEN.
WAS MAN NICHT WEISS, DAS EBEN BRAUCHT MAN,
UND WAS MAN WEISS, KANN MAN NICHT GEBRAUCHEN.

OH, HAPPY HE WHO STILL HOPES THAT HE CAN
EMERGE FROM ERROR'S BOUNDLESS SEA.
WHAT MAN KNOWS NOT, IS NEEDED MOST BY MAN,
AND WHAT MAN KNOWS, FOR THAT NO USE HAS HE.

(Faust)

--FAUST I, Vor dem Tor
Johann Wolfgang von Goethe

ACKNOWLEDGEMENTS

This research was funded by the National Oceanic and Atmospheric Administration Office of Sea Grant. The computer runs for the Gulf of Alaska study were financially supported by the Department of Civil Engineering and the MIT Sea Grant Office.

I appreciate the support and encouragement of my committee members Prof. Ken Melville, Dr. Bill Grant and Prof. Keith Stolzenbach. I am especially fortunate to have worked under the guidance of Prof. Ole Secher Madsen. His continuous advice and friendship were instrumental in starting and finishing this thesis and are greatly appreciated. Tak, Ole.

I like to thank Drs. Wolfgang Rosenthal and Heinz Günther for many helpful discussions and comments. Also, I'm grateful to Susanne Hasselmann for providing me with her results of the nonlinear energy transfer calculations. My gratitude goes to Drs. David Burdge and Mike Feifarek of Marathon Oil for making available to me the Gulf of Alaska wave data. I thank Dr. Allan Reece of Shell Oil for his help in obtaining the wave data of the Gulf of Alaska and also thank Dr. Vince Cardone of Oceanweather for leading me in the right direction and providing me with the wind fields of the Gulf of Alaska cyclone. I like to acknowledge the painstaking work of Mike Bruno in establishing the wind fields for the ARSLOE storm.

Pat Dixon, I still think that your initials are more important than those of my degree, since your friendship has always meant alot to me. To my office mates: John Shaw, Dave Langseth, John Trowbridge, Karl Helfrich and Kwok-Tai Shum, thanks for putting up with me. To everyone else in the Parsons Lab - past and present - I've enjoyed your comradery, but especially I like to mention Lloyd Townley, "the Aussie", Eric Adams, Rick Mercier and Mike Bruno. Karl, thanks for your time to go running, drinking, biking, etc. with me.

I'm grateful to Diane Hardy, without her expertise and patience in typing this dissertation I would not have finished on time. Also I enjoyed the music of "Morning Pro Musica" on WGBH which generated the necessary inspirations.

Finally I would like to say "Danke" to my parents and brothers for their continuous moral support and understanding in this endeavour.

TABLE OF CONTENTS

Page

ABSTRACT i

ACKNOWLEDGEMENTS iv

TABLE OF CONTENTS v

LIST OF FIGURES vii

LIST OF TABLES vii

1. INTRODUCTION xiii

2. HISTORICAL REVIEW OF WAVE PREDICTION METHODS 6

2.1 DEEP WATER DISCRETE SPECTRAL MODELS 12

2.2 DEEP WATER PARAMETRIC MODELS. 24

2.2.1 Diagnostic Parametric Models 24
2.2.2 Prognostic Parametric Windsea Models 27
2.2.3 Hybrid Models. 33

2.3 FINITE DEPTH WAVE MODELS. 36

3. THEORETICAL BACKGROUND 39

3.1 THE SPECTRAL DESCRIPTION OF A WINDSEA 42

3.1.1 The JONSWAP Spectrum and Related Wave Parameters 62

a) DEEP WATER 62
b) FINITE DEPTH. 80

3.2 THE ENERGY TRANSPORT EQUATION 90

3.3 GENERATION AND DISSIPATION OF WAVE ENERGY 108

3.3.1 Energy Flux from the Wind. 109
3.3.2 Nonlinear Energy Transfer and Wave-Wave Interactions 120
3.3.3 Dissipation by Wave Breaking 139
3.3.4 Dissipation by Finite Depth Mechanisms 144

3.4 WAVE ENERGY FLUX VERSUS WAVE MOMENTUM 161

Page

4. A PARAMETRIC WINDSEA MODEL FOR FINITE DEPTH 172

4.1 A PARAMETRIC TRANSPORT EQUATION USING AN ENERGY FLUX APPROACH 174

4.2 THE LINEAR TRANSFORMATION FUNCTIONALS 178

4.3 THE GENERALIZED PROPAGATION MATRIX FOR FINITE DEPTH . . 183

4.4 THE MEAN DIRECTION OF A WINDSEA 194

4.5 THE PARAMETRIC SOURCE FUNCTIONS 204

a) NONLINEAR TRANSFER 204
b) WIND INPUT 206
c) BOTTOM FRICTION. 209
d) REFRACTION, SHOALING, AND SPECTRAL SHAPE ADJUSTMENT. 211

4.6 ENERGY EXCHANGE BETWEEN WINDSEA AND SWELL 215

4.6.1 Windsea to Swell Transfer. 217
4.6.2 Swell to Windsea Transfer. 221
4.6.3 Propagation Treatment of Swell 224

5. MODEL APPLICATIONS 226

5.1 GULF OF ALASKA (Deep Water Case). 226

5.1.1 Meteorological Conditions and Wind Fields. . . . 231
5.1.2 Model Results. 234

5.2 ARSLOE (Finite Depth Case). 265

5.2.1 Meteorological Conditions and Wind Fields. . . . 268
5.2.2 Model Results. 268

6. CONCLUSIONS AND DISCUSSIONS 281

REFERENCES 287

APPENDIX A: Propagation Coefficients of the JONSWAP Parameters in Finite Depth 303

APPENDIX B: Propagation Coefficients of the Directional Parameter in Finite Depth 308

LIST OF FIGURES

No.		Page
3.1	The equilibrium range of the frequency spectrum of wind-generated surface waves in deep water.	47
3.2	The equilibrium range of one-dimensional wave number spectra of fetch-limited surface gravity waves	51
3.3	The depth-dependent transformation factor $\Phi(\omega_h)$.	59
3.4	Definition of the JONSWAP parameters	63
3.5	Schematic representation of the three functional forms making up the JONSWAP spectrum	65
3.6	a) Peak frequency vs. fetch according to Kitaigorodskii's scaling laws. b) Phillips' constant vs. fetch according to Kitaigorodskii's scaling laws.	67
3.7	Energy vs. fetch according to Kitaigorodskii's scaling laws.	68
3.8	Shape parameters γ, σ_a, σ_b vs. fetch	70
3.9	Examples of spectral and analytical fits of observed wave spectra from data sets: (a) Argus Island; (b) Western Atlantic; (c) Hurricanes AVA; and (d) CAMILLE.	71
3.10	Self-similar wave number spectra for different water depths. (a) Mean JONSWAP shape corresponding to fm = 0.1 Hz, α = 0.01, γ = 3.3; (b) Pierson-Moskowitz shape corresponding to fm = 0.1 Hz, α = 0.0081, γ = 1.	82
3.11	Self-similar frequency spectra for different water depths. (a) Mean JONSWAP shape with fm = 0.1 Hz, α = 0.01, γ = 3.3; (b) Pierson-Moskowitz shape fm = 0.1 Hz, α = 0.0081, γ = 1 .	84
3.12	Comparison of observed wave spectra from ARSLOE experiment with JONSWAP fit in deep water (---) and in finite depth (___).	86
3.13	The depth-dependent spectral ordinate factor $K^2(\omega_h)$. . .	104
3.14	Examples of wave refraction in the North Sea for a wave period T = 10 s. (a) convectional refraction diagram; (b) reverse ray projection	107
3.15	(a) The streamline pattern in a shear flow above a wavy surface. (b) The critical layer according to Miles' theory.	111

No.		Page
3.16	Schematic growth curves. (a) Conventional spectral growth according to a Phillips-Miles mechanism; (b) spectral growth including a nonlinear effect possibly due to wave-wave interactions.	115
3.17	Dimensionless growth rate parameter vs. dimensionless wind speed.	118
3.18	Observed mean JONSWAP spectrum F, net source function S and computed nonlinear transfer S_{nl} for fetch-limited conditions	123
3.19	Evolution of wave spectra with fetch for offshore winds during JONSWAP	125
3.20	Comparison of nonlinear energy transfer for a mean JONSWAP spectrum (γ = 3.3). Numerical integration by Sell and Hasselmann (x—x); narrow peak approximation by Fox (---); parameterization of exact calculations by Hasselmann and Hasselmann (——)	127
3.21	Comparison of nonlinear energy transfer for a sharp JONSWAP spectrum (γ = 7.0). Numerical integration by Sell and Hasselmann (x—x); narrow peak appoximation by Fox (---); parameterization of exact calculations by Hasselmann and Hasselmann (——)	128
3.22	Comparison of nonlinear energy transfer parameterization for typical windsea spectra. Top row: Barnett's parameterization. Bottom row: Resio's parameterization . . .	132
3.23	Ratio R of the nonlinear transfer in finite depth to the transfer rate in deep water. Narrow peak approximation by Herterich and Hasselmann (---); exact calculations by Hasselmann and Hasselmann (——).	137
3.24	Dissipation rate due to percolation as a function of permeability coefficient and wave period. (Isotropic sand properties are assumed; results are shown for 8 sec. (---) and 10 sec. (——) wave period.).	147
3.25	Comparison of wave friction factor theories.	152
3.26	Qualitative description of the interplay between near-bottom flow and resulting bottom roughness	153
3.27	Dissipation rate due to bottom friction as a function of wave friction factor, wave period and wave height. (Results shown correspond to a wave period T = 7 sec. and a wave height H_s = 2 m.).	157

No.		Page
3.28	Energy balance for a finite-depth storm-generated wave spectrum consisting of (a) wind input; (b) nonlinear energy transfer; (c) advection; (d) deep water dissipation (wave breaking); (e) bottom friction; (f) net source function. Water depth h = 35 m and wind speed U = 25 m/s	160
3.29	Comparison of typical angular spreading functions.	163
4.1	Depth-dependent advection coefficients of parameter fm for a family of γ values	187
4.2	Depth-dependent advection coefficients of parameter α for a family of γ values	189
4.3	Depth-dependent advection coefficients of parameter γ for a family of γ values	190
4.4	Depth-dependent advection coefficients of parameters fm, α, γ with respect to θ_o for a family of γ values.	192
4.5	Depth-dependent advection coefficients of parameter θ_o for a family of γ values	198
4.6	Ratio of advection coefficients (D_{6j}/D^m_{6j}) for parameter θ_o as a function of γ in deep water	200
4.7	Schematic representation of energy transfer from WINDSEA to SWELL	218
4.8	Schematic representation of energy transfer from SWELL to WINDSEA	223
5.1	Synoptic weather map of extratropical cyclone in the Gulf of Alaska for 0600 GMT, January 30, 1976	227
5.2	Location map of measuring stations in the Gulf of Alaska . .	229
5.3	Grid used in numerical wave model. Based on a polar stereographic projection, the average grid spacing is approximately 150 km	230
5.4	Examples of wind field input to the numerical model for 1500 GMT and 1800 GMT, January 28, 1976. The vectors show speed and direction of the wind. Dots indicate stations where wave measurements have been made	232
5.5	Storm track of extratropical cyclone	233
5.6	Examples of wind field input to the numerical model for 0000 GMT and 0300 GMT, January 30, 1976. The vectors show speed and direction of the wind. Dots indicate stations where wave measurements have been made	235

No.		Page
5.7	Evolution of hindcasted wave spectra at station NOAA EB03 (top) and Middleton Island (bottom) for the extratropical cyclone of January 27-31, 1976	237
5.8	Evolution of hindcasted wave spectra at station Sitkinak Island (top) and Amatuli Island (bottom) for the extratropical cyclone of January 27-31, 1976	238
5.9	Evolution of hindcasted wave spectra at station Icy Bay (top) and Yakutat Bay (bottom) for the extratropical cyclone of January 27-31, 1976	239
5.10	Time series of hindcasted spectral wave parameters and measurements (+++) at station NOAA EB03 using a model with directional relaxation	241
5.11	Time series of hindcasted spectral wave parameters and measurements (+++) at station NOAA EB03 using a model without directional relaxation	243
5.12	Comparison between hindcasted (——) and measured (*—*) wave spectra at station NOAA EB03 for 0600 GMT, January 30, 1976. (Left: with directional relaxation; right: without directional relaxation).	245
5.13	Comparison between hindcasted (——) and measured (*—*) wave spectra at station NOAA EB03 for 0900 GMT, January 30, 1976. (Left: with directional relaxation; right: without directional relaxation).	246
5.14	Comparison between hindcasted (——) and measured (*—*) wave spectra at station NOAA EB03 for 1200 GMT, January 30, 1976. (Left: with directional relaxation; right: without directional relaxation).	247
5.15	Time series of hindcasted spectral wave parameters and measurements (+++) at station Middleton Island using a model with directional relaxation.	248
5.16	Time series of hindcasted spectral wave parameters and measurements (+++) at station Middleton Island using a model without directional relaxation	250
5.17	Comparison of hindcasted significant wave heights from three wave models with data for Middleton Island. (——) GAPS model; (---) HYPA model, no directional relaxation; (.....) HYPA model, with directional relaxation.	251
5.18	Time series of hindcasted spectral wave parameters and measurements (+++) at station Sitkinak Island using a model with directional relaxation.	252

No.		Page
5.19	Time series of hindcasted spectral wave parameters and measurements (+++) at station Sitkinak Island using a model without directional relaxation	254
5.20	Time series of hindcasted spectral wave parameters and measurements (+++) at station Amatuli Island using a model with directional relaxation.	255
5.21	Time series of hindcasted spectral wave parameters and measurements (+++) at station Amatuli Island using a model without directional relaxation	257
5.22	Time series of hindcasted spectral wave parameters and measurements (+++) at station Icy Bay using a model with directional relaxation	258
5.23	Time series of hindcasted spectral wave parameters and measurements (+++) at station Icy Bay using a model without directional relaxation	260
5.24	Time series of hindcasted spectral wave parameters and measurements (+++) at station Yakutat Bay using a model with directional relaxation.	262
5.25	Time series of hindcasted spectral wave parameters and measurements (+++) at station Yakutat Bay using a model without directional relaxation	263
5.26	Contours of hindcasted significant wave heights in the Gulf of Alaska for the extratropical cyclone on 1200 GMT, January 28, 1976	264
5.27	Location map of ARSLOE experimental area off the North Carolina coast	266
5.28	Synoptic weather map of frontal system over the ARSLOE site showing the streamline pattern at 1200 GMT, October 25, 1980	267
5.29	Examples of wind field input to the numerical wave model for the ARSLOE storm at 1200 GMT and 1500 GMT, October 25, 1980. The vectors show speed and direction of the wind. The dot indicates location of XERB buoys	269
5.30	Evolution of hindcasted wave spectra at station XERB for the ARSLOE storm of October 23-26, 1980. (a) pre-storm development; (b) post-storm development.	271
5.31	Time series of hindcasted spectral wave parameters at station XERB for the ARSLOE storm.	272

No. Page

5.32 Comparison of measured and hindcasted significant wave height, spectral peak frequency and mean wave direction at station XERB. 275

5.33 Comparison of measured and hindcasted wave spectrum at station XERB for the ARSLOE storm at 1800 GMT, October 24, 1980 279

5.34 Comparison of measured and hindcasted wave spectrum at station XERB for the ARSLOE storm at 1300 GMT, October 25, 1980 280

LIST OF TABLES

No.		Page
3.1	Summary of theoretical spectral wave parameters as a function of fetch and duration. Examples are calculated for a mean JONSWAP and Pierson-Moskowitz spectrum, corresponding to fm = 0.1 Hz, U = 15.7 m/s, and f_{PM} = 0.1 Hz, U = 12.75 m/s, respectively	79
3.2	Transformation parameters for finite depth nonlinear energy transfer as a function of γ	135

CHAPTER 1

INTRODUCTION

Ein grosser Vorsatz scheint im Anfang toll. An ambitious plan at first seems mad.

(Wagner)

--FAUST II, Laboratorium
Johann Wolfgang von Goethe

The design and operation of most marine related activities in coastal and offshore areas require an adequate assessment of the ambient and extreme wave conditions. Sufficient information on wave statistics is only available at a few locations around the world (Gulf of Mexico, North Sea). To provide adequate information of the wave climate, a numerical wave prediction model can be employed to hindcast and forecast ocean surface waves from known meteorological data.

Design criteria for offshore engineering projects are based on the most extreme wave conditions to be expected during the structure's lifetime. A key ingredient for developing such design criteria is a knowledge of severe wave conditions. The extreme data required as input to design considerations should be determined from a data base which is a representative sample of wave conditions in the area of interest. To establish an adequate data base, there are several possibilities to accomplish this task. One way would be the availability of measurements of sufficient size and duration. Such records rarely exist and to undertake such a data gathering program is often economically infeasible. Sometimes a limited set of observations may exist in the vicinity of the area of interest, but in subsequent deliberations on design criteria for offshore structures, this set may not suffice to extrapolate to the design life of the structure. Typically, a record of ten years is required to extrapolate reliable

estimates of extreme conditions for return periods of 25 years. Extrapolation to return periods larger than those could seriously jeopardize not only the structure's economic feasibility, but also reduce the safety level of offshore operations. The primary unknown factor in a limited data base of field measurements is the relative severity of the worst storm. It is difficult to decide for a small sample if the worst storm is a 100-year storm or only a 50-year storm. Such a decision has a strong bearing on the derivation of design criteria. Therefore, the only feasible method, either to generate a data base or to supplement existing wave statistics is by means of hindcasting analyses using a numerical wave model. A data base can be compiled from hindcasts of the wave climatology for historical storm events in all areas of interest. In addition, these model predictions can be compared to existing data to verify their accuracy and if necessary the model can be calibrated to ensure reliable answers. Presently, the application of numerical wave models to known meteorological data seems to be the most promising source of information for the estimation of extreme wave conditions in either deep or shallow water.

Knowledge of ambient wave conditions are of importance for the general operation of offshore facilities, and in planning strategies concerning the clean-up of oil spills or rescue operations. The ongoing efforts to develop a reliable wave prediction method or to improve existing ones is still a much sought after goal. Many applications of numerical wave predictions can be put to practical use in ship routing, marine-related offshore operations, the coupling with storm surge (wave set-up) and sediment transport models (erosion and deposition).

In the past, these wind wave models have been primarily developed and/or applied to deep water conditions. Therefore, it was not uncommon to use deep water models to predict wave conditions in situations where the deep water assumption was violated. Clearly, a wind wave model should include finite depths effects, if applied to forecast wave conditions on the continental shelf and in coastal seas. In addition to the well-known effects of refraction and shoaling, a finite depth wave model should also account for the interaction between the near-bottom wave motion and the bottom sediments. This mechanism is responsible for the generation of bottom bedforms (ripples) and/or significant transport of bottom sediments (erosion and deposition), which in turn influences the resistance experienced by the waves (bottom friction) and results in a considerable loss of wave energy. The incorporation of the bottom friction effect in a wave model may yield considerably smaller wave heights, which by itself translates into reduced cost for offshore structures. Of all wave motions present in the ocean, surface gravity waves possess considerable amounts of energy and have the most potential for adverse impacts on most marine activity.

Most modern wind wave models are based on the energy transport equation which describes the evolution of the wave spectrum in space and time due to various physical processes which generate or dissipate energy. In Chapter 2 a historical review of wave prediction methods is presented, with particular emphasis on the theoretical concepts and underlying physics included in standard discrete spectral models and parametric models for deep water. A brief discussion of first generation shallow water models is also given.

Chapter 3 describes in detail the theoretical background needed to develop a hybrid parametric wave model for arbitrary water depths. Specifically, the derivation of the finite depth JONSWAP spectrum is discussed and various spectral parameters relating wave properties to the energy spectrum are also defined. The major portion of this chapter is devoted for a rigorous derivation of the energy transport equation and possible analytical solutions. In this context, the individual sections deal with the source functions such as wind input, nonlinear wave-wave interactions, wave breaking and bottom friction. The last sections of this chapter develops the concept of a mean wave direction based on energy flux arguments.

The arbitrary depth parametric wave model is described in Chapter 4. Based on an energy flux transport equation, the derivation of an equivalent set of prognostic parametric equations is outlined. The transformation functionals are constructed in the following section so that the JONSWAP parameters are recovered again. The propagation coefficients reflecting a depth dependent group velocity are calculated and Appendices A and B present some detailed example computations. The directional relaxation parameter is formulated using an energy flux concept and compared with an analogously derived parameter but instead using wave momentum. The parametric source functions are determined which in addition includes the effect of bottom friction and refraction. The final section gives a general outline of the transfer criteria between the windsea and swell domains.

Two test cases to verify the model's applicability are presented in Chapter 5. The first case describes a model application to an extratropical storm event in the Gulf of Alaska. The objective of this

test was to demonstrate the model's performance in situations of rapidly turning winds and in windsea-swell transition regions. The second case deals with the model's application to finite depth conditions. At the same time, the fact that wave directional data was available for the ARSLOE storm provided an additional test of the model's sensitivity to a 180° shift in the winds resulting from a frontal passage of the North Carolina coast.

The numerical wind wave model described here is an extension of a previous deep water hybrid parametric model to account for finite depths effects such as bottom friction, refraction and shoaling. At the same time, the model spectrum includes a depth dependent transformation factor which retains a f^{-5} spectral shape in deep water and reduces to a f^{-3} dependence in shallow water. Furthermore, the concept of directional relaxation of the windsea spectrum is re-derived using more general energy flux arguments instead of wave momentum.

CHAPTER 2

HISTORICAL REVIEW OF WAVE PREDICTION METHODS

Verzeiht! es ist ein gross Ergötzen,
Sich in den Geist der Zeiten zu versetzen.
Zu schauen, wie vor uns ein weiser
Mann gedacht und wie wir's dann
zuletzt so herrlich weit gebracht.

Excuse me! but it is a great delight
To enter in the spirit of the ages and
To see how once a sage before us
Thought and then how we have brought
Things on at last to such a splendid height.

(Wagner)

--FAUST I, Nacht
Johann Wolfgang von Goethe

Scientists and engineers have spent more than 100 years to explain the generation processes of surface gravity waves. In this context, even today Ursell's (1956) opening statement seems still appropriate: "Wind blowing over a water surface generates waves in the water by physical processes which cannot be regarded known." This is not to say that no progress has been made. On the contrary, extensive advances have been achieved both in a theoretical and experimental sense, but these efforts often come to a temporary stop, until newly developed methodologies and techniques open up the next door. At the same time it should be understood that wind-driven gravity waves are not the only wave motion occurring on the ocean surfaces. Various other types of wave motion are present either at the sea surface or within the ocean itself. In this study we restrict our attention to surface gravity waves generated by the wind. On a schematic energy spectrum of oceanic variability, surface waves occupy a broad range of periods (1~30 seconds) and wavelengths (10 cm ~ 1 km) and make a large contribution to the oceanic energy spectrum.

Since our interest is primarily concerned with the mechanism by which the wind generates waves, it is obvious to investigate this phenomenon first. The earliest theories applied to wave generation

were introduced by Helmholtz (1888) and Kelvin (1871), who both studied the effect of oscillations set up at the interface of two media (air and water) with different densities and flowing with different velocities relative to each other. The Kelvin-Helmholtz mechanism predicts a minimum wind speed 6.5 m/s for which waves grow, but ocean waves are observed to be initiated at much lower wind speeds. For this reason and others (Miles, 1959), this mechanism is believed not to be too effective in generating waves for those wind speeds and wave lengths typically observed at sea. An extensive discussion of these theories can be found in Lamb (1932).

The next important step forward was made by Jeffreys (1924, 1925) who re-examined the problem and suggested the "sheltering hypothesis" to be responsible for wave growth. He introduced the reasonable concept that when a turbulent wind blows over a hydrodynamically rough sea (pre-existence of ripples), flow separation occurs on the downwind side of the wave crests with presumed re-attachment somewhere on the upwind slope of the next wave crest. The resulting pressure field is asymmetrically distributed over the wave profile. The pressure component in phase with the wave slope does work on the wave and results in a positive energy transfer from the air flow to the waves, as long as the wave moves slower than the wind. If the imparted energy is greater than the dissipation by viscosity, the waves will grow according to

$$\frac{\partial E}{\partial t} = \frac{1}{2} \rho_a \, s \, c(U - c)^2 \, (ka)^2$$

where s is less than unity and commonly referred to as a "sheltering

coefficient". Some weak points of this theory may be pointed out. For one, Jeffreys neglects transfers from tangential stresses. The coefficient s depends on $(U_{min})^3$ and a correct choice of U_{min} was critical in calculating s, as remarked by Dobson (1969). Choosing U_{min} = 1.1 m/s and considering a balance between the energy gained from the wind and that lost by viscous effects, a value of s approximately equal to 0.27 is calculated. However, Jeffreys' theory quickly lost support, when measurements of wind passing over solid wavy surfaces gave values of s which were smaller by an order of magnitude. From this it was concluded that Jeffreys' mechanism was ineffective in accounting for the observed wave growth.

Other theories were developed by Eckart (1953), Lock (1954) and Wuest (1949), which still could not satisfactorily explain observed wave growth or were either too idealized or too complicated to be realistically used. Ursell's (1956) review provided the catalyst for a major progress in wind-wave research. Independently Phillips (1957) and Miles (1957) proposed two new, complementary theories. Philips' theory was an improvement over Eckart's model, whereby waves are generated on initially quiet water by normal pressure fluctuations after the onset of a turbulent wind. Miles' theory advanced the notion of an instability mechanism causing wave growth by improving the earlier shear flow models of Kelvin, Helmholtz, Wuest and Lock. The underlying physics of these two mechanisms are discussed in some detail in Section 3.3.1.

An appropriate utilization of these theoretical efforts explaining wind-generated surface waves is obviously seen in wave prediction. The earliest form of a wave forecasting model was developed by Sverdrup and

Munk (1947). Based on simple principles and some sparse observational evidence, these authors proposed a reasonable model which was capable of describing the behavior of a wave on the ocean surface in terms of its total energy content, phase speed and propagation velocity of energy. From this they were able to construct several simple parameters involving the wind speed, fetch, duration, wave height and period. Transforming these relationships into a set of nomographs, the prediction of wave heights was readily obtained, once the proper parameters were derived from synoptic weather maps. This approach is known as "the significant wave concept" and with the later improvements by Bretschneider (1952) is synonymous with the acronym "SMB method". It is clear that the SMB method is parametric and there is no connection with the physics of air-sea interactions.

With the introduction of the wave spectrum concept by Pierson, Neumann and James (1955) and Dabyshire (1952), the forecasting methods at last had a variable that could adequately describe the highly irregular appearance of waves at the sea surface. The PNJ method did not bring about the desired success in forecasting. This lack of success in both methods is mainly attributed to their largely subjective nature in making practical predictions. At the same time, one must understand that these methods tried to solve extremely complex problems with rather simple manual procedures. Today, the problem is still awaiting a satisfactory solution, although considerable progress has been made in closing this gap.

Evidence for this fact has been given by the recent results of the SWAMP (Sea Wave Modeling Project, 1982) study. The main purpose of this study was to test and to elicit our understanding of the physics

governing the generation of surface gravity waves from a wave modeling aspect. Specifically, this modeling exercise was designed to clarify the general physical concept of surface waves, how it is represented numerically, and the quantitative prediction of the evolution of a two-dimensional wave spectrum in space and time for a given wind field. In order to reveal the inherent differences between the models, a series of hypothetical, idealized wind fields were defined in such a way as to uncover each model's response to asymmetrical boundary conditions, sudden changes in wind directions, discontinuous spatial wind distributions, etc. A final test was to investigate the models' response to wind fields typically found in intense hurricanes, for the cases of a stationary and a moving storm. The principal conclusion of this intercomparison study was that the models, in all test cases, produced results which not only significantly differed from model to model, but also often behaved quite to the contrary of what was expected. In other words, forecasting results are still strongly dependent on the specific wave model used, aside from the meteorological uncertainties.

In the next sections we will present a brief look at some types of wave models of the past and present. We will also mention briefly specific applications and model validity as well as highlight distinct features. For additional information on the subject of wind wave research, the reader should see Kinsman (1965) or Barnett and Kenyon (1975) who presented an excellent account of the state-of-the-art on this subject. Similarly, Phillips (1977) and LeBlond and Mysak (1978) can be consulted for a wide range of wave theories and their relations to various physical processes and types of motions. General

hydrodynamic principles and fundamental properties of waves are excellently described in Lighthill (1978), and Mei (1983). Finally, for more practical advice the reader may consider the "Handbook on Wave Analysis and Forecasting" by the WMO (1976).

2.1 Deep Water Discrete Spectral Models

The general framework of spectral models is the energy balance or transport equation which governs the evolution of the surface wave field in space and time. In deep water, this equation can be written as

$$\frac{\partial E}{\partial t} + \underline{c}_g \cdot \underline{\nabla} E = S \equiv S_{in} + S_{nl} + S_{ds} \qquad (2.1.1)$$

where $E(f,\theta; \underline{x}, t)$ is the two-dimensional wave spectrum which is a function of frequency f and propagation direction θ, as well as the space-time coordinates $\underline{x}$, t; $\underline{c}_g = \underline{c}_g(f,\theta)$ is the group velocity, and the net source function S is represented as the sum of three processes: S_{in}, the energy input by the wind; S_{nl}, the nonlinear energy transfer by resonant wave-wave interactions; S_{ds}, the dissipation of energy by wave breaking, for example. Refraction effects resulting from the interaction with slowly varying currents are generally considered to be small and are neglected. This equation was independently proposed by Gelci et al. (1956) and Hasselmann (1960). Once a mathematical representation of S is specified, a solution to (2.1.1) can be obtained by numerical integration. Differences among models are mainly associated with the chosen form of the source function S, and the specific numerical technique to perform the integration of (2.1.1).

Nowadays spectral wave models are divided into two classes: decoupled and coupled spectral models. In the decoupled models, each

spectral component is assumed to grow, decay and propagate independently of the other modes. A new generation of discrete spectral models are called "coupled" spectral model, because they take advantage of the efficiency in the parametric approch for the high-frequency part of the spectrum. The basic discrete spectral representation is still retained for the entire energy spectrum (wind sea and swell). These wave model are now capable of including the resonant interactions of different wave modes, which cannot be done in ray-decoupled models.

The first wave forecasting model, based on the transport equation (2.1.1) was introduced by Gelci et al. (1957). Although the model included the simulation of growth and decay, these source terms were entirely derived from empiricism. The theoretical formulation of the three source functions, as utilized today, got their start with the fundamental works of Phillips (1957) and Miles (1957). The introduction of a universal equilibrium range concept for the spectrum by Phillips (1958) and the breakthrough in analyzing the nonlinear transfer due to resonant wave-wave interactions by Hasselmann (1960, 1962, 1963a,b), set the stage for the development of wave models thereafter.

The first generation of physical spectral wave models were mainly based on decoupled wave dynamics (Pierson et al. 1966; Inoue, 1967; Barnett, 1968; Ewing, 1971; Isozaki and Uji, 1973; Cardone et al. 1976). In these models wave growth is simulated by a linear source function S_{in} which comprises a linear and exponential growth term

$$S_{in} = A + B \cdot E \qquad (2.1.2)$$

Here, the A term represents Phillips' resonantly interacting turbulent pressure components and the B term corresponds to the growth function of Miles' instability (linear feedback) mechanism. Typically, the two-dimensional spectrum is characterized by discrete frequency-direction wave packets. Each energy packet, for a specific (f,θ), will separately grow to its limiting saturation level. To ensure an asymptotic approach to the universal equilibrium level, the dissipation function S_{ds} plays the role of a delimiter preventing the spectrum from exceeding this level. Since it is believed that the saturation level is controlled by wave breaking, S_{ds} is often presented as a wave breaking mechanism. Advection is handled on characteristic coordinates which means each energy packet is propagated at its appropriate group velocity along its own ray path. Generally, the nonlinear transfer S_{nl} has been omitted, since its inclusion poses new numerical problems which are associated with ray coupling. The Barnett and Ewing models, however, included simple parameterizations of S_{nl}, but the overall impact on the evolution of the spectrum was minor.

In the following paragraphs we will briefly describe some of the ray-decoupled models. Specifically, we address the choice of the source function S, the numerical integration method and the scope of applications.

The Pierson-Tick-Baer Model:

Commonly known as the PTB model and the parent of most discrete spectral models. Pierson et al. (1966) developed this model for global operational forecasting on a hexagonal grid system resulting from a

global gnomonic projection. The propagation is treated in a combined manner, using first-order upstream differencing and a discontinuous "jump" technique. The spectrum is resolved into 13 frequency and 24 direction bands. Wave components travelling against the wind are explicitly attenuated at a rate proportional to $[f \cdot E(f)]^4$. The growth-dissipation algorithm is based on a direction independent parameterization of the Phillips-Miles terms with an asymptotic limit specified by the PM spectrum. The right-hand side of (2.1.1) is given by

$$S = S_{in} + S_{ds} = A(U_o) + B(f,U_o)\, E(f) - D(f,U_o) \qquad (2.1.3)$$

where

$$A(U_o) = 1.4 \times 10^{-8}\, U_o^{\,3} \qquad (2.1.4)$$

$$B(f,U_o) = 6.27(U_o/c_g)^2 \exp[-0.017(U_o/c_g)^{-4}]f \qquad (2.1.5)$$

$$D(f,U_o) = (A - A^*) + (B - B^*)E \qquad (2.1.6)$$

in which

$$A^* = A[1 - (\frac{E}{E_\infty})^2]^{3/2}$$

$$B^* = B[1 - (\frac{E}{E_\infty})^2]$$

and $$E_\infty \equiv E_{PM}(f) = 0.0081\, g^2(2\pi)^{-4} f^{-5} \exp[-0.74(\frac{f}{f_o})^{-4}] \qquad (2.1.7)$$

is the fully developed PM spectrum, with $f_o = g/2\pi U_o$, and U_o corresponds to the wind speed at 19.5 m and the group velocity $c_g = g/4\pi f$. Thus, for an initial spectrum $E_o(f)$, the energy of this component at some time later, $E(f,t)$, is analytically calculated by integrating (2.1.3), i.e.,

$$E(f,t) = \frac{A \exp[B(t + t_o) - 1]}{B\{1 + [\frac{A}{B E_\infty} \exp(B(t + t_o) - 1)]^2\}^{0.5}} \qquad (2.1.8)$$

where t_o is an equivalent duration for the initial spectrum $E_o(f)$ at the new wind speed and is given by:

$$t_o = \frac{1}{B} \ln\{1 + \frac{B E_o \Delta f}{A[1 - (\frac{E_o}{E_\infty})^2]^{1/2}}\} \quad .$$

The PTB approach calculates the energy wave growth for all discrete directions θ at fixed frequency f. The final directional spectrum is determined by directionally spreading according to

$$E_{PM}(f,\theta,U_o) = E_{PM}(f,U_o)\, \Omega(\tilde{\theta},f,U_o) \qquad (2.1.9)$$

with an empirically specified angular distribution

$$\Omega(\tilde{\theta},f,U_o) = \frac{1}{\pi}\{1 + [\frac{1}{2} + .82 \exp(-\frac{1}{2}(\frac{f}{f_o})^4)] \cos 2\tilde{\theta}$$

$$+ .32 \exp(-\frac{1}{2}(\frac{f}{f_o})^4) \cos 4\tilde{\theta}\} \qquad (2.1.10)$$

where $\tilde{\theta}$ is the angle between the wind vector and the direction of the wave component. A modified version of the original PTB model has been implemented at the U.S. Navy Fleet Numerical Weather Central and is still in use to provide routine operational wave forecasts for the oceans in the Northern Hemisphere (Lazanoff and Stevenson, 1975).

The Inoue Model:

The Inoue (1967) model essentially has the same features as the PTB model. There are some refinements over the PTB model, primarily in

the specification of the terms A and B. In addition, the two-dimensional form of this model treats the directional aspect somewhat different than in the PTB approach. A model description and hindcast results can be found in Bunting (1970).

The Barnett Model:

Barnett (1968) probably presented the first model to contain delineations of all three processes in the source function. The major advancement was ascribed in the incorporation of a parameterized nonlinear transfer term S_{nl}. Based on Hasselmann's (1963b) early computations of nonlinear transfer rates for a fully developed Neumann spectrum, Barnett derived reasonably simple parameterizations of S_{nl} (see Section 3.3.2). Incorporation of these simple algebraic expressions did not decrease the relative computational efficiency of the model. Now, the model could no longer be solved on a ray-decoupled system, but this proved not to be too critical, so long as the nonlinear transfer was not the dominating term in S. Later tests showed that the nonlinear growth amplification turned up around the same region of the spectrum (at the peak) as the input from the wind. Qualitatively this implied that the overall effect of the nonlinear transfer in this form was relatively unimportant. Obviously, a numerical solution of (2.1.1) by ray methods was no longer feasible, since different wave modes are now coupled through a nonlinear mechanism. Numerical integration of the transport equation is carried out on a two parallel (30°; 60°) Lambert conformal projected grid system using a fourth-order Runge-Kutta technique. The linear growth term due to Phillips' resonance theory is related to the three-

dimensional spectrum of random atmospheric pressure fluctuations $P(k,\omega)$, as shown by Hasselmann (1960)

$$A = \frac{(2\pi)^2 k \omega^3}{\rho_w^2 g^3} P(k,\omega) \qquad (2.1.11)$$

where $\omega = 2\pi f$, k is the wave number and ρ_w is the density of water. From measurements of Priestley (1965) and Snyder and Cox (1966) the pressure spectrum is suitably described by

$$P(k,\omega) = \frac{\psi(\omega)}{\pi^2}\left[\frac{\nu_1}{\nu_1^2 + (k\cos\tilde{\theta} - \omega/U)^2}\right]\cdot\left[\frac{\nu_2}{\nu_2^2 + k^2 \sin\tilde{\theta}}\right] \qquad (2.1.12)$$

where $\psi(\omega)$ is the pressure power spectrum, given by

$$\psi(\omega) = 1.23\, \omega^{-2}\, \psi_o(U,s) \qquad (2.1.13)$$

with ψ_o representing a turbulent scaling coefficient which depends on the wind speed U and the atmospheric stability s and is taken as $\psi_o \sim U^6$. ν_1 and ν_2 are empirical functions determined by Priestly (1965) as

$$\nu_1 = 0.33\left(\frac{\omega}{U}\right)^{1.28} \quad ; \quad \nu_2 = 0.52\left(\frac{\omega}{U}\right)^{0.95} \qquad (2.1.14)$$

and $\tilde{\theta}$ specifies the angle between the wind and wave directions. The exponential growth term was slightly modified by Barnett to be consistent with field data of Snyder and Cox (1966) and Barnett and Wilkerson (1967). He takes

$$B = 5\frac{\rho_a}{\rho_w} f\left[\frac{U_o \cos\tilde{\theta}}{c} - 0.90\right] \qquad (2.1.15)$$

for $\frac{U_o \cos\tilde{\theta}}{c} > 0.90$, otherwise B = 0.

Wave growth is limited by the saturated value of each component in accordance with Phillips' (1958) "equilibrium range" hypothesis. The dissipation term is essentially a representation of the wave breaking process and is accounted for by multiplying the input term S_{in} by the quantity (1-r), where

$$r = 0.8 \exp[-\frac{1}{2}(E_\infty - E)/E] \qquad (2.1.16)$$

and the saturation spectrum E_∞ is specified as

$$E_\infty(f,\tilde{\theta}) = \frac{\alpha g^2}{(2\pi)^4} f^{-5} \Omega(\tilde{\theta}) \qquad (2.1.17)$$

with an angular spreading factor set as $\Omega(\tilde{\theta}) = \frac{8}{3\pi} \cos^4 \tilde{\theta}$. The nonlinear transfer term S_{nl} are taken in the form as defined in (3.3.14 - 3.3.18). Barnett discretizes the wave spectrum into 18 frequency and 12 direction bands. The model has been successfully applied in predictions of two-dimensional wind-wave spectra in the North Atlantic Ocean.

The Ewing Model:

This model (Ewing, 1971) is without distinction very similar to Barnett's model. The differences principally reside with the detailed specification of the individual terms making up the source function S. Again, Ewing represents all three wave processes and we briefly give an outline as to their differences below.

The nonlinear transfer is approximated in terms of a Fourier-Chebyshev series for a family of spectra for which Hasselmann's (1963b)

integrals were calculated. These parameterizations are given in equations 3.3.19 - 3.3.21 (see section 3.3.2). The linear growth term is identical to the expression in (2.1.11), except the turbulent scaling factor is taken $\psi_o \sim U^4$. Unlike Barnett's B term, Ewing proposes another empirical fit to the same data set which is continuous for the range (U/c) of interest, i.e.,

$$B = 7 \times 10^{-4} f \left(\frac{U}{c} \cos \tilde{\theta}\right)^4 \qquad (2.1.18)$$

The damping term is a simulated wave breaking process where Ewing sets

$$r = \left(\frac{E}{E_\infty}\right)^2 \qquad (2.1.19)$$

and the equilibrium range spectrum E_∞ is given by the limiting form of the PM spectrum, i.e.

$$E_\infty(f,\tilde{\theta}) = \frac{8.1 \times 10^{-3}\, g^2}{(2\pi)^4} f^{-5} \Omega(\tilde{\theta}) \qquad \text{for } \tilde{\theta} \leq |\pi| \qquad (2.1.20)$$

and the angular spreading factor is taken as $\Omega(\tilde{\theta}) = \frac{4}{3\pi} \cos^4 \left(\frac{\tilde{\theta}}{2}\right)$. Ewing considers the directional spectrum as the composition of 8 frequency and 12 direction components. The grid points are defined on a conical projection and the energy balance equation (2.1.1) is numerically integrated by means of an explicit fourth-order difference scheme for the homogeneous equation. The nonhomogeneous equation is solved by first calculating the homogeneous part of (2.1.1) over the entire grid and then computing the induced change in energy which results from integration of S over the previous time step holding the wind field parameters constant. Model applications were mainly carried out for the North Atlantic ocean.

The Isozaki-Uji Model:

An improved version of the original PTB model, Isozaki and Uji (1973) attempted to remedy some of the numerical problems associated with unrealistic concentrations of energy. Since the tendency of waves is to disperse, they resorted to a more complex variation of the "jump" technique which now could effectively simulate lateral spreading and longitudinal dispersion of energy. Additional refinements of this model by Uji (1975) included an attenuation mechanism for spectral components that propagate against locally generated windseas. The model was tested by hindcasting wave conditions in typhoon wind fields.

The Cardone Model:

Also known as ODGP (Ocean Data Gathering Program) model, it belongs to the family of PTB models, but with considerable advances in treating wave growth and decay. Cardone et al. (1976) developed this discrete spectral model specifically for forecasting wave spectra under extreme wind conditions such as in hurricanes. The model was calibrated to resolve adequately differences such as the response of the directional wave spectrum to rapidly turning winds (directional relaxation); the effect in representing the high-frequency equilibrium range with a f^{-4} or a f^{-5} dependence; the transition from a windsea to a fully developed sea; the proper choice of velocity in the growth terms (friction velocity u_* versus 10 m or 20 m winds, U_a). The ODGP model's specific task was to predict maximum storm generated sea states in selected areas as for example, the Gulf of Mexico. These models are rarely applicable to wind fields and physical geometries other than those they are tuned for. Many of the features found in the

PTB model have been improved and some of the salient differences are given below.

The principal difference arises in allowing each spectral component (f,θ) to grow independently, as opposed to the integrated PTB approach. Energy is redistributed over direction after all components travelling within $\pm$ 90° of the local wind have undergone growth. According to Cardone et al. (1981) this produces an effect which is believed to be similar to the capability of nonlinear wave-wave interactions to redistribute energy directionally in a turning wind field. The linear growth term has been changed to reduce the growth tendency of low frequency wave modes for large wind speeds. Based on Stacy's (1974) study, the limiting saturation range is modified to reflect a wind dependent form with (-4) frequency power law. The model has been successfully applied to extensive hurricane and tropical storm events in the Gulf of Mexico and along the east coast of the U.S. (Reece and Cardone, 1982). Several other versions of the ODGP model have since been developed with specific attention to the physical and meteorological parameters of the area of interest.

Spectral wave models, representative of the coupled class, are described in the recent wave modeling intercomparison study SWAMP (1982). The major distinctive feature in coupled models is the parametric treatment of the high-frequency tail of the spectrum. Although discrete spectral models are conceptually much simpler, the major drawback lies in the computational economics. The construction of the two-dimensional spectrum typically requires the solution of several hundred frequency-direction bins. Even with current computer speeds this is still a formidable task, especially if real-time

forecasts are needed. This fact may explain to some extent the slow drift of discrete spectral models to look more like parametric models.

2.2 Deep Water Parametric Models

2.2.1 Diagnostic Parametric Models

The inception of practical wave forecasting can be traced to the days of WWII, when the need for wave conditions arose in connection with the planning and preparation of amphibious operations on distant shorelines. Prior to this time, most knowledge regarding waves was entirely empirical and often inconsistent. Based on the hydrodynamic principles governing surface waves, Sverdrup and Munk (1947) introduced the conceptual wave parameters: significant wave height, H_s, and significant wave period, T_s. Although "significant waves" do not conform to the laws of classical wave theory, the idea was vital for the development of their forecasting theory, because only the significant waves are empirically known. These two parameters formed the basis for the Sverdrup and Munk (S-M) method. From theoretical considerations and empirical evidence, Sverdrup and Munk (1947) derived relationships relating these two wave parameters to three important variables: the wind speed at the sea surface; the fetch, indicating the distance over which the wind blows; and the duration, a measure of how long the wind has blown. A series of nomographs were established for various relationships among nondimensional variables involving these wind and wave parameters. Application of the S-M method is carried out to a reasonable degree of accuracy if adequate and consecutive surface weather maps are available. A forecast of sea and swell at a specific location is obtained by determining the appropriate values of surface

wind speed, fetch and duration and upon entering the graphs with their dimensionless combinations, the significant wave height, H_s, and significant wave period, T_s, are read off. Additional simple theories were developed to forecast graphically the propagation and decay of swell waves. A detailed derivation of the fundamentals for the S-M method can be found either in the authors original work or in Kinsman (1965).

The simplicity and cheap economics of the significant wave method explains its quick success as a widely applied technique to predict waves. Bretschneider (1952, 1958) made several improvements and corrections of the original S-M method. Further efforts to extend the range of application to more complex situations was undertaken by Wilson (1955), who incorporated the effect of time and spatially varying wind fields. For the preparation of objective wave forecasts, the SMB method has been programmed to be solved on digital computers (Hubert, 1964; Pore and Richardson, 1969). Until recently, the offshore oil and technology industries have based most of their engineering designs on wave parameters predicted from modified significant wave methods during extreme wind conditions as those occurring in hurricane systems (Patterson, 1972; Bea, 1974; Ward et al., 1977). Even today, the significant wave method still enjoys a wide user audience, primarily in the field of engineering. This is largely due to its simplicity and speed of application in obtaining significant wave estimates which agree reasonably well with observations. But there are numerous relationships from which to choose and each claims an improvement over previously determined relationships. All these empirical formulae are derived from a

best-fit to the general relation involving the dimensionless wave height, $\tilde{H}$, and dimensionless wave period, $\tilde{T}$; and the dimensionless fetch:

$$\tilde{H} = \frac{gH}{U^2} = a_1 \tanh (b_1 \tilde{F}^m) \qquad (2.2.1)$$

$$\tilde{T} = \frac{gT}{U} = a_2 \tanh (b_2 \tilde{F}^n) \qquad (2.2.2)$$

where a_1, a_2, b_1, b_2 are empirically determined constants; m,n are exponents; and $\tilde{F} = gx/U^2$ is the dimensionless fetch. Below we just present a few of the better known empirical formulae.

Wilson (1955):

$$\tilde{H} = 0.26 \tanh (0.01 \tilde{F}^{0.5}) \qquad \text{for } \tilde{F} \geq 10^{-1} \qquad (2.2.3)$$

$$\tilde{T} = 1.4\ 2\pi \tanh (0.0436 \tilde{F}^{0.33})$$

It is not clear from the author's original work if $U = U_{10}$, but $H = H_S$ and $T = T_S$.

Bretschneider (1973):

$$\tilde{H} = 0.283 \tanh (0.0125 \tilde{F}^{0.42}) \qquad (2.2.4)$$

$$\tilde{T} = 1.2 \cdot 2\pi \tanh (0.077 \tilde{F}^{0.25})$$

These expressions are probably the most widely used, since they are identical to those given in the Shore Protection Manual (CERC, 1975). Here $H = H_S$ and $T = T_S$.

Ou and Tang (1974):

$$\tilde{H} = 0.184 \tanh (0.02 \tilde{F}^{0.4}) \qquad (2.2.5)$$

$$\tilde{T} = 0.971 \cdot 2\pi \tanh (0.0406 \tilde{F}^{0.32})$$

Their original work specifies the constants multiplying $\tilde{F}$ by a factor 10 too large which appears to be a misprint.

Although contemporary versions of the significant wave method are still applied to solve today's offshore engineering design problems (Bretschneider and Tamaye, 1976; Earle, 1978), its decline is inevitable. There are several inherent problems associated with the significant wave method. First, the wave predictions are only diagnostic, because time does not appear explicitly in any of its formulations. This means that the wave field is only a function of the local wind vector at a certain fetch. Second, the increasing need for adequate and detailed descriptions of the ocean surface (wave spectra, wave direction) as required by cost-competitive offshore structural designs, cannot be provided by the significant wave method. Third, as remarked by Kinsman (1965), the underlying physical principles are just inadequate to describe the complexity of ocean surface waves and as a result of this, the significant wave method fundamentally lacks the framework which is suitable for progress and self-improvement.

2.2.2 Prognostic Parametric Windsea Models

The fundamental justification for a parametric representation of the windsea resides in the conclusions of the JONSWAP experiment. If one accepts the fact that the evolution of a wind-driven wave field is dominated by the nonlinear energy transfer, then there appears to be little reason to describe the spectrum and the source terms in any greater detail than the nonlinear transfer itself. A rigorous numerical calculation of the nonlinear transfer is computationally

still infeasible in the context of a modern wave prediction model. Not only the need to parameterize the nonlinear transfer predicated the parametric wave model, but also the shape stabilizing feature of these wave-wave interactions which ultimately leads to a quasi-equilibrium form. In accordance with this reasoning, Hasselmann et al. (1976) proposed that the growth of the windsea spectrum can adequately be described by a limited set of coupled transport equations for a small number of spectral parameters. The formulation of the parametric model is delineated by transforming the whole energy transport equation inclusive source functions into a set of prognostic equations in the parameters of the self-similar spectral form. The general procedure is shown for all JONSWAP parameters in Hasselmann et al. (1973). For a prescribed directional distribution and spectral shape, Hasselmann et al. (1976) argues that two parameters suffice to define the energy level and the frequency scale of the one-dimensional energy spectrum. The derived parametric transport equations for the parameter pair $\nu = fmU/g$ and α are:

$$\frac{1}{\nu}\left(\frac{\partial \nu}{\partial \tau} + P_{\nu\nu}\frac{\partial \nu}{\partial \eta}\right) + P_{\nu\alpha}\frac{1}{\alpha}\frac{\partial \alpha}{\partial \eta} = -N_\nu \alpha^2 \nu + \frac{1}{U}\left(\frac{\partial U}{\partial \tau} + \frac{\partial U}{\partial \eta}\right) \qquad (2.2.6)$$

$$\frac{1}{\alpha}\left(\frac{\partial \alpha}{\partial \tau} + P_{\alpha\alpha}\frac{\partial \alpha}{\partial \eta}\right) + P_{\alpha\nu}\frac{1}{\nu}\frac{\partial \nu}{\partial \eta} = I^{7/3} - N_\alpha \alpha^2 \nu + \frac{0.2}{U}\left(\frac{\partial U}{\partial \eta}\right) \qquad (2.2.7)$$

where

$$\begin{bmatrix} P_{\nu\nu} & P_{\nu\alpha} \\ P_{\alpha\nu} & P_{\alpha\alpha} \end{bmatrix} = \begin{bmatrix} 1.0 & -0.07 \\ 0.2 & 0.47 \end{bmatrix}; \quad N_\nu = 0.54,\ N_\alpha = 5,\ I = 5.1 \times 10^{-3}$$

and $\partial/\partial\tau \equiv (U/g)\partial/\partial t$, $\partial/\partial\eta \equiv (U/g)\underline{V}_m \cdot \nabla$, with $\underline{V}_m$ parallel to the wind direction, $|\underline{V}_m| = qg/(4\pi fm)$, $q = 0.85$. The nondimensional gradient, $\partial/\partial\eta$, corresponds to the rate of advection of wave properties

with the group velocity $\underline{V}_m$, where $\underline{V}_m$ is determined from waves around the spectral peak. The factor q arises from averaging over the directional distribution of the spectrum. The angular spreading function was taken as a frequency independent cosine-square law.

Special analytical solutions can be obtained for (2.2.6) and (2.2.7) for simply prescribed wind fields depending on fetch or duration according to the power laws

$$U = U_o(gx/U_o^2)^m \qquad (2.2.8)$$

$$U = U_o(gt/U_o)^n \qquad (2.2.9)$$

with U_o = constant and m,n are exponents. The complete solution of equations (2.2.6) and (2.2.7) requires numerical integration by finite difference techniques. The windsea spectrum is easily recovered from ν and α together with the mean JONSWAP values for the remaining parameters γ, σ_a, σ_b (cf. section 3.1.1). A further simplification is suggested by Hasselmann et al. (1976) by assuming a quasi-equilibrium relation between α and ν, which results in only one prognostic equation in ν.

If the quasi-equilibrium concept of the one and two parameter model applies, then it seems that this model approach should be sufficient to predict the sea state. According to Hasselmann (1978) the validity of the parametric windsea approach should generally hold for large-scale wind regions and for typical synoptic depressions such as mid-lattitude cyclonic disturbances. For small-scale wind systems, e.g., hurricanes, or nearly fully-developed seas the quasi-equilibrium

concept breaks down and thus one must resort to a multi-parameter model.

A similar wave prediction model was proposed by Toba (1978) who considered a single-parameter growth equation for the windsea based on similarity principles of growing wind waves. Toba (1978) chooses the single parameter E, the wave energy per unit area, to characterize the sea state, which in turn is related to the significant wave height by $E = H_s^2/16$. His parametric model is formulated as

$$\frac{\partial}{\partial t_*} E_*^{2/3} + \frac{E_*^{1/3}}{a} \frac{\partial}{\partial x_*} E_*^{2/3} = A\,[1 - \mathrm{erf}(bE_*^{1/3})] \qquad (2.2.10)$$

in which $E_* = g^2E/u_*^4$, $x_* = gx/u_*^2$, $t_* = gt/u_*$, where x is the fetch, t is time and u_* is the friction velocity. The error function erf is defined by

$$\mathrm{erf}(x) = \frac{2}{\sqrt{\pi}} \int_0^x \exp(-\xi^2)\,d\xi \qquad (2.2.11)$$

and the dimensionless empirical constants have the following values: $A = 2.4 \times 10^{-4}$, $a = 0.74$, and $b = 0.12$.

The odd two-thirds exponent in his model equation (2.2.10) can be deduced from the conspicuous similarity relation between nondimensional wave height and nondimensional period for significant waves.

$$H_* = BT_*^{3/2} \qquad (2.2.12)$$

where $H_* = gH/u_*^2$, $T_* = gT/u_*$ and for significant waves $B = 0.062$ is a nondimensional constant. Equation (2.2.10) then

states that the growth of nondimensional energy of a windsea can be regarded as a simple stochastic process in which the single parameter representing it, approaches its final value independent of its past history, but dependent on its present state, as long as the wind continues to blow. This method has been applied and tested for cases of different time and space scales (Kawai et al., 1979).

Generally, higher order corrections can be systematically incorporated in such models by introducing additional spectral parameters. Obviously, in the limit of a large number of parameters, the same degree of detail as in traditional discrete spectral models is ultimately recovered. Nevertheless, most parametric windsea models typically contain only few parameters ranging from one to normally six. The philosophy of a parametric windsea description is simply to reduce the large number of wave groups of different frequencies and directions found in standard discrete spectral models. However, there are shortcomings with the parametric approach for wave prediction. It is clear that the parametric concept of the wave field is not appropriate to describe spectral modes in the swell domain, because the nonlinear coupling among swell components or swell and windsea components is very weak. Thus, sea states dominated by a swell field or sea states engaged in exchanging energy between the swell and windsea domains cannot be simulated by a parametric windsea model. For such cases, a hybrid model is required, which combines the parametric windsea model and a ray-decoupled discrete swell model. This type of model is discussed next. Other situations also exist where simple one parameter models are expected to fail. In such models, the assumption is made that the nonlinear interactions always act fast enough to turn

the wave field into the direction of the local wind, which is valid as long as the changes associated with the wind field occur on space-time scales much smaller than those of the nonlinear interactions. This is clearly violated for rapidly varying wind fields as in fronts and hurricanes. However, this limitation can be removed by including a directional relaxation parameter governing the rate at which the wave field is turned into the direction of the wind.

Another parametric windsea model worthy of mention, because it is unique regarding its simplicity as well as its specific purpose of usage. On the basis of the parameterization technique outlined in Hasselmann et al. (1976), Ross (1976) developed a simple parametric wave model specifically for estimating the wave field in hurricanes. From a regression analysis involving the JONSWAP variables, ν, α, γ and ε, Ross determined their dependence on the dimensionless radial fetch $R = gr/U^2$, where r is the radial distance to the eye of the hurricane. The data sets of hurricanes Ava, Camille and Eloise produced the following power laws:

$$\begin{aligned} \nu &= 0.97\, R^{-0.21} \\ \alpha &= 0.034\, R^{-0.17} \\ \gamma &= 4.7\, R^{-0.13} \\ \varepsilon &= 2.25 \times 10^{-5}\, R^{0.45} \end{aligned} \qquad (2.2.13)$$

where $\nu = fmU/g$ and $\varepsilon = g^2\tilde{E}/U^4$ with $\tilde{E}$ the total energy.

An opportunity to test the model presented itself during hurricanes Belle, 1976 in the Atlantic and Anita, 1977 in the Gulf of Mexico. When compared with buoy observations the model was found to

give quite accurate specifications of the deep water wave field in tropical cyclones. Furthermore, Ross and Cardone (1978) systematically elucidated the differences in the results obtained from the simple parametric model and the complete discrete spectral model of Cardone et al. (1976). In general, it was concluded that Ross' model for predicting extreme wave states is warranted when no detailed information on the directional characteristics of the wave spectrum is required.

2.2.3 Hybrid Models

Parametric windsea models as outlined in the previous section are only appropriate for a growing windsea. During the stages of active growth, the nonlinear wave-wave interactions are the dominant processes controlling the evolution of the spectral shape. As the spectrum approaches that of a fully developed sea, the nonlinear transfer becomes weak and the advective terms prevail in the energy balance. Swell can be regarded as the dynamical complement to a developing windsea, since, according to linear wave theory, all wave components are decoupled and are primarily controlled by advection with some possible weak damping. The propagation of discrete swell packets is best represented by the method of characteristics where each swell component is tracked independently along ray paths with its associated group velocity.

To predict both sea states, parametric windsea models are therefore combined with a discrete spectral swell model into a hybrid model. As a result of the NORSWAM (North Sea Wave Model) study, two

hybrid parametric wave models were developed in collaborating efforts by Günther et al. (1978) and Weare and Worthington (1978). Both models include dynamical exchange criteria that controls the energy tansfer from to windsea to swell and back. Transition from one wave regime to another is simply treated as an instantaneous energy exchange between the windsea and swell domains. The resulting loss or gain of energy is instantaneously redistributed in the modified windsea spectrum. Either energy interchange between the two wave regimes conserves total energy. The swell model is based on a technique first introduced by Barnett et al. (1969). The NORSWAM model has been extensively applied to hindcast long-term wave-height statistics in the northern North Sea (Ewing et al., 1979). The HYPA (Hybrid-Parametric) model has been systematically tested in many situations of different scales involving the geometry of the prediction area and spatially and temporally varying wind fields (Günther et al, 1978; Günther and Rosenthal, 1979). A practical application of HYPA model is reported in Richter et al. (1982) where hindcasted wave conditions were used to reconstruct the sea states during the ship disasters involving the German container ship "München" north of the Azores and the tragic event of the 1979 Fastnet Race. From this analysis it was concluded that the "München" must have encountered maximum significant wave heights of 11 m, with peak periods of 14.3 seconds which correspond to a wave length of 320 m. These values are in close agreement with wave heights reported by ships in the same area. An earlier version of the HYPA model has been also applied to an extratropical storm in the Gulf of Alaska (Graber, 1979). The overall agreement of hindcast wave heights with buoy measurements were quite good.

A significant shortcoming of earlier HYPA versions was its limitations in directional resolution, because by assumption the waves were tied to the local wind direction with a fixed angular distribution. Thus wave directions could only be treated implicitly, since the response time of the spectral shape parameters was on scales too slow when compared to those of the directional waves. The introduction of a directional parameter θ_o by Günther et al. (1981) eliminated this restriction. Inclusion of a prognostic equation for this parameter improved the HYPA model's ability to transfer continuously portions of windsea energy to swell. Usually, for turning winds, the energy for windsea components traveling at large angles to the new wind direction is radiated into swell. The Toba model only allows a loss of energy to swell, when the wind direction changes more than 30° within a time step. This restriction results in a considerably reduced trasfer of windsea energy to swell for turning winds.

Additional descriptions of other hybrid models can be found in the SWAMP (1982) study. Results from idealized test situations are intercompared with other hybrid and spectral wave models. From the above description of hybrid parametric models it should be recognized that in modeling swell by a discrete spectral approach, these parametric models tend to look more like a coupled discrete spectral model.

2.3 Finite Depth Wave Models

When waves propagate into regions, where they feel the presence of the bottom topography, additional effects on the energy balance must be considered due to wave-bottom interactions. The fundamental equation governing the evolution of the wave field in shallow water is

$$\frac{\partial E}{\partial t} + \dot{\underline{x}} \cdot \underline{\nabla}_x E + \dot{\underline{k}} \cdot \underline{\nabla}_k E = S \qquad (2.3.1)$$

in which S represents the net contribution of energy gained or lost by atmoshperic wind input, nonlinear wave-wave interactions, dissipation due to wave breaking and bottom friction. In addition to bottom friction, other dissipation mechanisms such as percolation, soft bottom motions and bottom scattering could be important. However, these processes seem to be primarily site specific and often of local importance, whereas bottom friction is generally the dominant damping mechanism for waves propagating in coastal waters. Bottom friction and sediment transport are intimately related to each other, which means to specify either, knowledge of the other is required. The third term on the left-hand side of (2.3.1) describes the effect of refraction and shoaling on the wave spectrum. Local bottom inhomogeneities such as shoals or canyons are generally not resolved on the scales used by standard wave prediction models. The validity of physical wave models is also limited to not too shallow water, in particular the nearshore zone, where the involved processes are highly nonlinear.

However, early versions of shallow water wave models based on the energy transport equation have been successfully applied to numerous cases where water depths are shallow enough such that deep water approximations are clearly violated. The extension of a standard discrete spectral model is conceptually easy, because the major modification comes about in the use of curved rather than straight ray characteristics. The first applications of a modified deep water model was the Barnett model for hindcasting wave conditions in the South China Sea (Barnett et al., 1969). The wave climate in the North Sea, where depths are less than 30 m especially in the southern part, can not realistically be predicted by deep water forecasting methods. Golding (1978) convincingly demonstrated the sensitivity of the wave field to the presence or absence of bottom topography in the North Sea. In his model the effect of bottom friction was not yet included, thus leading to excessively high wave predictions.

Coastal erosion and sedimentation is a critical problem to the coastline around Venice in the Adriatic Sea and is directly related to the prevailing wave conditions in this area. For a number of selected points in the northern Adriatic Sea, Cavaleri and Malanotte-Rizzoli (1978) hindcasted wave spectra by employing a reverse ray projection technique as proposed by Collins (1972). A similar effort has been reported by Forristall et al. (1978) where a modified PTB model was used to hindcast directional wave spectra generated by a tropical storm in the Gulf of Mexico.

All these models belong to the ray-decoupled class, which means that generally the influence of nonlinear interactions is not incorporated. Herterich and Hasselmann (1980) have shown that resonant

nonlinear wave-wave interactions are greatly amplified in finite depth. Inclusion of this mechanism is only viable in a coupled model as those described in SWAMP (1982). The description of a coupled hybrid parametric wave model for waters of arbitrary depth is described in the following sections.

CHAPTER 3

THEORETICAL BACKGROUND

Grau, mein teurer Freund, ist alle Theorie
Und grün des Lebens goldner Baum.

Gray, my dear friend, is every theory,
And green the golden tree of life.

(Mephistopheles)

--FAUST I, Studierzimmer
Johann Wolfgang von Goethe

Waves appearing on the ocean surface can be described in many different ways. If one is interested in the large-scale features of oceanic waves, as they are generated and propagated over vast ocean surfaces, it usually suffices to consider only their principal characteristics. These vary slowly enough in space and time so that even at large distances away from their generation region they still can be detected. However, on a scale associated with local wind-generated waves, a more detailed description of the wave field is desirable. On these small scales, the main wave characteristics can be regarded constant, but the sea surface configuration is highly irregular both in a spatial and temporal sense. The forces and mechanisms responsible for the generation and evolution of waves include the turbulent wind and the interaction of the waves themselves, which are by far too complicated to be accounted for in detail. This implies that an exact prediction of the sea surface is virtually impossible. Early theories have relied on the superposition of many individual waves, but a typical ocean wave record hardly resembles the shape of a single sinusoidal wave.

In order to overcome this apparent disorder an integral representation of the sea surface can be used. This representation

would provide a more prolific approach for a general description of the ocean wave field. The fundamental part of such a formalism is to join theory and observations by means of a variable, which is capable of representing many aspects of the wave field and also can be determined directly from measurements. This variable is known as the wave energy spectrum and denotes the energy contents of the waves, as a function of frequency, wave number and direction. In particular, the wave number and frequency spectra reflect the spatial and temporal dependencies of the wave field.

Since the spectral description of events or a process is well-known in the theory of probability, many of its assumptions and methodologies find analogous counterparts in the statistical description of wave fields. Using standard spectral analysis techniques, various types of energy spectra can be constructed from observed wave records. The two most common forms are the two- and one-dimensional energy spectrum. In the past and the present, the most important and most utilized spectrum is the frequency wave spectrum. Extensive studies of this spectrum have been conducted under many diverse conditions, ranging from controlled laboratory experiments to the complex nature of hurricanes. These experiments were primarily carried out in deep water. However, recently some field experiments specifically dealt with measuring wave spectra in finite water depths, where the influence of the sea bottom on the surface wave field can no longer be neglected. Similarly, few studies are available describing the directional aspect of the waves. Possible reasons for the lack of directional data are the need for sophisticated measuring devices and

the fact that engineers and scientists only recently began to request more directional wave information for design purposes.

In this chapter, we are primarily concerned with the mathematical description of the wave energy spectrum, both in deep and shallow water, and how it evolves in space and time due to physical processes.

3.1 The Spectral Description Of A Windsea

The waves found on the ocean surface are almost always random in appearance due to the irregular variation of the surface, itself, in both space and time. An adequate representation of this motion is usually accomplished by means of a statistical description of observable and/or measurable quantities. The one most commonly used in the description of ocean waves is the surface elevation $\eta(\underline{x},t)$ as a function of the location $\underline{x}$ and time t. If we assume that a wave record $\eta(\underline{x},t)$ is the realization of some stochastic process, then it follows that the covariance of the surface elevation is given by

$$C(\underline{r},\tau) = \overline{\eta(\underline{x},t)\,\eta(\underline{x}+\underline{r},\, t+\tau)} \qquad (3.1.1)$$

where the overbar denotes averaging with respect to space and time, $\underline{r}$ is a displacement vector and τ is a time lag. However, the study of ocean waves is more conveniently performed in terms of the spectrum, which is defined as the Fourier transform of the covariance function

$$\psi(\underline{k},\omega) = (2\pi)^{-3} \iiint_{-\infty}^{\infty} C(\underline{r},t) e^{-i(\underline{k}\cdot\underline{r}-\omega\tau)} d\underline{r}\, d\tau \,. \qquad (3.1.2)$$

Here ψ is the three-dimensional variance density spectrum, $\underline{k}$ is the wave number vector and ω is the radian frequency.

From this general description, we can look at some specific cases, which are more practical but also more restrictive in the information they provide. For a homogeneous wave field, which is invariant by adding a constant, horizontal space-vector, the instantaneous wave

number variance spectrum of the free surface elevation is

$$F(\underline{k}) = (2\pi)^{-2} \int\int_{-\infty}^{\infty} \overline{\eta(\underline{x},\tau)\, \eta(\underline{x}+\underline{r},\tau)}\, e^{-i\underline{k}\cdot\underline{r}}\, d\underline{r} \ . \qquad (3.1.3)$$

Similarly, for a stationary wave field, which is invariant to the addition of a time constant, the frequency variance spectrum at a fixed point is

$$E(\omega) = (2\pi)^{-1} \int_{-\infty}^{\infty} \overline{\eta(\underline{x},t)\, \eta(\underline{x},t+\tau)}\, e^{i\omega\tau}\, d\tau \ . \qquad (3.1.4)$$

The total variance or energy of the waves is equal to the following integral expressions,

$$\overline{\eta^2} = \int\int_{-\infty}^{\infty} F(\underline{k})\, d\underline{k} = \int_0^{\infty} E(\omega)\, d\omega \ . \qquad (3.1.5)$$

Strictly speaking, the variance is related to energy by the factor [ρg], where ρ is the density of water and g is the acceleration of gravity. Since for oceanographical conditions this term ρg is constant, it has become common practice to drop it and simply refer to (3.1.3) - (3.1.5) as energy quantities.

If, in addition, we assume that $\eta(\underline{x},t)$ can be regarded in a linear approximation as a Gaussian random process (Hasselmann, 1967), then the wave field is completely specified, in a statistical sense, by the spectrum $F(\underline{k})$.

Now, let a turbulent wind commence to blow over an initially tranquil ocean surface. Small wavelets appear and continue to grow if

the mean speed and direction of the wind is maintained for a period of time. If the wind action continues for a sufficiently long time and large fetch, the waves grow until they are saturated with energy. At this time, according to Phillips (1958, 1977), the waves become locally unstable and break to dissipate the excess energy. In the deep ocean, this physical limit is reached when the local downward acceleration of the fluid particles near the wave crest is equal to or exceeds the gravitational acceleration, g. Phillips further hypothesizes that there exists an "equilibrium range" in the spectrum of wind-generated waves which is entirely determined by the physical parameters governing the continuity of the wave surface. If true, the physical quantities to be considered are the densities, ρ_a and ρ_w, of air and water, respectively; the surface tension and viscosity of water, σ_w and ν_w; the gravitational acceleration, g; the friction velocity, u*; the surface roughness length, z_o, and the wave number, k, or the frequency, ω. If one were to limit the analysis to wave numbers and frequencies well below those of capillary waves, such that

$$k << \left[\frac{\rho_w g}{\sigma_w}\right]^{1/2} = k_u; \quad \omega << \left[\frac{4\rho_w g^3}{\sigma_w}\right] = \omega_u \qquad (3.1.6)$$

then the effect of surface tension can be ignored. Similarly, the influence of viscosity, as related to wave damping (Lamb, 1932, §348, §349), can also be omitted for the present condition. Furthermore, as long as we are not concerned with quantities containing the dimensions of mass, then ρ_a and ρ_w could only appear as the ratio ρ_a/ρ_w. Under oceanographic conditions with an air-water interface, this ratio

is virtually a constant and therefore, need not to be taken into consideration. The roughness length parameter, z_o, shows some evidence that it depends on the friction velocity, $u*$, as suggested by Ellison (1956). An up-to-date review of the relation between the friction velocity and the roughness length is given in Garratt (1977). If this is true, then Phillips concludes that the equilibrium range properties of the wave field are accurately characterized by the parameters $u*$ and g, together with k or ω, provided the later satisfy the conditions (3.1.6).

From the functional form of the surface displacement spectrum, we conclude that the wave number spectrum (3.1.3) has dimension $[L^4]$ and the frequency spectrum (3.1.4) has dimensions $[L^2T]$. Applying dimensional analysis arguments, Phillips obtained the following expressions;

$$F(\underline{k}) = k^{-4}\, \xi_1(\theta, \frac{ku_*^2}{g}) \qquad \text{for } (k_\ell << k << k_u) \qquad (3.1.7)$$

and

$$E(\omega) = g^2\omega^{-5}\, \xi_2(\frac{\omega u_*}{g}) \qquad \text{for } (\omega_\ell << \omega << \omega_u) \qquad (3.1.8)$$

where ξ_1 and ξ_2 are two undetermined functions of the dimensionless wave number and frequency, respectively, and θ is the direction of the wave number vector $\underline{k}$. The limits k_ℓ and ω_ℓ represent the smallest wave number and frequency of the wave field below which nonlinear effects become important even for waves of relatively small height.

From (3.1.7) it follows that the moduli wave number spectrum, describing the energy distribution over k regardless of the direction of propagation, is designated by the integral

$$F(k) = \int_{-\pi}^{\pi} F(\underline{k})k\,d\theta = k^{-3}\xi_3\left(\frac{ku_*^2}{g}\right)\int_{-\pi}^{\pi} \Omega(\theta)\,d\theta \qquad (3.1.9)$$

where $\Omega(\theta)$ is an angular spreading factor and satisfies the normalization condition

$$\int_{-\pi}^{\pi} \Omega(\theta)\, d\theta = 1 \qquad (3.1.10)$$

If the surface drift is of no importance to the breaking process, i.e. breaking of essentially irrotational waves, Wu (1975) found from surface drift measurements that $\omega u_*/g \ll 2$ must be strongly satisfied. This implies that the spectrum is given by the breaking process under the influence of gravity only. Then (3.1.8) and (3.1.9) can be simplified

$$E(\omega) = \alpha g^2 \omega^{-5} \qquad \text{for } \left(\omega_\ell \ll \omega \ll \frac{2g}{u_*}\right) \qquad (3.1.11)$$

$$F(k) = \beta k^{-3} \qquad \text{for } \left(k_\ell \ll k \ll \frac{2g}{u_*^2}\right) \qquad (3.1.12)$$

where α and β are two non-dimensional constants, which must be determined from measurements. From the asymptotic behavior of (3.1.11) and (3.1.12), and making use of the dispersion relation $\omega^2 = gk$; it turns out that the following relation holds

$$\alpha = 2\beta \quad . \qquad (3.1.13)$$

Measurements of ocean waves basically confirm the -5 power law (Figure 3.1) of the high-frequency portion of the spectrum in deep

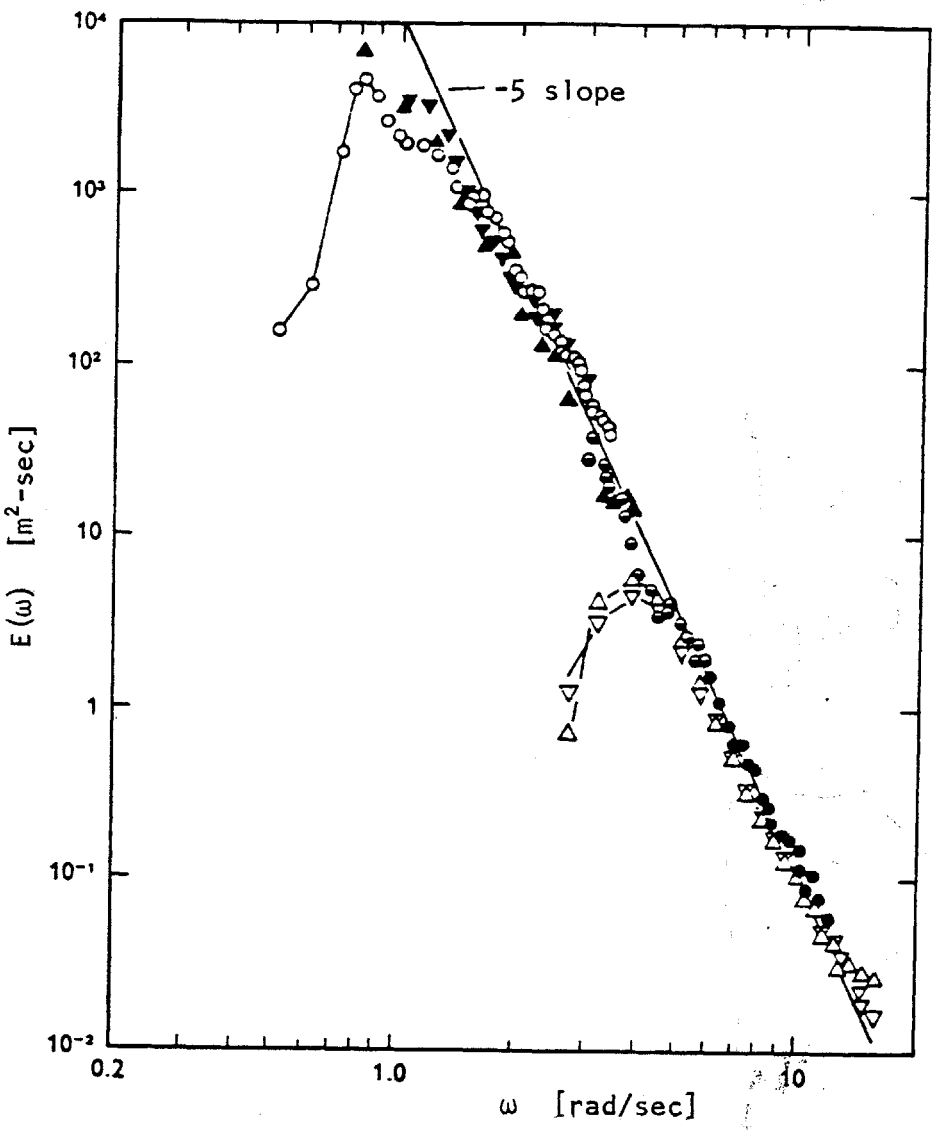


Fig. 3.1 The equilibrium range of the frequency spectrum of wind-generated surface waves in deep water. (From Phillips, 1977).

water. However, the observed values of the equilibrium range constant α (also known as Phillips' constant) exhibit some scatter in the range $(0.65 - 1.6) \times 10^{-2}$. A summary of α values as determined from various data sets can be found in Kahma (1981) and Graber (1979). Longuet-Higgins (1969) calculated a semi-theoretical estimate of Phillips' constant for a spectrum of the form (3.1.11) and obtained a value of 1.35×10^{-2}.

In recent years much attention has been focused on Phillips' -5 power law. Kitaigorodskii (1962) first suggested that certain high-frequency ranges are best fit to a -4 slope. A possible source of the discrepancy in the saturation range slope could be attributed to Doppler-shifted frequencies in the presence of currents. Kahma (1981) has shown that the Doppler shift could only account for a relatively small correction to the power law in the equilibrium range. Forristall (1981) analyzed hurricane data which supported both the hypothesis of an inverse fifth power law at higher frequencies, as well as an inverse fourth power law with a dependence on the friction velocity for lower frequencies of the saturation range. In a similar analysis of wave spectra during hurricane Camille, Stacy (1974) also found a departure from the classical f^{-5} relation.

Theoretical support came from Kitaigorodskii (1983), who demonstrated that an exact analog of Kolmogoroff's spectrum for weakly nonlinear ocean waves yields a spectral form proportional to ω^{-4} in the equilibrium range. His arguments are primarily based on a generalization of the wave-breaking limited equilibrium range concept, whereby the shorter waves in this range may not grow due to the direct energy transfer from the wind, but rather due to energy fluxes from the

lower wave numbers. From this Kitaigorodskii conjectured that the equilibrium range of wind-generated waves really has two asymptotic regions: Kolmogoroff's and Phillips' type. The former type of equilibrium corresponds to a wind-dependent saturation which has the frequency spectral form

$$E_K(\omega) = \alpha_u g U_a \omega^{-4} \tag{3.1.14}$$

where U_a is the mean wind speed at a reference height and α_u represents a non-dimensional constant analogous to Phillips' constant. The theoretically determined value of $\alpha_u = 4.4 \times 10^{-3}$ is almost equal to the observed value $\alpha_u = 4.5 \times 10^{-3}$ reported by Kahma (1981) and the calculated average $\alpha_u = 4.5 \times 10^{-3}$ reported by Forristall (1981). Donelan et al. (1982) proposed an asymptotic form for wind-generated high-frequency spectra:

$$E_D(\omega) = \alpha_m g^2 \omega^{-4} \omega_m^{-1} \tag{3.1.15}$$

where the dimensionless coefficient α_m varies implicitly as a function of dimensionless fetch and ω_m corresponds to the frequency of the peak. The empirical formula for α_m as suggested by Donelan et al. (1982) is approximately

$$\alpha_m = 0.006 \left(\frac{U_a}{c_m}\right)^{1/2} \tag{3.1.16}$$

where $c_m = g/\omega_m$ corresponds to the linear deep water phase velocity of the spectral peak. Upon equating (3.1.14) and (3.1.15), it follows that

$$\alpha_u = 6 \times 10^{-3} \left(\frac{U_a}{c_m}\right)^{-1/2} \quad . \tag{3.1.17}$$

For a range of $U_a/c_m \approx 1 - 5$, an average value of $\alpha_u \approx 4.3 \times 10^{-3}$ can be calculated.

Although recent field observations of the saturation range in ocean wave spectra point towards a negative fourth power law with a linear dependence on wind speed, Kitaigorodskii (1983) concludes that a relatively rapid transition from the Kolmogoroff to the Phillips equilibrium takes place, as can be interpreted from experimental data, but additional investigation is needed to make an accurate quantitative description. However, an asymptotic spectral form of this type may have some consequential impact on wave prediction models and deserves further attention.

Since the frequency spectrum can be related to the wave number spectrum, the question arises, why not measure F(k) instead? To date very few data sets exist. This is partially due to the complicated methodology required to obtain measurements. The wave number spectrum is best suited for remote sensing techniques such as airborne laser (Schule, et al., 1971), radar altimeter (Barnett and Wilkerson, 1967) and synthetic aperture radar (SAR). An example of a wave number spectrum is shown in Figure 3.2. The equilibrium constant β for this data set was estimated at 4.2×10^{-3}, which approximately confirms the relation given in (3.1.13). However, since there is little information about the directional distribution $\Omega(\theta)$ of the wave field, it can be shown that for the case of unidirectional waves [i.e., $\Omega(\theta) \propto \delta(\theta)$], $\beta = B$ where B is the actual saturation constant. For a

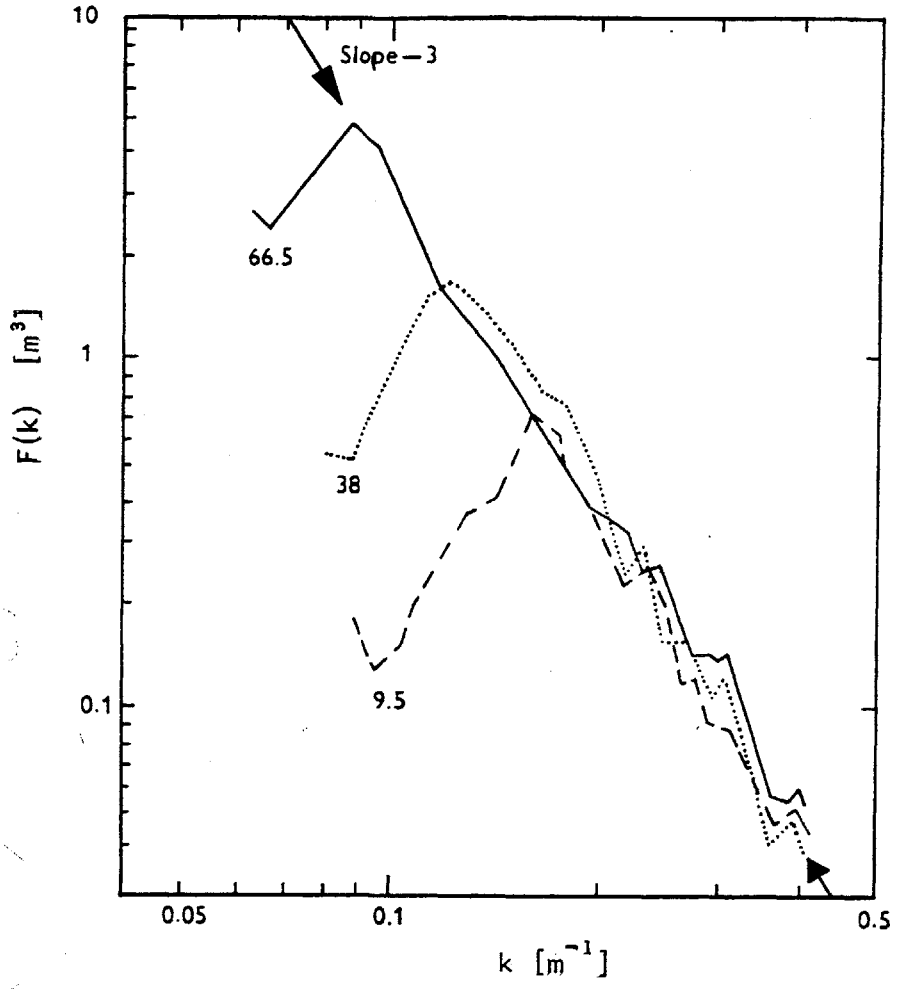


Fig. 3.2 The equilibrium range of one-dimensional wave number spectra of fetch-limited surface gravity waves. Numbers refer to fetches in nautical miles. (From Schule et al. 1971).

uniformly distributed wave field [i.e., $\Omega(\theta)$ = constant for $-\pi/2 < \theta < \pi/2$ and zero outside this range], then $\beta = 1/2\ B$, while if $\Omega(\theta) = \cos^2\theta$, then $\beta = 3/4\ B$.

Kitaigorodskii (1962) applied the similarity theory of atmospheric turbulence to the problem of wind-generated wave motion. In addition to the external parameters considered by Phillips' dimensional analysis, Kitaigorodskii also investigated the dependence of the wave spectrum on the fetch and duration of the wind action. Shortly after the wind begins to blow, the sea is partitioned into two regions. In the leeward region, the wave field is independent of time and depends only on the distance (fetch) to the shore. The waves in this region are steady and referred to as fetch-limited. In the upwind region with essentially unlimited fetch, the wave motion is transient or duration-limited. Waves in this domain are called unsteady. A steady-state wave motion is established at the boundary between the two domains. Ultimately, when the wind has blown over a sufficiently long fetch and after a sufficiently long duration, the waves cease to grow. This limiting form is designated as a fully developed sea, whose average properties are only a function of wind speed. Although this seems to be the simplest kind of waves in the ocean, it is difficult to observe. Under these assumptions, Kitaigorodskii proposed that

$$E(\omega) = S(\omega, u_*, g, x) \qquad (3.1.18)$$

where x is the fetch. The single parameter x is valid as long as the waves are fetch-limited and the boundary conditions and wind field are stationary and homogeneous along the direction perpendicular to x.

Then, from the similarity theory, the following expression may be obtained

$$E(\omega) = g^2\omega^{-5} S_1\left(\frac{u_*\omega}{g}, \frac{gx}{u_*^2}\right) \tag{3.1.19}$$

where S_1 is a universal non-dimensional function of two parameters, the dimensionless frequency $\tilde{\omega}$ and the dimensionless fetch $\tilde{x}$. From (3.1.19), one can conclude that the dimensionless frequencies $\tilde{\omega}$, corresponding to specific points of $E(\omega)$, depend only on $\tilde{x}$. In particular, when $E(\omega)$ has a maximum at some frequency ω_{max}, then,

$$\frac{\omega_{max} u_*}{g} = S_2\left(\frac{gx}{u_*^2}\right) \tag{3.1.20}$$

Similarly, other non-dimensional parameters involving the significant wave height H_s and the significant wave period T_s defined as m_o/m_1 (cf. 3.1.69), can be expressed as a function of dimensionless fetch:

$$\tilde{H}_s = \frac{H_s g}{u_*^2} = S_3\left(\frac{gx}{u_*^2}\right) \tag{3.1.21}$$

$$\tilde{T}_s = \frac{T_s g}{u_*} = S_4\left(\frac{gx}{u_*^2}\right) \tag{3.1.22}$$

In the limit, where the fetch dependence vanishes, for a fully developed wave field, it follows from (3.1.19) - (3.1.22) that

$$E(\omega) = g^2\omega^{-5} S_5\left(\frac{u_*\omega}{g}\right) \tag{3.1.23}$$

$$\frac{\omega_{max} u_*}{g} = C_1 \tag{3.1.24}$$

$$\tilde{H}_s = \frac{H_s g}{u_*^2} = C_2 \tag{3.1.25}$$

$$\tilde{T}_s = \frac{T_s g}{u_*} = C_3 \tag{3.1.26}$$

where C_1, C_2 and C_3 are constants.

Pierson and Moskowitz (1964) applied Kitaigorodskii's similarity theory to data of fully developed wind seas. Based on a best fit to the observed spectral data the following form of the spectrum was suggested

$$E(\omega) = \alpha g^2 \omega^{-5} e^{-A(\omega_o/\omega)^4} \tag{3.1.27}$$

The exponential term in (3.1.27) acts as a high-pass filter on the asymptotic high-frequency form and $\omega_o = g/U_{19.5}$, where $U_{19.5}$ is the wind speed at an anemometer height of 19.5 m, A = 0.74 and α = 0.0081. Using the Pierson-Moskowitz spectrum (hereafter called PM spectrum) to determine the constants C_1, C_2 and C_3, one finds (in metric units)

$$\omega_{max} = 8 \cdot U^{-1} \tag{3.1.28}$$

$$H_s^{PM} = 0.025\ U^2 \tag{3.1.29}$$

$$T_s^{PM} = 0.57\ U \tag{3.1.30}$$

where the wind speed at 10 m is substituted from the relation $U_{10} = 0.93 \cdot U_{19.5}$ (Pierson, 1964, 1977).

An alternative approach to the saturation range in the frequency spectrum was presented by Thornton (1977), who rederived Phillips' results from the kinematics of the wave motion. Thornton argues that wave breaking occurs as a result of kinematic instability, when fluid particles near the free surface attain speeds greater than the wave speed c. Hence, the relevant parameter at breaking should be the wave speed rather than the acceleration of gravity, as originally proposed by Phillips. Melville (personal communication) supports this hypothesis based on experimental evidence found in breaking waves. Thus, dimensional reasoning yields

$$E(\omega) = \alpha c^2 \omega^{-3} \tag{3.1.31}$$

The wave speed can be found from linear wave theory to a first approximation,

$$c^2 = \frac{g}{k} \tanh kh \tag{3.1.32}$$

where k is the wave number and h is the water depth. The deep water limit

$$c^2 = \frac{g}{k} = \frac{g^2}{\omega^2} \tag{3.1.33}$$

which reproduces Phillips' result when substituted into (3.1.31),

$$E(\omega) = \alpha g^2 \omega^{-5} \tag{3.1.34}$$

According to Thornton, this is so because the dispersion relation and hence, the wave speed, is derived from the dynamic free surface

boundary condition.

Whether (3.1.11) and (3.1.12) only hold for deep water waves ($kh \gg 1$) or whether they can also be applied to the equilibrium range for a gravity wave spectrum in waters of finite depth, (i.e., for arbitrary values of kh) can not be conclusively drawn from Phillips' (1958) original derivation of these equations. Of greater significance is the fact as pointed out by Phillips (1958) that if a function has discontinuities in its first derivatives, then its Fourier transform has an asymptotic k^{-2} shape. Since the wave spectrum is essentially given by the average square of the Fourier transform, this implies that spatial equilibrium spectra must be proportional to k^{-4} for large k. From this, one can reason that the equilibrium shapes of wave number spectra of ocean waves at large k will be identical for both deep and shallow seas. On the other hand, the same is not true for the frequency spectrum $E(\omega)$, since in transforming ω and thus $E(\omega)$ by means of a dispersion relation, the frequency spectrum may, in addition, depend on h.

A consistent approach on the self-similarity of depth dependent frequency spectra was originally demonstrated by Kitaigorodskii, Krasitskii and Zaslavskii (1975), hereafter abbreviated as KKZ. Adopting the asymptotic shape of the wave number spectrum (3.1.12) to be valid in any water depth, the frequency and wave number spectrum are related as

$$E(\omega) = F(k) \frac{dk}{d\omega} \qquad (3.1.35)$$

where $d\omega/dk$ represents the group velocity.

In linear theory the dispersion relation, connecting the radian frequency ω with the wave number k, is

$$\omega(k,h) = (gk \tanh kh)^{1/2} \tag{3.1.36}$$

where h designates the water depth.

In the absence of any mean currents, the wave field is regarded isotropic and the group velocity can be determined from (3.1.36),

$$c_g = \frac{d\omega}{dk} = \frac{1}{2}\frac{\omega}{k}\left(1 + \frac{2kh}{\sinh 2kh}\right) \tag{3.1.37}$$

Introducing the wave number spectrum (3.1.12), and the group velocity c_g in (3.1.35) yields a general expression for the frequency spectrum, i.e.,

$$E(\omega) = \alpha g^2 \omega^{-5} \phi(\kappa) \tag{3.1.38}$$

where $\kappa = kh$ is a dimensionless wave number and $\phi(\kappa)$ is a universal dimensionless function. The functional form of $\phi(\kappa)$ is readily found to be

$$\phi(\kappa) = \frac{\tanh^2 \kappa}{\left(1 + \frac{2\kappa}{\sinh 2\kappa}\right)} \tag{3.1.39}$$

An equivalent expression of ϕ, but in terms of dimensionless frequency $\omega_h = \omega\sqrt{h/g}$ was given by KKZ,

$$\Phi(\omega_h) = \chi^{-2}(\omega_h)\left\{1 + \frac{2\omega_h^2 \chi(\omega_h)}{\sinh[2\omega_h^2 \chi(\omega_h)]}\right\}^{-1} \tag{3.1.40}$$

where $\chi(\omega_h)$ is the solution of the transcendental algebraic equation

$$\chi \cdot \tanh(\omega_h^2 \chi) = 1 \tag{3.1.41}$$

Figure 3.3 shows a plot of $\Phi(\omega_h)$. It is easily ascertained that in deep water

$$\lim_{\kappa \to \infty} \phi(\kappa) = \lim_{\omega_h \to \infty} \Phi(\omega_h) = 1 \tag{3.1.42}$$

and in shallow water,

$$\lim_{\kappa \to 0} \phi(\kappa) = \frac{(kh)^2}{2} = \lim_{\omega_h \to 0} \Phi(\omega_h) = \frac{\omega_h^2}{2} \tag{3.1.43}$$

It follows from (3.1.38) that the high-frequency part of the spectrum in shallow water leads to the similarity form

$$E(\omega) = \frac{\alpha}{2} gh\, \omega^{-3} \tag{3.1.44}$$

Using Thornton's (1977) hypothesis, we have for (3.1.32) in shallow water

$$c^2 = gh \tag{3.1.45}$$

which yields a finite depth equilibrium shape

$$E(\omega) = \alpha_T gh\, \omega^{-3} \tag{3.1.46}$$

in agreement with the result obtained by KKZ, except for the equilibrium range constant α_T.

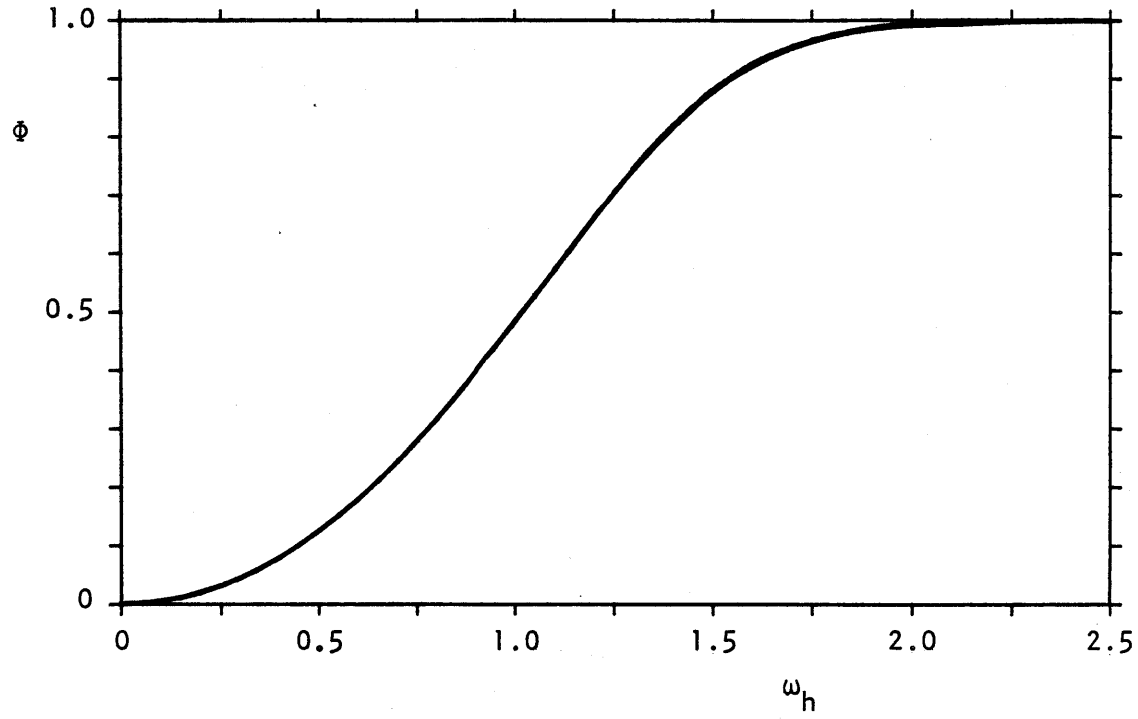


Fig. 3.3 The depth-dependent transformation factor $\Phi(\omega_h)$. (From Kitaigorodskii et al. 1975).

Thus comparing (3.1.44) with (3.1.46) shows that both spectral equilibrium ranges are equivalent if $\alpha_T = \alpha/2$. The discrepancy of a factor 2 results from the transformation formulae, which involve the group velocity for one and the phase speed for the other.

However, it should be noted that (3.1.44) is only valid for waves generated in areas where the bottom can be considered essentially horizontal. Other wave transformation mechanisms, such as refraction, may produce ambiguities in the deviation from the -5 power law. KKZ examined their similarity theory on empirical data by Dreyer (1973), which were collected in a region of shallow water where the depth did not vary over the whole extend of wave generation. They concluded that the transformation of the wave number spectrum into frequency spectrum, using the transfer function $\Phi(\omega_h)$, yields results which are in agreement with observations not only in deep water ($kh \gg 1$) but also in shallow water ($kh \ll 1$). Estimates of the Phillips constant $\alpha = 4 \times 10^{-3}$ are within the variability of values found by previous investigators.

Further evidence supporting this extension of Phillips' hypothesis to finite depth was given by Gadzhiyev and Krasitskiy (1978), who performed measurements in depths ranging from 40 m to 6 m to verify the theoretical relation of $\Phi(\omega_h)$. They obtained a mean value of $\alpha = 6 \times 10^{-3}$.

Data from Goda (1975) show that in shallow water some equilibrium ranges can be approximated by a -3 slope, whereas some spectra in very shallow water indicate slopes of less than -2. In a laboratory experiment, Ou (1980) demonstrated that waves generated in a wind-wave tank for finite depth conditions could satisfactorily be described by

the asymptotic form given in (3.1.44). Frequency spectra measured in Albermarle Sound by Knowles (1982) additionally uphold the validity of an ω^{-3} law for shallow seas.

3.1.1 The JONSWAP Spectrum And Related Wave Parameters

a) DEEP WATER

During the Joint North Sea Wave Project (JONSWAP), extensive measurements of growing sea states for deep water conditions were obtained along a profile extending 160 km into the North Sea westward from the island of Sylt. From the analysis of the fetch-limited wave spectra, Hasselmann et al. (1973) suggested a parametric form of the wave energy spectrum, which well describes the various stages of development occuring in windsea spectra. The one-dimensional form of the spectrum with its five free parameters for infinitely deep oceans is

$$E(f) = \alpha g^2 (2\pi)^{-4} f^{-5} \exp\{-\frac{5}{4}(\frac{f}{fm})^{-4} + \ell n\ \gamma\ \exp[-\frac{(f/fm-1)^2}{2\sigma^2}]\} \qquad (3.1.45)$$

The JONSWAP spectrum is illustrated in Figure 3.4 from which the five free parameters are defined as follows:

fm - the frequency at the peak of the spectrum;

α - the Phillips constant of the high-frequency tail of the spectrum, which asymptotically approaches a f^{-5} power law for large f/fm;

γ - the peak enhancement factor, or the ratio of the peak spectral energy to the maximum of the corresponding Pierson-Moskowitz spectrum with the same values of fm and α;

σ_a - the left-sided bandwidth of the spectral peak, i.e., $\sigma = \sigma_a$ for $f \leq fm$;

σ_b - the right-sided bandwidth of the spectral peak, i.e., $\sigma = \sigma_b$ for $f > fm$.

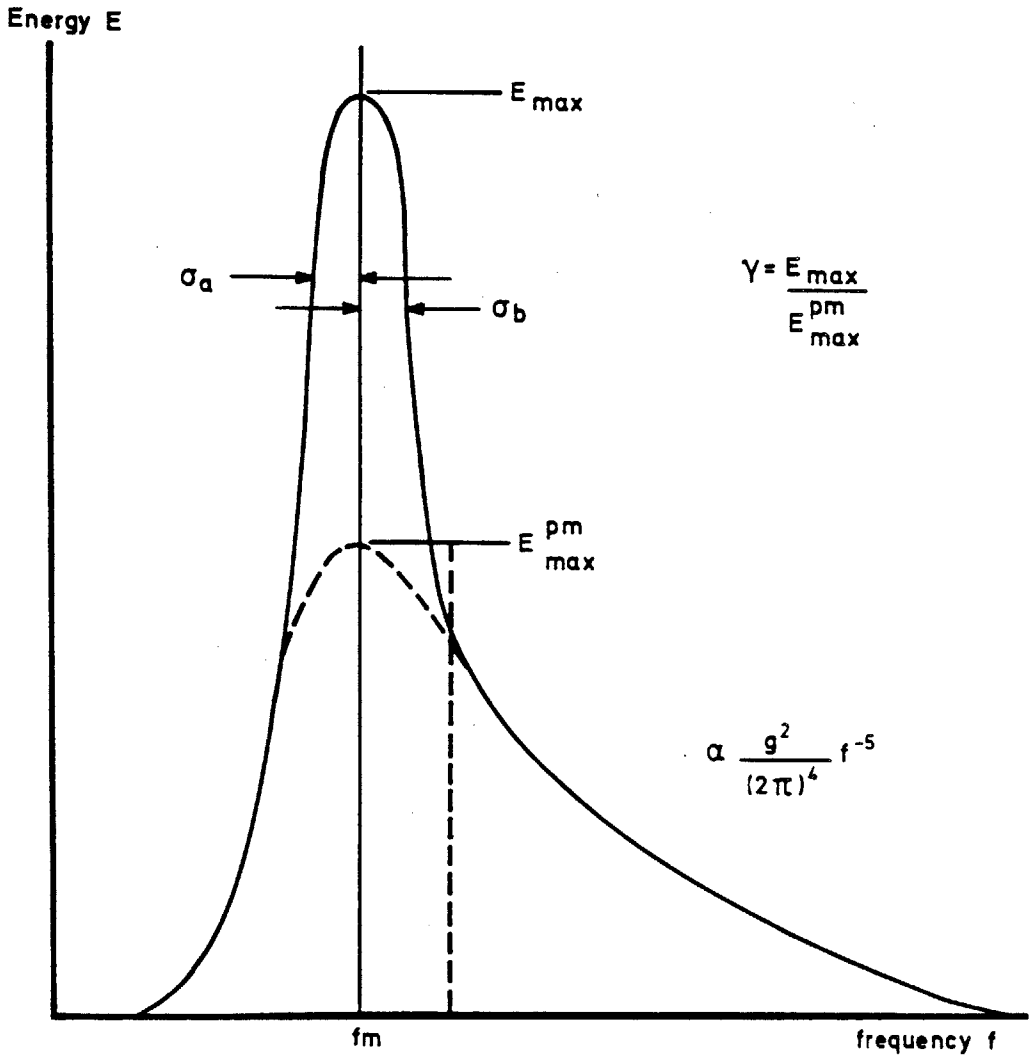


Fig. 3.4 Definition of the JONSWAP parameters.

The contribution of the parameters to the JONSWAP spectral shape is easily realized by representing E(f) as a product of three functions

$$E(f) = a \cdot \Psi_1 \cdot \Psi_2 \cdot \Psi_3 \tag{3.1.46}$$

where a = equilibrium constant,

$$\Psi_1 = f^{-5},$$

$$\Psi_2 = \exp\left[-\frac{5}{4}\left(\frac{f}{fm}\right)^{-4}\right],$$

$$\Psi_3 = \gamma^{\exp\left[-\frac{(f/fm-1)^2}{2\sigma^2}\right]}.$$

These three functions are schematically displayed in Figure 3.5, which give a good impression of the order of magnitude for the various parameters. Furthermore, inspection of the JONSWAP spectrum (3.1.45) reveals that as $\gamma \to 1$, the spectrum reduces to the PM spectrum for a fully developed sea state,

$$E_{PM}(f) = \alpha g^2 (2\pi)^{-4} f^{-5} \exp\left[-\frac{5}{4}\left(\frac{f}{fm}\right)^{-4}\right] \tag{3.1.47}$$

The original form of the PM spectrum allows only the fm parameter to vary as a function of wind speed, while α is fixed at 0.0081. The peak frequency for a fully developed sea state can be determined from

$$fm = \left(\frac{0.74}{1.25}\right)^{1/4} \frac{g}{2\pi U_{19.5}} = 0.13\,\frac{g}{U} = f_{PM} \tag{3.1.48}$$

which accounts for the adjustment of the wind speed due to the different anemometer heights (cf. Pierson, 1977). The peak frequency in the original PM spectrum corresponds to the frequency for which the

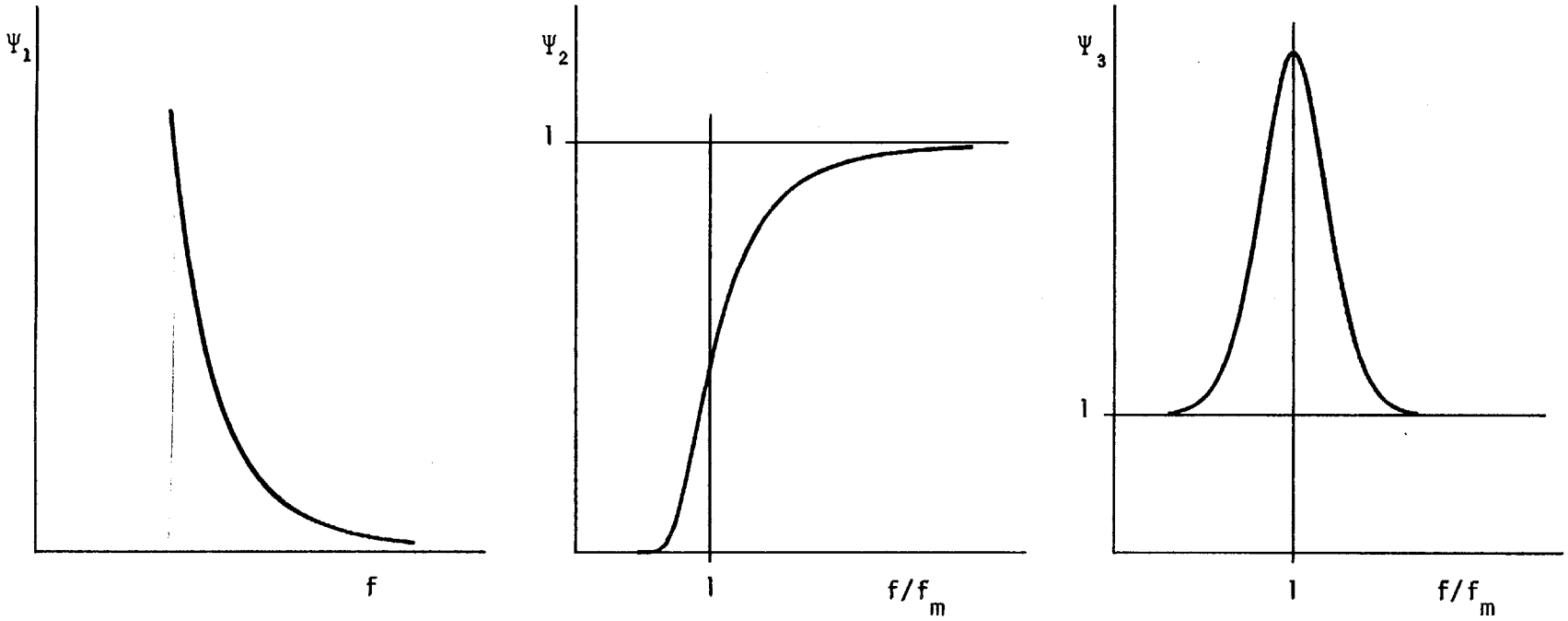


Fig. 3.5 Schematic representation of the three functional forms making up the JONSWAP spectrum.

deep water phase speed of the waves equals the wind speed, i.e., $f_p = g/2\pi U_{19.5}$.

The JONSWAP results showed that for growing sea states, the two scaling parameters fm and α are explicitly dependent on fetch and wind speed. Following Kitaigorodskii's (1962) similarity hypothesis, which states that for a uniform, stationary wind blowing perpendicular off a straight coastline, all wave parameters when non-dimensionalized by g and U should only depend on the dimensionless fetch,

$$\xi \equiv \frac{gx}{U^2} \tag{3.1.49}$$

where x is the fetch in meters. Over the non-dimensional fetch range $10^{-1} < \xi < 10^4$, the dimensionless peak frequency ν and α are satisfactorily described by the power-law expressions (Figure 3.6).

$$\nu \equiv \frac{fmU}{g} = 3.5\, \xi^{-0.33} \tag{3.1.50}$$

$$\alpha = 0.076\, \xi^{-0.22} \tag{3.1.51}$$

An alternative scale parameter (Figure 3.7), relating the average total wave energy to fetch, is given in non-dimensional form

$$\varepsilon \equiv \frac{\tilde{E}g^2}{U^4} = 1.6 \times 10^{-7} \xi \tag{3.1.52}$$

where $\tilde{E} = \int E(f)df$ is the total variance of the surface displacement.

Ample evidence from field and wave tank experiments support the validity of the scaling laws for fetch and duration limited wave conditions (Mitsuyasu, 1968, 1969, 1973; Ross, 1978; Liu and Ross,

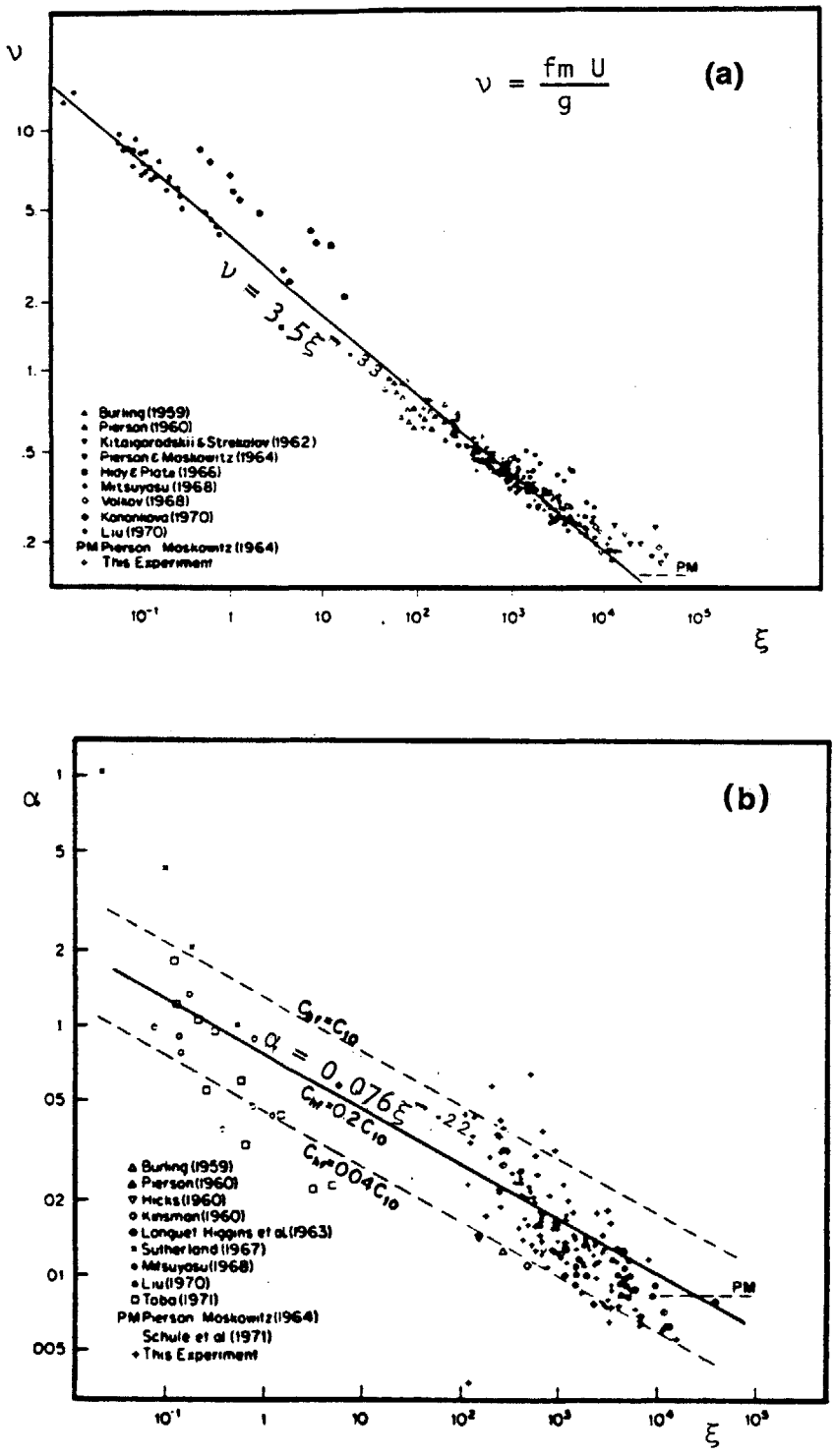


Fig. 3.6 a) Peak frequency vs. fetch according to Kitaigorodskii's scaling laws.
b) Phillips' constant vs. fetch according to Kitaigorodskii's scaling laws.
(From Hasselmann et al. 1973).

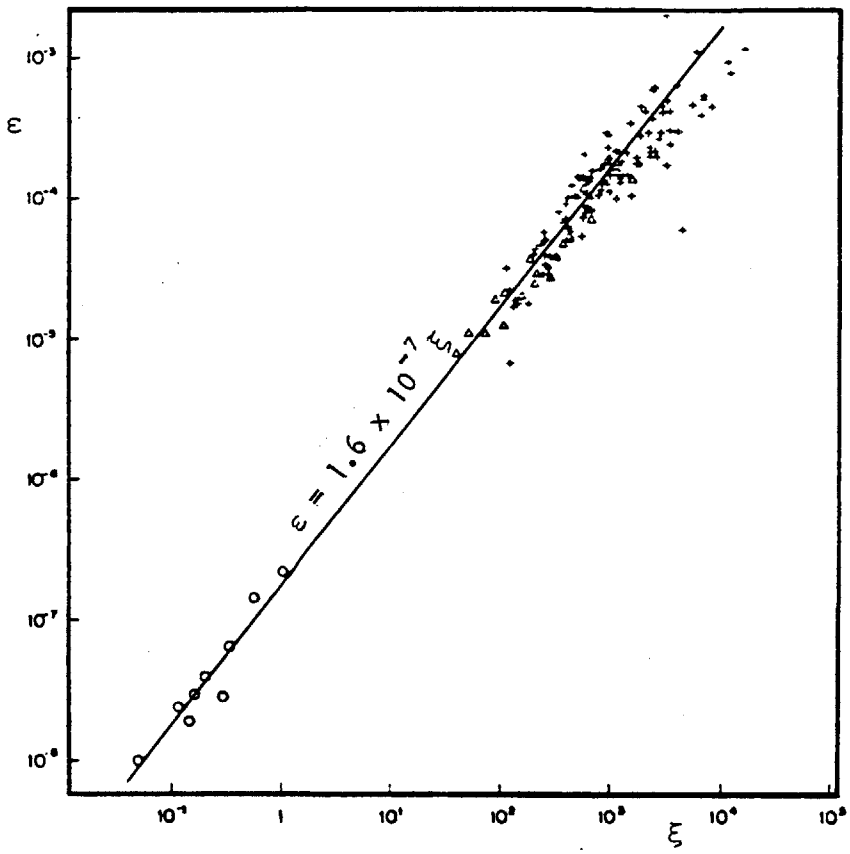


Fig. 3.7 Energy vs. fetch according to Kitaigorodskii's scaling laws. (From Hasselmann et al. 1973).

1980; Kahma, 1981; Rottier and Vincent, 1982).

The remaining three shape parameters γ, σ_a and σ_b, however, show no discernible trend with respect to dimensionless fetch for the JONSWAP data (Figure 3.8). The scatter in the parameters appears to be real and, according to Hasselmann et al. (1973), is attributed to the statistical indeterminacy associated with spectral measurements, since they generally characterize only the properties in proximity of the narrow spectral peak. A mean spectral shape was derived from the analysis of the JONSWAP spectra, which fixes these parameters at

$$\gamma = 3.3; \quad \sigma_a = 0.07; \quad \sigma_b = 0.09 \ . \tag{3.1.53}$$

Comparison of the mean JONSWAP spectrum (3.1.45, 3.1.53) with other observed fetch-limited spectra of growing windseas (Barnett and Wilkerson, 1967; Mitsuyasu, 1968, 1969; Ross et al., 1971; Schule et al., 1971; Ross and Cardone, 1974; Rye et al, 1974; Houmb and Øyan, 1981) was generally very good. Favorable agreement was also obtained when fitted to duration-limited windsea spectra (DeLeonibus et al., 1974; Mitsuyasu and Rikiishi, 1978). The JONSWAP spectral shape was successfully fit also to wave data taken during hurricanes (Patterson, 1974; Ross and Cardone, 1974). This is a surprising result, since hurricanes can generate complex wave fields which are associated with a moving, circular wind-field. A more detailed discussion of this subject can be found in Hasselmann et al. (1976). Some examples of spectral fits to these types of wave fields are shown in Figure 3.9.

Since the JONSWAP shape parameters γ, σ_a and σ_b are too sensitive to small perturbations of the spectral peak, an alternative

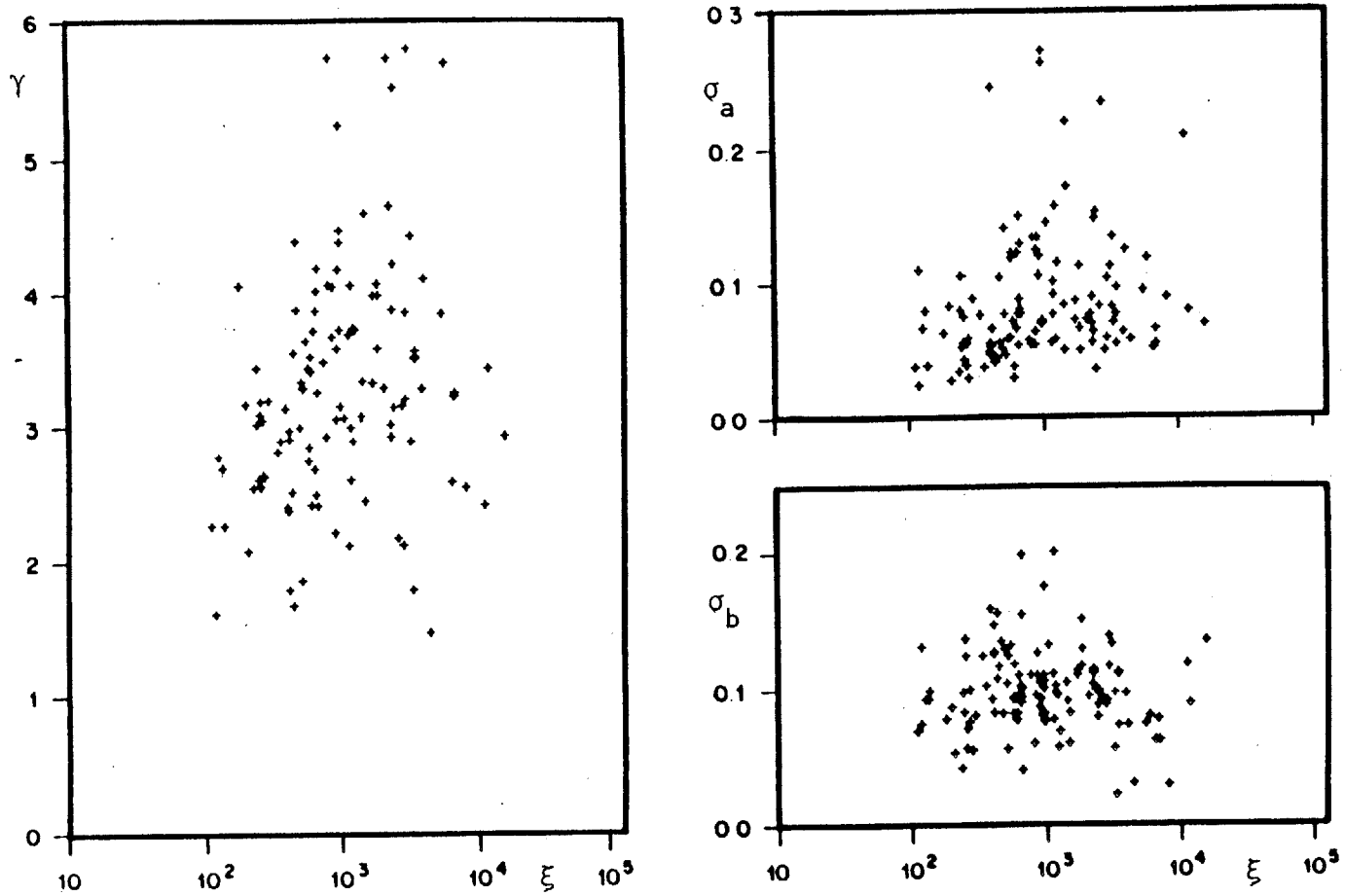


Fig. 3.8 Shape parameters γ, σ_a, σ_b vs. fetch.
(From Hasselmann et al. 1973).

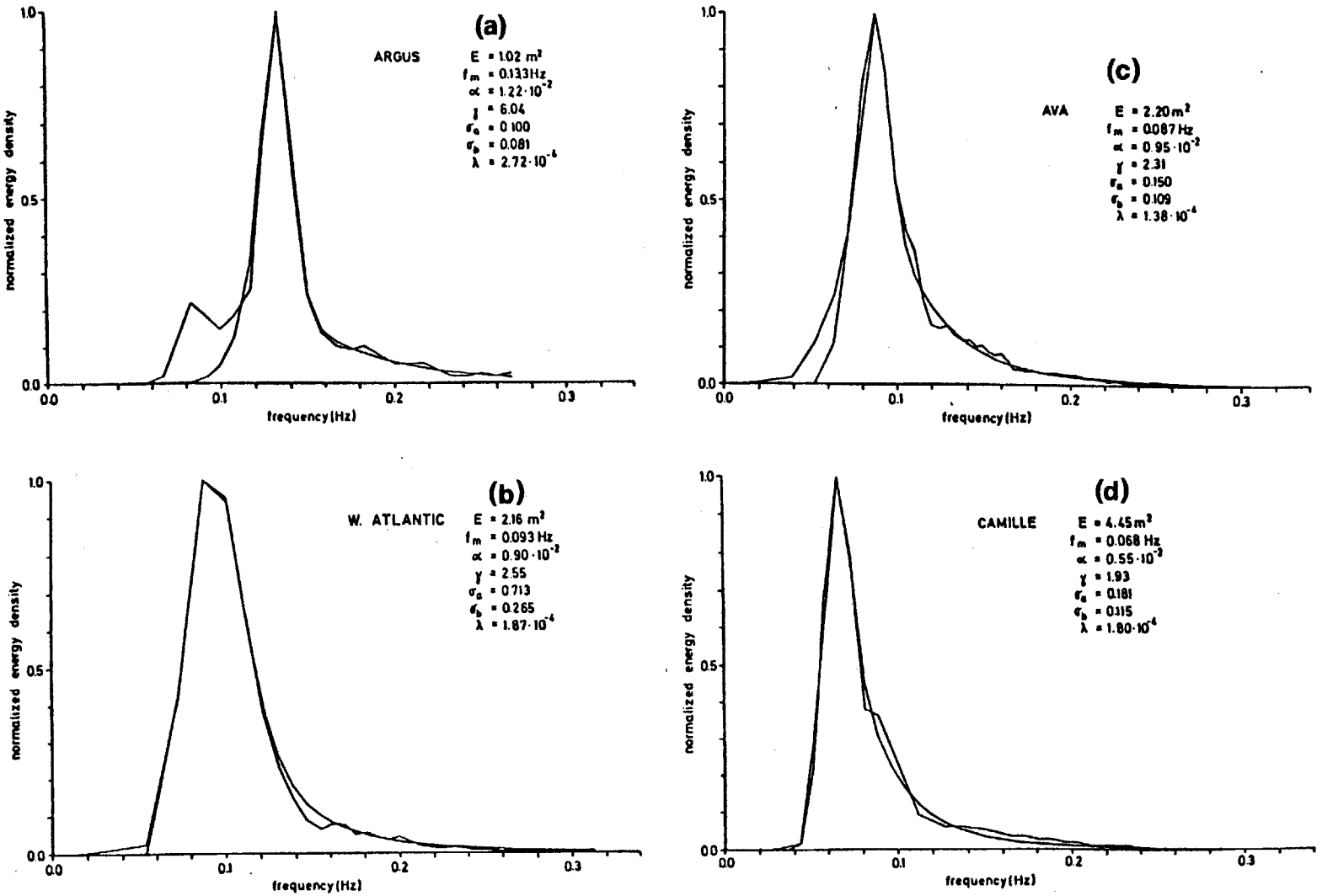


Fig. 3.9 Examples of spectral and analytical fits of observed wave spectra from data sets: (a) Argus Island; (b) Western Atlantic; (c) Hurricanes AVA; and (d) CAMILLE. (From Hasselmann et al. 1976).

shape parameter, which depends on the average spectral properties, can be directly derived from the JONSWAP spectrum. Thus, we define

$$\lambda = \frac{\tilde{E} fm^4}{\alpha g^2} = (2\pi)^{-4} I(z) \qquad (3.1.54)$$

where the total variance is given by

$$\tilde{E} = \alpha g^2 (2\pi)^{-4} fm^{-4} \int_0^\infty z^{-5} \Psi(z) dz$$

with $z = f/fm$ and $I(z) = \int_0^\infty z^{-5} \Psi(z) dz$ is only a function of the spectral shape.

The shape parameter λ is readily rewritten in terms of dimensionless scale variables

$$\lambda = \frac{\varepsilon \nu^4}{\alpha} \qquad (3.1.55)$$

which imply a weak fetch dependence, $\lambda \sim \xi^{-0.1}$, upon substitution of their fetch relations (3.1.50) - (3.1.52). For the mean JONSWAP spectrum, using (3.1.54) yields a value of $\lambda = 1.96 \times 10^{-4}$. For truly self-similar spectra, the shape should be invariant and hence, λ remains constant. For the sake of consistency, Hasselmann et al. (1976) slightly modified the empirical power laws (3.1.50) and (3.1.51) to the relations

$$\nu = 2.84\, \xi^{-0.3} \qquad (3.1.56)$$

and

$$\alpha = 0.0662\, \xi^{-0.2} \qquad (3.1.57)$$

which now yield a fetch-independent value of $\lambda = 1.58 \times 10^{-4}$, in

accordance with shape invariance.

Conversely, the fetch laws for ν, α and ε can also be expressed in terms of duration t or in its dimensionless form $T \equiv gt/U$. An approximate relationship which transforms fetch into an equivalent duration, can be derived in the following manner.

Consider a turbulent, uniform wind blowing sufficiently long over a fetch x, such that at fetches less than x the sea is steady and fetch-limited. A small distance δx downwind, the sea remains unsteady until the wave energy at x had time to travel the distance δx. Therefore, at $(x + \delta x)$ and further downwind, the wave field is said to be duration-limited. Then, the minimum time required for a wave group associated with a narrow-peaked spectrum to propagate from the upwind boundary to a fetch $(x + \delta x)$ is approximately given by

$$t = \int_0^x \frac{1}{\bar{c}_g} \, dx \tag{3.1.58}$$

where $\bar{c}_g$ is the average group velocity and is determined from

$$\bar{c}_g = \frac{\iint c_g(f,\theta) E(f,\theta) \, df d\theta}{\iint E(f,\theta) \, df d\theta} \, . \tag{3.1.59}$$

Assuming a mean JONSWAP spectrum and a cosine-squared angular spreading function, $\bar{c}_g$ is given in deep water by

$$\bar{c}_g = 0.767 \frac{g}{4\pi f_m} \tag{3.1.60}$$

On substituting (3.1.60) and the ν-fetch law into (3.1.58) and carrying out the integration leads to a fetch-duration relation

$$\xi = 2.5 \times 10^{-3} T^{10/7} \qquad (3.1.61)$$

Introducing (3.1.61) in the empirical fetch laws yields the following power laws for a fetch-equivalent duration

$$\nu = 17.14\, T^{-3/7} \qquad (3.1.62)$$

$$\alpha = 0.22\, T^{-2/7} \qquad (3.1.63)$$

$$\varepsilon = 4 \times 10^{-10} T^{10/7} \qquad (3.1.64)$$

From laboratory measurements of duration-limited wind waves Mitsuyasu and Rikiishi (1978) empirically found formulae for peak frequency fm and wave energy $\tilde{E}$. They are

$$\begin{aligned} \nu &= 20\, T^{-.57} \\ \varepsilon &= 0.9 \times 10^{-10} T^{1.44} \end{aligned} \qquad (3.1.65)$$

where we have assumed a drag coefficient $c_d = 1.83 \times 10^{-3}$ to relate the friction velocity u_* to the kinematic surface wind stress $\tau = c_d U^2$.

Similarly, Hasselmann et al. (1976) considered analytical solutions for their two-parameter (fm and α) wave model under idealized conditions, when the wind direction is constant and the wind speed depends only on some power p of either fetch or duration. When the wind velocity remains uniform, $p \equiv 0$. This indicates independence of fetch or duration, and so the solutions reduce to

$$\begin{aligned} \nu &= 16.8\, T^{-3/7} \\ \alpha &= 0.203\, T^{-2/7} \\ \varepsilon &= 4.08 \times 10^{-10} T^{10/7} \quad . \end{aligned} \qquad (3.1.66)$$

In a similar approach Carter (1982) also obtained duration-dependent formulae, which are analogous to the set in (3.1.62) - (3.1.64).

Up to now, most of the wave-related parameters have been deduced from empirical evidence. Since the wave spectrum resembles, in appearance, a statistical distribution of events and is treated with methods analogous to those well-known in statistical theory, other useful wave parameters can be derived in terms of the moments of the "distribution". The nth order moment m_n of the spectrum is denoted by

$$m_n = \int_0^\infty f^n E(f) df \quad . \tag{3.1.67}$$

From the above definition it immediately follows that the zeroth-order moment, m_o, represents the area under the spectrum or the total (variance) energy. Thus, the significant wave height, $H_{1/3}$, is related to the spectrum as

$$H_s = H_{1/3} = 4\sqrt{m_o} \quad . \tag{3.1.68}$$

The corresponding significant wave period T_s is given by the ratio

$$T_s = \frac{m_o}{m_1} \quad . \tag{3.1.69}$$

However, a more useful wave period parameter is the mean zero-crossing period T_z, since it reflects more accurately the relative distribution of energy within the spectrum. The zero-crossing period T_z can be calculated from

$$T_z = \left(\frac{m_o}{m_2}\right)^{1/2} . \qquad (3.1.70)$$

Finally, two additional parameters, which provide information of the spectral shape, can be determined from the spectral moments. The first gives a measure of the irregularity of the sea state and is commonly called the spectral width parameter ε_s. Originally introduced by Cartwright and Longuet-Higgins (1956), it is defined by

$$\varepsilon_s = \left(1 - \frac{m_2^2}{m_o m_4}\right)^{1/2} . \qquad (3.1.71)$$

If the spectrum is narrow, $\varepsilon_s \to 0$. This indicates that the wave heights approach a Rayleigh distribution and the waves can be considered regular. In the case of a broad spectrum, $\varepsilon_s \to 1$ and the statistical distribution of heights approaches a Gaussian form, or the wave pattern can be visualized as irregular. The usefulness of this parameter is somewhat limited, since it involves the fourth moment, which is extremely sensitive on the choice of the high-frequency cut-off. Since the spectral high-frequency tail is proportional to f^{-5}, then taking the fourth moment means that the integrated result will depend on the natural logarithm of the high-frequency cut-off. For measured wave records, this cut-off limit is typically set at the Nyquist frequency f_N, which is readily calculated from the inverse of twice the sampling interval. The data of frequencies larger than f_N will be folded into the lower range and create ambiguities in interpreting energy located there. This phenomenon is commonly known

as aliasing. In order to avoid aliasing, a small enough sampling interval should be chosen, so that no energy is likely to be found at frequencies above f_N. Generally, the Nyquist frequency is selected two to three times larger than the expected maximum frequency in a spectral time series. However, Rye and Svee (1976) have shown that for the PM spectrum ε_s varies between 0.4 and 0.8 depending on the choice of cut-off frequency. In addition, they concluded that ε_s poorly distinguishes between a very sharply peaked JONSWAP spectrum ($\gamma = 7$) and a PM spectrum ($\gamma = 1$). For computational purposes, in this study we set the upper integration limit for m_4 at $z_u = f/fm = 7.5$.

The second parameter, also a spectral width parameter, but derived from the joint distribution of wave period and amplitude (Longuet-Higgins, 1975), is given by the expression

$$\nu_s = \left(\frac{m_2 m_o}{m_1^2} - 1 \right)^{1/2} . \qquad (3.1.72)$$

Similarly, ν_s is a measure for the concentration of wave energy within a narrow frequency band ($\nu_s \to 0$) or not ($\nu_s \to 1$). From the analysis by Rye and Svee (1976) and recently by Longuet-Higgins (1983) it appears that ν_s is more sensitive in differentiating between typical windsea spectra (see Table 3.1). An additional parameter, describing the peakedness of a wave spectrum, was suggested by Goda (1970):

$$Q_p = \frac{2}{m_o^2} \int_0^\infty f|E(f)|^2 \, df. \qquad (3.1.73)$$

It turns out, as can be seen from the integral relation above that Q_p is independent of the high-frequency cut-off.

A summary of the above wave parameters, including typical values for the Pierson-Moskowitz and mean JONSWAP spectrum are given in Table 3.1. Osborne (1982) has developed similar mathematical expressions for the spectral wave parameters and made comparisons with random waves from a Monte-Carlo-type simulation.

Parameter	Definition	Pierson-Moskowitz spectrum	mean JONSWAP spectrum	Fetch laws	Duration laws
Peak Frequency	$\nu = \frac{fmU}{g}$	0.13	0.16	$2.84\ \xi^{-0.3}$	$17.14\ \tau^{-3/7}$
Phillips Constant	α	0.0081	0.0097	$0.0662\ \xi^{-0.2}$	$0.22\ \tau^{-2/7}$
Peak Enhancement Factor	$\gamma = \frac{E(fm)}{E_{PM}(fm)}$	1	3.3	-	-
Total Energy	$\epsilon = \frac{m_o g^2}{U^4}$	3.64×10^{-3}	2.90×10^{-3}	$1.6 \times 10^{-7} \xi$	$4 \times 10^{-10}\ \tau^{10/7}$
Spectral Shape	$\lambda = \frac{\epsilon \nu^4}{\alpha}$	1.28×10^{-4}	1.96×10^{-4}	1.58×10^{-4}	1.58×10^{-4}
Significant Wave Height (m)	$H_s = 4\sqrt{m_o}$	4.0	5.4	-	-
Significant Wave Period (sec)	$T_s = \frac{m_o}{m_1}$	7.7	8.3	-	-
Zero-Crossing Wave Period (sec)	$T_z = (\frac{m_o}{m_2})^{1/2}$	7.1	7.8	-	-
Spectral Width Parameter	$\nu_s = (\frac{m_2 m_o}{m_1^2} - 1)^{1/2}$	0.425	0.390	-	-
Spectral Width Parameters	$\epsilon_s = (1 - \frac{m_2^2}{m_o m_4})^{1/2}$	0.753	0.753	-	-
Peakedness Parameter	Q_p	2.0	3.14	-	-

Table 3.1 Summary of theoretical spectral wave parameters as a function of fetch and duration. Examples are calculated for a mean JONSWAP and Pierson-Moskowitz spectrum, corresponding to fm = 0.1 Hz, U = 15.7 m/s, and f_{PM} = 0.1 Hz, U = 12.75 m/s, respectively.

b) FINITE DEPTH

Our present knowledge of wave spectra and the processes governing their evolution in shallow water is far from complete. Although an underlying basic theory exists, there are only a few measurements available to check the validity of the proposed theoretical formulations in a consistent manner. The first step in this direction has been taken by Bouws et al. (1984), who applied the similarity principle of KKZ to three distinct experiments of shallow water wind-wave growth: the Marine Remote Sensing Experiment in the North Sea (MARSEN), the Atlantic Remote Sensing Land-Ocean Experiment (ARSLOE), and wave measurements during a severe storm in the North Sea near the Dutch lightship TEXEL.

It was concluded that KKZ's similarity scaling could be extended to the entire spectral range. From this they proposed the self-similar TMA (TEXEL-MARSEN-ARSLOE) spectrum or finite-depth JONSWAP spectrum, which fairly well describes windsea spectra in deep, intermediate depth and shallow water.

Based on KKZ's similarity hypothesis the JONSWAP spectrum (3.1.45) can be expressed in wave number space as

$$F_J(k) = \frac{\alpha}{2} k^{-3} \psi(k, fm, h) \tag{3.1.74}$$

where ψ is a dimensionless shape function and $(\alpha/2)k^{-3}$ represents the Phillips-Kitaigorodskii equilibrium range scaling factor. Pierson and Stacy (1973) suggested an analogous expression of ψ for a deep water PM spectrum, i.e.,

$$\psi_{PM}(k, km, h=\infty) = \exp\left[-\frac{5}{4}\left(\frac{k}{k_m}\right)^{-2}\right] \tag{3.1.75}$$

where k_m is related to the peak frequency fm by the linear dispersion relation

$$(2\pi fm)^2 = g\, k_m \tag{3.1.76}$$

From (3.1.74), it appears that wave spectra irrespective of water depth always adjust to a constant shape in wave number space. Figure 3.10 illustrates the variations of the Pierson-Moskowitz and JONSWAP spectra in wave number space for different water depths. It should be noted how dramatically the total energy differs as a function of water depth.

Applying the results derived in the previous section, a depth dependent frequency spectrum E(f,h) can be obtained by transforming the corresponding wave number spectrum, i.e.,

$$E(f,h) = F\big(k(f,h)\big)\,\frac{\partial k(f,h)}{\partial f} \tag{3.1.77}$$

Since the dimensionless shape function is not affected by the translation to different water depths, we have

$$\psi(k,fm,h) = \frac{F\big(k(f,h)\big)}{\big[k(f,h)\big]^{-3}} = \frac{F\big(k(f,\infty)\big)}{\big[k(f,\infty)\big]^{-3}} = \psi(k,fm,\infty) \tag{3.1.78}$$

Substituting (3.1.78) for F(k(f,h)) along with the inverse transformation of F(k(f,∞)) into (3.1.77) yields

$$E(f,h) = E(f,\infty)\left\{\frac{\big[k(f,h)\big]^{-3}\,\frac{\partial k(f,h)}{\partial f}}{\big[k(f,\infty)\big]^{-3}\,\frac{\partial k(f,\infty)}{\partial f}}\right\} \tag{3.1.79}$$

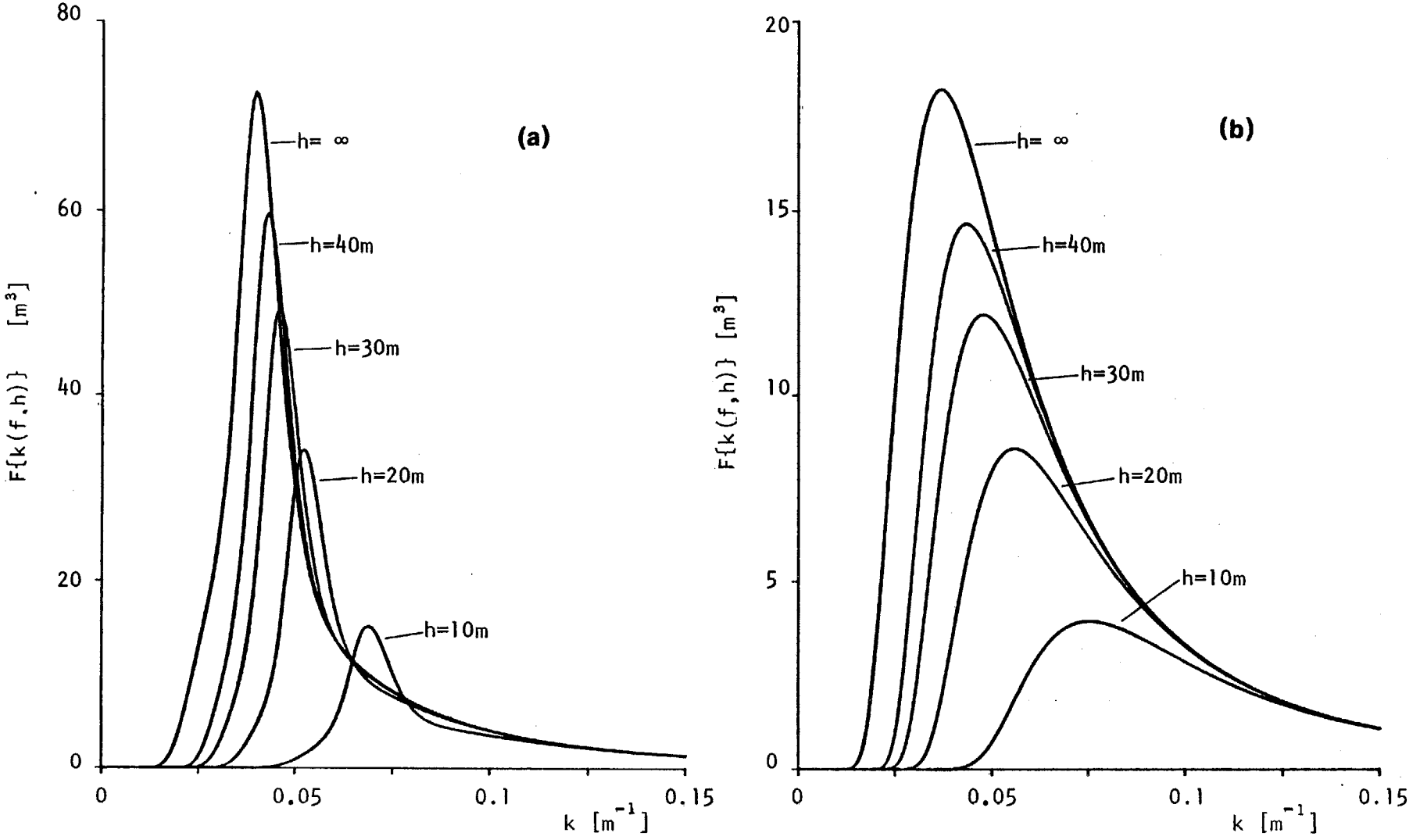


Fig. 3.10 Self-similar wave number spectra for different water depths. (a) Mean JONSWAP shape corresponding to fm = 0.1 Hz, α = 0.01, γ = 3.3; (b) Pierson-Moskowitz shape corresponding to fm = 0.1 Hz, α = 0.0081, γ = 1.

where $E(f,\infty)$ is the one-dimensional frequency spectrum for an infinitely deep ocean and

$$\Phi(\omega_h) = \left\{ \frac{[k(f,h)]^{-3} \frac{\partial k(f,h)}{\partial f}}{[k(f,\infty)]^{-3} \frac{\partial k(f,\infty)}{\partial f}} \right\} \tag{3.1.80}$$

with $\omega_h = 2\pi f \sqrt{h/g}$. This is an alternative derivation of the KKZ-factor but equivalent to (3.1.40). Equation (3.1.79) then formally states that the frequency spectrum in a sea of constant depth h is obtained by simply multiplying the corresponding deep water frequency spectrum with the KKZ-factor $\Phi(\omega_h)$. If the concept of quasi-equilibrium also holds for finite depth, then we can extend this to the JONSWAP shape, so that

$$E(f,h,a_j) = \Phi(\omega_h) \cdot E(f,\infty,a_j) \tag{3.1.81}$$

where $a_j = \{fm, \alpha, \gamma, \sigma_a, \sigma_b\}$, is the JONSWAP parameter set. Similarly, Figure 3.11 impressively displays the changes of windsea spectra with the same JONSWAP parameters in seas of different depths. In addition to the large variation of total energy, it is noteworthy to point out the migration of the actual spectral peak to slightly higher frequencies with diminishing depth. This is hardly noticeable for the JONSWAP spectrum, but becomes more prominent for the PM spectrum, where the frequency of maximum energy is located at approximately 1.1 fm when h = 10 m. This frequency drifting is still small enough and of little consequence for practical applications. Hence, no severe errors should accrue if the peak frequency is kept constant at its deep water value. Bouws et al. (1984) have convincingly demonstrated that the translation

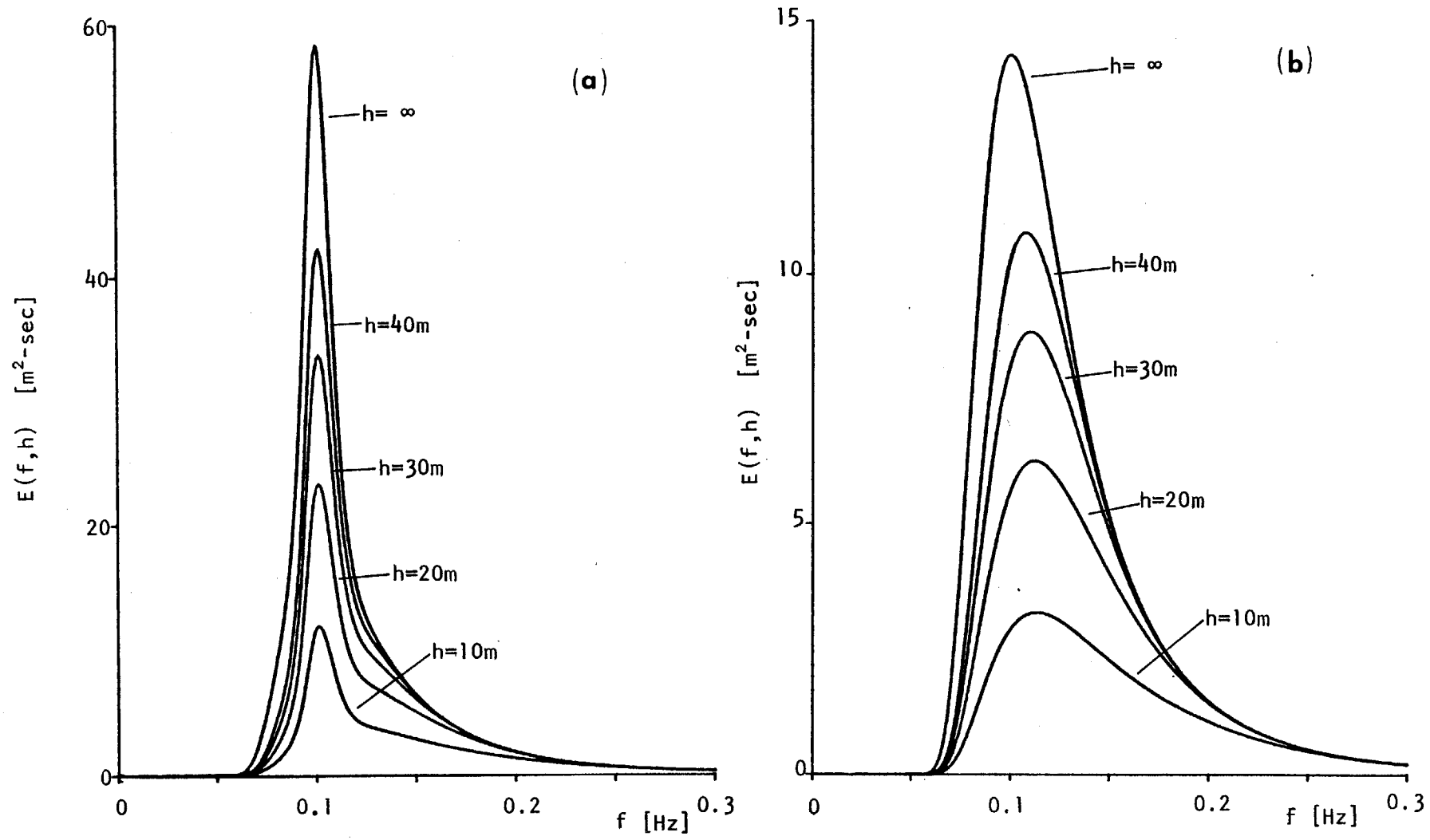


Fig. 3.11 Self-similar frequency spectra for different water depths. (a) Mean JONSWAP shape with fm = 0.1 Hz, α = 0.01, γ = 3.3; (b) Pierson-Moskowitz shape fm = 0.1 Hz, α = 0.0081, γ = 1.

of the deep water quasi-equilibrium spectra, by multiplying with the KKZ-factor, provide generally good fits to wind-wave spectra in constant depth and gently sloping coastal waters.

The fitting of the JONSWAP spectral shape to measured deep water spectra and the associated extraction of the spectral parameters can easily be accomplished by following the described procedure of Müller (1976). In light of the relationship given in (3.1.81) we simply perform an inverse transformation on a depth dependent spectrum by multiplying with $\Phi^{-1}(\omega_h)$ in order to obtain its associated deep water spectrum. Now we can proceed with the successive determinations of the five free parameters. Some examples, shown in Figure 3.12, provide an impression of how well observed spectra fit the finite depth JONSWAP spectral shape.

Bouws and Komen (1983) recently described a depth-limited windsea spectrum, which was generated by a severe storm in the Southern North Sea. From their analysis, they found that a JONSWAP shape defined by the parameters fm = 0.086 Hz, α = 0.01, γ = 2, and $\sigma_a = \sigma_b$ = 0.08 adequately describes the storm spectrum. However, in deriving the JONSWAP parameters, they neglected to account for the finite depth effect induced by $\Phi(\omega_h)$. If the effect of $\Phi(\omega_h)$ would have been included in their analysis, then the value of the enhancement factor γ would change to 3.35. This implies that the reduced value of γ may reproduce the KKZ effect at least within the range of ω_h corresponding to intermediate depths. This fact has already been noted by Bouws (1980). When examining the same set of storm spectra, he consistently determined γ values less than 2. Knowles (1982) essentially confirms these findings for his data set, where a mean γ

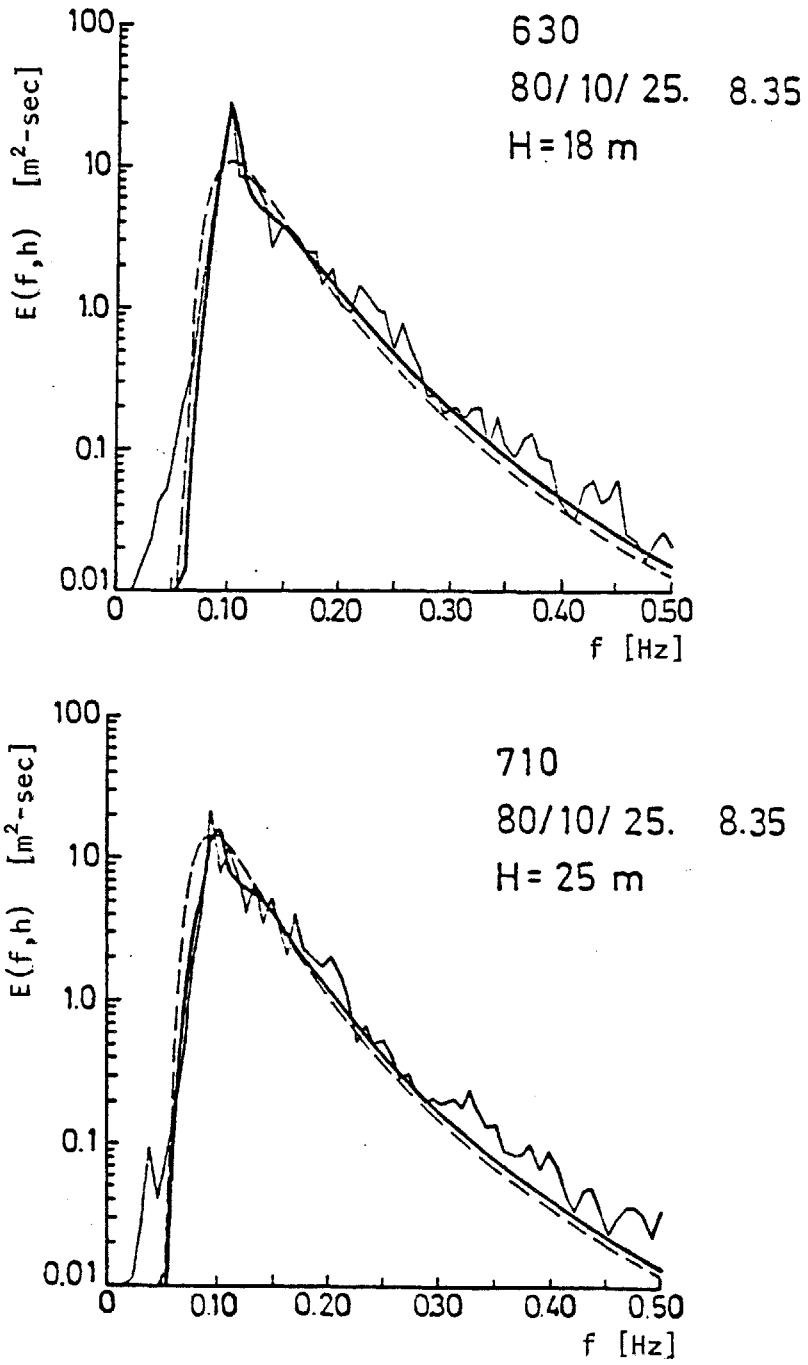


Fig. 3.12 Comparison of observed wave spectra from ARSLOE experiment with JONSWAP fit in deep water (---) and in finite depth (——). (From Bouws et al. 1984).

value of 1.5 was calculated.

Examination of empirically determined equilibrium constants indicate only a weak or almost no dependence on fetch (Knowles, 1982, Ou, 1980). This essentially supports the stipulation of KKZ that in accordance with Phillips' (1958) hypothesis, the equilibrium coefficient should be independent of fetch. The average value of α as reported by KKZ for finite depth sea spectra was estimated at $(4\pm2) \times 10^{-3}$. Although Knowles (1982) cites an α value in close agreement with the one above, it appears that there is an error of a factor of 10^{-1} or more. A rough estimate of α from his Fig. 3 gives an approximate value of $\sim 2 \times 10^{-2}$. Results from laboratory experiments by Ou (1980) suggest equilibrium range coefficients of $\sim (3\pm1) \times 10^{-3}$. A dependence on depth has been implied from the ARSLOE results (Vincent et al., 1982), where it was found that α increases with decreasing depth.

At this point it is anticipated that any spectral parameter in finite depth somehow must involve, either implicitly or explicitly, the depth itself. In the absence of mean currents, the frequency remains unaltered when waves propagate into shallow seas. Thus, the appropriate variable, reflecting a dependence on depth, is the wave number. From (3.1.74), we may compute the energy in the waves. Hence,

$$\tilde{E} = \int_0^\infty F_J(k)dk = \frac{\alpha}{2}\int_0^\infty k^{-3}\psi(k,fm,h)dk \qquad (3.1.82)$$

In a first approximation the above integral renders

$$\tilde{E} = \frac{\alpha}{2} k_m^{-2} \int_0^\infty y^{-3}\psi(y,fm,h)dy = K\frac{\alpha}{2} k_m^{-2} \qquad (3.1.83)$$

where K accounts for any net contribution to $\tilde{E}$ due to the spectral shape factor ψ. Similar to the spectral shape parameter λ for the frequency spectrum, we recognize that K essentially represents the shape parameter for the wave number spectrum, i.e.,

$$\Lambda = \frac{\tilde{E}k_m^2}{\alpha} = \frac{\varepsilon\kappa_m^2}{\alpha} = \frac{K}{2} \tag{3.1.84}$$

where ε is the dimensionless variance of the surface displacement defined in (3.1.52) and

$$\kappa_m = \frac{k_m U^2}{g} \tag{3.1.85}$$

is the dimensionless wave number, corresponding to the peak frequency fm of the FDJ spectrum and the water depth h.

By means of the deep water dispersion relation, ν in (3.1.56) can be replaced by κ_m, so that

$$\kappa_m = 318.42\ \xi^{-0.6} \tag{3.1.86}$$

Then substituting the deep water relations for ε, α and κ_m into (3.1.83), yields

$$\varepsilon_\infty = 0.25\ \alpha_\infty\ \kappa_m^{-2} \tag{3.1.87}$$

from which one infers that $\Lambda = 0.25$. The general form of (3.1.87) is precisely the relation Bouws et al. (1984) investigated by computing the values of ε, α and κ_m from the combined TMA data set and plotting them in terms of ε versus $\alpha\kappa_m^{-2}$. From a regression analysis, they

found that the data was well described by the empirical relationship

$$\varepsilon = 0.14\ (\alpha\kappa_m^{-2})^{0.88} \qquad (3.1.88)$$

The validity of extending the self-similar hypothesis to spectra in finite depth is inferred by the degree to which (3.1.88) is linear. Their results manifest not only that windsea spectra in shoaling water are self-similar, but also that the proper variable to describe finite depth spectral wave parameters should be the wave number rather than the wave frequency. From the limited number of examples (eight) given by Bouws et al. (1984), we recalculated Λ using (3.1.84) and found an average value of 0.28, which is in close agreement with the theoretical value in (3.1.87).

It is unfortunate that previous investigators of finite depth wind wave spectra (Knowles, 1982; Rottier and Vincent, 1982; Bouws, 1980; Goda, 1975) have not performed a similar analysis, as shown by Bouws et al. (1984), but rather attempted to force their empirical relationships to resemble the previously determined deep-water relations of various spectral wave parameters.

3.2 The Energy Transport Equation

In the previous section we introduced the definition and derivation of the energy density spectrum for ocean waves. For the problem of predicting waves in an ocean of arbitrary configuration, we need to discuss the changes of the local wave energy balance due to dynamical processes. A general theoretical framework is needed to describe the evolution of the spectrum in $(\underline{k},\underline{x},t)$ space, where $\underline{k}$ is the horizontal wave number vector (k_x,k_y), $\underline{x}$ is the horizontal space vector (x,y), and t is time.

Let us suppose that at time t_o, the total energy density of the waves per unit phase volume $[d\underline{k}_o d\underline{x}_o]$ is given by its initial value $F(\underline{k}_o,\underline{x}_o,t_o)$. At a later time $t = t_o + dt$, the phase volume has moved and its total energy may be altered due to the inflow and outflow of energy. Let $Q(\underline{k}',\underline{x}',t')$ represent the net rate of change of energy per unit phase volume resulting from any sources and sinks of wave energy. Then the energy balance may be stated in integral form

$$F(\underline{k},\underline{x},t) = F(\underline{k}_o,\underline{x}_o,t_o) + \int_{t_o}^{t} Q(\underline{k}',\underline{x}',t')dt' \qquad (3.2.1)$$

where $\underline{k}'$, $\underline{x}'$, t' vary along the path of a wave group from an initial value $\underline{k}_o,\underline{x}_o,t_o$ to the point $\underline{k},\underline{x},t$. Since the source function in the integral depends on the spectrum itself, equation (3.2.1) cannot, generally, be regarded as a solution of the energy balance, except in certain special cases.

In the absence of any energy sources and sinks, i.e., $Q \equiv 0$, we obtain

$$F(\underline{k},\underline{x},t) = F(\underline{k}_o,\underline{x}_o,t_o) \tag{3.2.2}$$

Equation (3.2.2) states that the spectrum F is invariant along the trajectory of a wave group, despite dispersion and the influences of refraction. This fundamental relation was originally derived by Longuet-Higgins (1957) by means of a geometrical-optics method. The same result can also be obtained more directly, as was pointed out by Dorrestein (1960), by applying Liouville's theorem.

From the integral form of the energy balance equation (3.2.1), a more convenient differential form may be derived. Expanding $F(\underline{k},\underline{x},t)$ in a Taylor series yields

$$\begin{aligned} F(\underline{k},\underline{x},t) &= F\left(\underline{k}_o + \frac{d\underline{k}}{dt}\,dt,\ \underline{x}_o + \frac{d\underline{x}}{dt}\,dt,\ t_o + dt\right) \\ &= F(\underline{k}_o,\underline{x}_o,t_o) + \frac{\partial F}{\partial t}\,dt + \frac{d\underline{x}}{dt}\,\underline{\nabla}_x F\,dt + \frac{d\underline{k}}{dt}\,\underline{\nabla}_k F\,dt \end{aligned} \tag{3.2.3}$$

Upon substitution of (3.2.3) into (3.2.1) and approximating the integral by $T(\underline{k},\underline{x},t)\,dt$, we obtain

$$\frac{DF}{Dt} \equiv \frac{\partial F}{\partial t} + \dot{\underline{x}} \cdot \underline{\nabla}_x F + \dot{\underline{k}} \cdot \underline{\nabla}_k F = T \tag{3.2.4}$$

where

$$\dot{\underline{x}} \equiv \frac{\partial}{\partial \underline{k}}\,\omega(\underline{k},\underline{x}) = \underline{c}_g(\underline{k},\underline{x}) \tag{3.2.5}$$

$$\dot{\underline{k}} \equiv -\frac{\partial}{\partial \underline{x}}\,\omega(\underline{k},\underline{x}) \quad . \tag{3.2.6}$$

Here DF/Dt is the Lagrangian rate of change of the spectrum relative to a wave group moving along the ray paths determined by equations (3.2.5) and (3.2.6). $\nabla_{\underline{x}}$ and $\nabla_{\underline{k}}$ are the horizontal gradient vector operators of the position vector $\underline{x}$ and the wave number vector $\underline{k}$, respectively. The source function T now represents the net contribution of energy added to or subtracted from the spectrum at the wave number $\underline{k}$ due to all interaction processes which affect the component $\underline{k}$. Equations (3.2.5) and (3.2.6) describe the path of motion taken by a wave group, and are usually referred to as the wave rays, which coincide with the wave orthogonals, if there are no currents present. For equations (3.2.4) - (3.2.6) to be valid, it is assumed that both the amplitude and the wave number vectors of individual spectral components are slowly varying functions of $\underline{x}$ and t, such that

$$\frac{1}{kF}\frac{\partial F}{\partial \underline{x}} \ll 1, \qquad \frac{1}{\omega F}\frac{\partial F}{\partial t} \ll 1 \quad . \tag{3.2.7}$$

Equation (3.2.7) implies that the wave field can still be described locally by the spectrum $F(\underline{k},\underline{x},t)$. Furthermore, it is assumed that the water depth $h(\underline{x})$ is also slowly varying, i.e.,

$$\frac{1}{kh}\frac{\partial h}{\partial \underline{x}} \ll 1 \tag{3.2.8}$$

so that the geometrical-optics approximation is valid. A more detailed account of the exact conditions when the geometrical-optics law applies was formulated by Keller (1958) for surface gravity waves propagating in a fluid of arbitrary depth $h(\underline{x})$. For nearly-plane waves and within the geometrical-optics approximation, the non-homogeneous

dispersion relation connecting the local radian frequency ω with the wave number k is given by

$$\omega = \omega(\underline{k},\underline{x}) = (gk \tanh kh)^{1/2} \tag{3.2.9}$$

where $k = |\underline{k}|$ and $h = h(\underline{x})$ has an arbitrary dependence on the horizontal space coordinates. One derives this same equation in the case of waves in uniform depth. The group velocity associated with the wave properties at fixed $\underline{x}$ follows from differentiation of (3.2.9) with respect to $\underline{k}$, and is already stated in (3.2.5). From the conservation of crests equation

$$\frac{\partial \underline{k}}{\partial t} + \nabla_{\underline{x}} \omega = 0 \tag{3.2.10}$$

an equation for the variation of $\underline{k}$ along the ray path can be deduced by introducing ω above and writing the result in tensor notation

$$\frac{\partial k_i}{\partial t} + \frac{\partial \omega}{\partial k_j} \frac{\partial k_j}{\partial x_i} + \frac{\partial \omega}{\partial x_i} = 0 \quad . \tag{3.2.11}$$

Noting that $\underline{k}$ is irrotational, i.e.,

$$\frac{\partial k_j}{\partial x_i} = \frac{\partial k_i}{\partial x_j} \tag{3.2.12}$$

and making use of this result, (3.2.11) can be rewritten upon reverting to vector notation

$$\frac{\partial \underline{k}}{\partial t} + \underline{c}_g \cdot \nabla_{\underline{x}} \underline{k} = - \frac{\partial \omega}{\partial \underline{x}} \tag{3.2.13}$$

Equation (3.2.13) states that the rate of change of $\underline{k}$ at a position moving with the group velocity $\underline{c}_g$ is caused by spatial inhomogeneities, or refraction. Hence, in general, when ω is also a function of $\underline{x}$, the characteristic curves in the $(\underline{x},t)$ plane defined by $d\underline{x}/dt = \underline{c}_g$ are not straight lines. Since time does not appear explicitly in ω, the frequency ω remains constant on these characteristics. This can be shown by taking the scalar product of (3.2.10) with $\underline{c}_g$ so that we get

$$\frac{\partial \omega}{\partial t} + \underline{c}_g \cdot \underline{\nabla}_x \omega = 0 \qquad (3.2.14)$$

and also noting that $\underline{c}_g \cdot \partial \underline{k}/\partial t = \partial \omega/\partial t$. A complete and detailed treatment of the kinematics of wave trains in a general medium may be found in Whitham (1960), Synge (1963) and Lighthill (1965).

Formally, the energy transport equation (3.2.4) describes then the evolution of the energy spectrum of surface gravity waves due to horizontal advection and refraction of energy and the net transfer of energy from the various physical processes along the path of a wave group, as determined from the characteristic equations (3.2.5) and (3.2.6). These equations (3.2.5) and (3.2.6) are analogous to Hamilton's equations for a material particle moving in the $\underline{x}$ plane. This set of equations is applicable to a plane ocean and was originally presented by Gelci, et al. (1956) and Hasselmann (1960, 1968). Extension of this set for wave propagation on a spherical earth was given by Groves and Melcer (1961) and Backus (1962). Willebrand (1975) carefully examined the approximations, which yield the more general form of the transport equations in terms of the action density

variable, and derived the nonlinear corrections for the left-hand side of (3.2.4), due to the generally nonlinear source functions. However, it was concluded that the nonlinear corrections can be omitted for deep ocean waves, but they should be taken into account for waves in shallow seas.

In oceans, where the water depth is large (deep water limit) compared with all wave lengths, the frequency is independent of position and the refraction term $[\underline{k}\cdot\underline{\nabla}_{\underline{k}}F]$ in (3.2.4) vanishes. In the absence of any currents, the wave rays are straight lines. The same result occurs in waters of finite, but constant depth. In coastal waters, where the depth is small (shallow water limit) compared with the wave length, the waves are refracted by the presence of a spatially varying sea bottom. Now, the wave rays are generally curved lines. If the spectrum is stationary, hence independent of position, the advection term $[\underline{x}\cdot\underline{\nabla}_{\underline{x}}F]$ in (3.2.4) disappears.

Although, in general, the energy transport equation and the accompanying set of equations governing the rays are solved numerically, an important analytical result can be derived quite readily. Consider a narrow swell peak centered around a wave number $\underline{k}_o$, so that

$$F(\underline{k},\underline{x},t) = \varepsilon_o(\underline{x},t)\ \delta(\underline{k} - \underline{k}_o) \qquad (3.2.15)$$

where δ is Dirac's delta. Applying equation (3.2.4) to the swell beam, we may integrate over wave number space to obtain a propagation equation for the total swell energy ε_o,

$$\frac{\partial \varepsilon_o}{\partial t} + \frac{\partial}{\partial x_i}(c_{g_i}\varepsilon_o) = T_o \qquad (3.2.16)$$

where $\underline{c}_g = c_g(\underline{k}_o, \underline{x})$ and $T_o = \int T d\underline{k}$. This was the equation proposed by Sverdrup and Munk (1947) in order to forecast sea and swell from weather data to aid in naval landing activities on foreign beaches. Hasselmann et al. (1973) reduced (3.2.16) into an equivalent energy flux equation and applied this form to the analysis of swell data.

The formulation of energy transport in terms of the directional wave number spectrum, as presented in (3.2.4), is concise and can be solved numerically for a wide variety of applications in both shallow and deep water. However, a more convenient approach to the wave prediction problem is performed by employing the frequency-direction spectrum. In practice, it is easier to collect data of the directional frequency spectrum, which then can be compared with numerical model solutions. Besides being interested in the wave heights, we also would like to know the periods and directions of the waves. These two variables (period = inverse of frequency) are already incorporated in the two-dimensional frequency spectrum by definition and therefore, fall out quite naturally.

Then, the energy per unit surface area contained within an elemental area of wave number space can be related to the polar wave number space by

$$F(\underline{k};\underline{x},t)\, d\underline{k} = F(k,\theta;\underline{x},t)\, k\, dk\, d\theta \qquad (3.2.17)$$

where $\theta = \tan^{-1}[k_x/k_y]$ is the direction of the wave number vector $\underline{k} \equiv (k_x = k\cos\theta,\ k_y = k\sin\theta)$ and $k = |\underline{k}|$. Now (3.2.17) is

readily transformed into frequency-direction space by equating elemental areas. We have

$$F(k,\theta;\underline{x},t)\, k\, dk\, d\theta = E(f,\theta;\underline{x};t)\, df\, d\theta \tag{3.2.18}$$

from which the following relation can be deduced

$$F(\underline{k};\underline{x},t) = J \cdot E(f,\theta;\underline{x},t) \tag{3.2.19}$$

where J is the Jacobian of the transformation

$$J \equiv \frac{\partial(f,\theta)}{\partial(k_x,k_y)} = \frac{cc_g}{2\pi\omega}\ , \quad c_g = |\underline{c}_g|\ , \quad c = \frac{\omega}{|\underline{k}|}\ . \tag{3.2.20}$$

Substitution of (3.2.19) into (3.2.4) and after some algebra, yields a transport equation for the frequency-direction spectrum

$$\frac{D}{Dt}(cc_gE) \equiv \frac{\partial}{\partial t}(cc_gE) + \underline{c}_g \cdot \underline{\nabla}_x(cc_gE) - \frac{\partial\omega}{\partial\underline{x}} \cdot \underline{\nabla}_k(cc_gE) = 2\pi\omega S\ . \tag{3.2.21}$$

The refraction term in (3.2.21) may be expressed more appropriately in terms of a change with respect to the directon θ. Noting that the gradient operator $\underline{\nabla}_k$ can also be written as

$$\underline{\nabla}_k = \frac{\partial}{\partial\underline{k}} = \frac{\partial\theta}{\partial\underline{k}}\frac{\partial}{\partial\theta} \tag{3.2.22}$$

where $\partial\theta/\partial\underline{k} = [-\sin\theta/k,\ \cos\theta/k]$ upon making use of the fact that

$$\theta = \cos^{-1}\left[\frac{k_x}{k}\right] = \sin^{-1}\left[\frac{k_y}{k}\right]\ . \tag{3.2.23}$$

Furthermore, the derivative $-\partial\omega/\partial\underline{x}$ can be transformed into

$$-\frac{\partial\omega}{\partial\underline{x}}\bigg|_k = \frac{\partial\omega}{\partial k}\frac{\partial k}{\partial\underline{x}}\bigg|_\omega \tag{3.2.24}$$

where the vertical bar and subscript mean holding ω or k constant. Evaluating the scalar product in (3.2.21) and using (3.2.24), we get

$$-\frac{\partial\omega}{\partial\underline{x}}\cdot\frac{\partial\theta}{\partial\underline{k}} = -\frac{c_g\sin\theta}{k}\frac{\partial k}{\partial x} + \frac{c_g\cos\theta}{k}\frac{\partial k}{\partial y} \tag{3.2.25}$$

Since $\underline{k}$ is irrotational so that $\underline{\nabla}\times\underline{k} = 0$, one can show that

$$\cos\theta\frac{\partial\theta}{\partial x} + \sin\theta\frac{\partial\theta}{\partial y} = -\frac{\sin\theta}{k}\frac{\partial k}{\partial x} + \frac{\cos\theta}{k}\frac{\partial k}{\partial y} \tag{3.2.26}$$

From simple ray theory, we know that the orthogonal trajectories of constant phase lines define the direction of wave propagation (Huygen's principle) and along these lines a moving particle experiences no change of phase. Let this characteristic curve be denoted by the function $s(\underline{x})$ (Courant and Hilbert, 1968), where s represents the arc length along the curve. Then a particle travelling a distance ds in the time interval dt along such a curve, moves with the phase speed

$$c = \frac{ds}{dt}\,. \tag{3.2.27}$$

Consequently, the cartesian coordinates of a particular ray can be expressed as $x = x(s)$, $y = y(s)$. Taking the derivative with respect to s gives the direction cosines of the ray,

$$\frac{dx}{ds} = \cos\theta\;; \qquad \frac{dy}{ds} = \sin\theta\;. \tag{3.2.28}$$

Total differentiation along the ray may be expressed in terms of partial derivatives along the fixed cartesian coordinates (x,y),

$$\frac{d}{ds} = \frac{dx}{ds}\frac{\partial}{\partial x} + \frac{dy}{ds}\frac{\partial}{\partial y} \quad . \tag{3.2.29}$$

Applying (3.2.29) to the direction θ and using (3.2.28) yields

$$\frac{d\theta}{ds} = \cos\theta \frac{\partial\theta}{\partial x} + \sin\theta \frac{\partial\theta}{\partial y} \quad . \tag{3.2.30}$$

This is readily recast to denote the spatial curvature of θ upon substitution from (3.2.26)

$$\frac{d\theta}{ds} = -\frac{\sin\theta}{k}\frac{\partial k}{\partial x} + \frac{\cos\theta}{k}\frac{\partial k}{\partial y} \quad . \tag{3.2.31}$$

Since, from the dispersion relation (3.2.9), we have

$$\frac{\partial k}{\partial x} = \frac{\partial}{\partial x}\left(\frac{\omega}{c}\right) = -\frac{\omega}{c^2}\frac{\partial c}{\partial x} = -\frac{k}{c}\frac{\partial c}{\partial x}$$

and

$$\frac{\partial k}{\partial y} = \frac{\partial}{\partial y}\left(\frac{\omega}{c}\right) = -\frac{\omega}{c^2}\frac{\partial c}{\partial y} = -\frac{k}{c}\frac{\partial c}{\partial y}$$

we can rewrite (3.2.31) as

$$\frac{d\theta}{ds} = \frac{1}{c}\left(\sin\theta \frac{\partial c}{\partial x} - \cos\theta \frac{\partial c}{\partial y}\right) \tag{3.2.32}$$

Therefore, making use of the above, (3.2.25) may equivalently be written as

$$-\frac{\partial\omega}{\partial \underline{x}} \cdot \frac{\partial\theta}{\partial \underline{k}} = \frac{c_g}{c}\left(\sin\theta \frac{\partial c}{\partial x} - \cos\theta \frac{\partial c}{\partial y}\right) \tag{3.2.33}$$

Introducing (3.2.33) in (3.2.22) and dividing by c_g, we finally have

$$\frac{1}{c_g}\frac{\partial}{\partial t}(cc_gE) + \cos\theta\,\frac{\partial}{\partial x}(cc_gE) + \sin\theta\,\frac{\partial}{\partial y}(cc_gE) + \frac{1}{c}\left(\sin\theta\,\frac{\partial c}{\partial x} - \cos\theta\,\frac{\partial c}{\partial y}\right)\frac{\partial}{\partial\theta}(cc_gE) = \frac{2\pi\omega}{c_g}S \qquad (3.2.34)$$

It should be remarked that the set of parametric equations (3.2.28) and (3.2.32) completely specify the ray paths in a non-homogeneous medium, as described by (3.2.9). Furthermore, (3.2.28) is equivalent to (3.2.5), since the direction of the group velocity $\underline{c}_g$ is identical with the direction of the phase velocity $\underline{c}$, if no mean currents are present. The physical significance of this fact is that both the waves and their associated energies propagate along the same trajectories. This is not true for the case when waves advance into regions where the medium is moving too.

For steady state (3.2.34) simplifies

$$\frac{d}{ds}(cc_gE) = \frac{2\pi\omega}{c_g}S \qquad (3.2.35)$$

which is the equation solved by Collins (1972) for cases of irregular bottom contours. When S = 0, the result of Longuet-Higgins (1957) is easily recovered, i.e.,

$$cc_gE = \text{constant} \qquad (3.2.36)$$

An equivalent form of writing (3.2.34) is presented by Krasitskiy (1974),

$$\frac{\partial e}{\partial t} + c_{g_i}\frac{\partial e}{\partial x_i} - c_g\left(\sin\theta\,\frac{\partial\Xi}{\partial x} - \cos\theta\,\frac{\partial\Xi}{\partial y}\right)\frac{\partial e}{\partial\theta} = T_e \qquad (3.2.37)$$

where $e \equiv e(\omega,\theta,\underline{x},t) = c_g E(\omega,\theta,\underline{x},t)$ and $\Xi = \ell n\ k$.

In general, the evolution of the energy spectrum in waters with varying bottom topography can only be solved by numerical techniques, such as integration along the ray paths or by finite difference methods. Analytical solutions of the spectral development are contingent on simple geometries of the sea bottom. To demonstrate this, let us consider a narrow coastal zone, where the bottom contours are essentially straight and parallel to the shore line. Furthermore, suppose that either the time of the wind acting on the waves or the fetch is short, and that energy fluxes into or out of the waves due to air-sea and sea-bottom interactions are presumed to be small enough and so can be neglected together with any redistribution of energy within the spectrum due to nonlinear wave-wave interactions. Then, it is reasonable to set $S = 0$ and by assuming a steady-state wave field, (3.2.34) takes the reduced form,

$$\cos\theta \frac{\partial}{\partial x}(cc_g E) - \frac{\sin\theta}{c}\frac{\partial c}{\partial x}\frac{\partial}{\partial \theta}(cc_g E) = 0 \qquad (3.2.38)$$

Furthermore, we restrict ourselves to outside the surf zone, and neglect any effects due to reflection from the shore. Then, (3.2.38) represents only the advection and refraction effects. A solution of (3.2.38) can be obtained from the method of characteristics. The resulting two equations are:

$$\frac{d\theta}{dx} = \frac{\tan\theta}{c}\frac{dc}{dx} \qquad (3.2.39)$$

and

$$\frac{d}{dx}(cc_g E) = 0 \qquad (3.2.40)$$

The last equation is familiar and yields the solution

$$E(f,\theta,x) = \frac{c_o c_{g_o}}{c c_g} E_o(f,\theta_o) \tag{3.2.41}$$

where the subscript o refers to a point, say $x = x_o$, and where the spectrum is known. The first equation can be integrated for an arbitrary c(x) relation and gives

$$\ell n \sin\theta = \ell n\, c + \text{constant}$$

or

$$\frac{\sin\theta}{c} = \text{constant} \tag{3.2.42}$$

This is the familiar statement of Snell's Law. With the above result, we can write (3.2.41) as

$$E(f,\theta,x) = \frac{c_o c_{g_o}}{c c_g} E_o(f,\sin^{-1}[\frac{c_o}{c}\sin\theta]) \tag{3.2.43}$$

and in partilcular, if the origin is in deep water, we obtain from (3.2.43), (3.2.9) and (3.1.41)

$$E(f,\theta,x) = K^2(\omega_h) \cdot E_o(f,\sin^{-1}[\frac{c_o}{c}\sin\theta]) \tag{3.2.44}$$

where

$$K^2(\omega_h) = \frac{\chi^2(\omega_h)}{1 + \omega_h{}^2(\chi^2(\omega_h) - 1)} \quad . \tag{3.2.45}$$

Several observations can be made about (3.2.44). One feature is that the coefficient $K^2(\omega_h)$ represents the combined effect of refraction and shoaling. Figure 3.13 shows a plot of $K^2(\omega_h)$. In depths corresponding to values of $\omega_h \leq 1$, which are typical for coastal regions, $K^2(\omega_h)$ rapidly increases beyond unity. This simply implies that the shallow water spectrum ordinates are substantially larger than their connected deep water ones.

The second fact inferred from (3.2.44) requires that the inequality

$$\frac{c}{c_o} \sin\theta_o \leq |1| \tag{3.2.46}$$

must be satisfied. Returning to our example, we note that the phase velocity monotonically decreases with decreasing depth. This is the case for waves propagating towards shallow coastal areas. At fixed frequency f and incident angle θ, c is always less than c_o and if (3.2.46) is initially true, it will remain so. However for certain combinations (f,θ_o,x_o), (3.2.46) can be violated. The meaning of this is that this spectral component is not present at location x. Hence, we put $E(f,\theta,x) = 0$ for this particular set (f,θ_o,x_o). Conversely, if the waves travel towards deeper water, then the left-hand side of the inequality (3.2.46) increases up to $\sin\theta_o$ and the condition is always met. Depending on the incident angle, some waves escape into deeper water, whereas others are turned back again. The later situation is analogous to the optical phenomenon of total internal reflection. The location where this occurs is called a "turning point", and the wave ray becomes asymptotically tangent to the

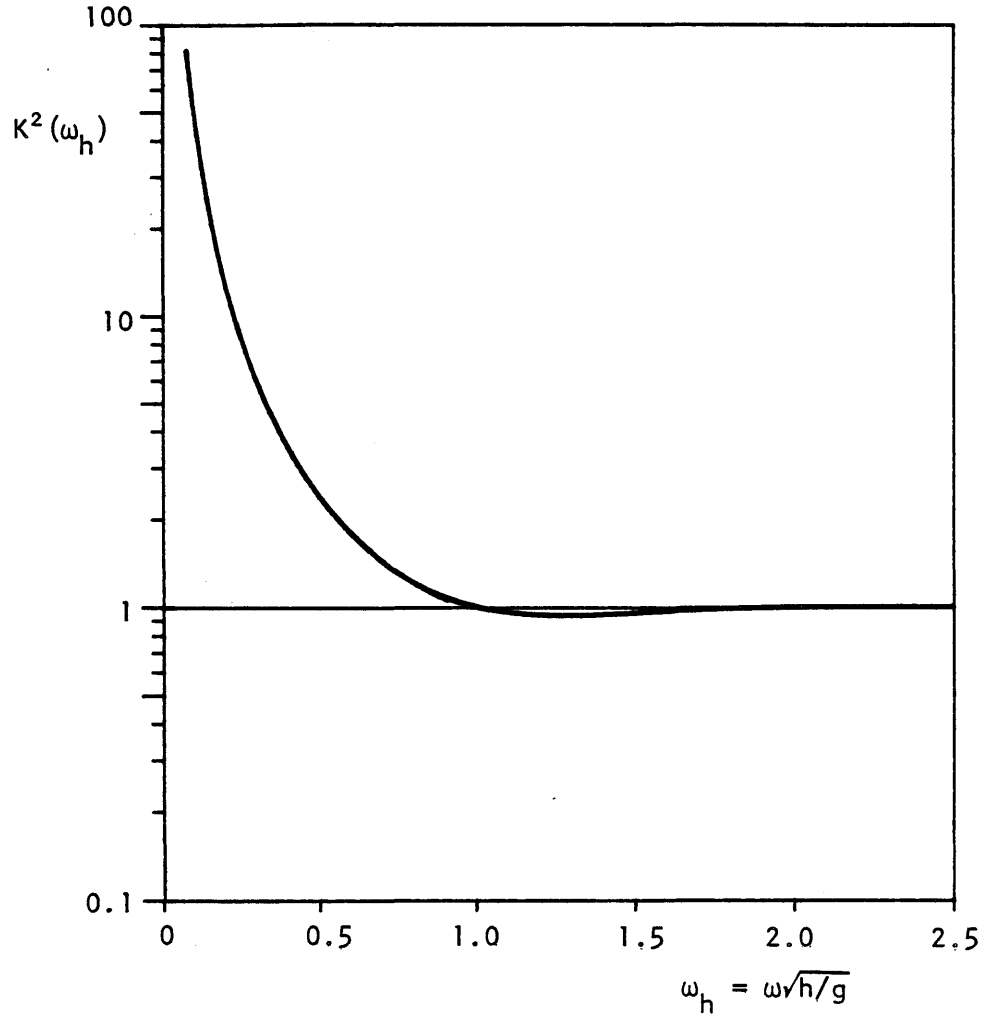


Fig. 3.13 The depth-dependent spectral ordinate factor $K^2(\omega_h)$.

underlying bottom contour. The line formed by many such points is the envelope of all these rays and is known as a caustic. It is well known from linear theory of monochromatic waves that in the vicinity of a caustic the geometrical-optics approximation breaks down. The wave heights grow without limit at a caustic. In order to overcome this inadequacy of the ray approximation, within the caustic region, a finite value of the wave amplitude may still be obtained by treating the monochromatic wave field as a boundary-layer type of problem. A theoretical development of this type for surface gravity waves was presented by Chao (1971), and experimental confirmation for simple bottom geometries can be found in Chao and Pierson (1972). A wide variety of problems concerned with wave refraction, due to slowly varying depth contours and currents, is excellently treated in Mei (1983).

Returning to a windsea spectrum with many different f and θ values, the above suggests that each pair of (f,θ) values has its own caustic. Hence, the entire spatial region must contain numerous caustics. But from relation (3.2.44) we know that as long as the depth is finite, the shallow water spectral density is bounded by $K^2(\omega_h)$ times the deep water spectral density. Therefore, it readily follows that (3.2.44) never becomes singular, even at (f,θ) values where monochromatic wave theory would predict infinite heights.

One might ask, what has happened to all these anomalies associated with caustics? If we consider, in an analytical sense, $E(f,\theta)$ and $E_o(f,\theta_o)$ as continuous surfaces in the frequency-direction plane, we realize that each caustic shows up as a local plateau of finite but small area. Thus, their contributions to the integrals of $E(f,\theta)$ with

respect to f and θ are relatively insignificant. The primary merits, using a spectral refraction approach for wind waves, are that the results are always bounded for coastal areas with finite depths. The problems associated with converging or crossing wave rays [i.e., caustics] are simply interpreted to mean that waves with spectral components (f_1, θ_1) propagate along different ray paths than waves with components (f_2, θ_2). Typical examples of a conventional refraction diagram and the reverse projection technique of Dorrestein (1960) are shown in Figure 3.14.

Karlson (1969) solved equation (3.2.34) for steady-state conditions and no source terms by finite differences for geometries of straight coastlines with a uniform bottom slope and for concave, straight and convex coastlines with a curved depth profile. Abernethy and Gilbert (1975) applied the form of spectral transformation given by Longuet-Higgins directly. In order to determine the wave field at some selected point inshore, they computed for all chosen combinations (f,θ) the rays trajectories emanating out to deep water. Since refraction is reversible (Dorrestein, 1960), this provided a method to find the corresponding deep water direction θ_o. If in deep water a directional spectrum is known along the whole offshore boundary, then the shallow water directional spectrum can be constructed quite easily. An excellent review on the state-of-the-art for refraction methods of wave spectra can be found in Dingemans (1978).

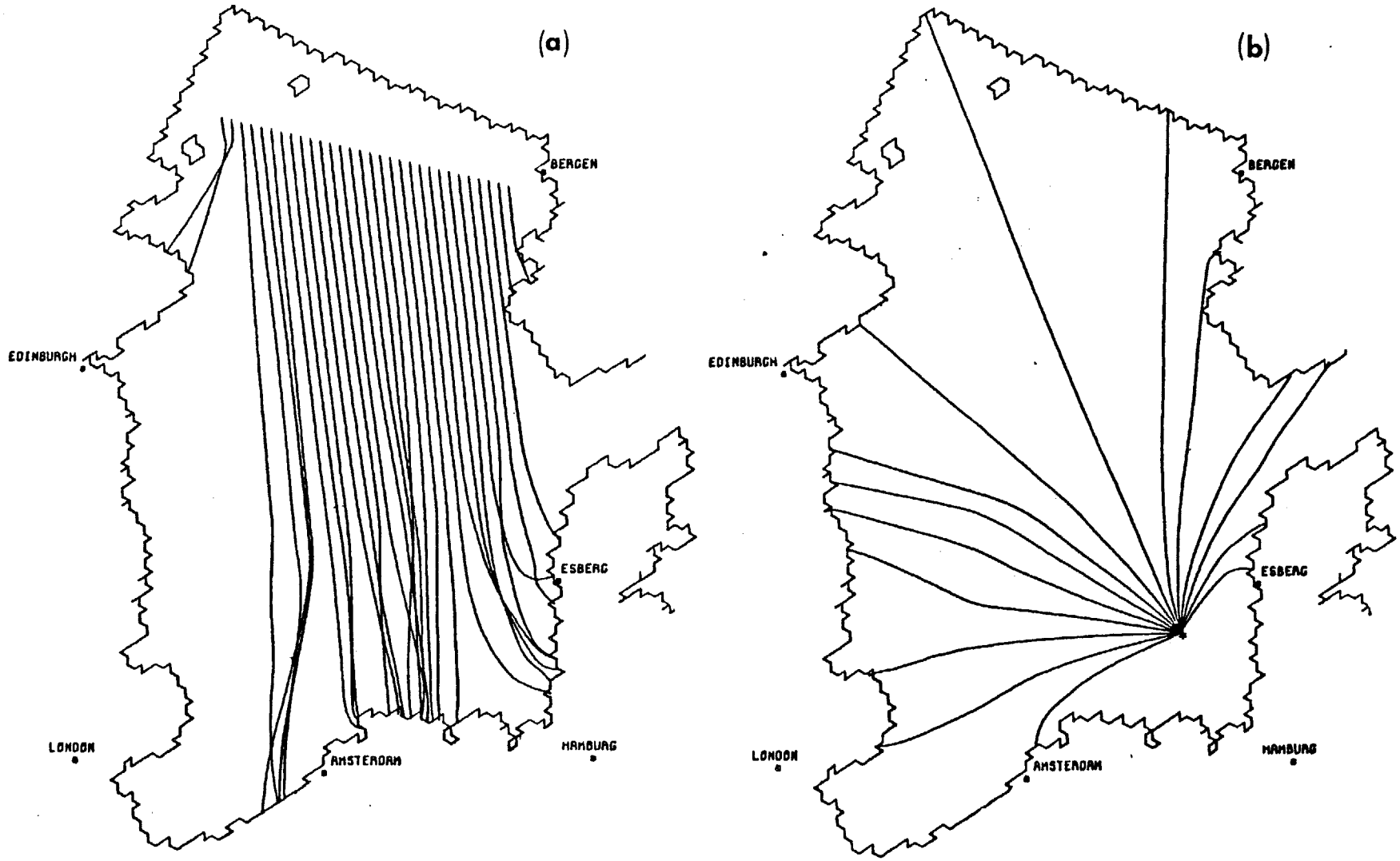


Fig. 3.14 Examples of wave refraction in the North Sea for a wave period T = 10 s. (a) convectional refraction diagram; (b) reverse ray projection.

3.3 Generation And Dissipation Of Wave Energy

The growth and decay of surface waves is the result of various physical, linear and nonlinear processes transferring energy to and from the wave field as well as redistributing energy within the spectrum itself. These processes are due to two distinguishable types of interactions: external interactions, involving both the components of the wave field and the external field, and internal or wave-wave interactions, involving wave components only. The dominant external interactions in the context of ocean wave models can be identified as wave-atmosphere, wave-bottom, and wave-ocean interactions. The major process of the wave-atmosphere interactions is the flux of energy from the wind. Interactions between the waves and the ocean are represented by wave-current refraction and the dissipative mechanism due to white-capping. In finite depth water the waves are affected by numerous wave-bottom interactions which can be of different importance depending on the depth and seabed properties. These mechanisms include refraction, shoaling, bottom friction, percolation, bottom scattering and bottom motion. Wave-wave interactions are prominent processes both in deep and shallow water. Following Hasselmann (1968) we assume that the net source function S can be expressed by the linear superposition of all individual source terms S_i, i.e., $S = \sum_i S_i$. These source terms and others are discussed in a full theoretical context by Hasselmann (1968). However, here we will present only a summary of the various mechanisms and describe recent theoretical and empirical results and their possible importance for wave prediction models.

3.3.1 Energy Flux From The Wind

Wave generation takes place in several phases. The first phase of wave growth is due to random normal pressure fluctuations of a turbulent wind over a calm ocean surface. This is the mechanism considered by Phillips (1957), who found that wave growth should be considered in two stages: the "initial" stage and the "principal" stage, where the elapsed time is respectively much less or much greater than the time scale associated with the development of the pressure fluctuations. The initial stages of development are characterized by ripples or capillary-gravity waves of wave length L_r = 1.7 cm. Two notable features of these waves are readily observed on any water surface. For one, the rhombic pattern they form is a consequence that the prominent waves move in the two directions $\cos^{-1}(c_m/U_a)$, where $c_m = (4g\,\sigma_w/\rho_w)^{1/4}$ is the minimum phase speed of the 1.7 cm waves and U_a is an average wind speed at a height, of approximately L_r above the sea surface. Two, if the wind would suddenly cease to blow, these ripples would die out quite rapidly, since at this stage of growth they still are under the influence of capillary effects.

The greatest growth occurs in the principal stage, when the speed of a surface pressure component is now locked to the phase velocity of the free surface wave of the same wave number. Resonance provides continuous growth of the waves. The resulting induced spectral growth is constant and increases linearly with time until the wave slopes become large enough that nonlinearities, which are ignored in the theory, become important.

However, Phillips' theory could not supply the necessary rate of growth observed in wind waves. Longuet-Higgins (1961) pointed out that pressure fluctuations were much smaller than those originally considered by Phillips in his theoretical evaluations. Also attenuation of waves by adverse winds could not be explained by the resonance theory. Yet, the resonance mechanism is still significant, since this provides an efficient way by which waves can be generated on an initially flat ocean surface. Wave development continues to a level, where more effective growth processes can take over.

The second phase of wave generation is attributed to Miles (1957) who considered an instability mechanism coupling the wave field and the mean boundary layer flow. In a series of papers, Miles (1959a,b, 1960, 1962) developed his shear flow instability model as an improvement over the classical Kelvin-Helmholtz models (Kelvin, 1887 and Helmholtz, 1888).

Suppose air is flowing over a wavy sea surface, which in turn deforms the immediate streamlines of the otherwise plane, parallel air flow above so that they take on a similar wavy image (Figure 3.15). The induced pressure disturbance in phase with the wave slope does work on the waves, and consequently transfers energy to the moving waves. Although the problem statement was quite general, an analytical solution was only feasible for an idealized situation. To proceed, Miles needed to make the following assumptions: the air motion is quasi-laminar, inviscid and incompressible and in the absence of any waves, the mean wind speed had a prescribed profile as a function of height; the turbulent fluctuations, necessary to maintain the mean shear flow, were neglected in the coupling of wind and waves. In

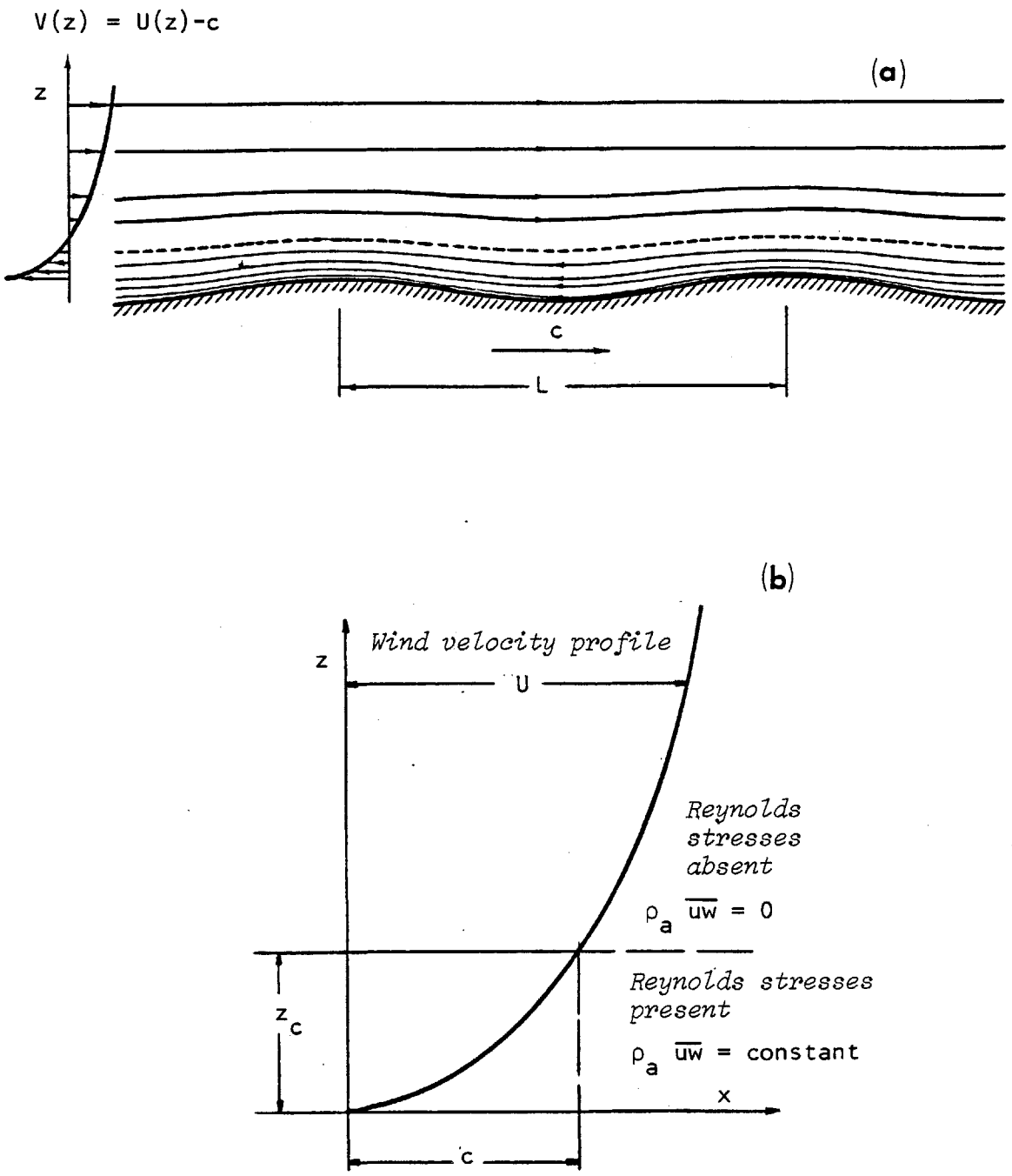


Fig. 3.15 (a) The streamline pattern in a shear flow above a wavy surface.
(b) The critical layer according to Miles' theory.

addition the water motion was also assumed to be inviscid, irrotational and incompressible, as well as the wave slopes were supposed to be small enough so nonlinear terms can be disregarded. Furthermore, any drift motions in the waters induced by the wind are ignored. The resulting energy flux to the waves from this coupled mechanism yields an exponential growth rate for the wave spectrum.

Later observations, however, indicated that the transfer of wind energy to waves in an open ocean exceeded the theoretical transfer of Miles' mechanism by at least an order of magnitude. In addition, the mathematical description of Miles' shear flow model entails too many difficulties which prevents a clear understanding of the physics involved as in the case of Kelvin-Helmholtz theory. Lighthill (1962) made an important contribution by giving a physical explanation of the shear flow model in terms of fluid concepts. However, it is possible to improve on Miles' original theory as progress is made, not only in terms of measuring techniques, but also in our advancement in solving more complicated problems. West and Seshardri (1981) generalized the Miles-Phillips process to include fluctuations of the air-sea coupling parameter. Although their growth rates were still not sufficient to match those observed, the increased rates were higher than the ones predicted by Miles' model. Janssen (1982) considered a quasi-linear approximation for wind-wave spectrum and thereby extended the validity of Miles' calculations to permit the analysis at large time.

Nevertheless, it appears that both the Phillips and Miles mechanism must play an active role in generating wind waves, but each dominating at different times during the growth stages. While the

resonance model of Phillips provides the initial broad energy transfer to the waves, the shear flow model of Miles continues the influx of energy via a linear frequency-selective feedback mechanism. Miles (1960) took the next step by combining both mechanisms into one model. An equivalent expression for the wave number density spectrum resulting from this model is given by Phillips (1977) as

$$F(\underline{k},t) = \frac{\pi P(\underline{k},\omega)}{\rho_w^2 c^2} \left[\frac{\sinh(\xi\omega t)}{\xi\omega}\right] \qquad (3.3.1)$$

where $P(\underline{k},\omega)$ is the wave number-frequency spectrum of the pressure fluctuations, c is the phase speed of the waves at wave number $\underline{k}$ and ξ is a dimensionless air-sea coupling parameter representing the fractional increase in wave energy per radian. From the above equation the principal results of the Miles-Phillips model can be deduced. Let $T \equiv (\xi\omega)^{-1}$ mark the time when a component reaches the transition where the growth changes from a forced to an unstable mode.

Thus, it follows from (3.3.1) that when the wind duration t is small compared with T, the prevailing active mechanism of wave growth is only due to the influence of the pressure fluctuations. The wave spectrum develops linearly with time,

$$F(\underline{k},t) = \frac{\pi P(\underline{k},\omega)}{\rho_w^2 c^2} t \qquad \text{for } \xi\omega t \ll 1 \qquad (3.3.2)$$

As the winds prolong and t becomes large, hence $\xi\omega t$ surpasses beyond unity, the induced surface stress becomes effective, creating a feedback link. The continuous flux of energy yields a more rapid

growth rate, which is reflected by an exponential time dependence of the wave spectrum,

$$F(\underline{k},t) = \frac{\pi P(\underline{k},\omega)}{\rho_w^2 c^2 \xi\omega} e^{\xi\omega t} \qquad \text{for } \xi\omega t >> 1 \qquad (3.3.3)$$

Figure 3.16 illustrates schematically the two growth rates for a single wave component. Contrary to past beliefs, the linear and subsequently exponential wave growth is not succeeded by a gradual transition to its ultimate equilibrium level. Barnett and Sutherland (1968) found from spectral measurements of growing waves that the Miles-Phillips region is followed by a pronounced "overshoot" beyond its eventual equilibrium value and then decays back (see Figure 3.16). The rapid decay indicates that a nonlinear process might be the responsible cause for this phenomenon. Such a process could possibly be nonlinear wave-wave interactions, which exhibit typically a positive energy transfer to frequencies lower than the spectral peak and a negative transfer on the high-frequency side.

Combined, the two wave generation processes are commonly known as the Miles-Phillips mechanism and because both the resonance and shear flow model are linear, the total input of energy from the wind is usually written as the sum of two concurrently acting processes

$$S_{in} = S_1 + S_2 \qquad (3.3.4)$$

Hasselmann (1960) has shown that S_1 is related to a linear growth parameter α^*

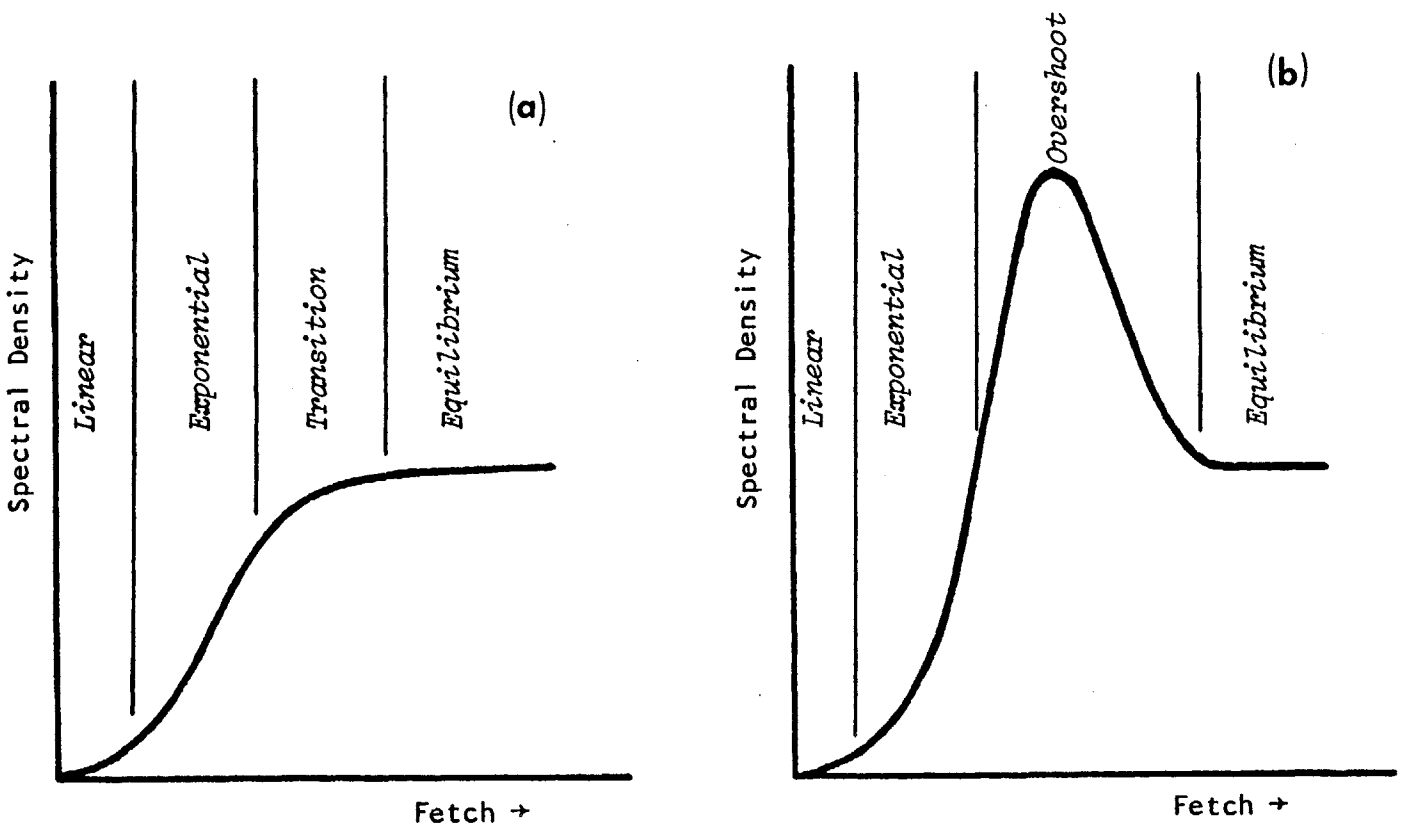


Fig. 3.16 Schematic growth curves. (a) Conventional spectral growth according to a Phillips-Miles mechanism; (b) spectral growth including a nonlinear effect possibly due to wave-wave interactions. (From Barnett and Sutherland, 1968).

$$S_1 = \frac{\pi P(\underline{k},\omega)}{\rho_w^2 c^2} = \alpha^* . \qquad (3.3.5)$$

Similarly, S_2 can be represented by

$$S_2 = \xi\omega F(\underline{k},t) = \beta^* F(\underline{k},t) \qquad (3.3.6)$$

where β^* is the exponential growth parameter, and is the subject of numerous experiments both in the field and laboratory. Hence, the source function of the atmospheric input is generally written as

$$S_{in} = \alpha^* + \beta^* F(\underline{k},t) \qquad (3.3.7)$$

where the coefficients α^* and β^* are assumed to have known functional dependencies on the wind field.

The two pioneering field experiments, directed to investigate Miles' theory, were carried out by Snyder and Cox (1966) and Barnett and Wilkerson (1967). The major conclusion reached from both data sets was that Miles' (1957) theory was consistently underpredicting the observed wave growth by at least one order of magnitude. The initial phase of wave growth was found to be in good agreement with observations. Additional field measurements (Barnett and Sutherland, 1968; Schule, et al. 1971; Ross, et al., 1971; Dobson, 1971; Elliot, 1972; Snyder, 1974; Dobson and Elliot, 1978) and laboratory experiments (Shemdin and Hsu, 1967; Bole and Hsu, 1969) could only verify in a qualitative manner Miles' exponential growth theory. From their data, Snyder and Cox (1966) determined an empirical form for the exponential growth parameter

$$\beta = c_* \frac{\rho_a}{\rho_w} (\underline{k} \cdot \underline{U} - \omega) \ . \qquad (3.3.8)$$

This functional form seemed to fit well all subsequently observed growth rates. However, the large discrepancies in the value of c_* (0.1 - 1) a nondimensional coefficient related to the portion of momentum flux into the waves, stimulated new discussions. Since c_* appears to be very sensitive to the choice of drag coefficients when calculating the momentum transfers, a possible explanation for the large variation in c_* could be measurement accuracy.

In a recent experiment by Snyder et al. (1981) careful measurements were made to resolve this question. A generally accepted parameterization of Miles' mechanism for use in wave prediction models, based on the results of Snyder et al. (1981), is given by

$$S_{in} = 0.2 \frac{\rho_a}{\rho_w} \omega \left[\frac{\underline{k} \cdot \underline{U}}{\omega} - 1\right] F(\underline{k}) \qquad \text{for } \frac{\underline{k} \cdot \underline{U}}{\omega} > 1$$

$$= 0 \qquad \text{for } \frac{\underline{k} \cdot \underline{U}}{\omega} < 1 \qquad (3.3.9)$$

It should be noted that this formulation is valid in any water depth, since the growth rate parameter β depends only on the ratio U/c, where $c = \omega/k$ is the wave phase speed.

The most recent experimental investigation of fetch-limited wave growth was performed by Kahma (1981), who derived a growth-rate parameter β for a f^{-4} spectrum which is different than the empirical relation (3.3.8). Figure 3.17 shows a comparison of dimensionless growth parameters β from Kahma (1981), Benilov et al. (1978a,b) and Snyder and Cox (1966) with data.

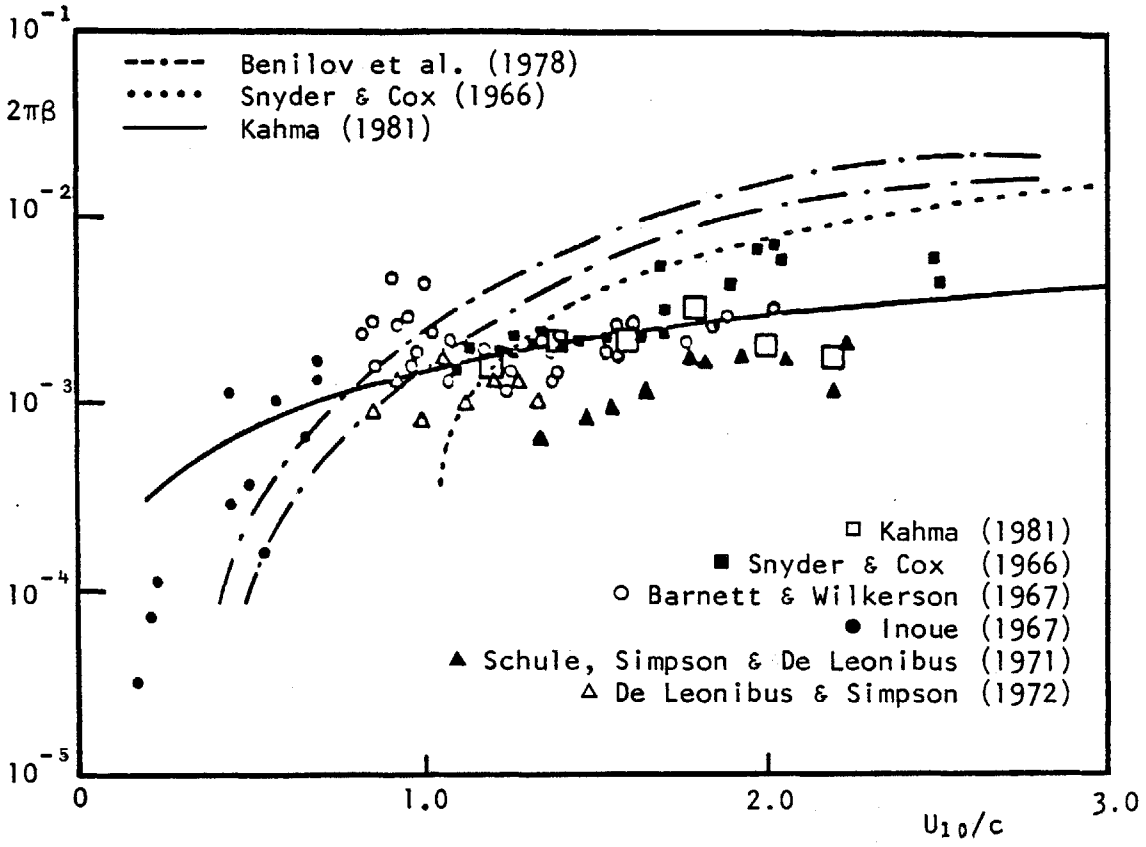


Fig. 3.17 Dimensionless growth rate parameter vs. dimensionless wind speed. (From Kahma, 1981).

Although a wave component acquires most of its energy in the second stage of development where rapid, exponential growth takes place, the wave does not continue to grow indefinitely. Eventually a time will be reached, where nonlinearity and other processes either dominate or place a limit on wave development. This limiting process, as will be discussed in a later section, is wave breaking, which is predominantly found in the high-frequency range of the spectrum. Another process is triggered, when the fetch or duration of the wind gets large, so that lower frequencies are engulfed by this phase of rapid growth. Now wave-wave interactions prevail and produce a nonlinear energy transfer within the spectrum, whereby energy is removed from the central region of the spectrum (around the peak) and transported to lower and higher frequencies. This redistribution of energies, by itself causing an exponential growth, progressively shifts the spectral peak to lower frequencies. The wave-wave interaction process is recognized to explain adequately some more features during the active growth stages of wind-generated waves.

3.3.2 Nonlinear Energy Transfer And Wave-Wave Interactions

The existence of a nonlinear mechanism during the growth stages of surface gravity waves has been conjectured for a long time. The necessary theoretical development and experimental confirmation proceeded at an incremental pace with many researchers working on this problem. An enjoyous and readable essay on the history of weak resonant wave interactions was written by Phillips (1981), who contributed significantly to shape a mere idea into an extensively applied phenomenon in a variety of geophysical contexts.

For ocean surface waves, the nonlinearity is introduced by the surface boundary conditions. Stokes (1847) investigations demonstrated that individual waves may distort and appear with sharper crests and flatter troughs due to finite amplitude limitations. This nonlinear effect can be shown to result from a small perturbation on the linear solution. As long as these nonlinear terms are small, the response is only seen in the bounded second-order distortions of the wave profile. As perturbation parameter the wave slope, $\mu = ka$, is used, which gives a measure of the nonlinearity. Hence, the smaller the wave slope, the progressively smaller will be the contribution of the nonlinear terms in successive expansion approximations. In terms of Fourier components this means that harmonics of the fundamental wave are generated and if the spectrum is narrow-banded, secondary peaks may occur at multiples of the fundamental mode. Tick (1959) carried out a second-order perturbation analysis for a random gravity wave field to explain a secondary spectral peak, which was observed during the Stereo-Wave

Observation Project (Chase et al., 1957). Kinsman (1960) observed these as well and made extensive comments about their origin.

In order to alter the wave height, interactions of three wave components are necessary to produce an energy transfer. Phillips (1960) extended the perturbation expansion about the linear solution to third order. At this point Phillips found that under certain resonance conditions unsteady excitations were possible to produce a linear growth in a third wave of the interacting triad. These interactions, however, could not describe the energy transfer in wind-generated wave spectra. A fourth-order analysis was necessary to examine the effect of resonantly interacting wave components in a continuous surface gravity wave spectrum. In a series of three papers, Hasselmann (1962, 1963a,b) derived the theoretical formulation that permitted calculation of nonlinear energy transfer rates in a random wave field. These weakly nonlinear wave-wave interactions could only take place when the following resonance conditions were identically or almost satisfied,

$$\begin{aligned} \underline{k}_1 + \underline{k}_2 &= \underline{k}_3 + \underline{k}_4 \\ \omega_1 + \omega_2 &= \omega_3 + \omega_4 \end{aligned} \qquad (3.3.10)$$

and $$\omega_j = (gk_j)^{1/2} \quad .$$

The details involved in deriving an expression for the energy exchange among ocean surface wave components are complicated and the reader is referred to Phillips (1977) and West (1981) for a more complete account. In summary, the transfer integral, expressing the nonlinear interactions between the components of a gravity wave spectrum has the form

$$\frac{\partial F(\underline{k}_4)}{\partial t} = \iiint_{-\infty}^{+\infty} [F_1F_2(\omega_4F_3 + \omega_3F_4) - F_3F_4(\omega_2F_1 + \omega_1F_2)]$$

$$\times \; Q\,\delta(\underline{k}_1 + \underline{k}_2 - \underline{k}_3 - \underline{k}_4)\,\delta(\omega_1 + \omega_2 - \omega_3 - \omega_4)$$

$$\times \; d\underline{k}_1\, d\underline{k}_2\, d\underline{k}_3 \qquad (3.3.11)$$

and $Q = \pi\omega_4(3g^2D/2\omega_1\omega_2\omega_3\omega_4)^2$ where D is the coupling coefficient and $F_i = F(\underline{k}_i)$ is the variance spectrum at wave number $\underline{k}_i$. Qualitatively, the nonlinear transfer integral can be interpreted as the interaction process of a wave number tetrad which under certain resonance conditions transfers energy from three "active" components to a "passive" fourth component. These resonant interactions are also conservative, and in the case of a continuous spectrum, Hasselmann (1963b) has shown that total energy as well as other quantities, are conserved over the entire wave spectrum. This result is very significant since it implies that conservative resonant interactions by themselves can obviously not generate or dissipate wave energy. Then what is their significance with respect to wave dynamics? The major effect of resonant interactions is the provision of a capability to redistribute the energy among the spectral components. Experimental evidence was obtained from the JONSWAP experiment, where the source functions of partially developed wave spectra displayed a typical plus-minus signature (Figure 3.18). The same behavior was also predicted quantitatively by the nonlinear energy flux due to resonant wave-wave interactions (Hasselmann, 1963b). This provided the basis for the importance of the nonlinear interactions during the stages of active wave growth. Now this was the mechanism

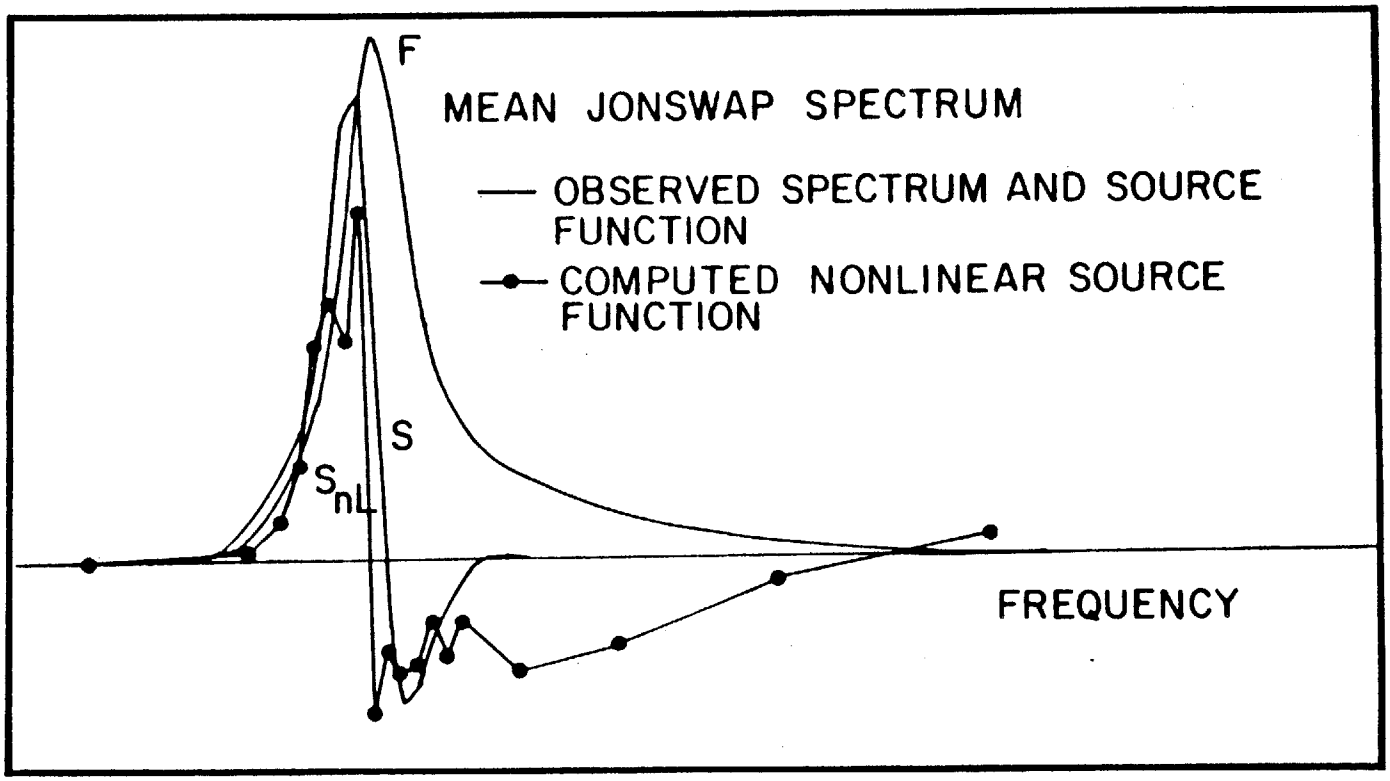


Fig. 3.18 Observed mean JONSWAP spectrum F, net source function S and computed nonlinear transfer S_{nl} for fetch-limited conditions. Frequency and ordinate scales are arbitrary. (From Hasselmann, 1974).

which could redistribute the influx of energy from the wind at the central portion of the spectrum to lower and higher frequencies. Consequently, if the initial spectrum is sharply peaked, the resonant wave-wave interactions will work towards a reduction or broadening of the spectral peak. At the same time, the flux of energy to the low-frequency forward face of the spectrum causes the spectral peak to migrate towards lower frequencies (Figure 3.19). If the energy transfer from the wind into the waves prevails and the energy exchange among the wave components is not fast enough, then the waves will ultimately dissipate their excess energy by breaking. This led to the principal conclusion of JONSWAP (Hasselmann et al. 1973) that the spectral shape is primarily determined by the nonlinear energy transfer mechanism. Furthermore, the evolution of the pronounced spectral peak could be deduced from the self-stabilizing feature of the nonlinear wave-wave interactions.

Before the set of extensive wave growth measurements from JONSWAP two important laboratory tests were independently conducted by Longuet-Higgins and Smith (1966) and McGoldrick et al. (1966) to verify experimentally that resonant wave interactions indeed exist and transfer rates were of the order of magnitude as predicted by theory.

A severe drawback in applying Hasselmann's theory to practical situations is that for a general wave spectrum the formally six-dimensional integral (3.3.11) can only be evaluated numerically (Hasselmann, 1963b; Sell and Hasselmann, 1972; Webb, 1978; Masuda, 1981). Calculations of transfer rates for representative windsea spectra required extensive computing times of the order of minutes. Hence, incorporating the original form of the nonlinear transfer

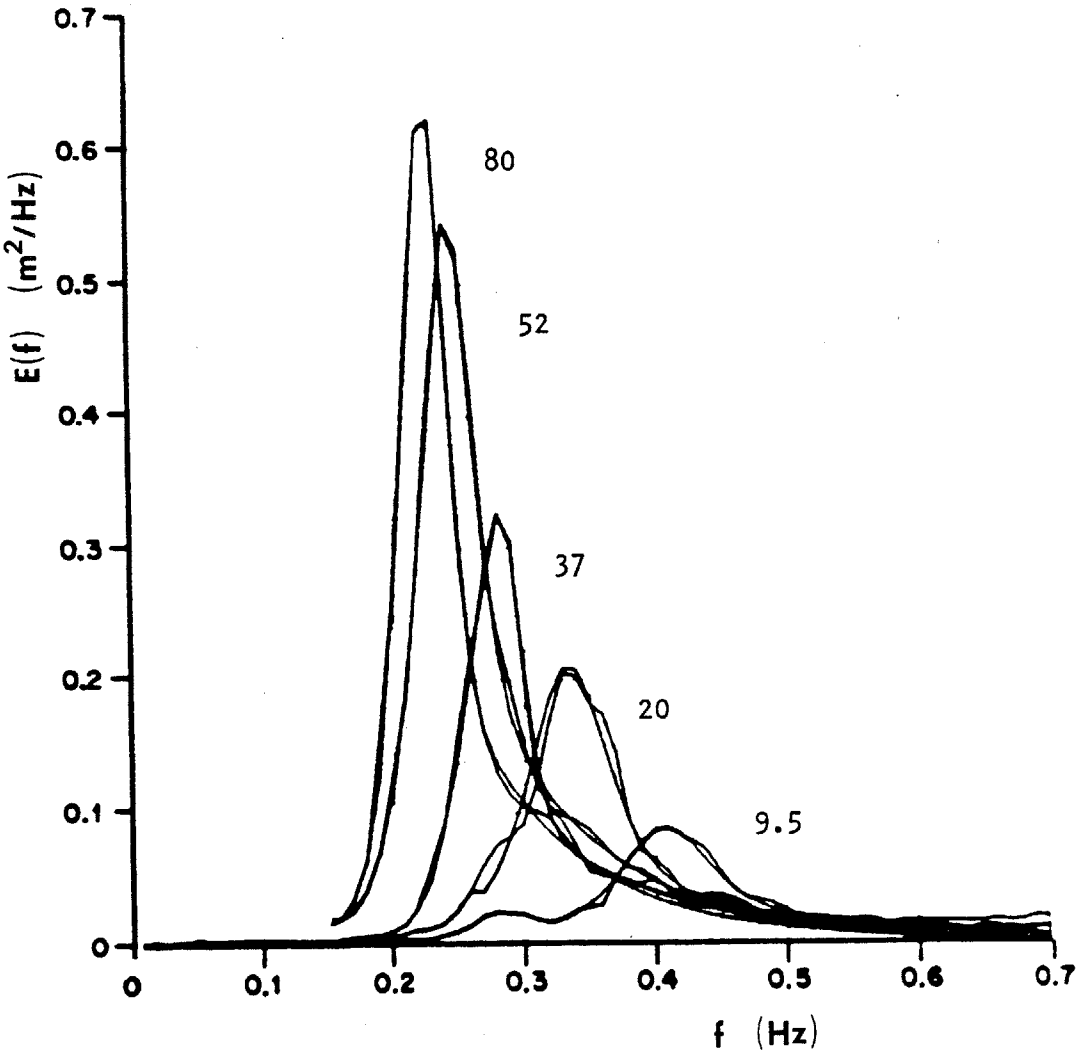


Fig. 3.19 Evolution of wave spectra with fetch for offshore winds during JONSWAP. Numbers refer to fetches in kilometers. (From Hasselmann et al. 1973).

expression in a modern wave prediction model was infeasible, unless the computation speeds could drastically be increased. In the past years this promoted efforts towards either a parameterization of the wave interaction process or an approximation of the transfer integral itself. Both approaches had the ultimate goal to arrive at a suitable expression for wave prediction models.

In the limiting case of a very narrow gravity wave spectrum, Longuet-Higgins (1976) has shown that a simple analytical solution of (3.3.11) is possible. Consider the interactions to be confined to the region around the peak, such that $\underline{k}_1 \approx \underline{k}_2 \approx \underline{k}_3 \approx \underline{k}_4 \approx \underline{k}_m$, where $\underline{k}_m$ is the wave number of the spectral peak. For this case, we obtain for Q in (3.3.11)

$$Q = 4\pi g k_m^5 . \qquad (3.3.12)$$

with $D = D_o = -4/3(\omega_m^8/g^4)$ (Hasselmann, 1963b). This is identical with Longuet-Higgins' result (see Phillips, 1977, eq. 4.4.4), when performing the proper transformation from the wave action density per unit mass defined by $A(\underline{k}) = gF(\underline{k})/\omega$.

Fox (1976) adopted the transfer equation previously derived by Longuet-Higgins (1976) along with the narrow-peak approximation and calculated the flux of energy for the mean JONSWAP and a sharply peaked spectrum (Figures 3.20 and 3.21). Dungey and Hui (1979) also considered narrow-peak approximations but perturbed the coupling coefficient to first order in spectral width. Longuet-Higgins and Fox neglected the effect of spectral width in their analysis. In summary, it can be argued that although these approximations duplicate many of the qualitative features of the exact integral, for quantitative research of windsea spectra the approximations are not adequate.

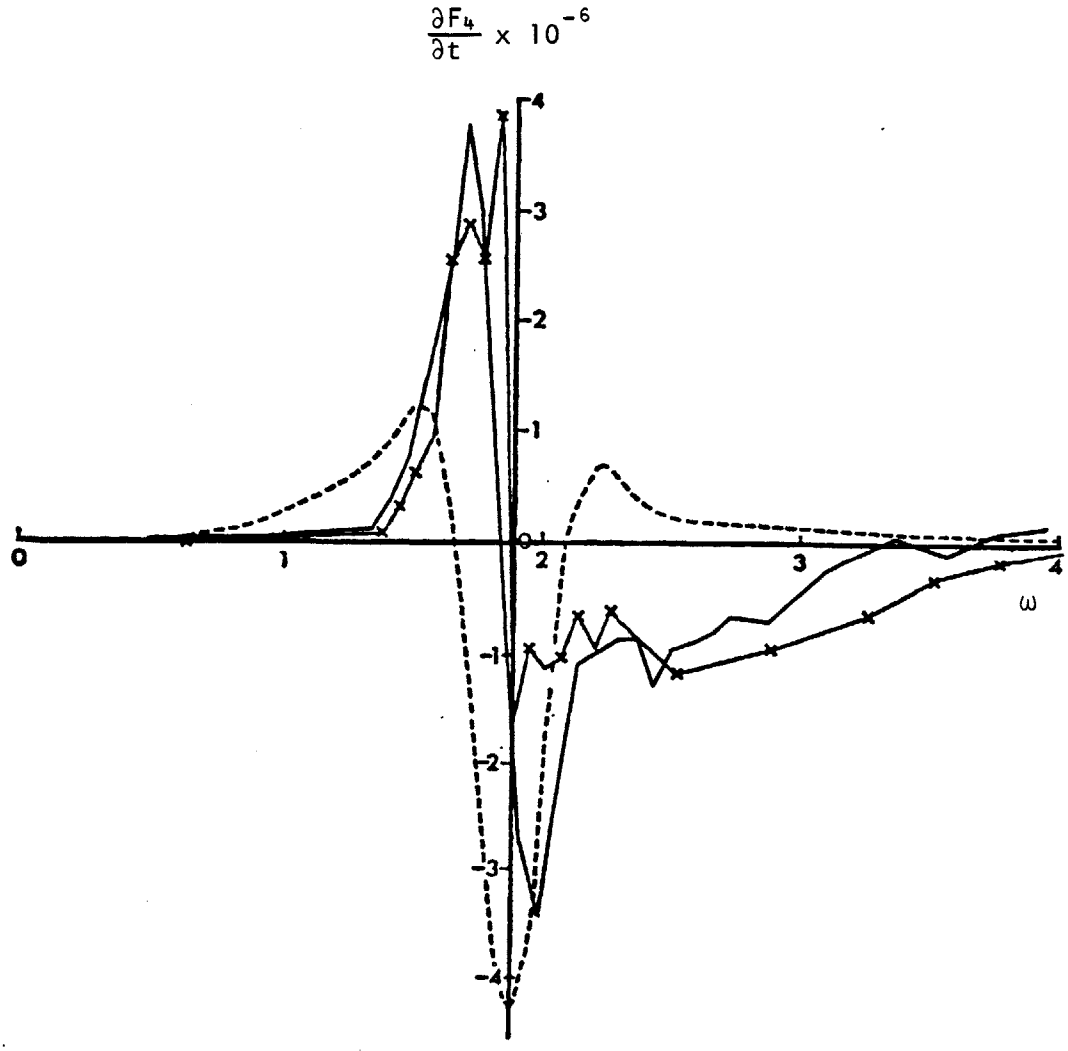


Fig. 3.20 Comparison of nonlinear energy transfer for a mean JONSWAP spectrum (γ = 3.3). Numerical integration by Sell and Hasselmann (x—x); narrow peak approximation by Fox (---); parameterization of exact calculations by Hasselmann and Hasselmann (——).

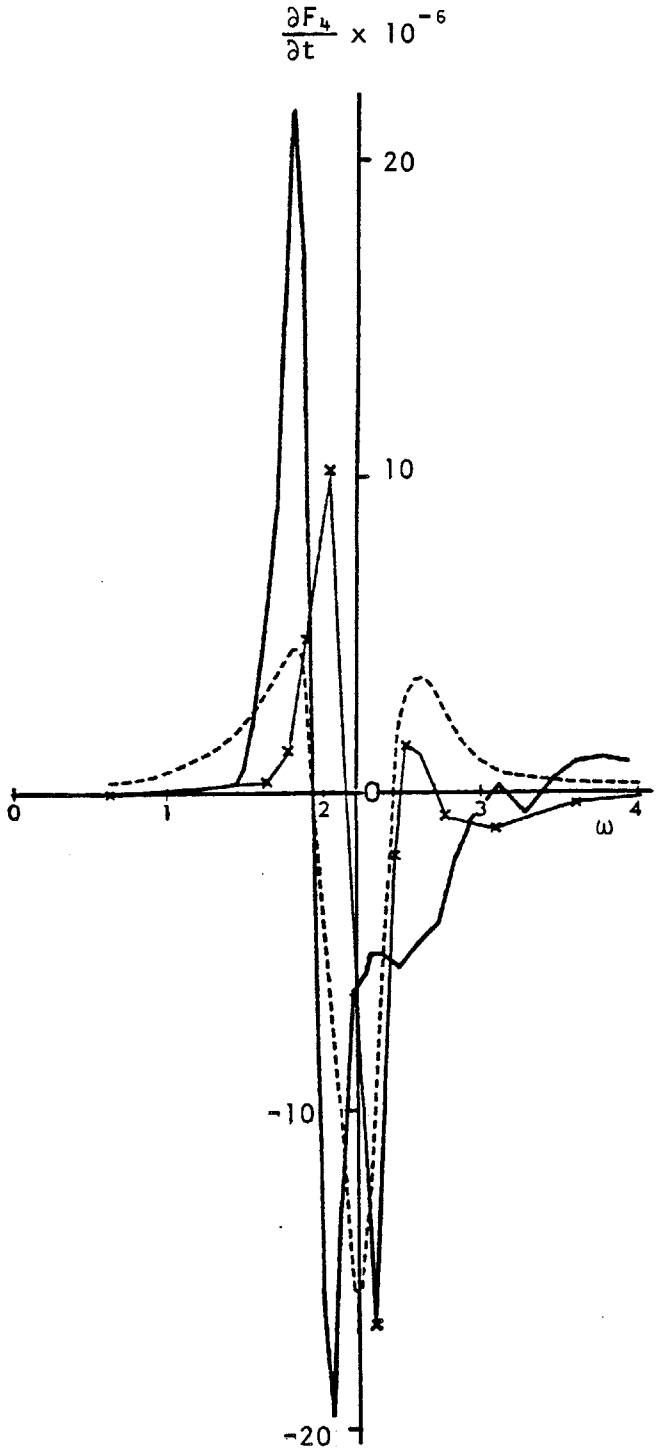


Fig. 3.21 Comparison of nonlinear energy transfer for a sharp JONSWAP spectrum (γ = 7.0). Numerical integration by Sell and Hasselmann (x—x); narrow peak appoximation by Fox (---); parameterization of exact calculations by Hasselmann and Hasselmann (——).

An alternative approach is to develop accurate parameterizations of the exact results. The first step in this direction was taken by Barnett (1966) who proposed to represent the nonlinear interaction mechanism as the sum of two processes. Then, the general expression of the rate of energy transfer is closely described by

$$\frac{\partial E(f,\theta)}{\partial t} \approx \Gamma(f,\theta) - \tau(f,\theta)E(f,\theta) \qquad (3.3.13)$$

where $E(f,\theta)$ is the two-dimensional wave spectrum, $\Gamma(f,\theta)$ characterizes the rate at which the "passive" component receives energy and $\tau(f,\theta)$ denotes the reciprocal of a decay time, or the rate of transfer from the "active" mode. The principal features of the wave field are characterized by the parameters energy, mean frequency and direction, respectively:

$$E_o = \iint E(f,\theta)\,df\,d\theta \qquad (3.3.14)$$

$$f_o = \frac{1}{E_o}\iint fE(f,\theta)\,df\,d\theta \qquad (3.3.15)$$

$$\theta_o = \frac{1}{E_o}\iint \theta E(f,\theta)\,df\,d\theta \qquad (3.3.16)$$

Using dimensional arguments and the general qualitative features of Hasselmann's results, the subsequent functional forms of Γ and τ were deduced,

$$\Gamma(f,\theta) = 4.76\times10^{4}\, f_o^{8}\, E_o^{3}(1 - 0.42p)^{3} \exp[-4(1-p)^{2}+0.1p^{5}]\cos^{4}(\theta-\theta_o)$$

$$\text{for } p = \frac{f_o}{f} < 2.38 \text{ and } |\theta-\theta_o| < \frac{\pi}{2} \qquad (3.3.17)$$

$$= 0, \text{ otherwise}$$

$$\tau(f,\theta) = 8.1\times10^{3}\, f^{9}\, E_o^{\,2}\, p^{7}(1 - 0.53p)^{3}[1 + 16|\cos(\theta-\theta_o|]$$

$$\text{for } p = \frac{f_o}{f} < 1.89 \qquad (3.3.18)$$

$$= 0, \text{ otherwise}$$

These parametric expressions for the nonlinear energy transfer are quite compatible with practical wave prediction schemes. However, their range of application to ocean wave spectra was limited to shapes which were not too different from a fully developed sea. Nevertheless, comparison with partially developed spectra showed reasonably good agreement (Barnett, 1968; Mitsuyasu, 1968; Wu et al., 1977), although the results could be enhanced by including spectral shape factors.

In a similar effort, Ewing (1971) used parametric representations of the wave-wave interactions which have been developed by Cartwright (unpublished) in terms of Fourier-Chebyshev series:

$$\Gamma(f,\theta) = f_1^{\,8}\, p^2\, E_o^{\,3} \sum_{n=0}^{12} \sum_{m=0}^{6} a_{mn}\, T_n(q) \cos m(\theta-\theta_o) \qquad (3.3.19)$$

$$\tau(f,\theta) = f_1^{\,9}\, p^7\, E_o^{\,2} \sum_{n=0}^{12} \sum_{m=0}^{6} b_{mn}\, T_n(q) \cos m(\theta-\theta_o) \qquad (3.3.20)$$

$$\text{for } \frac{1}{2} \leq p \leq \frac{9}{2}$$

with $f_1 = 0.816 f_o$; $p = \frac{f}{f_1}$; $q = \frac{1}{2}(p - 2.5)$; and $T_n(q)$ is the Chebyshev polynomial of degree n and is defined by

$$T_n(x) = \frac{(x + \sqrt{x^2 - 1})^n + (x - \sqrt{x^2 - 1})^n}{2^n} \qquad (3.3.21)$$

The predetermined coefficients a_{mn} and b_{mn} are given in two matrices. Furthermore, it is assumed

$$\Gamma = \tau = 0 \qquad \text{for } p > 1/2$$

and

$$T_n(q) = 1 \qquad \text{for } p > 9/2.$$

Based on the above, it appears that the results from this parameterization would not be too dissimilar to the ones of Barnett. However, (3.3.17) and (3.3.18) should be computationally more efficient and thus are preferable in a practical wave forecasting model.

More recently, Resio (1981) proposed another parameterization of the nonlinear wave-wave interactions, but based on Webb's (1978) entropy concept. In this approach, the interaction process is similarly described by two transfers; these are called "diffusive" and "pumped". Unfortunately, Resio's derivation is rather confusing and difficult to follow. A major drawback in his formulation is the need to determine several constants from comparison with the complete solution. This may not be suitable for practical calculations.

Nevertheless, Figure 3.22 displays a comparison of Resio's parameterized nonlinear wave interactions with Barnett's model for a PM, a mean JONSWAP and a very sharp spectrum. It is clear from Figure 3.22 that Resio's parameterization shows better agreement for the PM spectrum over Barnett's result, but over-estimates the negative lobe of the mean JONSWAP spectrum by at least a factor 2. Similarly, for the sharp spectrum, both parameterization underpredict the negative value. On the whole this is an improvement over Barnett's parametric nonlinear transfer, but the approximated transfer rates are still not of the

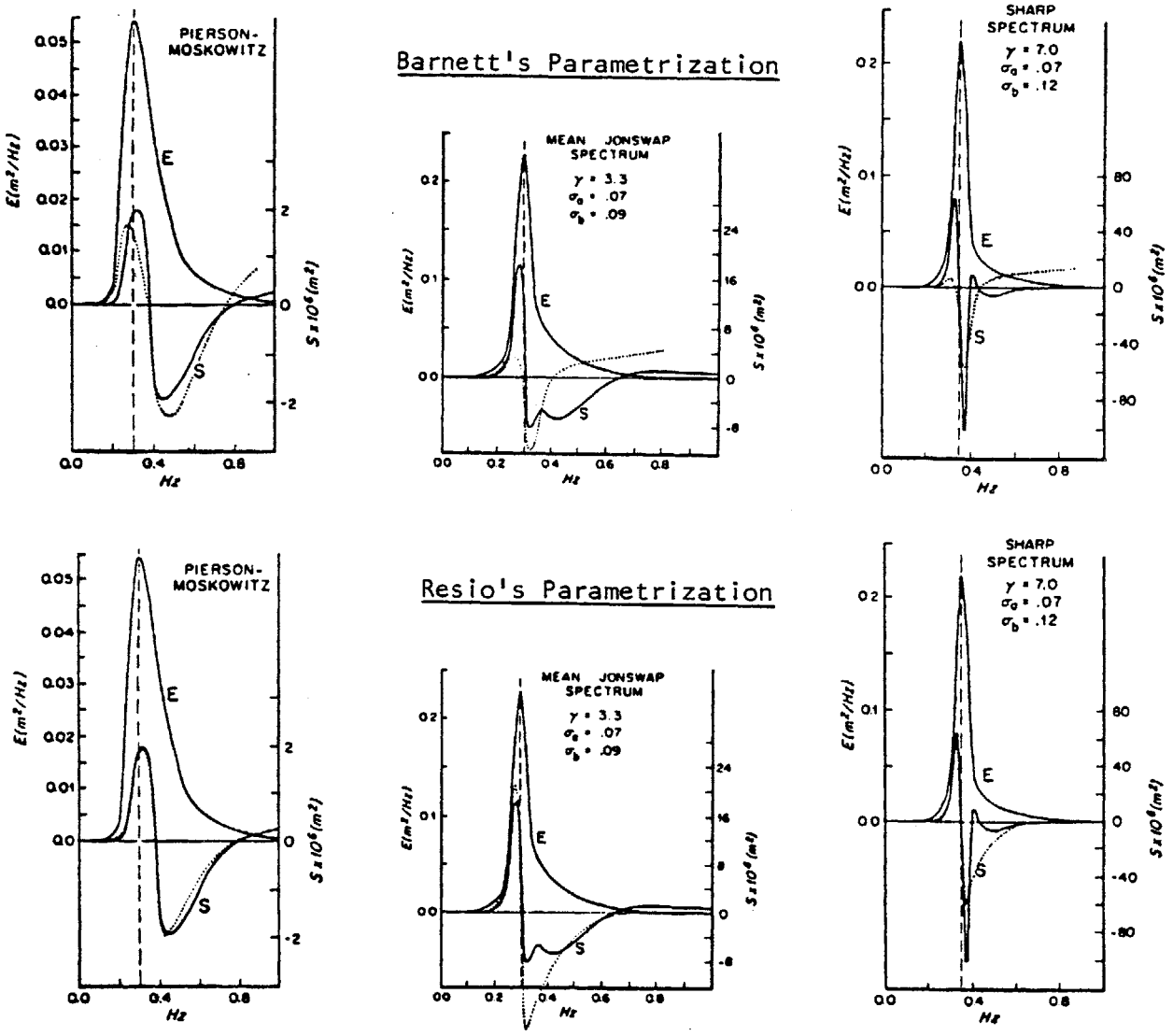


Fig.3.22 Comparison of nonlinear energy transfer parameterization for typical windsea spectra. Top row: Barnett's parameterization. Bottom row: Resio's parameterization. (From Resio, 1981).

desired accuracy, especially for calculating energy fluxes in a wave model.

Currently, the most efficient parameterization of the nonlinear transfer for a discrete spectral model and with sufficient accuracy has been introduced by Hasselmann and Hasselmann (1981) (hereafter abbreviated as HH). From the evaluation of the exact integration of the nonlinear interaction process for numerous windsea spectra, Hasselmann and Hasselmann (1981) concluded that all windsea spectra and their associated nonlinear transfer rates are interrelated and can be deduced from a reference spectrum. Defining the mean JONSWAP spectrum as the reference spectrum, it was found that the nonlinear transfer for a spectrum with shape parameter $\gamma \neq 3.3$ is just distorted relative to the one of the mean JONSWAP. This distortion can be rectified by simply transforming the frequency axis according to:

$$\nu^* = \Psi(\gamma) \cdot (\nu - \nu_o) + \nu_o^* \qquad (3.3.22)$$

and by multiplication of a scaling factor Ξ, such that:

$$S_{nl}(\nu,\theta) = \Xi(\gamma) \cdot S_{nl}^*(\nu^*,\theta) \qquad (3.3.23)$$

where $\nu^* = f^*/fm^*$ and $\nu = f/fm$ are the normalized frequencies of the reference JONSWAP and windsea spectrum ($\gamma \neq 3.3$), respectively, but with the same α value. The zero-transfer point ν_o of the one-dimensional transfer defines the transition from the positive low frequency lobe to the negative high-frequency lobe, and is generally a function of γ. For the mean JONSWAP spectrum, this null point is located at $\nu_o^* = 1.0092$. $S_{nl}(\nu,\theta)$ and $S_{nl}^*(\nu^*,\theta)$ refer to

the nonlinear transfer of the windsea and reference spectrum, respectively. It should be noted that in the two-dimensional case they have the same angular arguments, while the frequency arguments diverge, as is easily seen from (3.3.23). The transformation coefficients Ψ, Ξ and ν_o are all dependent on the peak enhancement factor γ and are listed in Table 3.2.

This simple parameterization reflects quite accurately the influence of the spectral shape on the nonlinear transfer. Inspection of Table 3.2 shows that as $\gamma \to 1$, i.e., a fully developed sea, the nonlinear transfer shifts towards higher frequencies [increasing ν_o], the distribution becomes broader [decreasing Ψ] and the interactions get weaker [decreasing Ξ]. For comparisons of the transformed transfer rates with the exact one-dimensional nonlinear transfers, the reader should see to HH (1981).

Hasselmann et al. (1973) have demonstrated that for self-similar spectra of the type

$$E(f,\theta) = \alpha g^2 f^{-5} \Psi(f/fm,\theta)$$

the nonlinear transfer $S_{n\ell}$ can be scaled with respect to α and fm according to

$$S_{nl}(f,\theta) = \alpha^3 g^2 fm^{-4} \Psi_*(f/fm,\theta) \qquad (3.3.24)$$

Introducing this relation in (3.3.24), we can establish a generalized formula for the parameterized nonlinear transfer which now accounts for different α values too. Hence, the one-dimensional form yields

γ	Ξ	Ψ	ν_o^*
1.00	.14135	.31378	1.1832
1.25	.17783	.34799	1.1132
1.50	.21845	.36257	1.0802
1.75	.26047	.36256	1.0544
2.00	.28773	.43563	1.0370
2.25	.37653	.54560	1.0262
2.50	.49220	.72983	1.0184
2.75	.61914	.87806	1.0125
3.00	.75797	.97729	1.0088
3.30	1.00000	1.00000	1.0092
3.50	1.07279	1.04830	1.0034
3.75	1.24936	1.07432	1.0014
4.00	1.44900	1.13048	0.9997
4.50	1.93931	1.16076	0.9969
5.00	2.50794	1.16069	0.9948
6.00	3.89577	1.13023	0.9917
7.00	5.64199	1.19251	0.9896

Table 3.2 Transformation parameters for finite depth nonlinear energy transfer as a function of γ. (From Hasselmann and Hasselmann, 1981).

$$S_{nl}(\nu;\alpha) = \left(\frac{\alpha}{\alpha^*}\right)^3 \left(\frac{fm}{fm^*}\right)^{-4} \Xi(\gamma)\, S_{nl}{}^*(\nu^*;\alpha^*) \ . \qquad (3.3.25)$$

The quality of this simple, efficient algorithm for the nonlinear transfer is superposed onto Fox's results and illustrated in Figures 3.20 and 3.21. In particular, it shows its superiority over the narrow-peak results for the "sharp" JONSWAP spectrum.

An important extension of the nonlinear energy transfer to finite depth gravity-wave spectra was derived by Herterich and Hasselmann (1980). For waves in water depths greater than approximatly one tenth of the wave length ($kh \geq 0.7$), the finite-depth nonlinear transfer is related to the infinitely deep ocean transfer rate by a similarity transformation. These results apply for the asymptotic narrow-peak aproximation of Longuet-Higgins (1976) and Fox (1976). From their study Herterich and Hasselmann (1980) found that the finite-depth transfer $S_{nl}(f,\theta;\, k_m h) \equiv S_{nl}{}^h$ could be determined from the infinite depth case, $S_{nl}(f,\theta;\, k_m h = \infty) \equiv S_{nl}{}^\infty$ by multiplying with a depth-dependent transformation factor, i.e.,

$$S_{nl}{}^h = R(k_m h) \cdot S_{nl}{}^\infty \qquad (3.3.26)$$

where $k_m h$ is the dimensionless depth and k_m is the wave number corresponding to the spectral peak frequency fm. Figure 3.23 shows the theoretically determined ratio R from the narrow-peak assumption of their analysis and the empirically derived values of R from the exact calculations by HH (1981). The results of the exact integral computations indicate that the restrictions on the transformation can be relaxed to $k_m h \approx 0.5$, which corresponds to waves with wave lengths

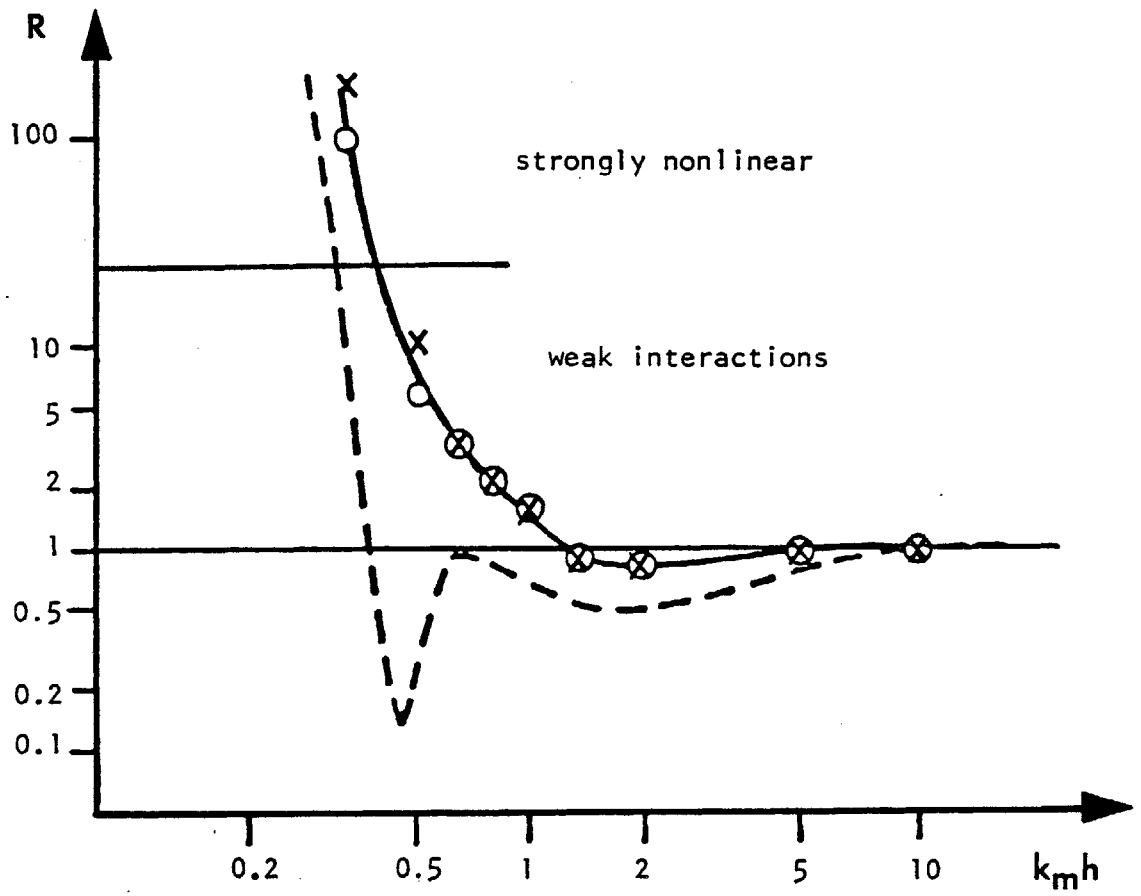


Fig. 3.23 Ratio R of the nonlinear transfer in finite depth to the transfer rate in deep water. Narrow peak approximation by Herterich and Hasselmann (---); exact calculations by Hasselmann$_h$ and Hasselmann (——). o = max and x = min values of exact S_{nl}^h.

less than 30 times the water depth. For values of $k_m h$ less than 0.5, the nonlinear energy transfer rapidly intensifies and the waves deform by becoming steeper until they break. In this region the interactions gain in strength and the governing weak interaction theory breaks down.

In conclusion, the relation given in (3.3.26) can readily be generalized using the above results, to express the nonlinear energy transfer for finite depth waves. For examples, the reader is referred to HH (1981).

3.3.3 Dissipation By Wave Breaking

One of the most visual and interesting features of surface gravity waves in a deep ocean is the formation of "white caps" which result from air entrainment during the breaking process. Similarly, as waves approach the shore, they grow to a limiting steepness which triggers the onset of breaking. At this point, the wave collapses, releasing its energy through a plunging or spilling motion. In general, wave breaking is regarded as the process limiting the wave amplitude. But it takes place with such a tempestuous force and on a time scale so short that a rigorous study of the breaking process in the field is extremely difficult. Recent observations of white caps at sea have focused on their spatial distribution as a function of wind speed and intervals of recurrence (Donelan et al., 1972; Ross and Cardone, 1974).

However, more progress has been made in studying wave breaking under controlled laboratory conditions (Banner and Phillips, 1974; Van Dorn and Pazan, 1975; Wu et al., 1977; Melville, 1983). Although these studies have significantly contributed to the understanding of the breaking process for individual or a group of waves, no experimental results under typical ocean conditions are available to test its effect as a dissipative mechanism for the wave spectrum. In the context of practical wave prediction schemes, the wave breaking process is commonly represented by a weighted or reduced generation source function. This condition may be stated as

$$S = S_{in} - S_{wb} = (1-r)\, S_{in} = (1-r)(\alpha^* + \beta^* E) \qquad (3.3.28)$$

where S_{in} is a Phillips-Miles type wave generation source term and the coefficient $r \to 0$ for $E \ll E_\infty$, or $r \to 1$ for $E \geq E_\infty$. The saturated wave spectrum E_∞ after Phillips (1958) is given by

$$E_\infty = E_\infty(f,\theta) = \alpha g^2 (2\pi)^{-4} f^{-5} \Omega(\theta) \qquad (3.3.29)$$

where $\Omega(\theta)$ is the angular spreading function. The determination of the empirical coefficient r varies from one model to another. Barnett (1968) used the following expression for r:

$$r = d_1 \exp[-d_2 (E_\infty - E)/E] \qquad (3.3.30)$$

where $E = E(f,\theta)$, and the constants were chosen as $d_1 = 0.8$ and $d_2 = 0.5$. Alternatively, Ewing (1971) and Cardone et al. (1976) expressed r in their models as

$$r = \left(\frac{E}{E_\infty}\right)^2 \qquad (3.3.31)$$

whereas Collins (1972) and Cavaleri and Malanotte-Rizzoli (1977) simply adopt that r is appropriately given by

$$r = \begin{cases} 1 & \text{for } E < E_\infty \\ 0 & \text{for } E \geq E_\infty \end{cases} \qquad (3.3.32)$$

A semi-theoretical treatment of the energy loss due to wave breaking is given by Longuet-Higgins (1969). A theoretical account of

white capping and its effect on the spectral energy distribution of surface gravity waves was first presented by Hasselmann (1974). Although, wave breaking is locally a highly nonlinear process, Hasselmann has shown that the dissipation can be related to the wave spectrum in a quasi-linear manner,

$$S_{wb}(\underline{k}) = -\gamma_d(\underline{k})\, F(\underline{k}) \qquad (3.3.33)$$

where γ_d is a damping coefficient which depends only on wave number and integral spectral parameters, such as the average wave steepness. For the case, when white capping occurs on space-time scales which are short compared with the characteristic periods and wave lengths of the spectrum, Hasselmann (1974) found that $\gamma_d \sim k$. A complete analysis of $\gamma_d(\underline{k})$, however, is still an oustanding problem in wave research. Transforming (3.3.33) into frequency-direction space yields

$$S_{wb}(f,\theta) = -\lambda_d (2\pi f)^2 E(f,\theta) \qquad (3.3.34)$$

Unfortunately, λ_d cannot readily be computed from first principles and must indirectly be determined from the energy balance in the high-frequency equilibrium range. Applying the assumption that the net contribution of wind input, nonlinear transfer and white capping vanishes at high frequencies, this condition may be stated as

$$S_{in}^{hf} + S_{nl}^{hf} + S_{wb}^{hf} = S_{net}^{hf} \equiv 0 \; . \qquad (3.3.35)$$

Furthermore, if it is assumed that two of the contributing source functions in (3.3.35) are known, the remaining one can therefore be

calculated. As a result, Hasselmann found

$$\lambda_d = fm^{-1}\{3.5 \times 10^{-5}[1 - 4.8 \times 10^{-2}\nu^{-1}] + 0.5\alpha^2\kappa_s\} \qquad (3.3.36)$$

with α the Phillips constant, fm the peak frequency, $\nu = fmU/g$ and κ_s a spectral shape factor between 0.12 and 0.16. It is clear that λ_d is really not a constant, but rather depends explicitly on spectral parameters as fm, α and shape factors. This is a consequence of the fact that the nonlinear energy transfer in the high-frequency portion of the spectrum is coupled to the wave-wave interactions near the spectral peak.

In an effort, describing the relative importance of various physical processes contributing to the growth and dissipation of waves, Bouws and Komen (1983) appplied (3.3.34) to a depth-limited windsea. Since no vanishing equilibrium balance could be found with λ_d given by (3.3.36), λ_d was subsequently determined from the requirement that

$$\Sigma\, S^2_{net}(f_i) = \text{minimum}, \qquad \text{for } 0.8\ fm < f_i < 2fm \qquad (3.3.37)$$

such that

$$\int_{0.8fm}^{2fm} S_{net}\, df = 0.$$

This gave the value of $\lambda_d = 1.9 \times 10^{-4}$ sec, which is only a factor of 2 smaller, than the values one would calculate from (3.3.36) using their spectral parameters of fm = 0.086 Hz, $\alpha = 0.01$, $\gamma = 2$ and U = 25 m/s.

Under considerations to simulate observed fetch-limited wave growth in deep oceans, Hasselmann and Hasselmann (1984) proposed the

following parameterized dissipation function

$$S_{wb}(f,\theta) = - d_o\left(\frac{f}{fm}\right)^3 f \left[\frac{\tilde{E}\,\omega_m^4}{g^2}\right]^6 E(f,\theta) \qquad (3.3.38)$$

with the constant $d_o = 7.8 \times 10^9$. Here $\tilde{E}$ defines the total energy and $\omega_m = 2\pi fm$ is the peak radian frequency. In an attempt to investigate the existence of a fully-developed spectrum, Komen et al. (1984) generalized the specification of the wave damping coefficient as

$$\gamma_d = -d\,\omega_o\left(\frac{\omega}{\omega_o}\right)^n \cdot \left(\frac{\hat{\alpha}}{\hat{\alpha}_{PM}}\right)^m \qquad (3.3.39)$$

where $\hat{\alpha}$ is the integral wave steepness parameter defined as $\hat{\alpha} = \tilde{E}\omega_o^4/g^2$, $\omega_o = \tilde{E}^{-1}\int\omega F(\underline{k})d\underline{k}$, d is a constant and n,m are exponents which must be determined. The theoretical value of the wave steepness for the PM-spectrum is $\hat{\alpha}_{PM} = 4.5 \times 10^{-3}$. The objective of their study was to determine the conditions under which an equilibrium solution can exist for the energy balance equation. In summary, the results of their analysis demonstrated that for the combination n = m = 2 and $d = 3.33 \times 10^{-5}$, a quasi-stationary solution could be obtained. For this case, the net residual of the energy balance was two orders of magnitude smaller than the individual source terms. Surprisingly enough, they found that the resulting one-dimensional spectral distribution closely resembled the shape of the conventional Pierson-Moskowitz spectrum. On the other hand, the directional distribution did not reproduce the functional behavior of commonly accepted angular spreading factors. It appears that such an approach should lead to a more definitive specification of the source functions

and their directional dependence for waves in deep water. A complementary investigation should also be carried out for waves in finite depth to examine in detail the influence of the sea bottom characteristics on the wave spectrum.

3.3.4 Dissipation By Finite Depth Mechanisms

As ocean waves propagate onto the continental shelf, waves, with a wave length greater than twice the local water depth, will feel the presence of the sea bottom and begin to interact with the sea bed characteristics. In a wave spectrum, the low frequency components are transformed first, while the high-frequency portion still behaves as in deep water. To demonstrate this numerically, let us define the high-frequency cut-off at approximatly twice the peak frequency. Then, for a wave spectrum with a peak frequency, fm = 0.1 Hz, all spectral components would feel the bottom in waters less than 20 m deep. Both linear and nonlinear mechanisms will affect the transformation of the wave spectrum in finite depth seas. Among the linear transformation mechanisms one can enumerate the dissipative effects of percolation, soft bottom motion and bottom scattering and the non-dissipative impacts due to refraction and shoaling. The nonlinear processes, such as wave-wave interactions and bottom friction are equally dominant when waves enter shoaling waters. A survey of these mechanisms can be found in Shemdin et al. (1980). In this section we shall only focus on the dissipative mechanisms resulting from percolation, bottom motion, bottom scattering and primarily bottom friction.

When surface waves propagate over a rigid porous seabed, the varying wave pressure can induce a considerable flow in the underlying permeable soil layer. In turn, the induced flow will dissipate some of the wave energy. This mechanism is called percolation and was first treated by Putnam (1949) for an isotropic and infinitely deep sand layer. Reid and Kajiura (1957) re-examined the same problem but in a more rigorous approach, and disclosed an error in Putnam's dissipation function. The average rate of energy dissipation due to percolation is equal to the average rate of work done by the upper fluid on the fluid within the permeable medium at the interface. In this manner one obtains

$$\frac{\partial E}{\partial t} = -k\sqrt{ab}\,\frac{\tanh\sqrt{a/b}\,kd}{\cosh^2 kh}\,E(f,\theta) \tag{3.3.40}$$

where a,b are the horizontal and vertical permeability coefficients, respectively, and d is the depth of the permeable layer. If the porous medium is isotropic, $a = b$, and the layer is sufficiently deep, i.e., kd > 2, the equation simplifies

$$\frac{\partial E}{\partial t} = -\frac{a\,k}{\cosh^2 kh}\,E(f,\theta) \tag{3.3.41}$$

which is equivalent to Putnam's result, except for a missing factor of 4. Then the fractional decrease of wave energy per radian can be defined as the damping ratio

$$\zeta_p = -\frac{1}{\omega E}\frac{\partial E}{\partial t} = \frac{2\,\omega\,a}{g\,\sinh\,2kh}\,. \tag{3.3.42}$$

Sleath (1970) investigated the wave-induced flows in a sand bed under laboratory conditions. For a coarse sand with mean diameter D_{50} = 1.13 mm and a fine sand with D_{50} = 0.39 mm, the following isotropic permeability coefficients of 1.1 cm/sec and 0.121 cm/sec were calculated for the coarse and fine sand, respectively. Figure 3.24 illustrates the strength of the damping coefficient ζ_p for an 8 and 10 second wave. The sand properties are assumed isotropic, corresponding to typical values for coarse and fine sands.

Real sea bottom sediments rarely consist of just rigid sand layers, but are more likely to resemble that of a poro-elastic medium. In this case, the pressure forces of the waves may deform and displace the bottom. Wave damping results due to the imperfect elasticity of the bottom soil. Recently, much effort has focused on the dynamic behavior of marine sediments. The general analytical treatment of this type of wave-seabed interaction is derived from the theory of Biot (1962), which describes the propagation of elastic waves through fluid-filled porous media. Mei (1983) gives a detailed account of the basic equations governing such a deformable porous medium, as well as several examples relevant to ocean engineering. Bottom motions are also of interest in seismology. Theories describing the origin of microseisms can be found in Longuet-Higgins (1950) and Hasselmann (1963c). Wave-induced stresses in a porous sea bed have also been dealt with by Madsen (1978). Calculations of wave transformation over soft mud bottoms were performed by Hsiao and Shemdin (1980) and Yamamoto (1981). The energy transfer from surface gravity waves to the sediment was also calculated by Rosenthal (1978). When compared with the attenuation rates for the JONSWAP results, it was inferred that

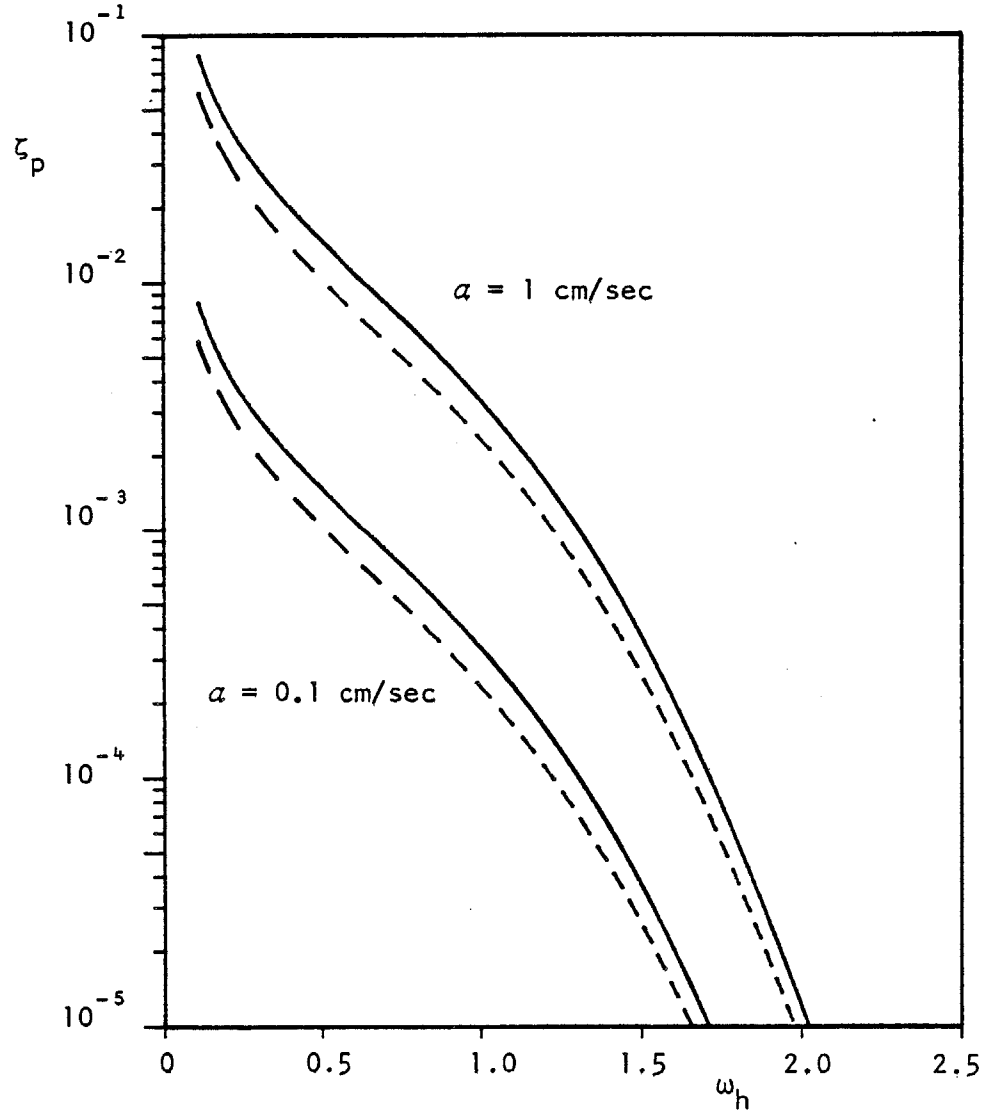


Fig. 3.24 Dissipation rate due to percolation as a function of permeability coefficient and wave period. (Isotropic sand properties are assumed; results are shown for 8 sec. (---) and 10 sec. (——) wave period.)

wave damping due to bottom motions was at least one order of magnitude smaller for the JONSWAP site. However, it seems that bottom motions as a means of wave damping are only dominant in the vicinity of large river deltas such as the Mississippi and Orinoco. Furthermore, a clear determination of the mud properties such as viscosity, shear modulus, density and layer thickness is extremely difficult. Very often these properties are inferred from observed energy dissipation rates.

Another potential sink of energy could be attributed to the scattering of surface waves by topographical irregularities. This particular mechanism was studied by Long (1973) and applied to the JONSWAP data. For this case, it could not conclusively be shown that bottom scattering is the process responsible for the observed swell attenuation. A more definitive verification of this mechanism is needed and awaits more accurate measurements of the directional wave characteristics at both inshore and offshore sites, as well as better estimates of the bottom spectrum.

By far the most studied and explored wave-bottom interaction process is bottom friction. Generally speaking, bottom friction is not only important in damping shallow water surface waves, but also plays a significant role in sediment transport, bottom boundary-layer flows and shelf currents. Once the wave motion feels the bottom, a bottom boundary-layer is generated as result of a non-zero bottom shear stress. The viscous effects within this boundary-layer causes a dissipation of mechanical energy and hence attenuates the waves. In nature this boundary layer is almost always fully rough turbulent and analogous to boundary layer theory of steady flows, the bottom shear stress depends upon the roughness of the boundary. In turn, the

boundary roughness must then be expressed in terms of the actual, physical features of the sea bed, i.e., sediment size, bedform geometry (ripples), and sediment transport (Grant and Madsen, 1982). Therefore, it is essential for accurate predictions of wave energy dissipation due to bottom friction that the fluid-sediment interaction, e.g., bedform geometry, be accounted for as precisely as possible.

The shear stress τ_b acting on the ocean bottom under a wave can be expressed as

$$\underline{\tau}_b = \frac{1}{2} \rho f_w |\underline{u}_b| \underline{u}_b \tag{3.3.43}$$

where f_w is the wave friction factor and $\underline{u}_b$ is the near-bottom wave orbital velocity. If the flow is fully rough turbulent, the friction factor f_w depends only on the relative boundary roughness k_b/A_b, where A_b represents the near-bottom excursion amplitude and k_b is an "equivalent roughness height" which is analogous to the "equivalent grain size roughness height" concept introduced first by Nikuradse (1933). From linear wave theory, an estimate of the particle excursion length for a monochromatic wave is given by

$$A_b = \frac{1}{2} \frac{H}{\sinh kh} \tag{3.3.44}$$

with H the wave height. It is clear that f_w relates the bottom shear stress to the roughness of the sea bottom. This immediately implies that a successful transformation of deep water wave conditions to shallow water involves an accurate calculation of the friction factor f_w. The theoretical work of Kajiura (1964) provided a consistent approach for determining f_w in an oscillatory flow. In his model

Kajiura introduced an eddy-viscosity concept to relate the tangential boundary stress to the velocity gradient within the boundary layer. Semi-empirical evidence supporting Kajiura's findings was furnished by Jonsson (1966) and Jonsson and Carlsen (1976) from two laboratory experiments on artificially roughened bottoms. A purely empirical study was performed by Kamphuis (1975), who measured the shear stress directly. In a theoretical study improving his original model Kajiura (1968) obtained predictions in good agreement with Jonsson's experimental results. In summary, based on Jonsson's data, the friction factor f_w is commonly determined from the relation

$$F_w + \log_{10} F_w = \log_{10} \frac{A_b}{k_b} - 0.08 \tag{3.3.45}$$

where we use the definition $F_w \equiv (16 f_w)^{-1/2}$. In a similar analysis for waves in the presence of currents, Grant and Madsen (1979) derived an expression relating the friction factor to the bottom boundary roughness, when the flow is fully rough turbulent. In the absence of currents, i.e., pure wave motion only, their expression for f_w reduces to

$$f_w = 0.08 \left[\mathrm{Ker}^2 \left(2\xi_o^{1/2} \right) + \mathrm{Kei}^2 \left(2\xi_o^{1/2} \right) \right]^{-1} \tag{3.3.46}$$

which is valid for $k_b/A_b \leq 1$. Here Ker and Kei refer to Kelvin functions of zero'th order. The dimensionless roughness length ξ_o for fully rough turbulent flow is taken as

$$\xi_o = \frac{k_b}{30\ell} \tag{3.3.47}$$

where ℓ is a characteristic length scale of the wave boundary layer and is given by

$$\ell = \kappa u_{*,max}/\omega \tag{3.3.48}$$

in which $\kappa = 0.4$ is von Karman's constant and

$$u_{*,max} = \sqrt{\frac{1}{2} f_w} A_b \omega \tag{3.3.49}$$

For small ξ_o, Grant (1977) has shown that (3.3.46) reduces to the form of (3.3.45), except for the constant factor 0.08. Figure 3.25 shows a comparison of commonly accepted, but different formulae for f_w. In essence, this ascertains that the key factor for the bottom friction mechanism is an accurate prediction of the roughness on the ocean bottom. To exemplify this point, we consider the model proposed by Grant and Madsen (1982) as illustrated in Figure 3.26, which qualitatively describes the interplay between the near-bottom flow field and the resulting effective bottom roughness for non-cohesive sediments on a flat sea bed. For near-bottom flow intensities which are low and not strong enough to produce sediment movement, the bottom remains flat and stable. The resistance experienced by the wave motion is that due to skin friction of the sediment grains, and the friction factor f_w is small. As the wave intensity over the bed is increased above a certain threshold value (Madsen and Grant, 1976), small ripples appear due to bottom sediment movements. The bottom roughness is now on a scale comparable to the ripple height rather than the sediment grain size. The resulting resistance experienced by the wave is now attributed to the form drag, hence a larger f_w. Further increase of

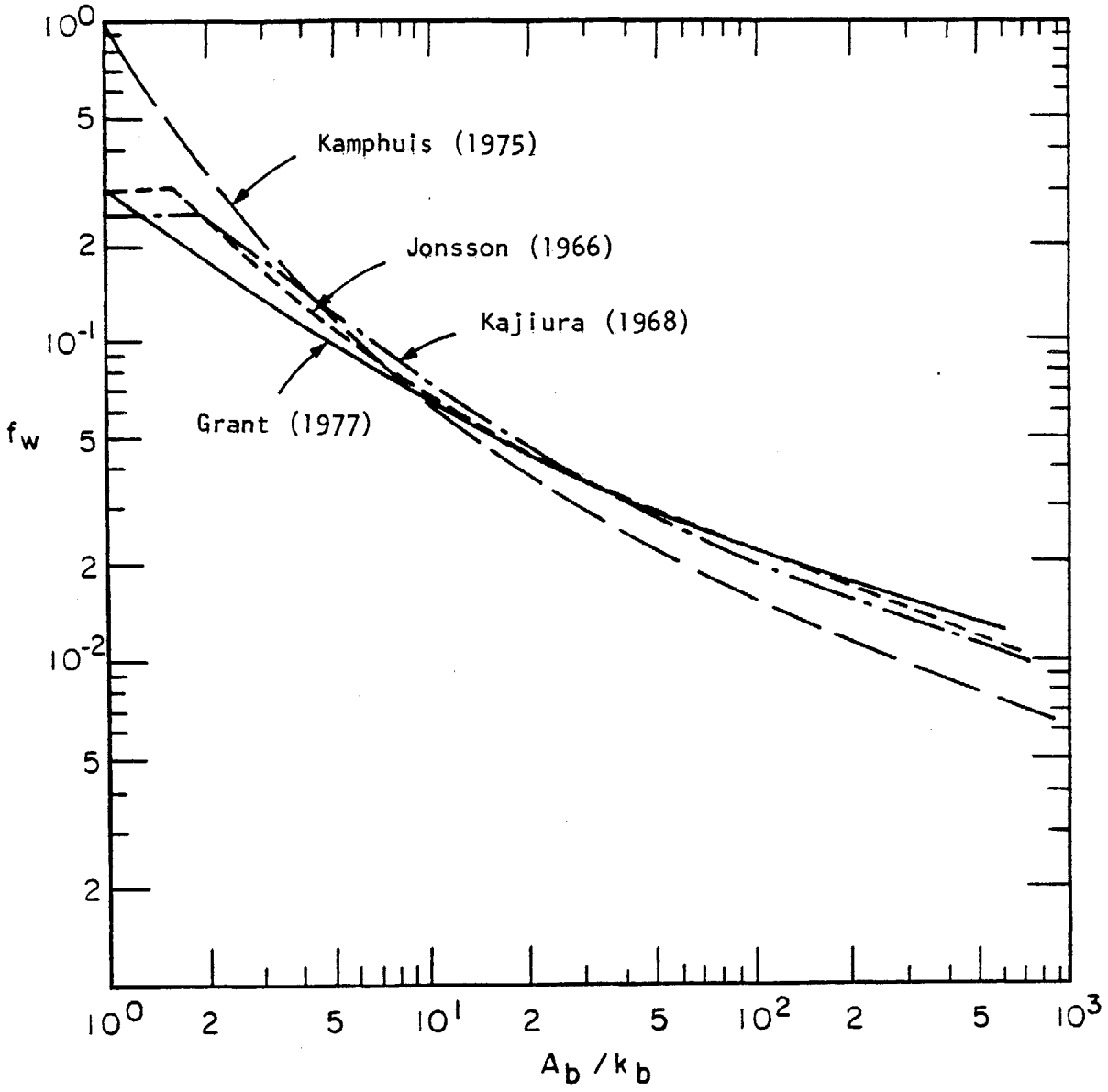


Fig. 3.25 Comparison of wave friction factor theories. (From Grant, 1977).

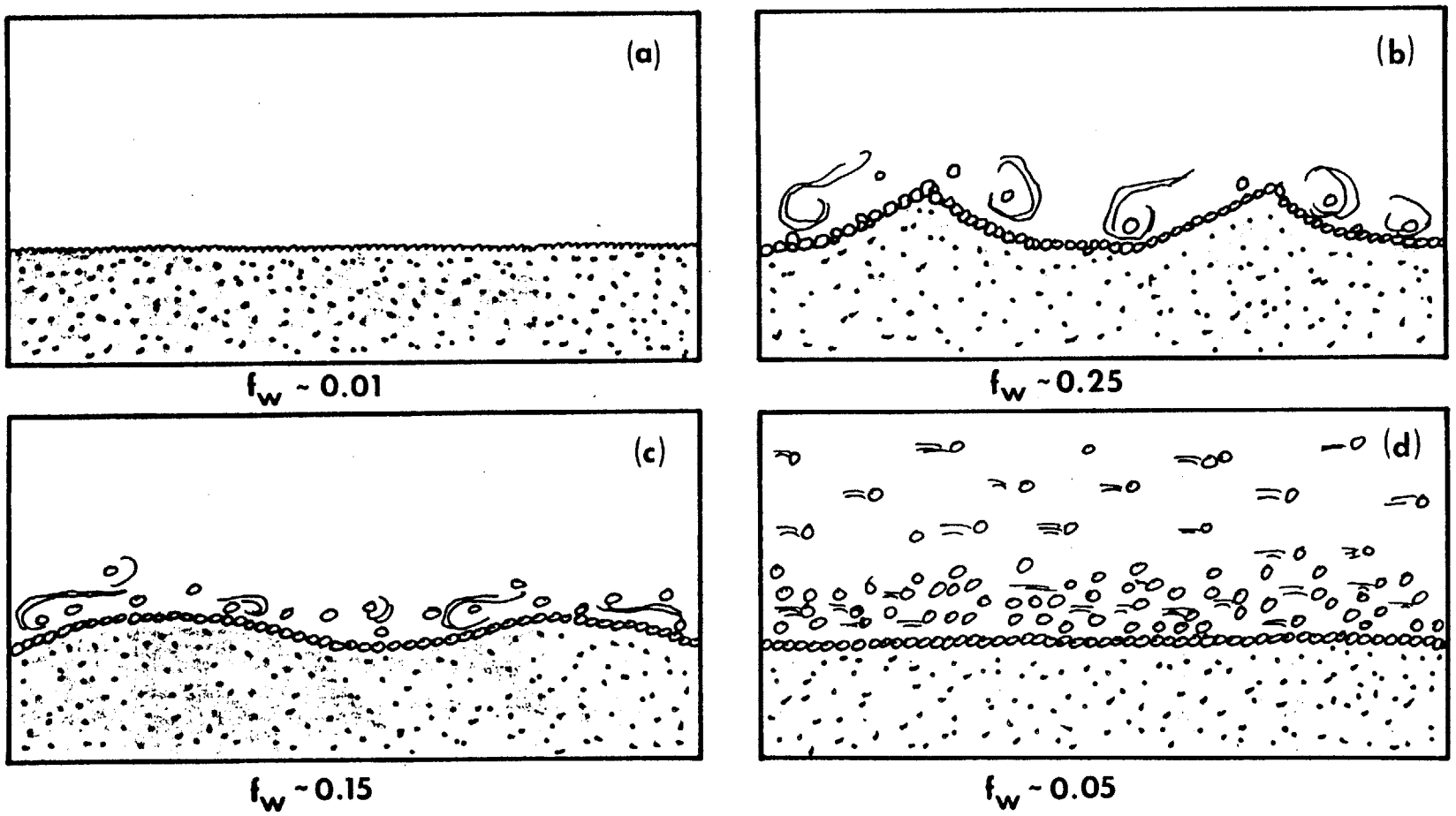


Fig. 3.26 Qualitative description of the interplay between near-bottom flow and resulting bottom roughness.

the wave orbital velocity results in a gradual trimming of the ripples, while sediment transport takes place at a higher rate. Eventually the bottom bedforms are completely washed out and the bed becomes flat again. Now the bottom roughness is entirely governed by the suspended sediment motion or sheet flow. The friction factor f_w is now relatively small again. Consequently, it should be realized that an empirically determined friction factor in a wave model may dangerously underpredict or overpredict the sea state and may lead to false conclusions, especially in terms of engineering designs. Grant and Madsen (1982) developed an efficient model to predict the boundary roughness in unsteady, oscillatory flows over movable, cohesionless beds (cf. Figure 3.25).

In a rigorous theoretical treatment, Hasselmann and Collins (1968) derived an expression for the dissipation rate of a wave spectrum. The average rate of energy dissipation in an oscillatory wave boundary layer (Kajiura, 1968) or for a random wave field (Hasselmann and Collins, 1968) can be expressed as

$$\frac{\partial E}{\partial t} = - E_{diss} = - \overline{\underline{\tau}_b \cdot \underline{u}_b} \tag{3.3.50}$$

where the overbar denotes averaging over the wave field. Following Hasselmann and Collins (1968), equation (3.3.50) can be rewritten in terms of the frequency-direction spectrum

$$\frac{\partial E}{\partial t} = - \frac{1}{2} \frac{f_w \omega^2}{g \sinh^2 kh} E(f,\theta) \cdot \langle u_b \rangle \tag{3.3.51}$$

and $\langle u_b \rangle$ represents the mean value of the bottom velocity spectrum, i.e.,

$$\langle u_b \rangle = \{ \langle |\underline{u}_b| \rangle + \cos^2(\theta - \zeta) \langle \frac{u_1^2}{|\underline{u}_b|} \rangle + \sin^2(\theta - \zeta) \langle \frac{u_2^2}{|\underline{u}_b|} \rangle \} \tag{3.3.52}$$

where ζ represents the angle for which the condition $\langle u_1 u_2 \rangle = 0$ is satisfied. Here, u_1 and u_2 denote the components of the near-bottom orbital velocity in the direction of ζ and perpendicular to ζ, respectively. The angle ζ, which is measured clockwise, may be derived from the orthogonality condition and is conveniently given by

$$\tan 2\zeta = - \frac{2\nu_{12}}{\nu_{11} - \nu_{22}} \tag{3.3.53}$$

with the following definitions:

$$\begin{aligned} \nu_{11} &= \iint \frac{\omega^2}{\sinh^2 kh} E(f,\theta) \cos^2\theta \, df d\theta \\ \nu_{12} &= \iint \frac{\omega^2}{\sinh^2 kh} E(f,\theta) \sin\theta \cos\theta \, df d\theta \\ \nu_{22} &= \iint \frac{\omega^2}{\sinh^2 kh} E(f,\theta) \sin^2\theta \, df d\theta \quad . \end{aligned} \tag{3.3.54}$$

It should be noted, that the equivalent expression of (3.3.53) given in Collins (1972) (his equation 13) is incorrect. For the zero-current case, closed form analytical soutions for (3.3.52) may be obtained,

$$\langle |\underline{u}_b| \rangle = (2/\pi)^{1/2} \lambda_1 E(x)$$

$$\left\langle \frac{u_1^2}{|\underline{u}_b|} \right\rangle = (2/\pi)^{1/2} \lambda_1 \left[\frac{E(x)}{x^2} - \frac{K(x)}{x^2} (1-x^2) \right] \qquad (3.3.55)$$

$$\left\langle \frac{u_2^2}{|\underline{u}_b|} \right\rangle = (2/\pi)^{1/2} \lambda_1 \left(\frac{1-x^2}{x^2} \right) [K(x) - E(x)]$$

where $x = (1 - \lambda_2/\lambda_1)^{1/2}$ and λ_1 and λ_2 are given by,

$$\lambda_1 = \nu_{11}\cos^2\zeta - 2\nu_{12}\sin\zeta\cos\zeta + \nu_{22}\sin^2\zeta$$

$$\lambda_2 = \nu_{11}\sin^2\zeta + 2\nu_{12}\sin\zeta\cos\zeta + \nu_{22}\cos^2\zeta \quad .$$

Here $K(x)$ and $E(x)$ are the complete elliptic integrals of the first and second kind, respectively. In a similar manner to Collins (1972) we approximate (3.3.52) by a representative near-bottom velocity value which is expressed as

$$u_{br} = \langle u_b \rangle = \left\{ 2 \int \frac{\omega^2}{\sinh^2 kh} E(f,h) \right\}^{1/2} \qquad (3.3.56)$$

with E(f,h) the finite depth JONSWAP spectrum (3.1.81). Analogously to (3.3.42), we may define a dimensionless damping ratio for bottom friction,

$$\zeta_f = -\frac{1}{\omega E}\frac{\partial E}{\partial t} = \frac{f_w}{2}\frac{\omega}{g \sinh^2 kh} u_{br} \quad . \qquad (3.3.57)$$

Here ζ_f not only depends on the wave frequency and friction factor, but also on the wave height through u_{br}. Figure 3.27 shows the

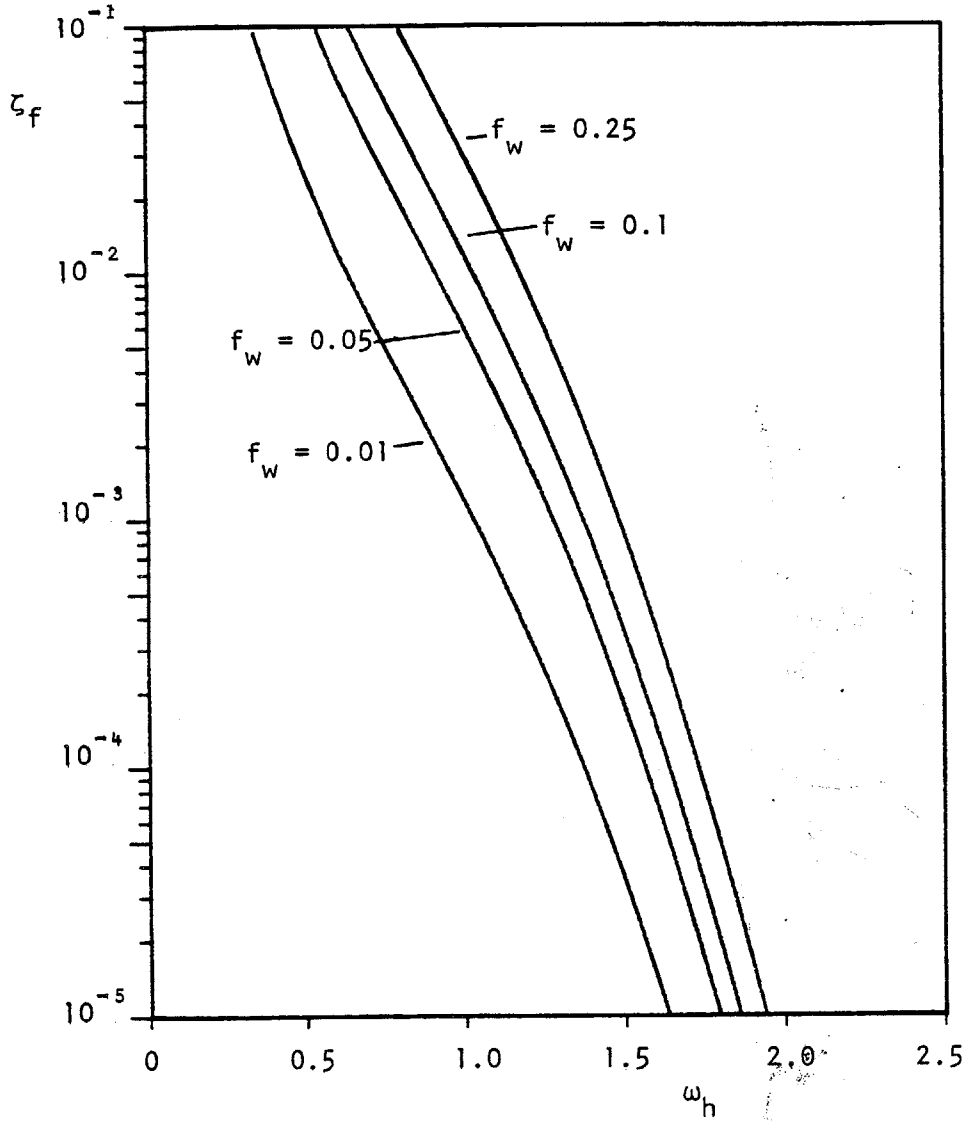


Fig. 3.27 Dissipation rate due to bottom friction as a function of wave friction factor, wave period and wave height. (Results shown correspond to a wave period T = 7 sec. and a wave height H_s = 2 m.)

variation of ζ_f as a function of f_w versus dimensionless frequency ω_h for a wave height of 2 m.

Hasselmann et al. (1973) applied (3.3.51) to the JONSWAP data, to investigate the mechanism responsible for the observed swell decay. They assumed that tidal currents were dominating the wave orbital velocities in the near-bottom boundary layer an assumption which can not be considered valid, in view of the results obtained by Grant and Madsen (1979). From the analysis of their swell data, an empirical swell decay rate was derived,

$$\Gamma = \frac{d \ln I}{d\xi} = c_f g V \qquad (3.3.58)$$

where I is the energy flux in a narrow swell band and ξ describes a normalized distance coordinate, referenced from the shoreline, and V is the mean current near the ocean bottom. From the analysis of 678 swell spectra during JONSWAP an average value $\Gamma = 0.038$ m^2/sec^3 was computed. For tidal currents with velocities of 20 - 40 cm/sec typically measured during JONSWAP, (3.3.58) yields friction factors f_w in the range 0.04 - 0.02. Recently Bouws and Komen (1983) represented the bottom friction mechanism based on empirical grounds from the JONSWAP results by

$$\hat{S}_{bf} = -\Gamma \left(\frac{\omega}{g \sinh kh}\right)^2 E(f,\theta) \quad . \qquad (3.3.59)$$

Comparing the above with the general expression of bottom frictional attenuation defined in (3.3.51) it follows that

$$f_w = \Gamma \frac{2}{g \langle u_b \rangle} \qquad (3.3.60)$$

When using the JONSWAP parameters for fm = 0.086 Hz, α = 0.01 and γ = 2.0 as reported by Bouws and Komen (1983) for the Texel storm spectrum, one calculates f_w = 0.015. Similarly, using the observed significant wave height H_s = 6.8 m and a grain size of 0.25 mm, the approach suggested by Grant and Madsen (1982) which accounts for the combined roughness under the wave, yields f_w = 0.05. These unequal friction factors are a consequence of using different wave variables to evaluate them. Conceptually this is correct, since, for example, the significant wave height is a factor $\sqrt{2}$ larger than the rms wave height. Hence, a larger f_w is needed to obtain the same dissipation rate. Therefore, as long as the proper wave fricton factor is attached to the appropriate variables, the final analysis should give equivalent results.

Finally, to illustrate the relative contributions of the various source functions we have discussed in the previous sections, we use the observed finite depth wind sea spectrum reported by Bouws and Komen (1983). Figure 3.28 shows the energy balance comprised of nonlinear wave-wave interacions, wind input, dissipation by wave breaking and bottom friction.

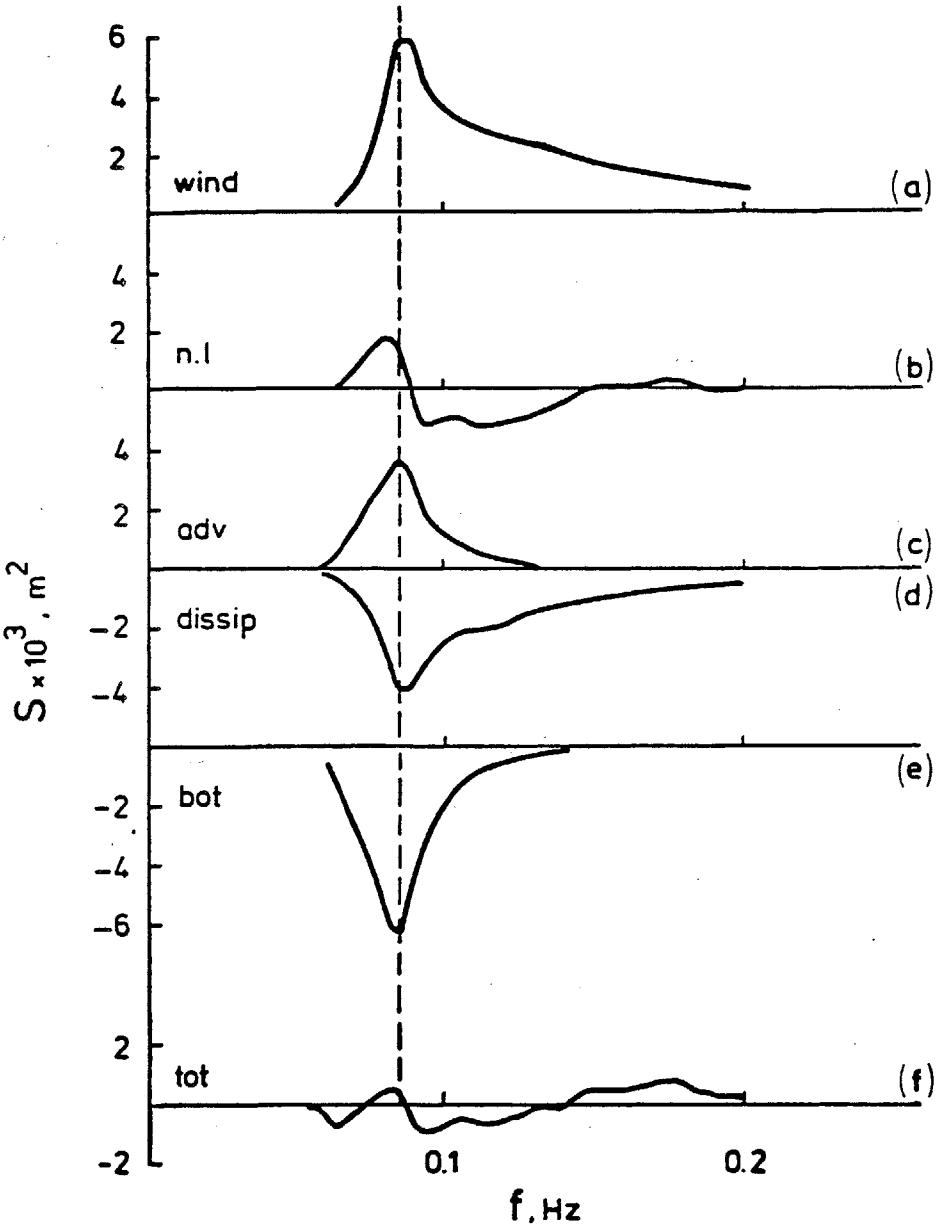


Fig. 3.28 Energy balance for a finite-depth storm-generated wave spectrum consisting of (a) wind input; (b) nonlinear energy transfer; (c) advection; (d) deep water dissipation (wave breaking); (e) bottom friction; (f) net source function. Water depth h = 35 m and wind speed U = 25 m/s. (From Bouws and Komen, 1983).

3.4 Wave Energy Flux Versus Wave Momentum

The directional distribution of wave energy is an important aspect concerning ocean waves. Recently some efforts have been directed towards the derivation of an equation which describes the response of the mean direction of a windsea spectrum to changes in wind directions. To accomplish this, an appropriate vector variable must be defined. In the past, it was assumed that the two-dimensional energy spectrum can be written as the product of the one-dimensional frequency spectrum and a frequency independent angular spreading function

$$E(f,\theta) = E(f) \cdot \Omega(\theta) \qquad (3.4.1)$$

Many models of $\Omega(\theta)$, where θ is the angle measured from the mean wave direction, have been proposed to represent the angular spreading of ocean waves. The most common form was given by Pierson et al. (1955),

$$\Omega(\theta) = \frac{2}{\pi} \cos^2(\theta) \qquad \text{for } -\frac{\pi}{2} \leq \theta \leq \frac{\pi}{2} \qquad (3.4.2)$$

The cosine-square model has a fixed direction width and a standard deviation $\sigma_o = 32.5°$. Another model, extensively applied to ocean swell, with a fixed angular width and $\sigma_o = 25.5°$ is

$$\Omega(\theta) = \frac{8}{3\pi} \cos^4(\theta) \qquad \text{for } -\frac{\pi}{2} \leq \theta \leq \frac{\pi}{2} . \qquad (3.4.3)$$

Substantial progress was made by Longuet-Higgins et al. (1963), who found that their buoy observations fit well a spreading function with a variable directional width

$$\Omega(f,\theta) = \Delta(s)\cos^{2s}(\theta/2) \quad \text{for } -\pi \leq \theta \leq \pi \qquad (3.4.4)$$

with a frequency dependent exponent s = s(f). The values of s ranged from 1 at high frequencies to 10 at low frequencies. The normalization factor $\Delta(s)$ is expressed as

$$\Delta(s) = \frac{2^{(2s-1)}}{\pi} \frac{\Gamma^2(s+1)}{\Gamma(2s+1)}$$

where Γ represents the Gamma function. The particular parameterization for s was studied by Hasselmann et al. (1980) using data collected during JONSWAP. Empirical evidence indicated that s could be related to the local peak frequency fm, in particular,

$$s = 10^{0.99}(f/fm)^{\rho} \qquad (3.4.5)$$

where $$\rho = \begin{cases} 4.06 & \text{for } f < fm \\ -2.34 & \text{for } f \geq fm \end{cases}.$$

Additional support for the directional parameterization in (3.4.4) was presented by Tyler et al. (1974) who concluded that (3.4.4) provided adequate estimates of the directional distributions for duration-limited wave fields as observed from radio backscatter. Mitsuyasu et al. (1975) reached a similar conclusion from their analysis of buoy measurements. Figure 3.29 gives an impression how these various angular spreading factors compare to one another.

It is clear from the definition of energy density (3.4.1) that no mean direction can be extracted. In order to assign a direction to the waves, a vector quantity is required. The particular choice of such a vector variable has provoked some controversy within wave research.

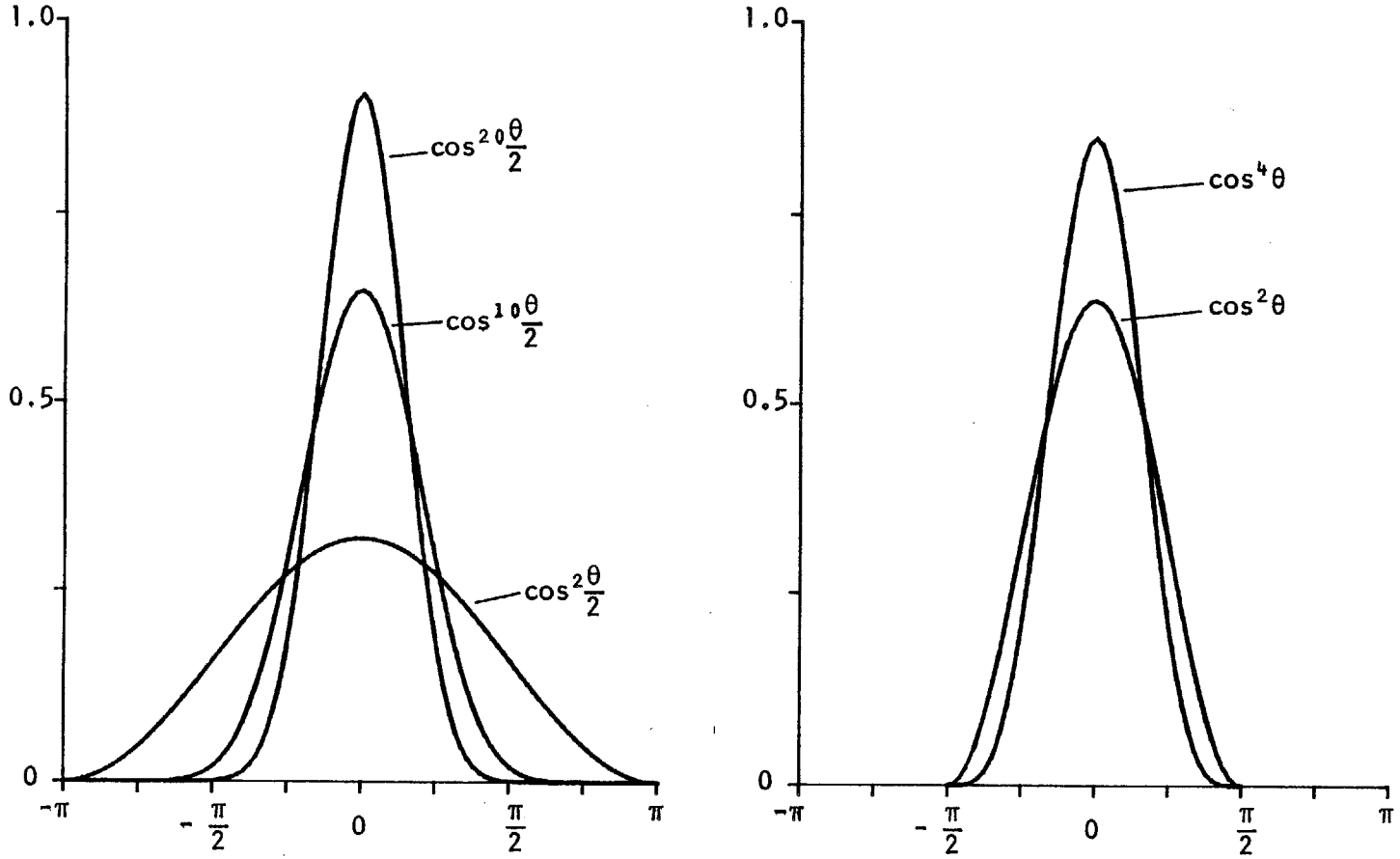


Fig. 3.29 Comparison of typical angular spreading functions.

Commonly wave momentum, a vector quantity, is employed in the mathematical formalism when the directional aspect of the waves is important. The controversy, whether waves possess momentum or not has repeatedly troubled the minds of scientists. McIntyre (1981) shed some light on the so-called "wave momentum myth", by demonstrating on some simple, classical examples the misuse of the meaning of wave momentum.

For strictly periodic surface gravity waves in an inviscid, incompressible fluid of large depth and with an irrotational motion, the total momentum is found near the surface. It turns out to be equal to the momentum of the Stokes drift. By definition, the Stokes drift velocity is the difference between the Lagrangian mean particle velocity and the Eulerian mean velocity, and can be expressed as (Bye, 1967; Kenyon, 1969)

$$U_s(z) = \frac{1}{\rho} \iint_{-\infty}^{\infty} F(\underline{k}) \frac{\underline{k}}{\omega} \left[\frac{2k \cosh 2k(z+h)}{\sinh 2kh}\right] d\underline{k} \qquad (3.4.6)$$

where z is the vertical coordinate measured positive upward. The Stokes drift is a generally non-zero wave property. In this case, it spatially coincides with the total mean momentum, since the Eulerian velocity can not change without the presence of any mean horizontal pressure gradients during wave generation. The average momentum per unit surface area is then defined by (Hasselmann, 1963b)

$$\underline{M} \equiv \int_{-h}^{\eta} \rho U(z)\, dz = \iint_{-\infty}^{\infty} F(\underline{k}) \frac{\underline{k}}{\omega} d\underline{k} \qquad (3.4.7)$$

For a single sinusoidal wave component, this relation is conveniently written (Phillips, 1977) as

$$\underline{M} = \frac{\tilde{E}}{c} \hat{k} \tag{3.4.8}$$

where $\hat{k}$ is the unit wave number vector. Starr (1959) has shown that momentum and energy are related through the phase velocity in analogy to Einstein's well-known law $E = mc^2$. This implies that the mean momentum, associated with the Stokes drift does, by definition, remain with the waves. However, as pointed out by McIntyre (1981), the extension to wave trains of finite length cannot be readily made since, in addition to the Stokes drift portion, there are other contributions to the momentum of the system. In particular, he cited examples where the resulting wave momentum can either be equal to zero or different from the momentum associated with the Stokes drift. Ursell (1950) and Hasselmann (1970) have noted that a steady Stokes drift velocity can not exist in an ocean, because there is no force that counteracts the effect of the Coriolis force on the translating fluid particles.

This verbal inaccuracy, as remarked by McIntyre (1981), shows up more readily when using simple wave theory. In terms of the velocity potential, the wave momentum is mathematically expressed as

$$\underline{M} = \rho \overline{\int_{-h}^{\eta} \underline{u} \, dz} \tag{3.4.9}$$

in which $\underline{u} = \nabla\phi$ and ϕ is the velocity potential. The above relation is also the precise statement of the mass flux associated with the wave motion. Consequently, the momentum flux is a scalar, since

$$\underline{u} \cdot \underline{M} = \rho \overline{\int_{-h}^{\eta} (\underline{u} \cdot \underline{u})\, dz} = \tilde{E} \tag{3.4.10}$$

and defines the energy of the wave motion. The next vector quantity gives

$$\underline{\tilde{E}}_f = \rho \overline{\int_{-h}^{\eta} (\underline{u} \cdot \underline{u})\underline{u}\, dz} = \underline{c}_g \tilde{E} \tag{3.4.11}$$

which is the energy flux. Therefore, it appears that the energy flux is a more suitable parameter to describe the direction of the wave motion, because the underlying physical principle of wave prediction is based on a wave energy transport equation. Previous approaches have derived the equations governing the directional relaxation of the wave field from wave momentum considerations (Günther et al. 1981). The energy flux and momentum approaches will both yield the same mean direction as long as there is no mean motion of the medium. In the case when currents are present, it can be shown that the wave momentum follows the direction of the absolute phase velocity vector, $\underline{c}_a$,

$$\underline{c}_a = \underline{c}_r + \underline{U} \cdot \hat{k} \tag{3.4.12}$$

where $\underline{c}_r = (\omega/k)\hat{k}$ is the relative phase velocity vector and $\underline{U}$ is the current vector. Similarly, the wave energy flux is in the direction of the absolute group velocity vector, $\underline{c}_{g_a}$,

$$\underline{c}_{g_a} = \underline{c}_{g_r} + \underline{U} \tag{3.4.13}$$

where $\underline{c}_{g_r} = \partial\omega/\partial\underline{k}$ is the group velocity of the waves relative to the fluid motion. In general, the directions specified by these two equations will not coincide. However, from this it appears that the energy flux approach is more general, since wave action, energy divided by the intrinsic frequency, also propagates along trajectories defined by (3.4.13) (Bretherton and Garrett, 1969). As a matter of fact, the wave energy flux can be expressed in terms of the wave action variable A. Let us define the energy flux of a wave spectrum or the wave energy flux density as $\underline{F}_f(\underline{k}) \equiv \underline{c}_g F(\underline{k})$. Then, the energy flux density

$$\underline{F}_f(\underline{k}) = \frac{F(\underline{k})}{\omega}\,\frac{g}{2}\left(\tanh kh + \frac{kh}{\cosh^2 kh}\right)\hat{n}(\underline{k})$$

$$= A(\underline{k})\, G(kh)\, \hat{n}(\underline{k}) \qquad (3.4.14)$$

might be thought of as the product of wave action times a gravity reduction factor, G(kh), which ranges from 1/2 g in deep water to g in shallow water. $\hat{n}(\underline{k})$ is a unit vector in the direction of $\underline{k}$.

Following Günther et al. (1981) we can analogously describe the wave energy flux as a function of frequency and direction by

$$\underline{F}_f(f,\theta) = c_g(f)\, E(f,\theta)\, \hat{n}(\theta) \qquad (3.4.15)$$

where $\hat{n}(\theta)$ is a unit vector pointing in the direction of wave propagation θ. Similarly, the x and y components are (θ is measured clockwise from north, $\theta = 0$);

$$F_{fx}(f,\theta) = \sin\theta \left|\underline{F}_f(f,\theta)\right|$$

$$F_{fy}(f,\theta) = \cos\theta \left|\underline{F}_f(f,\theta)\right| \qquad (3.4.16)$$

The total energy flux along the cartesian coordinates is given by the integrals

$$I_x = \iint F_{fx}(f,\theta)\, df\, d\theta$$
$$I_y = \iint F_{fy}(f,\theta)\, df\, d\theta . \qquad (3.4.17)$$

Then, a mean direction θ_o averaged over the entire windsea spectrum may be defined as the direction of the vector

$$\underline{I} = (I_x, I_y) \qquad (3.4.18)$$

and specifically,

$$\theta_o = \tan^{-1}[I_x/I_y] \qquad (3.4.19)$$

with $\sin\theta_o = I_x/|\underline{I}|$ and $\cos\theta_o = I_y/|\underline{I}|$.

Since the description of the wind wave field now incorporates a directional aspect, we must also generalize the transport equation previously defined in Section 3.2. Applying the Lagrangian operator D/Dt to $\underline{F}_f = \underline{c}_g F(\underline{k})$ yields

$$\frac{D}{Dt}\underline{F}_f(\underline{k}) = \underline{c}_g(\underline{k})\frac{DF(\underline{k})}{Dt} + F(\underline{k})\frac{D}{Dt}\underline{c}_g(\underline{k}) \qquad (3.4.20)$$

where the first term on the right-hand side is equal to (3.2.4) times the group velocity. Hence, the energy flux transport equation in wave number space is

$$\frac{D}{Dt}\underline{F}_f(\underline{k}) = \frac{\partial}{\partial t}\underline{F}_f(\underline{k}) + (\underline{c}_g \cdot \nabla_x)\underline{F}_f(\underline{k}) + (\dot{\underline{k}} \cdot \nabla_k)\underline{F}_f(k)$$
$$= \underline{c}_g\, T(\underline{k}) + \dot{\underline{c}}_g\, F(\underline{k}) \qquad (3.4.21)$$

The term $\dot{\underline{c}}_g F(\underline{k})$ is explicitly given by

$$\dot{\underline{c}}_g F(\underline{k}) = F(\underline{k}) (\underline{c}_g \cdot \nabla_x) \underline{c}_g = \underline{F}_f(\underline{k}) (\nabla_x \cdot \underline{c}_g) \qquad (3.4.22)$$

Here we assume $\frac{\partial}{\partial t} \underline{c}_g = (\dot{\underline{k}} \cdot \nabla_k) \underline{c}_g = 0.$

As before, the more convenient form of the transport equation will be in terms of frequency and direction. Using the same definition of the Jacobian J given in (3.2.20), we have the relation

$$\underline{F}_f(\underline{k}) = J \cdot \underline{E}_f(f,\theta) \qquad (3.4.23)$$

with $\underline{E}_f = \underline{c}_g E(f,\theta)$. Substituting (3.4.23) into (3.4.21) and noting that $\partial J/\partial t = \partial J/\partial \theta \equiv 0$, we obtain

$$\frac{\partial}{\partial t} \underline{E}_f + (\underline{c}_g \cdot \nabla_x) \underline{E}_f + (\dot{\underline{k}} \cdot \nabla_k \theta) \frac{\partial}{\partial \theta} \underline{E}_f =$$

$$J^{-1} [\underline{c}_g T - \underline{E}_f (\underline{c}_g \cdot \nabla_x) J] + \underline{E}_f (\nabla_x \cdot c_g) \qquad (3.4.24)$$

in which we made use of the relation (3.2.22). The dispersion relation (3.2.9) has previously been expressed as a function of ω_h (3.1.41),

$$\chi \cdot \tanh [\omega_h{}^2 \chi] = 1 . \qquad (3.4.25)$$

In terms of these variables, the group velocity is given as

$$c_g(f,h) = \frac{g}{2\omega\chi} [1 + \omega_h{}^2 (\chi^2 - 1)] \qquad (3.4.26)$$

From the dispersion relation we recognize that

$$\chi = \frac{1}{\tanh kh} \qquad (3.4.27)$$

and

$$kh = \chi \omega_h{}^2 . \qquad (3.4.28)$$

The refraction term in (3.4.24) is readily rewritten making use of (3.2.23)

$$(\dot{\underline{k}} \cdot \underline{\nabla}_k \theta) \frac{\partial}{\partial \theta} = -\frac{\omega}{2} \left(\frac{\chi^2 - 1}{\chi}\right) \left[\cos\theta \frac{\partial h}{\partial x} - \sin\theta \frac{\partial h}{\partial y}\right] \frac{\partial}{\partial \theta} = \dot{\theta} \frac{\partial}{\partial \theta} \qquad (3.4.29)$$

The shoaling term $J^{-1}(\underline{c}_g \cdot \underline{\nabla}_x)J$ gives in component form

$$S.T. = J^{-1} c_g \frac{\partial J}{\partial h} \frac{\partial h}{\partial \underline{x}} \begin{bmatrix} \sin\theta \\ \cos\theta \end{bmatrix} . \qquad (3.4.30)$$

The derivative of J with respect to depth h can be evaluated as follows,

$$\frac{\partial J}{\partial h} = \frac{\partial}{\partial h} \left[\frac{c\, c_g}{2\pi\omega}\right] =$$

$$\frac{g^2}{4\pi\omega^3} \left[-\frac{2}{\chi^3} \frac{\partial \chi}{\partial h} + \frac{\omega^2}{g} \left(\frac{\chi^2 - 1}{\chi^2}\right) + \omega_h^2 \frac{2}{\chi^3} \frac{\partial \chi}{\partial h}\right] \qquad (3.4.31)$$

From the partial differentiation of (3.4.25) we obtain

$$\frac{\partial \chi}{\partial h} = -\frac{\omega^2}{g} \frac{\chi(\chi^2 - 1)}{1 + \omega_h^2(\chi^2 - 1)} . \qquad (3.4.32)$$

Upon substitution of (3.4.32) into (3.4.31) and after some simplifications gives

$$\frac{\partial J}{\partial h} = \frac{1}{2\pi k} \frac{\omega}{2} \frac{(\chi^2 - 1)}{\chi} \left[1 + \frac{2(1 - \omega_h^2)}{1 + \omega_h^2(\chi^2 - 1)}\right] \qquad (3.4.33)$$

Introducing (3.4.33) and (3.4.26) in (3.4.30) and evaluating the remaining variables finally yields

$$S.T. = \frac{\omega}{2} \frac{(\chi^2 - 1)}{\chi} \left[1 + \frac{2(1 - \omega_h^2)}{1 + \omega_h^2(\chi^2 - 1)}\right] \left[\sin\theta \frac{\partial h}{\partial x} + \cos\theta \frac{\partial h}{\partial y}\right] \qquad (3.4.34)$$

The last term on the right-hand side of (3.4.24) can be determined in a similar manner, i.e.,

$$(\underline{\nabla}_x \cdot \underline{c}_g)\underline{E}_f = \underline{E}_f\{\frac{\omega}{2}\frac{(\chi^2-1)}{\chi}\left(2 - \frac{2\omega_h^2\chi^2}{1+\omega_h^2(\chi^2-1)}\right)\left[\sin\theta\frac{\partial h}{\partial x} + \cos\theta\frac{\partial h}{\partial y}\right]\} \quad (3.4.35)$$

Upon substitution of (3.4.29), (3.4.34) and (3.4.35) into (3.4.24) and combining like terms, finally yields

$$\frac{\partial \underline{E}_f}{\partial t} + (\underline{c}_g \cdot \underline{\nabla}_x)\underline{E}_f + \dot{\theta}\frac{\partial \underline{E}_f}{\partial \theta} = \underline{S}_f - \underline{E}_f\frac{\omega}{2}\frac{(\chi^2-1)}{\chi}\left[\sin\theta\frac{\partial h}{\partial x} + \cos\theta\frac{\partial h}{\partial y}\right] \quad (3.4.36)$$

in which $\underline{S}_f = \underline{c}_g S(f,\theta)$ is the net flux vector due to all sources and sinks of energy. This equation describes then the balance of the wave energy flux in frequency direction space due to refraction, shoaling and the net effect from the fluxes of energy in and out of the waves. We recognize that the term $(\sin\theta\,\partial h/\partial x + \cos\theta\,\partial h/\partial y)$ expresses the depth gradient parallel to the direction of wave propagation. The depth gradient perpendicular to the propagation direction as in $\dot{\theta}$ represents the effect due to refraction. For infinitely deep ocean, $h \to \infty$ and therefore $\chi \to 1$, equation (3.4.36) reduces to the familiar deep water version,

$$\frac{\partial \underline{E}_f}{\partial t} + \underline{c}_g \cdot \underline{\nabla}_x \underline{E}_f = \underline{T}_{deep} \quad (3.4.37)$$

CHAPTER 4

A PARAMETRIC WINDSEA MODEL FOR FINITE DEPTH

Es wird nachstens schon besser gehen,
Wenn Ihr lernt alles reduzieren
Und gehorig klassifizieren.

Next time, surely you will have more
Success, when you have learned how
To reduce and classify all by its use.

(Mephistopheles)

--FAUST I, Studierzimmer
Johann Wolfgang von Goethe

The concept of a parametric windsea description has originally been proposed by Hasselmann et al. (1973, 1976). Since the inclusion of the general nonlinear energy transfer integral in a wave prediction scheme is still computationally infeasible, it is necessary to represent the wave-wave interaction process by some parameterized form if it is to be incorporated in a wave model. The JONSWAP results have shown that in conjunction with the shape-stabilizing effect of the nonlinear wave-wave interactions, the JONSWAP spectrum with its five free parameters replicated strikingly well the actual sea state. For deep water, this approach has been extensively tested with considerable success (Günther et al. 1979a, 1979b; Ewing et al. 1979; Graber, 1979). The surface wave field is classified by two domains: a windsea domain, where the local wind plays an active role during the generation process and a swell domain, where waves are no longer under the influence of the local wind and the nonlinear interactions. Combined, this hybrid representation of the surface wave field is simulated by a parametric windsea description and by a propagation scheme along characteristics for the swell. The later method was first introduced by Barnett et al. (1969). Both wave domains are allowed to interchange energies if certain situations arise. Windsea energy is transferred to swell characteristics when the wind falls below a level such that

the Pierson-Moskowitz frequency, sustained by this wind, exceeds the local windsea peak frequency. On the other hand, swell energy can be picked up by the local windsea when the peak frequency is less than the frequency bins of ray characteristics with non-zero energy. A detailed description of these exchanges can be found in Günther et al. (1979b) and Graber (1979).

The extension of the parametric approach to finite depth will be discussed in the following sections.

4.1 A Parametric Transport Equation Using An Energy Flux Approach

In order to derive equivalent prognostic equations for the JONSWAP parameters and the directional relaxation parameter, we must make the following assumptions concerning the windsea wave spectrum in finite depth:

i. All one-dimensional energy spectra in arbitrary water depths can be modeled by the family of finite depth JONSWAP spectra.

ii. The TMA spectrum can always be related to its corresponding deep water spectrum by multiplication of the reciprocal KKZ factor.

iii. The two-dimensional windsea spectrum has a frequency independent directional distribution Ω, which is centered around the mean direction of the windsea, θ_o, i.e.,

$$F(f,h,\theta) = E(f,h)\,\Omega(\theta,\theta_o)\,, \tag{4.1.1}$$

where $$E(f,h) = \int F(f,h,\theta)\,d\theta \tag{4.1.2}$$

iv. The directional distribution is assumed to be given by

$$\Omega(\theta,\theta_o) = \frac{2}{\pi}\cos^2(\theta - \theta_o) \quad \text{for } |\theta-\theta_o| \leq \frac{\pi}{2}$$

$$= 0 \quad \text{for } |\theta-\theta_o| > \frac{\pi}{2} \tag{4.1.3}$$

v. The nonlinear wave-wave interactions are the prevailing process and ensure shape similarity of the windsea spectrum in any water depth.

Combining assumptions (i) - (iv), we can define the finite-depth energy flux density spectrum as

$$\underline{F}(f,\theta;h,a_i) = \underline{c}_g(f,\theta,h)\,\Phi(\omega_h)\,E(f;a_i)\,\Omega(\theta,\theta_o) \tag{4.1.4}$$

where $E(f;a_i)$ is the JONSWAP spectrum defined in (3.1.45) and $a_i = [fm,\alpha,\gamma,\sigma_a,\sigma_b]$ is the parameter vector, $\Phi(\omega_h)$ is the KKZ transformation factor as given in (3.1.40), $\underline{c_g}$ is the group velocity vector, and $\Omega(\theta,\theta_o)$ is the angular distribution from iv., with the mean direction parameter $a_6 = \theta_o$.

The next step is to introduce in general terms some algorithms which extract out of any given flux spectrum the set of individual parameters by some best-fitting methodology. Let ϕ_i designate an algorithm, so that,

$$a_i = \phi_i\{\underline{F}\} \qquad \text{for } i = 1,\ldots,6 \tag{4.1.5}$$

In particular, ϕ_i is a differentiable functional and the curly brackets indicate that the operation of ϕ_i is carried out on the enclosed argument. Then a small variation $\delta\underline{F}$ in $\underline{F}$ will evoke a variation δa_i in a_i, such that

$$\delta a_i = \phi_i'\{\underline{F}, \delta\underline{F}\} \equiv \phi_i'\{\delta\underline{F}\} \tag{4.1.6}$$

Here ϕ_i' is a linear function of $\delta\underline{F}$ and denotes the Fréchet or variation derivative of ϕ_i. Now the meaning of the curly brackets should read as: the transformation ϕ_i' applied to $\delta\underline{F}$ at the position $\underline{F}$. The Fréchet derivative is generally obtained from the linear term of the Taylor series expansion (Collatz, 1964),

$$\phi_i\{\underline{F} + \delta\underline{F}\} - \phi_i\{\underline{F}\} = \phi_i'\{\underline{F}\}\ \delta\underline{F} \tag{4.1.7}$$

A variation in $\underline{F}$ can be expressed by the differential

$$\delta \underline{F} = \frac{\partial \underline{F}}{\partial a_j} \delta a_j \tag{4.1.8}$$

and applying (4.1.6) yields the relation

$$\phi_i' \left\{ \frac{\partial \underline{F}}{\partial a_j} \right\} = \frac{\delta a_i}{\delta a_j} \equiv \Delta_{ij} \tag{4.1.9}$$

The Kronecker delta, Δ_{ij} is unity for $i = j$ and zero for $i \neq j$.

For the finite depth case, a small change in the energy flux spectrum (4.1.4) is approximated by the differential

$$\partial \underline{F} = \frac{\partial \underline{F}}{\partial a_j} \partial a_j + \frac{\partial \underline{F}}{\partial h} \partial h \tag{4.1.10}$$

and noting that $\partial h/\partial t \equiv \partial h/\partial \theta \equiv 0$, we can rewrite the energy flux transport equation (3.4.36) in component form

$$\frac{\partial \underline{F}}{\partial a_j} \frac{\partial a_j}{\partial t} + c_{g_x} \frac{\partial \underline{F}}{\partial a_j} \frac{\partial a_j}{\partial x} + c_{g_y} \frac{\partial \underline{F}}{\partial a_j} \frac{\partial a_j}{\partial y} =$$

$$\underline{S} - \dot{\theta} \frac{\partial \underline{F}}{\partial \theta} - \frac{\partial \underline{F}}{\partial h} (\underline{c}_g \cdot \underline{\nabla}_x h) - \Psi \underline{F} \tag{4.1.11}$$

where $\Psi = \frac{\omega}{2} \frac{(\chi^2 - 1)}{\chi} \left[\sin\theta \frac{\partial h}{\partial x} + \cos\theta \frac{\partial h}{\partial y} \right]$.

Applying the transformation ϕ_i' to (4.1.11) and invoking the relation (4.1.9) we obtain the parametric transport equation for arbitrary water depths

$$\frac{\partial a_i}{\partial t} + D_{ijx}\frac{\partial a_j}{\partial x} + D_{ijy}\frac{\partial a_j}{\partial y} = S_i + R_i \qquad \text{for } i,j = 1,\ldots,6 \qquad (4.1.12)$$

$$\text{in which } D_{ijx} = \phi_i'\{c_{g_x}\frac{\partial \underline{F}}{\partial a_j}\},\ D_{ijy} = \phi_i'\{c_{g_y}\frac{\partial \underline{F}}{\partial a_j}\} \qquad (4.1.13)$$

$$S_i = \phi_i'\{\underline{S}\} \qquad (4.1.14)$$

$$R_i = \phi_i'\{-\dot{\theta}\frac{\partial \underline{F}}{\partial \theta} - \Psi\underline{F} - \frac{\partial \underline{F}}{\partial h}(\underline{c}_g \cdot \underline{\nabla}_x h)\} \qquad (4.1.15)$$

The terms D_{ij} in (4.1.13) are the x and y components of the generalized finite depth propagation matrix, respectively. The source function S_i represents the net effect on the parameter a_i due to the sum of the following processes,

$$S_i = \phi_i'\{\underline{T}_{in} + \underline{T}_{nl} + \underline{T}_{bf} + \underline{T}_{ds}\} \qquad (4.1.16)$$

with $\underline{T}_{in}$, the energy flux into the waves from the wind; $\underline{T}_{nl}$, the transfer of energy within the spectrum due to nonlinear, resonant wave-wave interactions; $\underline{T}_{bf}$, the dissipation of energy due to bottom friction; $\underline{T}_{ds}$, the dissipation of energy due to wave breaking. The remaining terms enumerated in R_i describe the change of the parameter resulting from refraction, shoaling and the spectral adjustment to a varying bottom topography.

4.2 The Linear Transformation Functionals

As previously remarked, the purpose of the JONSWAP parameterization is to provide a computational tool by which the dependence of the spectral parameters on fetch, wind speed and direction and other factors can be studied in a consistent way during the development stages of the wave spectrum. The original procedures for determining the set of optimally fitted parameters of any measured windsea spectrum was presented by Müller (1976). The extension to a continuous description was made by Günther et al. (1979b), which proved to be more convenient for theoretical calculations. It should be realized that these methods have been specifically derived for the one-dimensional JONSWAP spectrum in deep water. Thus, from the definition of the energy flux spectrum (4.1.4) we may alternatively state the JONSWAP spectrum as

$$E(f;a_i) = [c_g(f,h)\Phi(\omega_h)]^{-1} \int \{F_x^2(f,\theta) + F_y^2(f,\theta)\}^{1/2} d\theta = \hat{F} \quad (4.2.1)$$

Now, we can redefine the functionals (4.1.5) operating on $\underline{F}(f,h,\theta)$ so that they reveal the parameters a_i of the JONSWAP shape

$$a_i = \phi_i\{\underline{F}\} \equiv \zeta_i\left\{ \frac{\int [F_x^2(f,\theta,h) + F_y^2(f,\theta,h)]^{1/2} d\theta}{c_g(f,h)\Phi(\omega_h)} \right\} = \zeta_i\{E\} \quad (4.2.2)$$

Here the operator ϕ_i applied to $\underline{F}$ should be interpreted as the operation ζ_i on the scalar $\hat{F}$. Since $\hat{F}$ is equal to E, by (4.2.1), we essentially apply ζ_i directly to E to recover the JONSWAP parameters. These functionals are previously defined in Graber (1979)

and Günther et al. (1979b). Then the functional derivative ζ_i' is straightforward from (4.1.7),

$$\delta a_i = \phi_i'\{\delta \underline{F}\} \equiv \zeta_i'\{ \frac{1}{c_g \Phi} \int \frac{F_x \delta F_x + F_y \delta F_y}{|\underline{F}|} d\theta\} = \zeta_i'\{\delta E\} \qquad (4.2.3)$$

These derivations are analogous to those described by Günther et al. (1981) in terms of the momentum density spectrum. Evaluation of the insides of ζ_i and ζ_i' recovers the previously defined functionals for the JONSWAP spectral shape (Günther et al. 1979b). A detailed derivation of the same functionals can also be found in Graber (1979).

Conceptually, the simplest parameter of a one-dimensional spectrum E(f) is the peak frequency fm. Thus, fm can be determined from the solution of the equation.

$$E'(f) = \frac{\partial E(f)}{\partial f} = 0 \qquad (4.2.4)$$

Equation (4.2.4) can be equivalently written in terms of the argument E, we get

$$a_1 = fm = \phi_1\{\underline{F}\} = \zeta_i\{E\} = \int f\, \delta[E']\, d[E] \qquad (4.2.5)$$

where δ is Dirac's delta and the prime indicates differentiation with respect to frequency. The α parameter is commonly determined in the range of 1.35fm to 2.0fm and is given by

$$a_2 = \alpha = \phi_2\{\underline{F}\} = \zeta_2[E, fm] \qquad (4.2.6)$$

$$= \frac{1}{0.65fm} \int_{1.35fm}^{2.0fm} \frac{E\, f^5 (2\pi)^4}{g^2} \exp\left[\frac{5}{4}\left(\frac{f}{fm}\right)^{-4}\right] df$$

Once the parameters fm and α are known, the Pierson-Moskowitz spectrum can be constructed and is restated here as

$$E_{PM}(f) = \alpha g^2 (2\pi)^{-4} f^{-5} \exp\left[-\frac{5}{4}\left(\frac{f}{fm}\right)^{-4}\right] \qquad (4.2.7)$$

The enhancement parameter γ can now be calculated from

$$a_3 = \gamma = \phi_3\{\underline{F}\} = \zeta_3\{E, fm, \alpha\} = \int \frac{E(f)}{E_{PM}(f)} \delta(f - fm)\, df \qquad (4.2.8)$$

For the remaining two spectral bandwidths σ_a and σ_b, we use the function, which is valid for $\gamma > 1$,

$$G(f) = \ell n \left[\frac{E(f)}{E_{PM}(f)} \right] - e^{-0.5} \ln \gamma \qquad (4.2.9)$$

The zeros of G(f) are

$$z_a = fm(1 - \sigma_a) \quad \text{and} \quad z_b = fm(1 + \sigma_b) \qquad (4.2.10)$$

Consequently, we can write for $f \leq fm$,

$$\sigma_a = 1 - \frac{f}{fm} \qquad (4.2.11)$$

which is generalized to

$$a_4 = \sigma_a = \phi_4\{\underline{F}\} = \zeta_4\{E, fm, \alpha, \gamma\} = 1 - \frac{1}{fm} \int_{f \leq fm} f\, \delta[G(f)]\, d[G(f)] \qquad (4.2.12)$$

Similarly, for $f > fm$, we have

$$\sigma_b = \frac{f}{fm} - 1 \qquad (4.2.13)$$

which is given in integral form by

$$a_5 = \sigma_b = \phi_5\{\underline{F}\} = \zeta_5\{E,fm,\alpha,\gamma\} = -1 + \frac{1}{fm} \int_{f>fm} f\, \delta[G(f)]\, d[G(f)] \quad (4.2.14)$$

Since $\delta\underline{F}$ is the variation of $\underline{F}(f,\theta,h)$, the functional derivative $\phi_i'\{\underline{F},\delta\underline{F}\} = \phi_i'\{\delta\underline{F}\}$ should be understood to mean the operation ϕ_i' at the position $\underline{F}(f,\theta,h)$ in the spectral space applied to $\delta\underline{F} = \underline{Z}(f,\theta,h)$, where $\underline{Z}$ is an arbitrary function in the spectral space (f,θ,h). Analogously, we use the same notation on ζ_i' and define $\zeta_i'\{E,\delta E\} = \zeta_i'\{\delta E\}$, where $\delta E = \hat{Z}(f)$ is an arbitrary function in frequency. For the sake of completeness we only state the final form of the functional derivatives for $i = 1,\ldots,5$, and the reader is refered to either Günther (1981) or Graber (1979) for a detailed derivation. Thus, we have with this definition

$$\phi_1'\{\underline{Z}(f,\theta,h)\} = \zeta_1'\{\hat{Z}(f)\} = -\frac{1}{E''(fm)} \int \delta(f - fm)\, \frac{d}{df}\, \hat{Z}(f)\, df \quad (4.2.15)$$

$$\phi_2'\{\underline{Z}(f,\theta,h)\} = \zeta_2'\{\hat{Z}(f)\} = \frac{\alpha}{0.65\ fm} \int_{1.35fm}^{2.0fm} \frac{\hat{Z}(f)}{E_{PM}(f)}\, df + \frac{\alpha}{fm}\, 0.72165\, \phi_1'\{\hat{Z}(f)\} \quad (4.2.16)$$

$$\phi_3'\{\underline{Z}(f,\theta,h)\} = \zeta_3'\{\hat{Z}(f)\} = \int \delta(f-fm)\, \frac{1}{E_{PM}(f)}\, [\hat{Z}(f)]\, df + \gamma\left[\frac{5}{fm}\, \phi_1'\{\hat{Z}(f)\} - \frac{1}{\alpha}\, \phi_2'\{\hat{Z}(f)\}\right] \quad (4.2.17)$$

$$\phi_4'\{\underline{Z}(f,\theta,h)\} = \zeta_4'\{\hat{Z}(f)\} = \frac{1}{fm}\left[\frac{z_a}{fm}\phi_1'\{\hat{Z}(f)\} + \frac{1}{G'(z_a)}\left(\int \delta(f-z_a)\frac{\hat{Z}(f)}{E(f)}\,df\right.\right.$$

$$+ \frac{5}{fm}\left(\frac{z_a}{fm}\right)^{-4}\phi_1'\{\hat{Z}(f)\} - \frac{1}{\alpha}\phi_2'\{\hat{Z}(f)\}$$

$$\left.\left. - \frac{e^{-0.5}}{\gamma}\phi_3'\{\hat{Z}(f)\}\right)\right] \qquad \text{for } f \leq fm \qquad (4.2.18)$$

$$\phi_5'\{\underline{Z}(f,\theta,h)\} = \zeta_5'\{\hat{Z}(f)\} = -\frac{1}{fm}\left[\frac{z_b}{fm}\phi_1'\{\hat{Z}(f)\} + \frac{1}{G'(z_b)}\left(\int \delta(f-z_b)\frac{\hat{Z}(f)}{E(f)}\,df\right.\right.$$

$$+ \frac{5}{fm}\left(\frac{z_b}{fm}\right)^{-4}\phi_1'\{\hat{Z}(f)\} - \frac{1}{\alpha}\phi_2'\{\hat{Z}(f)\}$$

$$\left.\left. - \frac{e^{-0.5}}{\gamma}\phi_3'\{\hat{Z}(f)\}\right)\right] \qquad \text{for } f > fm \qquad (4.2.19)$$

This specific set of linear transformation functionals for $i = 1,\ldots,5$ can now be applied to the energy flux transport equation to arrive at a set of equivalent prognostic transport equations for the individual parameters.

4.3 The Generalized Propagation Terms D_{ij} For Finite Depth

In this section we limit our treatment of the advection terms to the JONSWAP parameters. The terms involving the directional relaxation parameter θ_o are discussed in more detail in the subsequent section. The explicit mathematical expressions of the finite depth propagation terms are determined analogously to the deep water case by applying the appropriate transformation functional to the advection terms in the energy flux transport equation. We shall proceed as follows by writing the partial derivative of (4.1.4) with respect to the parameter a_j as

$$\frac{\partial \underline{F}}{\partial a_j} = \frac{g}{2\omega\chi^3} \frac{\partial E}{\partial a_j} \frac{2}{\pi} \cos^2(\theta-\theta_o) \begin{bmatrix} \sin\theta \\ \cos\theta \end{bmatrix} \tag{4.3.1}$$

in which we have substituted the explicit mathematical expressions of c_g, Φ and Ω. Further, it is understood that E subsequently refers to the JONSWAP spectrum (3.1.45). Introducing (4.3.1) in the definition of D_{ij} (4.1.13) and invoking the operation defined in (4.2.3), we get for the x and y components, respectively,

$$D_{ijx} = \phi_i' \{ c_g(f,h) \frac{\partial E}{\partial a_j} \frac{2}{\pi} \int [\cos^2(\theta-\theta_o) \sin\theta \,] \, d\theta \} \tag{4.3.2}$$

$$D_{ijy} = \phi_i' \{ c_g(f,h) \frac{\partial E}{\partial a_j} \frac{2}{\pi} \int [\cos^2(\theta-\theta_o) \cos\theta \,] \, d\theta \} \tag{4.3.3}$$

Since the functional ϕ_i' is linear in $\underline{Z}$ we can carry out the integrations and simplify so that

$$D_{ijx} = \frac{8}{3\pi} \sin\theta_o \, D_{ij} \tag{4.3.4}$$

and

$$D_{ijy} = \frac{8}{3\pi} \cos\theta_o \, D_{ij} \tag{4.3.5}$$

with $D_{ij} = \zeta_i' \{ c_g(f,h) \frac{\partial E}{\partial a_j} \}$.

The determination of the D_{ij}'s is straightforward and we will only sketch some of the pertinent steps and present a detailed example calculation in Appendix A. Starting with $i = j = 1$, we obtain

$$D_{11} = \zeta_1' \{ c_g(f,h) \frac{\partial E}{\partial fm} \} = c_g(fm,h)[1 + 5\Delta_1] \tag{4.3.6}$$

where $c_g(fm,h)$ is the group velocity at the peak frequency fm in a depth h. Here Δ_1 is given by

$$\Delta_1 = \frac{\sigma^2}{20\sigma^2 + \ln\gamma} \left[1 - 4 \frac{\omega_h{}^2(\chi^2 - 1)(1 - \omega_h{}^2)}{(1 + \omega_h{}^2(\chi^2 - 1)^2} \right] \tag{4.3.7}$$

with $\omega_h = 2\pi fm \sqrt{h/g}$ and $\chi = \chi(\omega_h)$ as determined from (3.1.41). Inspection of (4.3.7) reveals that as $h \to \infty$, we have $\chi \to 1$ and (4.3.6) becomes

$$\lim_{h\to\infty} D_{11} = \frac{g}{4\pi fm} [1 + 5K] \tag{4.3.8}$$

with $K = \sigma^2/(20\sigma^2 + \ln\gamma)$. This is exactly the deep water advection term for the combination (fm, fm) (cf. Graber, 1979; Günther, 1981). Similarly, as $h \to 0$, we find $\chi \to (kh)^{-1}$ and $\omega_h \to kh$. Hence, Δ_1 goes to zero, and (4.3.6) reduces to

$$\lim_{h \to 0} D_{11} = \sqrt{gh} \tag{4.3.9}$$

which states that in very shallow water all frequency components eventually propagate with the same group velocity depending only on the water depth. Furthermore, two additional results of significance can be revealed from (4.3.6). As the spectrum becomes extremely narrow, i.e., $\gamma \to \infty$, so that we can approximate the wave field as a single monochromatic wave, we find for any water depth

$$\lim_{\gamma \to \infty} D_{11} = c_g(fm,h) \tag{4.3.10}$$

since $\Delta_1 \to 0$. Conversely, for a very broad spectrum, i.e., $\gamma \to 1$, and the wave field can be described as a fully developed sea, we obtain

$$\lim_{\gamma \to 1} D_{11} = c_g(fm,h)[1.25 - \Delta_*] \tag{4.3.11}$$

with $\Delta_* = \dfrac{\omega_h^{\,2}(\chi^2 - 1)(1 - \omega_h^{\,2})}{(1 + \omega_h^{\,2}(\chi^2 - 1))^2}$. The group velocity corresponding to the mean frequency of the PM spectrum in deep water (i.e., $\Delta* = 0$) is approximately calculated as

$$c_g(\overline{f_{PM}},\infty) \simeq 1.3\, c_g(f_{PM},\infty) \quad . \tag{4.3.12}$$

Comparing (4.3.12) with (4.3.11) shows close agreement. This should demonstrate that switching to a parametric formulation does not necessarily imply a loss of the physics.

The remaining two non-zero advection coefficients for the fm functional are D_{12} and D_{13}. The effect of σ_a and σ_b on fm and other parameters is negligibly small so that these terms, Di4 and

D_{i5}, are effectively zero for i = 1,2,3. Then, for D_{12} and D_{13} we have

$$D_{12} = - c_g(fm,h) \frac{fm}{\alpha} \Delta_1 \tag{4.3.13}$$

and

$$D_{13} = - c_g(fm,h) \frac{fm}{\gamma} \Delta_1 \tag{4.3.14}$$

Figure 4.1 illustrates the variation of the D_{1j}'s as a function of ω_h and for a family of γ values.

The propagation terms for the α transport equation are calculated from the functional expression

$$D_{2j} = \phi_2' \left[c_g(f,h) \frac{\partial E}{\partial a_j} \right] \tag{4.3.15}$$

Upon evaluation of the appropriate derivatives, we obtain these final expressions

$$D_{21} = c_g(fm,h) \frac{\alpha}{fm} [\Delta_2 + 3.61\Delta_1] \tag{4.3.16}$$

$$D_{22} = c_g(fm,h) [\Delta_3 - 0.722\Delta_1] \tag{4.3.17}$$

$$D_{23} = - c_g(fm,h) \frac{\alpha}{\gamma} 0.722\Delta_1 \tag{4.3.18}$$

where Δ_2 and Δ_3 are integral expressions, which in general can not be evaluated analytically. They are given in terms of the variables defined in (4.3.7)

$$\Delta_2 = - \frac{5 \omega_h^4 \chi}{0.65[1 + \omega_h^2(\chi^2 - 1)} \int_{1.35\omega_h}^{2\omega_h} \frac{1 + s^2(\chi^2(s) - 1)}{s^5 \chi(s)} ds + 0.722 \tag{4.3.19}$$

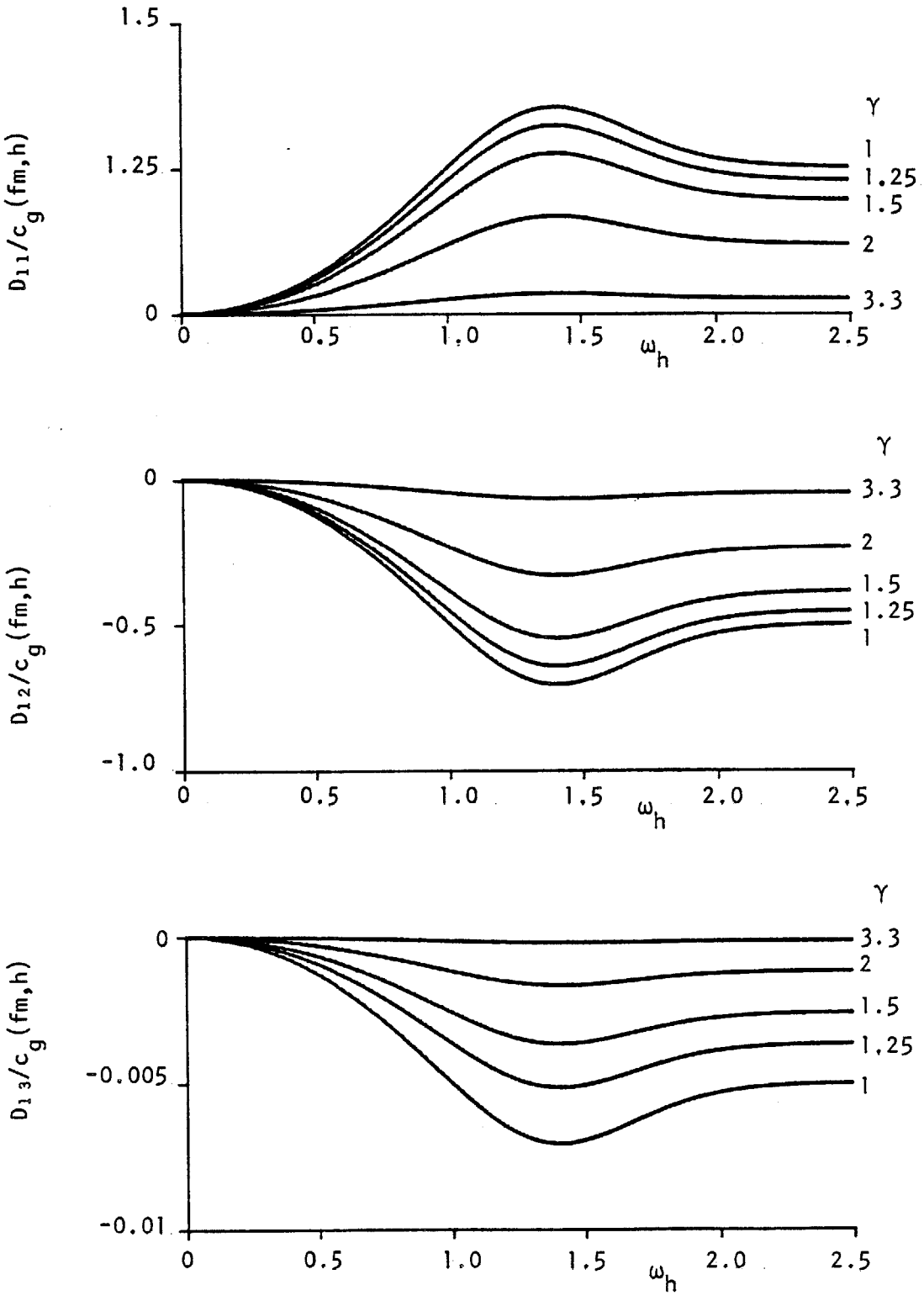


Fig. 4.1 Depth-dependent advection coefficients of parameter fm for a family of γ values. (Results correspond to fm = 0.1 Hz, α = 0.01.)

$$\Delta_3 = \frac{\chi}{0.65[1 + \omega_h{}^2(\chi^2 - 1)]} \int_{1.35\omega_h}^{2\omega_h} \frac{1 + s^2(\chi^2(s) - 1)}{s\chi(s)}\, ds \qquad (4.3.20)$$

The D_{2j}'s are shown in Figure 4.2 indicating their relative strength for different γ values over a range from deep to shallow water.

The coefficients for the γ equation are determined in an analogous manner by applying the functional ϕ'_3 to the advection terms. Thus, we obtain

$$D_{31} = c_g(fm,h)\frac{\gamma}{fm}[21.39\Delta_1 - \Delta_2] \qquad (4.3.21)$$

$$D_{32} = c_g(fm,h)\frac{\gamma}{\alpha}[1 - \Delta_3 - 4.28\Delta_1] \qquad (4.3.22)$$

$$D_{33} = c_g(fm,h)[1 - 4.28\Delta_1] \qquad (4.3.23)$$

in which Δ_1, Δ_2, Δ_3 are the same as previously defined.
Figure 4.3 depicts the D_{3j}'s for the same parameter values and depth ranges.

To determine the advection coefficients D_{i6} we need the partial derivative of (4.1.4) with respect to θ_o,

$$\frac{\partial \underline{F}}{\partial \theta_o} = c_g\, E(f,h)\frac{2}{\pi}\sin 2(\theta - \theta_o)\begin{bmatrix}\sin\theta \\ \cos\theta\end{bmatrix} \qquad (4.3.24)$$

Applying the functionals ϕ'_i, for $i = 1,\ldots,5$ to (4.1.13) with the $\partial\underline{F}/\partial a_j$ term given by (4.3.24), one gets for the x and y components, respectively,

$$D_{i6x} = \phi'_i\{c_g{}^2\, E\frac{2}{\pi}\int \sin 2(\theta - \theta_o)\sin\theta\, d\theta\} \qquad (4.3.25)$$

$$D_{i6y} = \phi'_i\{c_g{}^2\, E\frac{2}{\pi}\int \sin 2(\theta - \theta_o)\cos\theta\, d\theta\} \qquad (4.3.26)$$

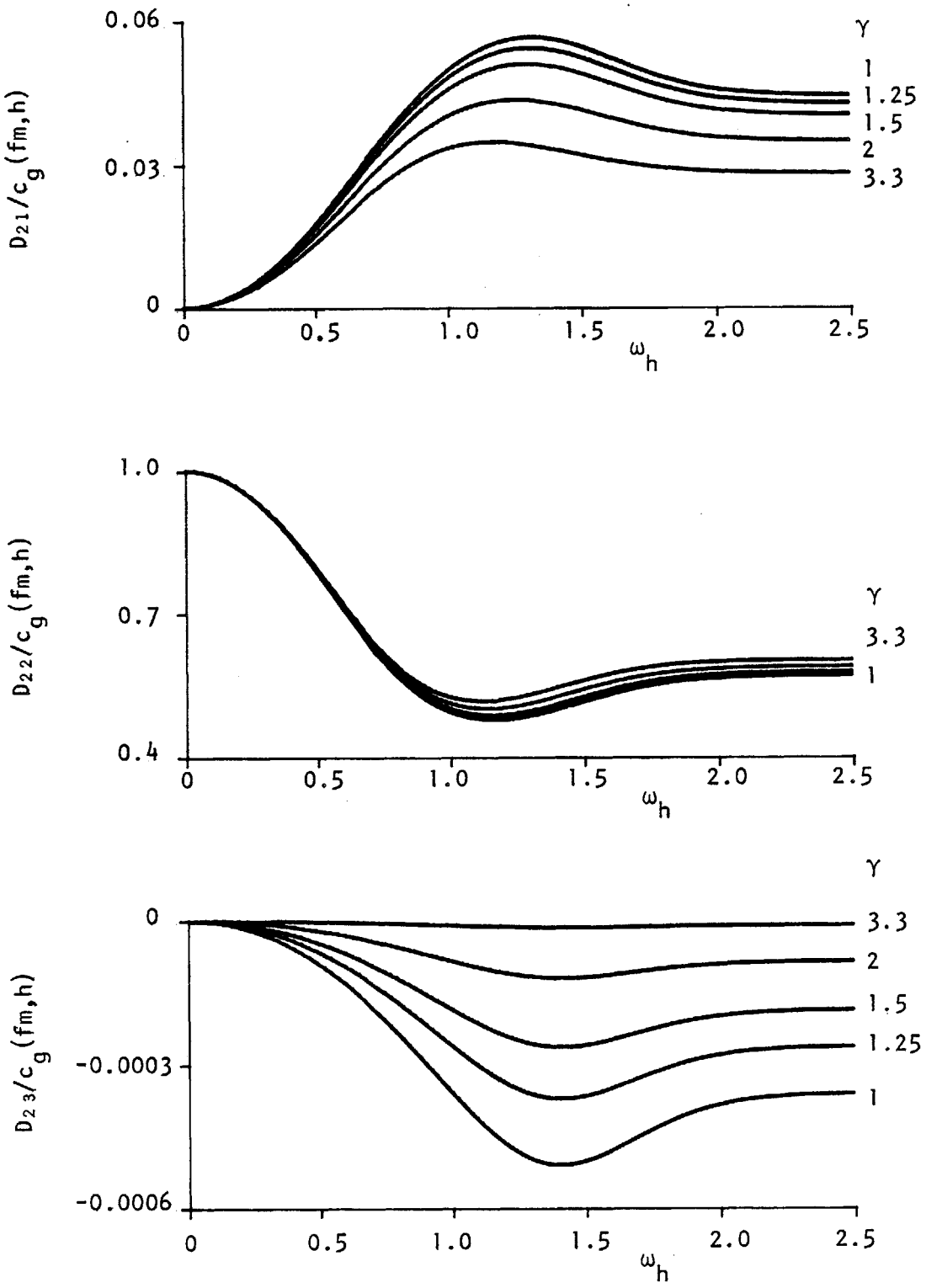


Fig. 4.2 Depth-dependent advection coefficients of parameter α for a family of γ values. (Results correspond to fm = 0.1 Hz, α = 0.01.)

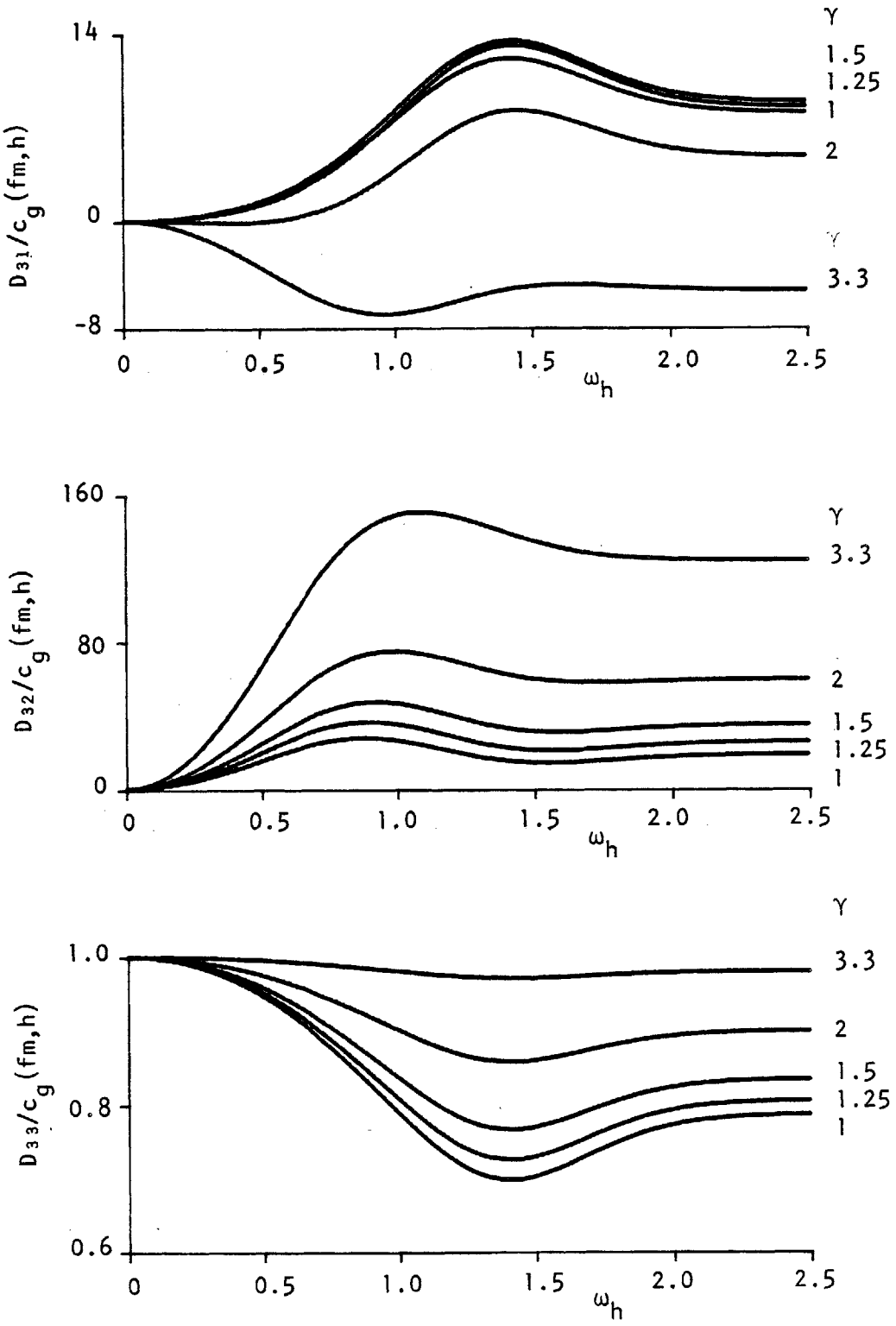


Fig. 4.3 Depth-dependent advection coefficients of parameter γ for a family of γ values. (Results correspond to fm = 0.1 Hz, α = 0.01.)

The integrals can be evaluated and pulled outside the curly brackets, which yield

$$D_{i6x} = \frac{8}{3\pi} \cos\theta_o \, D_{i6} \tag{4.3.27}$$

$$D_{i6y} = -\frac{8}{3\pi} \sin\theta_o \, D_{i6} \tag{4.3.28}$$

where $D_{i6} = \phi_i'\{c_g^2(f,h)\, E(f,h)\}$ for $i = 1,\ldots,5$.

It turns out that the D_{i6} are closely related to the coefficients D_{i2}:

$$D_{i6} = \alpha \, D_{i2} \tag{4.3.29}$$

with D_{i2} specified in (4.3.13), (4.3.17) and (4.3.22) for $i = 1,2,3$, respectively. Substitution of these expressions into (4.3.29) gives

$$D_{16} = -c_g(fm,h)\, fm\, \Delta_1 \tag{4.3.30}$$

$$D_{26} = c_g(fm,h)\, \alpha[\Delta_3 - 0.722\Delta_1] \tag{4.3.31}$$

$$D_{36} = c_g(fm,h)\, \gamma[1 - \Delta_3 - 4.28\Delta_1] \tag{4.3.32}$$

Figure 4.4 shows the variation of D_{i6} for a family of γ values. As one might expect, D_{26} is not too sensitive on the choice of γ, because α characterizes the high-frequency energy level which is quite independent of the properties around the spectral peak.

For practical applications, the solutions of the transport equations corresponding to the bandwidth parameters σ_a and σ_b are not explicitly included. In general, their influence on the overall solution for the wave field is only minor and it suffices to determine

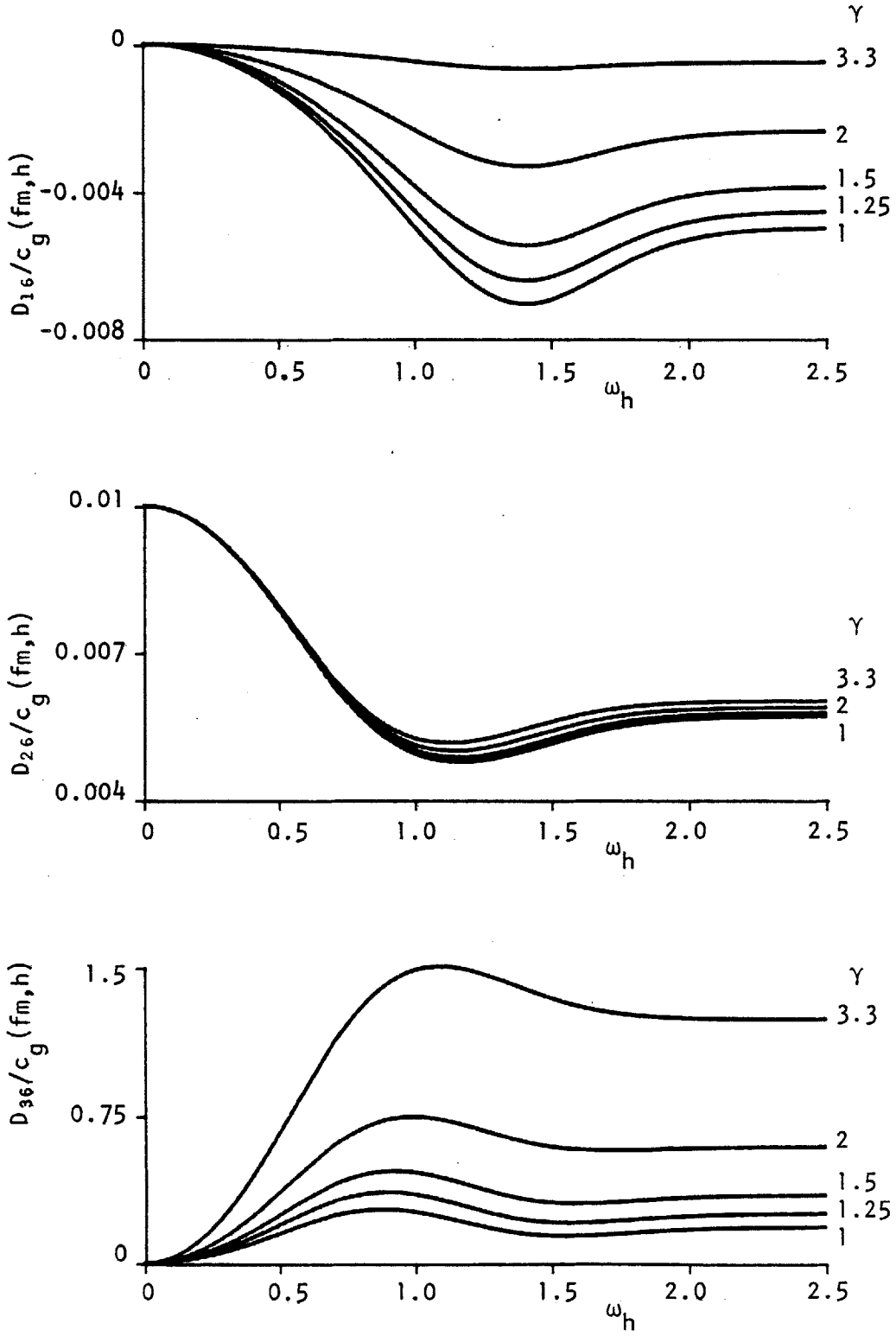


Fig. 4.4 Depth-dependent advection coefficients of parameters fm, α, γ with respect to θ_o for a family of γ values. (Results correspond to fm = 0.1 Hz, α = 0.01.)

their values from algebraic expressions as a function of γ (cf. Günther et al. 1979b). However, for the sake of completeness, the final expressions for the D_{4j}'s and D_{5j}'s are given in Appendix A.

4.4 The Mean Direction Of A Windsea

The inclusion of a directional parameter in the windsea parameterization predicated the use of a vector quantity. It is true that for most circumstances of practical concern the choice in using wave momentum or wave energy flux to derive a mean direction averaged over the windsea spectrum will probably result in only small deviations of the computed mean θ. However, based on considerations of the physics governing wave generation, it appears that a wave energy flux approach is not only more appropriate, but also more general, since it would also be valid in a moving medium. In deriving the functionals for performing the windsea parameterization, we will follow the wave momentum approach by Günther et al. (1981) and will point out differences and equalities of the final results.

The energy flux density $\underline{F}(f,\theta,h)$ is described by the product of the group velocity times the energy density

$$\underline{F}(f,\theta,h) = \underline{c}_g(f,h) \cdot E(f,\theta,h) \qquad (4.4.1)$$

with $E(f,\theta,h)$ denoting the two-dimensional spectrum in arbitrary water depth. Its x and y components are

$$\begin{bmatrix} F_x \\ F_y \end{bmatrix} = \left|\underline{F}\right| \begin{bmatrix} \sin\theta \\ \cos\theta \end{bmatrix} \qquad (4.4.2)$$

where the angle θ is counted clockwise from north (y-axis). The total energy flux along the x and y coordinates, respectivley, are defined by

$$I_x = \iint F_x \, df d\theta \; ; \quad I_y = \iint F_y \, df d\theta \tag{4.4.3}$$

The mean direction of the wave spectrum is then designated by the direction of the vector

$$\underline{I} = (I_x, I_y) \tag{4.4.4}$$

where $\sin\theta_o = I_x/|\underline{I}|$ and $\cos\theta_o = I_y/|\underline{I}|$. In explicit terms, θ_o may be calculated from

$$\theta_o = \tan^{-1}[I_x/I_y] \tag{4.4.5}$$

The definition of the functional $\phi_6\{\underline{F}\}$ can now be stated in terms of (4.4.3)

$$a_6 = \theta_o = \phi_6\{\underline{F}\} = \tan^{-1}\left[\frac{\iint F_x \, df d\theta}{\iint F_y \, df d\theta}\right] \tag{4.4.6}$$

Here the same definitions as stated in Section 4.2 do not apply to the mathematical meaning of ϕ_6. Obviously a direction can only be determined from a vector quantity such as $\underline{F}$ and not from the scalar E. Therefore, we can specify the functional ϕ_6 directly in terms of $\underline{F}$ without the transformation to energy density used in the determination of the JONSWAP parameters. Hence, following the same procedure in deriving the Frechet derivatives for the JONSWAP parameters, the first variation on (4.4.6) yields

$$\phi_6'\{\delta\underline{F}\} = \cos^2\theta_o \, \frac{\iint F_x \, df d\theta \iint \delta F_y \, df d\theta - \iint F_y \, df d\theta \iint \delta F_x \, df d\theta}{\left(\iint F_y \, df d\theta\right)^2} \tag{4.4.7}$$

Upon evaluation of all integrals and simplifying the results, we can write ϕ_6' more compactly as

$$\phi_6'\{\underline{Z}(f,\theta,h)\} = \frac{3\pi}{8} \frac{\iint (\cos\theta_o \, Z_y - \sin\theta_o \, Z_x) d\theta \, df}{\int c_g(f,h) \, E(f,h) \, df} \tag{4.4.8}$$

in which we replaced $\delta\underline{F}$ by an arbitrary function $\underline{Z}(f,\theta,h)$ of the spectral space.

When applying ϕ_6' to the energy flux transport equation (3.4.36), one arrives at the prognostic equation for the parameter θ_o,

$$\frac{\partial \theta_o}{\partial t} + D_{6jx} \frac{\partial a_j}{\partial x} + D_{6jy} \frac{\partial a_j}{\partial y} = S_6 + R_6 \tag{4.4.9}$$

The directional dependence of the coupling coefficients D_{6j}, for $j = 1,\ldots,5$, can be calculated first using (4.4.8) on (4.1.13)

$$\begin{aligned} D_{6jx} &= -\frac{3\pi}{32} \sin\theta_o \, D_{6j} \\ D_{6jy} &= \frac{3\pi}{32} \cos\theta_o \, D_{6j} \end{aligned} \tag{4.4.10}$$

It should be remarked that these components represent the advection in the direction perpendicular to the mean wave direction. Some of the details to derive D_{6j} are presented in Appendix B. Here, we only state the final results. Thus, we obtain

$$D_{61} = -\frac{3g}{128} \frac{J_2(\omega_h,\gamma)}{J_1(\omega_h,\gamma)} \quad 6 fm^{-2} \tag{4.4.11}$$

$$D_{62} = \frac{3g}{128} \frac{J_2(\omega_h,\gamma)}{J_1(\omega_h,\gamma)} \quad \alpha^{-1} \; fm^{-1} \tag{4.4.12}$$

$$D_{63} = \frac{3g}{128} \frac{J_2(\omega_h,\gamma=1)}{J_1(\omega_h,\gamma)} \; fm^{-1} \qquad (4.4.13)$$

in which J_1, J_2 are non-dimensional integrals depending only on the dimensionless water depth and the spectral shape. They are

$$J_1(\omega_h,\gamma) = \int_0^\infty \xi^{-6} \exp[-\frac{5}{4}\xi^{-4} + \ln\gamma \exp(-\frac{(\xi-1)^2}{2\sigma^2})] \chi^{-3} \, d\xi \qquad (4.4.14)$$

$$J_2(\omega_h,\gamma) = \int_0^\infty \xi^{-7} \exp[-\frac{5}{4}\xi^{-4} + \ln\gamma \exp(-\frac{(\xi-1)^2}{2\sigma^2})] \frac{1 + \omega_h^2 (\chi^2 - 1)}{\chi^4} \, d\xi \qquad (4.4.15)$$

where $\xi = f/fm$ and $\chi = \chi(\omega_h)$. Evaluation of J_1 and J_2 must be done numerically. The D_{6j}'s are depicted in Figure 4.5 for various spectral shapes as a function of dimensionless frequency, ω_h.

In the same manner the D_{66} term can be calculated and one finds

$$D_{66x} = \frac{3\pi}{16} \sin\theta_o \, D_{66} \quad ; \quad D_{66y} = \frac{3\pi}{16} \cos\theta_o \, D_{66} \qquad (4.4.16)$$

in which D_{66} is given by

$$D_{66} = \frac{3g}{64} \frac{J_2(\omega_h,\gamma)}{J_1(\omega_h,\gamma)} \; fm^{-1} \qquad (4.4.17)$$

The general behaviour of D_{66} is illustrated in Figure 4.5. The coefficients D_{64} and D_{65} can be neglected, since, as already remarked, they have only a minor influence on the total solution.

When deriving the same set of D_{6j}'s, but instead using the wave momentum concept of Günther et al. (1981) one finds notable differences in their numerical values. This distinct deviation manifests itself primarily in the integrals. This is so, because in the momentum

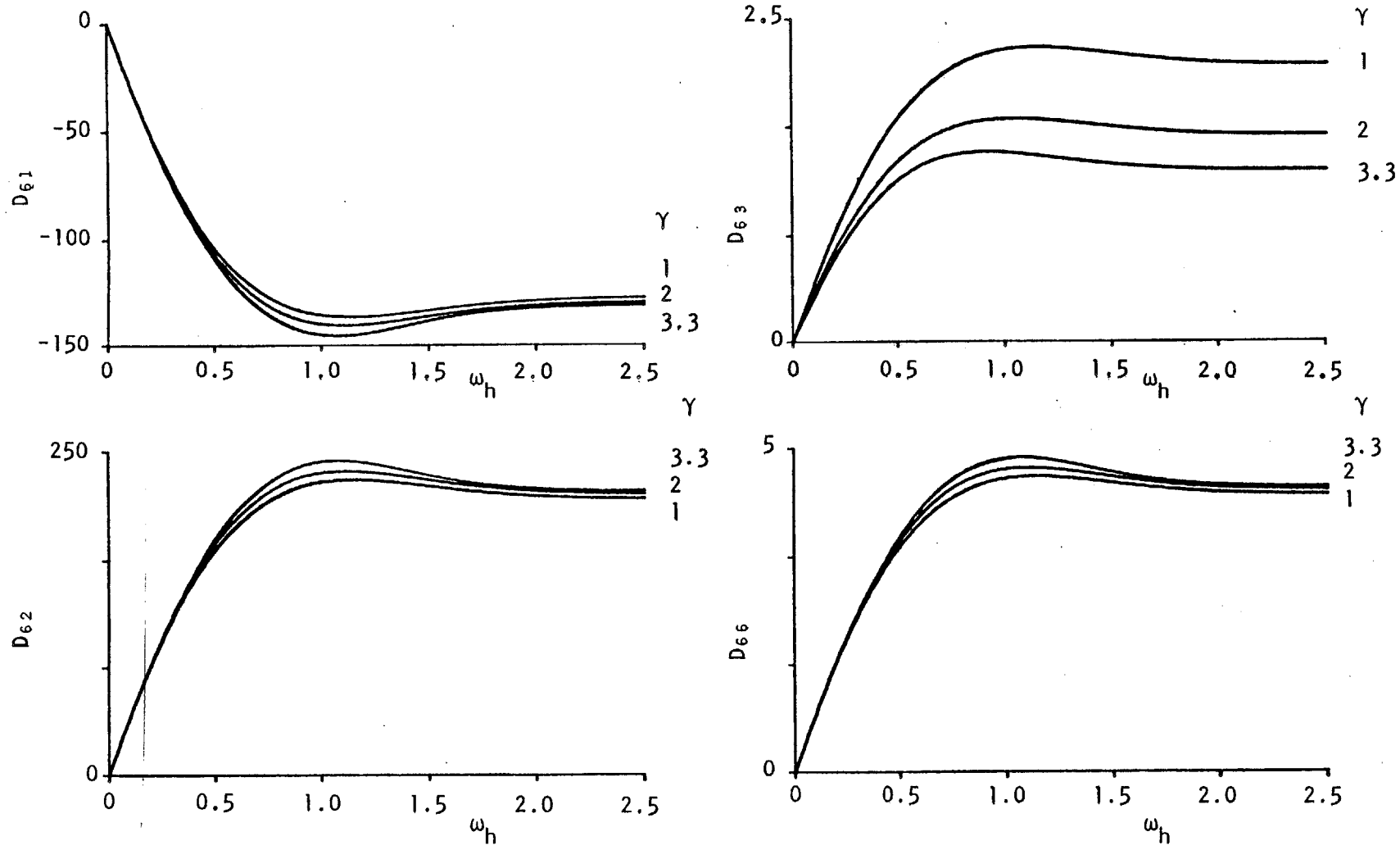


Fig. 4.5 Depth-dependent advection coefficients of parameter θ_o for a family of γ values. (Results correspond to fm = 0.1 Hz, α = 0.01.)

approach the integrals replacing J_1 and J_2 are proportional, to (-4) and (-5) power of the dimensionless frequency, respectively. Whereas, in the energy flux approach, the integrals (4.4.14) and (4.4.15) contain the dimensionless frequency to the powers (-6) and (-7), respectively. In summary, these advection terms for the wave momentum approach turn out to be

$$D^m_{61} = -\frac{3g}{128}\frac{M_2}{M_1} 4\ fm^{-2} \tag{4.4.18}$$

$$D^m_{62} = \frac{3g}{128}\frac{M_2}{M_1}\ \alpha^{-1}\ fm^{-1} \tag{4.4.19}$$

$$D^m_{63} = \frac{3g}{128}\frac{M_2}{M_1}\ fm^{-1} \tag{4.4.20}$$

$$D^m_{66} = \frac{3g}{64}\frac{M_2}{M_1}\ fm^{-1} \tag{4.4.21}$$

Here, the superscript m refers to the wave momentum approach. M_1 and M_2 are the appropriate integral expressions analogous to (4.4.14) and (4.4.15), derived from the wave momentum principle. As an example, we use the deep water form to illustrate the differences between the two approaches. Figure 4.6 shows a comparison of both approaches in terms of the ratios of their coupling coefficients for a range of γ values. This clearly reveals that the ratios are only slightly sensitive to the spectral shape, except for the γ terms, where this sensitivity is somewhat more pronounced.

When waves propagate into a region where the local direction of the wind differs from the direction of the waves, the wind component perpendicular to the wave trajectory does work to turn the waves so

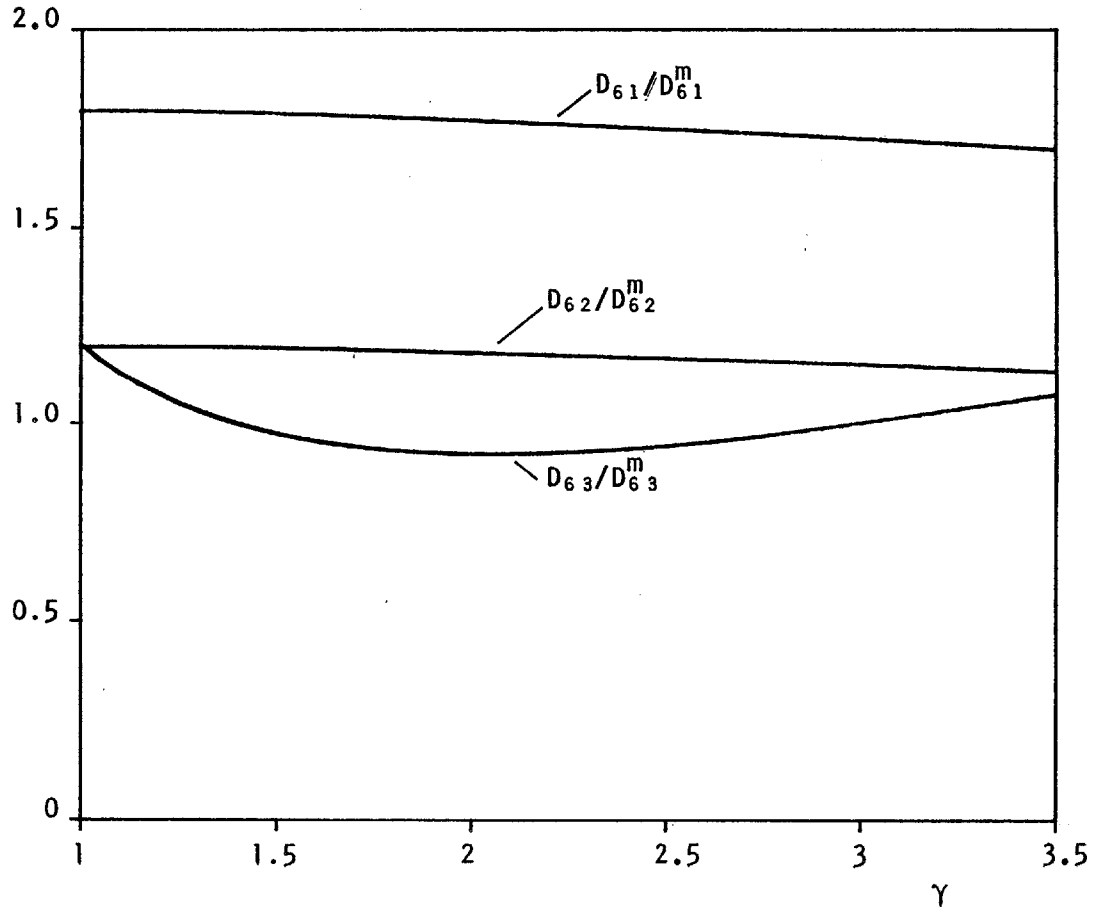


Fig. 4.6 Ratio of advection coefficients (D_{6j}/D^m_{6j}) for parameter θ_o as a function of γ in deep water.

that they eventually become aligned with the direction of the wind. Hasselmann et al. (1980) and Günther et al. (1981) have shown that the high-frequency components of the spectrum almost instantaneously respond to a sudden change in the wind direction and become aligned. The lower the frequency, the faster the wave moves relative to a fixed wind speed and therefore the impact of the wind on this spectral component is of diminishing strength. The transfer of energy from the wind takes place in the central region of the surface wave spectrum, and the nonlinear interaction generally redistribute this influx of energy over all frequencies. It seems reasonable that the nonlinear mechanism is also responsible in translating the new direction of the high-frequency components to lower frequencies until the entire windsea spectrum is turned parallel to the new wind direction. From this argument one expects that the source function of the directional relaxation parameter θ_o should involve the wind component perpendicular to the mean wave direction.

Thus, applying ϕ_6' to the Snyder-Cox input term as defined in (3.3.9) yields the parametric source term

$$S_6 = \phi_6'(\underline{T}_{in}) = - C_o \frac{fm^2}{g} U \sin(\theta_w - \theta_o) \qquad (4.4.22)$$

where θ_w is the direction of the new wind vector. The functional form of S_6 is identical to the source function derived from the wave momentum principle in Günther et al. (1981). Although momentum is proportional to (E/c) and energy flux is given by (c_gE), the functional expression of S_6 depends only on the ratios of integral expressions such as $(\int E/c_g df)/(\int c_g E df)$ for the energy flux approach

and $(\int E/c^3 df)/(\int E/c df)$ for the momentum approach. Both ratios result in f^2 dependence with the remaining differences contained in the proportionally constant C_o. If this constant C_o is determined from measurements, using (4.4.22), then both approaches yield the same results. Using field data from JONSWAP, Günther et al. (1981) have obtained an average value of

$$C_o = 0.12° = 0.21 \times 10^{-2} \text{ radians} \quad . \tag{4.4.23}$$

However, it can be shown that a theoretical value of C_o can also be obtained by evaluating the operation denoted in (4.4.22). For the mean JONSWAP spectrum this value is approximately $\approx 0.33 \times 10^{-2}$ radians for the energy flux approach, which is roughly off by a factor of 1.5. Similarly for the wave momentum approach, we find a value $\approx 0.6 \times 10^2$ radians. Based on these values one cannot conclude that one approach is better than the other, since there are still considerable uncertainties associated with the drag coefficient in the Snyder-Cox source function.

An alternative approach to investigate the directional relaxation of the mean wave direction was proposed by Hasselmann et al. (1980). Instead of the average direction for the entire spectrum, the response of the mean direction for individual frequency bands $\theta(f)$ was considered in the formulation

$$\frac{\partial \theta(f)}{\partial t} = 2\pi f \, b \, \sin[\theta_w - \theta(f)] \tag{4.4.24}$$

where $b = b(U/c;\ f/fm)$ is a constant. Their analysis led to the estimate $b \approx 3 \times 10^{-5}$. A similar study was performed by Allender et

al. (1983), but the dependence of U/c was explicitely retained in (4.4.24). From a simple regression analysis the values determined for $b = b_*(U/c)$ with $b_* \equiv 2 \times 10^{-5}$ were generally in good agreement with those reported by Hasselmann et al. (1980). Günther et al. (1981) have shown that under certain conditions, both descriptions give results of the same order of magnitude.

Since the source function S_6 is the same, both wave momentum and energy flux approaches would yield the same answer under spatially homogeneous conditions. Nevertheless, to demonstrate their differences we may consider the idealized situation of a steady wave field propagating into a region, where the wind direction undergoes a sudden step-like change. Furthermore, we assume that the JONSWAP parameters remain spatially homogeneous. Then, we can write (4.4.9) for a sea of constant depth and small angles $\tilde{\theta} = \theta_w - \theta_o$ as

$$\frac{\delta\tilde{\theta}}{\delta r} = -\frac{\tilde{\theta}}{R} \tag{4.4.25}$$

with

$$R = \left[\frac{1024}{9\pi} C_o \frac{f_m^3 U}{g^2} \frac{J_1}{J_2}\right]^{-1} \tag{4.4.26}$$

The resulting approximate solution is

$$\tilde{\theta} = \tilde{\theta}(r=0)e^{-r/R} \tag{4.4.27}$$

and R can be interpreted as a measure of the distance necessary for the steady wave field to travel to attain a direction coinciding with that of the wind.

For example, consider a PM spectrum with fm = 0.1 Hz and U = 12.75 m/s, we obtain $R \simeq 90$ km. Similarly, using the wave momentum approach, we get $R^m \simeq 75$ km.

4.5 The Parametric Source Functions

As previously discussed we represent the net effect of the various physical processes of an air-sea-bottom system by

$$S = S_{in} + S_{nl} + S_{ds} + S_{bf} + R \qquad (4.5.1)$$

in which S_{in}, S_{nl}, S_{ds} and S_{bf} are the average influx of energy from the wind, the nonlinear energy transfer due to wave-wave interactions, the dissipation of energy due to wave breaking and bottom friction, respectively. The influence of refraction, shoaling and the adjustment of the spectral shape resulting from a varying bottom topography are identified as R. To obtain an equivalent set of parametric source terms we apply the transformation functionals to (4.5.1),

$$S_i = \phi_i'\{\underline{S}\} \qquad \text{for } i = 1,\ldots,5 \qquad (4.5.2)$$

A discussion of the first three terms is given in Hasselmann et al. (1973, 1976) and the details in deriving their parametric expressions can be found in Günther et al. (1979b) and Graber (1979). We will limit our discussion to stating some of the pertinent points and focus our attention on changes resulting from the inclusion of the directional parameter and the extension to waters of finite depth.

a) NONLINEAR TRANSFER

From scaling arguments of the exact nonlinear transfer integral, the nonlinear source term S_{nl} can be deduced to be of the general

form (cf. 3.3.25)

$$S_{nl} = g^2 \alpha^3 fm^{-4} \psi_*(f/fm) \qquad (4.5.3)$$

Applying the functionals ϕ_i' to (4.5.3) yields the following analytical expressions

$$S_{nl}^{(1)} = -0.586\, \alpha^2 fm^2 \left(\frac{\gamma-1}{2.3}\right) \quad \text{for } \gamma > 1 \qquad (4.5.4)$$

$$= 0 \quad \text{otherwise}$$

$$S_{nl}^{(2)} = -5\, \alpha^3\, fm \qquad (4.5.5)$$

$$S_{nl}^{(3)} = -16(\gamma - \Gamma_o)\, \alpha^2 fm \qquad (4.5.6)$$

$$S_{nl}^{(4)} = -[25.5(\sigma_a - 0.07\sigma_o) - 0.5(\sigma_b - 0.09\sigma_o)]\alpha^2 fm \qquad (4.5.7)$$

$$S_{nl}^{(5)} = -[25.5(\sigma_b - 0.09\sigma_o) - 0.5(\sigma_a - 0.07\sigma_o)]\alpha^2 fm \qquad (4.5.8)$$

where

$$\Gamma_o = 3.3 \quad \text{for } \nu'' \geq 0.16$$

$$\Gamma_o = 1 + 2.3\, \frac{\nu'' - 0.13}{0.03} \quad \text{for } 0.16 > \nu'' < 0.13$$

$$\Gamma_o = 1 \quad \text{for } \nu'' \leq 0.13$$

$$\sigma_o = 16/(\gamma + 0.7)^2$$

and $\nu'' = fmU/g \cos(\theta_w - \theta_o)$ is the non-dimensional peak frequency parallel to the wave direction θ_o, and θ_w is the direction of the wind. The above nonlinear source terms are already modified to ensure a smooth transition from a growing sea to a fully developed sea state. This implies that for $\nu'' \to 0.13$, we require $\gamma \to 1$ which reduces the JONSWAP spectral shape to a Pierson-Moskowitz spectrum.

Since the nonlinear transfer rates in finite depths are related to the deep water nonlinear transfer by a similarity transformation involving the peak frequency fm (Herterich and Hasselmann, 1980), we simply multiply the parametric nonlinear source functions $S_{nl}^{(i)}$ by the depth dependent transformation factor $R(\omega_h)$ as defined in (3.3.27). The final expressions valid for finite and deep water depths are

$$S_{nl}^{(i)}(h) = R(\omega_h) \cdot S_{nl}^{(i)} \quad (h = \infty) \tag{4.5.9}$$

where $\omega_h = (k_m h/\chi)^{1/2}$ with χ given by (3.1.41).

b) WIND INPUT

Due to the difficulties associated with describing the wave breaking process by an exact analytic form, we consider the minimal dissipation case as discussed in Hasselmann et al. (1973). This essentially means that the loss of energy from breaking waves is restricted to the frequency range $f > 2$ fm. Then, it suffices to represent the net energy influx by

$$S_{in}^{net} = S_{in} + S_{ds} \simeq S_{in} \tag{4.5.10}$$

Further, we assume that wave generation is adequately predicted by a linear Miles mechanism, i.e.,

$$S_{in} = \beta(f,\theta)\, E(f,\theta) \tag{4.5.11}$$

and from empirical evidence, the growth parameter $\beta(f,\theta)$ can be approximated by the functional form proposed by Snyder and Cox (1966),

$$\beta(f,\theta) \approx (\underline{k} \cdot \underline{U} - \omega) \qquad (4.5.12)$$

$$= 0 \quad \text{for } (\underline{k} \cdot \underline{U} - \omega) \leq 0$$

Factoring ω, we can write (4.5.12) in terms of the ratio U/c,

$$\beta(f,\theta) \approx \omega(\frac{U}{c}\cos(\theta - \theta_w) - 1) \qquad (4.5.13)$$

which states that S_{in} vanishes for wave components with phase velocities larger than the wind velocity, if $\theta = \theta_w$. It is remarked that the rate of energy transfer from the wind to the waves depends only on the wind speed relative to the wave speed. This means that it makes no difference if the wave is in deep or shallow water. However, the total rate of input may not be equal for a constant ratio U/c, since the frequency ω will vary in different water depths. Nevertheless, we may also write

$$U/c = \frac{2\pi\, fU}{g\, \tanh\, kh} = \frac{2\pi\nu}{\tanh\, kh} \qquad (4.5.14)$$

in which ν is the dimensionless frequency. In deep water, when all spectral components are fully developed, wave growth ceases and this means the net source function (4.5.1) vanishes. This is characterized by the Pierson-Moskowitz frequency, f_{PM},

$$\nu = \frac{f_{PM}U}{g} = 0.13 \qquad (4.5.15)$$

which can be introduced in (4.5.14) as

$$U/c(f_{PM}) = 0.82 \qquad (4.5.16)$$

From this we infer for the case of a fully grown spectrum, that the frequencies containing most of the energy are found slightly below the frequencies, where the wind input is zero.

This poses the question of the existence of an equilibrium sea state in shallow waters, such that the sum of all source functions vanishes. For lack of empirical evidence, we may give some heuristic arguments as follows. The nonlinear wave-wave interactions main impact on the wave spectrum is to redistribute energies from the central portion of the spectrum to lower and higher frequencies. At the same time, this causes the spectral peak to migrate towards lower frequencies. Attenuation by bottom friction is strongest at the low frequency flank of the spectrum. This means that some of the energy transferred to these frequencies by the wave-wave interactions are dissipated by wave-bottom interactions as realized in bottom friction. Hence, the resulting effect is to slow down the rate of migration of the peak. Therefore, let us assume that these nonlinear processes both can be approximated as a reduced nonlinear transfer mechanism. From (4.5.14) it is clear that the atmopsheric input is increased for a fixed frequency in finite depth, since tanh kh < 1. If we now assume that wave breaking is similarly intensified, such that the net contribution of S_{in} and S_{ds} is still roughly given by S_{in}, then we may conjecture that in shallow water

$$S = (S_{nl} + S_{bf}) + (S_{in} + S_{ds}) \approx 0 \qquad (4.5.17)$$

but the overall rate has been increased by some factor. Since S_{in} is functionally the simplest one, we chose this factor to be proportional to tanh kh. From Figure 3.23 we can infer that the depth-dependent

transformation factor R for S_{nl} shows at least qualitatively the same behavior. Thus we may generalize the heuristic lower frequency limit (PM-frequency) for the peak frequency fm of a windsea spectrum in finite depth seas to be

$$\frac{f_{PM}U}{g \tanh kh} = \nu_h = 0.13 \qquad (4.5.18)$$

Applying ϕ_i' to (4.5.11) yields only one non-zero source function for the α-parameter

$$S_{in}^{(2)} = \alpha \, fm \, Q(\nu_h'') \qquad (4.5.19)$$

in which $Q(\nu_h'') = 5.022 \times 10^{-3}(\nu_h'')^{4/3}$ and ν_h'' refers to the depth dependent non-dimensional peak frequency determined from the wind component U'' parallel to the ~~mean~~ wave direction θ_o, i.e.

$$\nu_h'' = \frac{fm \, U''}{g \tanh kh} = \nu'' \chi(\omega_h) \qquad (4.5.20)$$

where χ is given by (3.1.41). The remaining input source terms are two orders of magnitude smaller than the corresponding nonlinear source terms (cf. Hasselmann et al. 1976) and therefore are neglected.

c) BOTTOM FRICTION

A parametric source function for bottom frictional effects can be deduced from either (3.3.51) or (3.3.59). The former equation is more general, since it allows specification of the friction factor f_w in terms of local bottom roughness and wave variables. Thus, the analytic form of S_{bf} to be used in the wave model is

$$S_{bf} = -\frac{f_w}{2} \frac{\omega^2}{g \sinh^2 kh} \langle u_b \rangle E(f,\theta,h) \qquad (4.5.21)$$

with $\langle u_b \rangle = u_{br} = \{2 \iint \frac{\omega^2}{\sinh^2 kh} E(f,h)\, df\}^{1/2}$

a representative mean near-bottom velocity. This integral can approximately be evaluated, so we obtain

$$u_{br} = \frac{\sqrt{\alpha}\, g}{2\pi f m} I(\omega_h, \gamma) \qquad (4.5.22)$$

where I can be calculated numerically from

$$I(\omega_h,\gamma) = \{2\int_0^\infty y^{-3} \exp[-\frac{5}{4} y^{-4} + \ln\gamma \exp(-\frac{(y-1)^2}{2\sigma^2})] \cdot \frac{\chi^2(y) - 1}{\chi^2(y)(1 + \omega_h^2(\chi^2(y) - 1))}\, dy\}^{1/2}$$

When applying the functionals ϕ_i' to (4.5.21), the result is the parametric source function

$$S_{bf}^{(1)} = -\frac{fw}{4} \sqrt{\alpha}\, g\, fm\, \Delta_o\, I(\omega_h,\gamma) \qquad (4.5.23)$$

where

$$\Delta_o = \frac{\sigma^2}{20\sigma^2 + \ln\gamma} \frac{(\chi^2 - 1)}{\chi} \{\frac{1 - \omega_h^2(\chi^2 + 3)}{1 + \omega_h^2(\chi^2 - 1)}\} \qquad (4.5.24)$$

Similarly, as is the case for the atmospheric input, the remaining terms are by orders of magnitude smaller and therefore omitted. This is of no surprise, since we do expect that the bottom frictional effect

should be strongest for the fm parameter and only of minor importance for the remaining others.

d) REFRACTION, SHOALING, SPECTRAL SHAPE ADJUSTMENT

In deriving the equivalent parametric energy flux transport equation we obtained, in addition to refraction and shoaling, a term relating the change of the spectral shape to the spatial variation of the bottom topography. They are, respectively,

$$\dot{\theta}\frac{\partial \underline{F}}{\partial \theta} = F\{\sin 2(\theta-\theta_o)\begin{bmatrix}\sin\theta\\ \cos\theta\end{bmatrix} - \cos^2(\theta-\theta_o)\begin{bmatrix}\cos\theta\\ -\sin\theta\end{bmatrix}\}$$

$$\times \frac{\omega}{\pi}\frac{(\chi^2-1)}{\chi}\left(\cos\theta\frac{\partial h}{\partial x} - \sin\theta\frac{\partial h}{\partial y}\right) \qquad (4.5.25)$$

$$\frac{\underline{F}}{J}\{(\underline{c}_g\cdot\underline{\nabla}_x)J + \dot{\underline{c}}_g\} = F\frac{\omega}{\pi}\frac{(\chi^2-1)}{\chi}\cos^2(\theta-\theta_o)\begin{bmatrix}\sin\theta\\ \cos\theta\end{bmatrix}$$

$$\times \cos^2(\theta-\theta_o)\begin{bmatrix}\sin\theta\\ \cos\theta\end{bmatrix}\left(\sin\theta\frac{\partial h}{\partial x} + \cos\theta\frac{\partial h}{\partial y}\right) \qquad (4.5.26)$$

$$\frac{\partial \underline{F}}{\partial h}(\underline{c}_g\cdot\underline{\nabla}_x h) = \frac{\partial \Phi c_g}{\partial h}E_J\frac{2}{\pi}\cos^2(\theta-\theta_o)\begin{bmatrix}\sin\theta\\ \cos\theta\end{bmatrix}c_g\left(\sin\theta\frac{\partial h}{\partial x} + \cos\theta\frac{\partial h}{\partial y}\right) \qquad (4.5.27)$$

where E_J is the JONSWAP spectrum defined in (4.2.1). The term $\partial/\partial h\,(\Phi c_g)$ is conveniently expressed as

$$\frac{\partial}{\partial h}\left(\frac{g}{2\omega}\chi^{-3}\right) = -\frac{3}{2}\frac{g}{\omega}\chi^{-4}\frac{\partial \chi}{\partial h} \qquad (4.5.28)$$

where we substituted for Φ and c_g as defined in (3.1.40) and (3.1.37), respectively. The derivative of χ with respect to h can be determined from implicitly differentiating (3.1.41), i.e.,

$$\tanh(\chi\omega^2)\frac{\partial\chi}{\partial h} + (1 - \tanh^2(\chi\omega^2))(\chi\frac{\omega^2}{g} + \omega^2\frac{\partial\chi}{\partial h})\chi = 0 \qquad (4.5.29)$$

Solving for $\partial\chi/\partial h$ one gets

$$\frac{\partial\chi}{\partial h} = -\frac{\omega^2}{g}\frac{(\chi^2 - 1)\chi}{1 + \omega_h^2(\chi^2 - 1)} \qquad (4.5.30)$$

Combining (4.5.25) - (4.5.27) and simplifying, yields the R term,

$$R = -F\frac{\omega}{\pi}\frac{(\chi^2-1)}{\chi}\cos^2(\theta-\theta_o)\{(2\tan(\theta-\theta_o)\begin{bmatrix}\sin\theta\\ \cos\theta\end{bmatrix} - \begin{bmatrix}\cos\theta\\ -\sin\theta\end{bmatrix})h_\perp + 4\begin{bmatrix}\sin\theta\\ \cos\theta\end{bmatrix}h''\} \qquad (4.5.31)$$

where $F = \Phi c_g E_J$ is the scalar energy flux spectrum, $h_\perp$ and h'' refer to the depth gradient perpendicular and along the direction θ of a wave component, respectively. The transformed parametric expressions are obtained from applying ϕ_i' to (4.5.31). It turns out, due to the linearity of the functional derivatives ϕ_i' that when evaluating the directional dependence first, the right-hand side of (4.5.31) simplifies to

$$R_i = -\hat{R}_i\frac{8}{\pi}\left(\sin\theta_o\frac{\partial h}{\partial x} + \cos\theta_o\frac{\partial h}{\partial y}\right) \qquad (4.5.32)$$

where

$$\hat{R}_i = \phi_i'\{\frac{\omega}{2}\frac{(\chi^2 - 1)}{\chi}E_J\} \qquad \text{for } i = 1,\ldots,5$$

When evaluating $\hat{R}_i$ we find

$$\hat{R}_1 = \pi \, fm^2 \, \Delta_o \tag{4.5.33}$$

$$\hat{R}_2 = 12.31 \, \alpha fm \, J(\omega_h) + \frac{\alpha}{fm} \, 0.72 \, \hat{R}_1 \tag{4.5.34}$$

$$\hat{R}_3 = \pi fm \, \gamma \, \frac{\chi^2 - 1}{\chi} + 5 \, \frac{\gamma}{fm} \, \hat{R}_1 - \frac{\gamma}{\alpha} \, \hat{R}_2 \tag{4.5.35}$$

The terms R_4 and R_5 are generally small and are neglected. The general form of (4.5.32) indicates that the net change of the JONSWAP parameters is proportional to the depth gradient along the mean wave direction θ_o.

Finally, applying ϕ_6', the functional derivative governing the directional relaxation, to (4.5.31) and integrating out the directional dependence, yields

$$R_6 = - \hat{R}_6 \, \frac{3}{4\pi} \, (\cos\theta_o \, \frac{\partial h}{\partial x} - \sin\theta_o \, \frac{\partial h}{\partial y}) \tag{4.5.36}$$

$$\text{with } \hat{R}_6 = \phi_6' \left\{ \frac{\int \Phi c_g E_J \, \frac{\omega}{2} \, \frac{(\chi^2 - 1)}{\chi} \, df}{\frac{8}{3\pi} \int \Phi \, c_g E_J \, df} \right\}.$$

Again, the integral expressions can only be determined from numerical quadrature. The final form of (4.5.36) can be stated as

$$R_6 = - \frac{9\pi^2}{32} \, fm \, \frac{I_1(\omega_h, \gamma)}{I_2(\omega_h, \gamma)} \, (\cos\theta_o \, \frac{\partial h}{\partial x} - \sin\theta_o \, \frac{\partial h}{\partial y}) \tag{4.5.37}$$

where I_1 and I_2 are non-dimensional integrals depending on the spectral shape in finite depth. It is clear that (4.5.37) represents the influence of a spatially varying sea bottom on the wave spectrum,

or better known as refraction. The other source term for the θ_o transport equation is due to the spatial inhomogeneity of the windfield which has already been derived in Section 4.4. For demonstration purposes we take a simple example to obtain some numerical values. Consider a mean JONSWAP spectrum with fm = 0.1 Hz in 20 m of water propagating at an angle θ_o = 45° to a constant bottom slope of 1/2500. The wind is blowing uniformly in the same direction parallel to the bottom contours, i.e., $\theta_w - \theta_o$ = 45°, at 20 m/sec. For R_6 and S_6, we calculate

$$R_6 = 3.02 \times 10^{-5} \text{ rad/sec}$$

and

$$S_6 = 3.03 \times 10^{-5} \text{ rad/sec.}$$

For these conditions both mechanisms are of equal strength, but if the waves were in waters 7.5 m deep, all other variables unchanged, we find

$$R_6 = 8.8 \times 10^{-5} \text{ rad/sec}$$

Now, refraction is clearly dominating the directional relaxation of the wave spectrum. To counter refraction, the wind speed would need to increase to almost 60 m/sec.

4.6 Energy Exchange Between Windsea and Swell

Situations can arise where spectral components, belonging to both the windsea and swell domain, are present independent of each other, but are likely to interact. If interaction takes place, then some criteria are warranted which control the transfer of energy from one domain to the other within the wave spectrum. Before we describe these transfer criteria in detail, it is appropriate to attach a more specific definition to each wave domain.

The lower heuristic limit of the windsea peak frequency fm is defined as the Pierson-Moskowitz frequency f_{PM}. Therefore, the energy of wave components, whose frequencies are greater than the local PM frequency, are refered to as "windsea", provided their mean wave direction θ_o is aligned with the local wind vector. It is remarked that wave modes satisfying the frequency requirement, but propagating in a direction differing by 90° or more, are excluded from the windsea domain and assigned to the swell domain. Also, it should be realized that with this definition, the limiting windsea spectrum is the PM spectrum. This spectrum still contains energy at frequencies less than $fm = f_{PM}$, but with decreasing frequency, the energy density rapidly diminishes too.

Then, surface waves, characterized as swell, are unaffected by the local wind. Swell energy of a certain frequency band will propagate with its associated group velocity along wave characteristics (rays) which are determined from refraction laws. In deep water, these characteristics are always straight and thus, the initial propagation angle remains unaltered.

The following two situations can occur when energy must be exchanged between the windsea and swell region. If the wind conditions suddenly change so that the local PM frequency is located above the windsea peak frequency, then the energy in excess of what can be supported by the local PM spectrum is transferred to swell (windsea → swell transfer). As we shall see, a change in wind conditions can come about either by a drop in wind speed, but maintaining the same direction, or by a veering of the wind angle, holding the wind speed constant, or by a combination of the two, such that the above rule is fulfilled.

The reverse happens, when swell is advected into a region, where the local peak frequency lies below the frequency of a swell bin with non-zero energy. This energy is instantaneously absorbed into the windsea spectrum (swell → windsea transfer).

In formulating these dynamical exchange criteria, one must rely mainly on intuitive arguments, since existing theories can not adequately explain the exact sequence of events which takes place through the interplay of two wave domains. The fundamental assumptions underlying these exchange rules are: First, conservation of total energy (windsea + swell) is ensured in any transfer; second, nonlinear interactions between wave modes of the windsea and swell region are generally very weak, except in cases where swell frequencies span the windsea frequency domain. Then, the coupling or decoupling process of two energy domains is rapidly sped up by nonlinear interactions, and achieved within one model time step. This concept is supported by calculations of Hasselmann (1963b) and more recently by numerical experiments of HH (1981) to test the response of these interactions for

general cases when swell is present.

In the next two sections we follow the approach presented by Gunther et al. (1981, 1979b) to derive in some detail and in general terms the adopted transfer criteria.

4.6.1 Windsea to Swell Transfer

As already mentioned, the frequency border between the windsea and swell domains results as a consequence of a vanishing source function. Explicitly, this frequency is defined as

$$f_{PM} = \frac{0.13\, g \tanh k_{PM} h}{U \cos(\theta_w - \theta_o)} \qquad \text{for } |\theta_w - \theta_o| < \frac{\pi}{2}$$

$$= \infty \qquad \text{for } |\theta_w - \theta_o| \geq \frac{\pi}{2} \tag{4.6.1}$$

where k_{PM} is the wave number corresponding to f_{PM}. In the deep water limit, (4.6.1) reduces to the equation given by Gunther et al. (1981). In order to illustrate the necessary sequential steps to achieve a smooth transition from windsea to swell, we consider the following example.

Let a uniform wind field $U_1 = U(u_1, \theta_1)$ exist over some finite region of constant depth h. The sea state in this region is growing accordingly to previously discussed wave theories. Further, the spectral peak of the wave field is located at fm, where fm > $f_{PM}(U_1) = f_{PM,1}$. Suddenly the wind field drops to a new value $U_2 = U(u_2, \theta_2)$ everywhere in this area, such that fm < $f_{PM}(U_2) = f_{PM,2}$ as determined from (4.6.1) (see Figure 4.7a). This means, that under these conditions the wind can support at

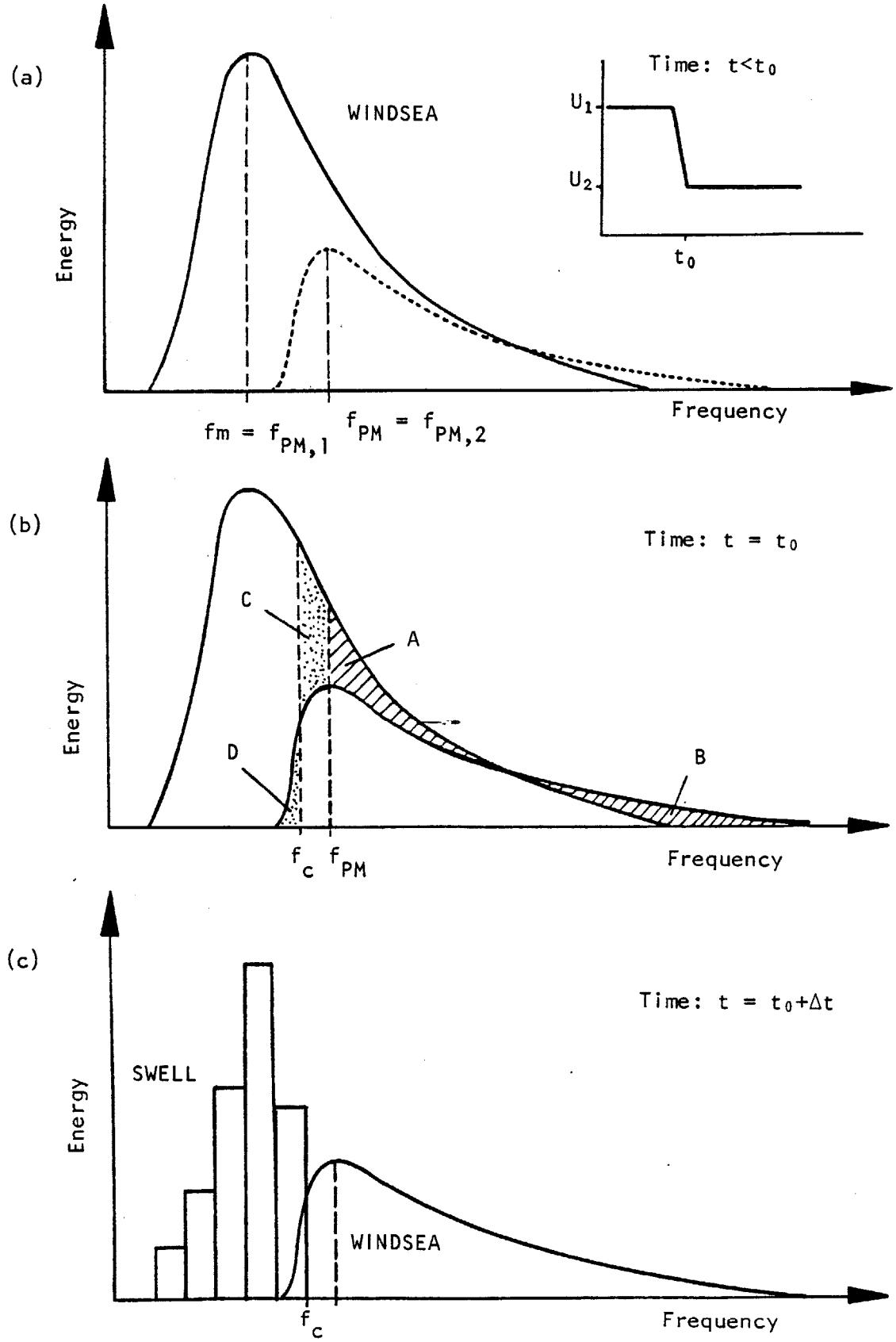


Fig. 4.7 Schematic representation of energy transfer from WINDSEA to SWELL.

most a new spectrum, corresponding to a fully developed sea which is characterized by $f_{PM,2}$. Hence, we set fm = $f_{PM,2}$ (Figure 4.7b). Energy in frequencies greater than the new fm (area A in Figure 4.7b) is instantaneously absorbed by adjusting the α parameter. This implies to conserve energy in the spectral range greater than the local fm, we must satisfy

$$\int_{f_{PM}}^{\infty} E_{ws}(\alpha, fm, \gamma)\, df = \int_{f_{PM}}^{\infty} E_{ws}(\alpha_o, f_{PM}, \gamma=1)\, df \qquad (4.6.2)$$

in which E_{ws} denotes the parametric windsea spectrum as defined in (3.1.81). Graphically (4.6.2) corresponds to an equality of areas A and B in Figure 4.7b. Again these integrals can not be evaluated analytically. Nevertheless, a close approximation to the exact solution is given by

$$\alpha_o = \alpha f^4 \frac{1 - \exp(-1.25\, f^{-4})}{0.7135}\, g(\gamma) \qquad (4.6.3)$$

where $f \equiv f_{PM}/fm$ is the ratio of the PM frequency to the windsea peak frequency before the change in the wind, and $g(\gamma)$ is a correction function resulting from a spectral shape with $\gamma \neq 1$. Finally, overall energy conservation is accomplished by transferring to swell all the excess energy remaining in the original windsea spectrum below a certain cut-off frequency f_c. The frequency f_c specifies the location for which areas C and D are equal (Figure 4.7b). In integral form, f_c is determined from

$$\int_{f_c}^{\infty} E_{ws}(\alpha, fm, \gamma)\, df = \int_{0}^{\infty} E_{ws}(\alpha_o, f_{PM}, \gamma=1)\, df \qquad (4.6.4)$$

Graphically, the integral equality (4.6.4) and the equality of areas C and D are not readily obvious. Splitting up (4.6.4) into a sum of two integrals each, yields

$$\int_{f_c}^{f_{PM}} E_{ws}(\alpha, fm, \gamma)\,df + \int_{f_{PM}}^{\infty} E_{w}(\alpha, fm, \gamma)\,df$$

$$= \int_{o}^{f_{PM}} E_{ws}(\alpha_o, f_{PM}, \gamma=1)\ df + \int_{f_{PM}}^{\infty} E_{ws}(\alpha_o, f_{PM}, \gamma=1)\ df \qquad (4.6.5)$$

The second integrals on both sides are clearly the same as given by (4.6.2). Hence, this simplifies (4.6.4) to the schematically depicted areas C and D,

$$\int_{f_c}^{f_{PM}} E_{ws}(\alpha, fm, \gamma)\ df = \int_{o}^{f_{PM}} E_{ws}(\alpha_o, f_{PM}, \gamma=1)\ df \qquad (4.6.6)$$

Similarly, the integrals in (4.6.6) can not be expressed analytically, but f_c is accurately approximated by

$$f_c = (1.25)^{0.25}\ fm\left\{-\ln\left[1 - \frac{\alpha_o}{\alpha} f^{-4}\right]\right\}^{-0.25} \qquad (4.6.7)$$

The windsea energy found at frequencies less than f_c are transferred to swell and are distributed with a cosine-squared spreading function centered around the local mean wave direction θ_o.

4.6.2 Swell to Windsea Transfer

In general, newly created swell will leave the generating area rapidly by means of simple advection without sources. However, distant, old swell can propagate into a region, where the local windsea is actively growing at frequencies close enough to/or overlapping the frequency bins of the swell. Two distinct situations can arise from this type of interplay which requires an energy exchange criterion between the two wave domains.

The first case comes into existence when swell energy is found at frequencies greater than 0.9 fm. Energies within this frequency range are instantaneously absorbed regardless of direction into the windsea as a result of nonlinear interactions. The interpretation in this case is that the nonlinear interactions are effective enough to engulf the swell modes and then redistribute the energy within the windsea domain to maintain shape similarity. Conservation of energy is obtained by adjusting the frequency of the windsea peak to a new value fm_o, but keeping α and γ fixed. This assumes that the high-frequency portion of the windsea spectrum remains initially unchanged and that the redistribution of the swell energy does not alter the spectral shape (i.e., γ) by any significant amount. Hence, in terms of integral expressions this can be stated as

$$\int_o^\infty E_{ws}(\alpha, fm_o, \gamma)\,df = \Delta E_{sw} + \int_o^\infty E_{ws}(\alpha, fm, \gamma)\,df \qquad (4.6.8)$$

where ΔE_{sw} represents the total swell energy to be absorbed. For illustrative purposes, we depict this procedure schematically in Figure

(4.8). Clearly, areas A and B are graphically equivalent representation of (4.6.8). Again, the integrals can not generally be evaluated in terms of closed form analytic expressions, due to the non-integrability of the JONSWAP spectral shape for $\gamma \neq 1$. The adjusted windsea peak is closely given by

$$fm_o = fm\{ 1 + \frac{80\pi^4}{\alpha g^2} fm^4 \frac{\Delta E_{sw}}{g(\gamma)} \}^{-0.25} \qquad (4.6.9)$$

The correction function $g(\gamma)$ can easily be determined from numerical integration of the JONSWAP spectral shape, i.e.,

$$g(\gamma) = \frac{(2\pi fm)^4}{\alpha g^2} \int_0^\infty E_{ws}(\alpha, fm, \gamma) df \qquad (4.6.10)$$

A least-square fit of the results to a third-order polynomial in γ yields the algebraic expression

$$g(\gamma) = -0.044 + 0.344\gamma - 0.112\gamma^2 + 0.012\gamma^3 \qquad (4.6.11)$$

The second case to be considered, emerges from the situation where swell energy exists at frequencies for which the associated phase speeds are less than the local wind speed, i.e., $f > f_u = g/(2\pi U\cos(\theta_w - \theta_s))$, where $\theta_w - \theta_s$ is the angle between the wind vector and the swell direction; but are outside the range of influence of nonlinear windsea interactions, i.e., $f_u < f < 0.9$ fm. These are assumed to grow again through a Phillips-Miles mechanism. This type of linear atmospheric input is commonly described by the Snyder-Cox source function (Snyder, 1974)

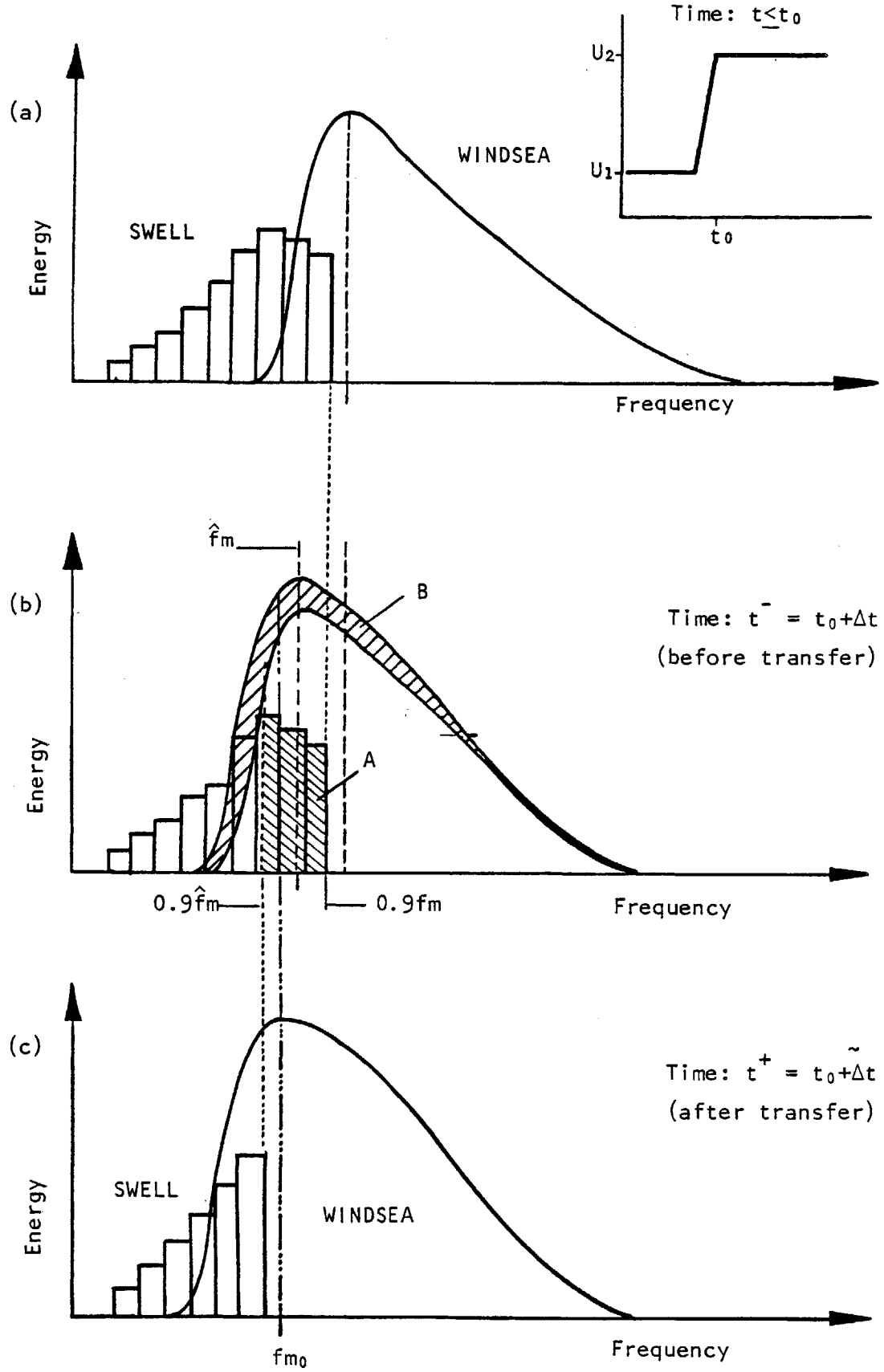


Fig. 4.8 .Schematic representation of energy transfer from SWELL to WINDSEA.

$$S(f,\theta) = \beta(f,\theta)\, E_{sw}(f,\theta) \qquad (4.6.12)$$

with

$$\beta = c_d \frac{\rho_a}{\rho_\omega} 2\pi f \left(\frac{f}{f_u} - 1\right) \qquad \text{for } f > f_u$$

$$= 0 \qquad \text{for } f \leq f_u$$

Here, E_{sw} is the swell energy density and ρ_a, ρ_w are the densities of air and water, respectively and c_d is a drag coefficient taken as 0.05. Although swell can grow again, it still remains in the swell domain and is further advected along prescribed characteristics.

These two outlined transfer criteria provide the vital link between the swell model and the parametric windsea model. Together they make up the hybrid wave model.

4.6.3 Propagation Treatment of Swell

The parametric description of the windsea domain is not applicable to the swell region. This means energy at frequencies $f < f_{PM} = 0.13g/(U\cos(\theta_w-\theta))$ are treated in a different manner. Since swell lies outside the range where either the wind or nonlinear interactions can influence its evolution in space and time, a characteristic approach is used in this model to represent the swell wave field. The concept of employing discrete spectral rays was originally introduced by Barnett et al. (1969) as a method to propagate swell over an ocean of arbitrary depth. If the medium is time independent, then the rays can be predetermined and for waters of varying bottom topography, the effects of depth refraction can be included. Generally, swell is

represented as discrete energy packets defined by their frequency f and direction θ. The rays are also classified by the pair (f,θ). Swell packets are then located at points along the ray. These incremental spacings are computed from

$$\Delta \ell = \Delta t \, c_g = \Delta t \frac{g}{4\pi f} \tanh kh \left(1 + \frac{2kh}{\sinh 2kh}\right) \qquad (4.6.13)$$

where Δt is the model time step and c_g is the local group velocity at frequency f and in depth h. The model area is covered with a mesh of rays at appropriate increments in frequency, angle and (x,y) spacings. In deep water, this is simplified considerably, since all rays are straight lines. Energy propagation by one or more time steps is easily simulated by a computer as an input-output process, by storing the ray points in a one-dimensional array. In deep water, where refraction effects are absent, as well as no sources and sinks, this procedure is rather efficient. In the case of finite depth, the inclusion of dissipation from bottom friction poses no difficulties (Graber et al., 1981). Swell packets reaching a model boundary are simply advected out by purging the energy contents for a given (f,θ).

Detailed accounts of the numerical and computational procedures employed in implementing the hybrid wave model can be found in Hydraulics Research Station (1977a,b) and Graber (1979).

CHAPTER 5

MODEL APPLICATIONS

Dieser Erdenkreis gewahrt noch Raum
Zu grossen Taten.

For this earthly sphere affords a place
For great deeds.

(Faust)

--FAUST II. Hochgebirg
Johann Wolfgang von Goethe

5.1 Gulf of Alaska (Deep Water Case)

Especially during winter, the Gulf of Alaska is constantly exposed to adverse meteorological and oceanographic conditions. These extreme storm conditions are produced by very large, rapidly moving extra-tropical cyclones. Typically, these storms develop as initially small depressions in the western part of the North Pacific and quickly intensify during their movements toward the Gulf of Alaska. The mountain ranges surrounding the shores of the Gulf present a natural barrier to the movement of these storm systems, which cause stagnation and influence the duration of the storms in this region. The combined effect of storm intensity and duration in conjunction with a very long storm track over the open ocean, can generate exceptionally high waves in the Gulf of Alaska.

Similar in structure to hurricanes, extratropical cyclones have ordinarily maximum winds of approximately 25 - 30 m/s, but engulf a large spatial area of the order of 750 km in diameter. The synoptic weather map for this model storm at its peak is shown in Figure 5.1. However, these cyclones strikingly differ from hurricanes in their very high forward velocities and the capability to intensify very rapidly. These features seem to provide a good test to verify the model's response to rapidly turning winds. At the same time, this would also

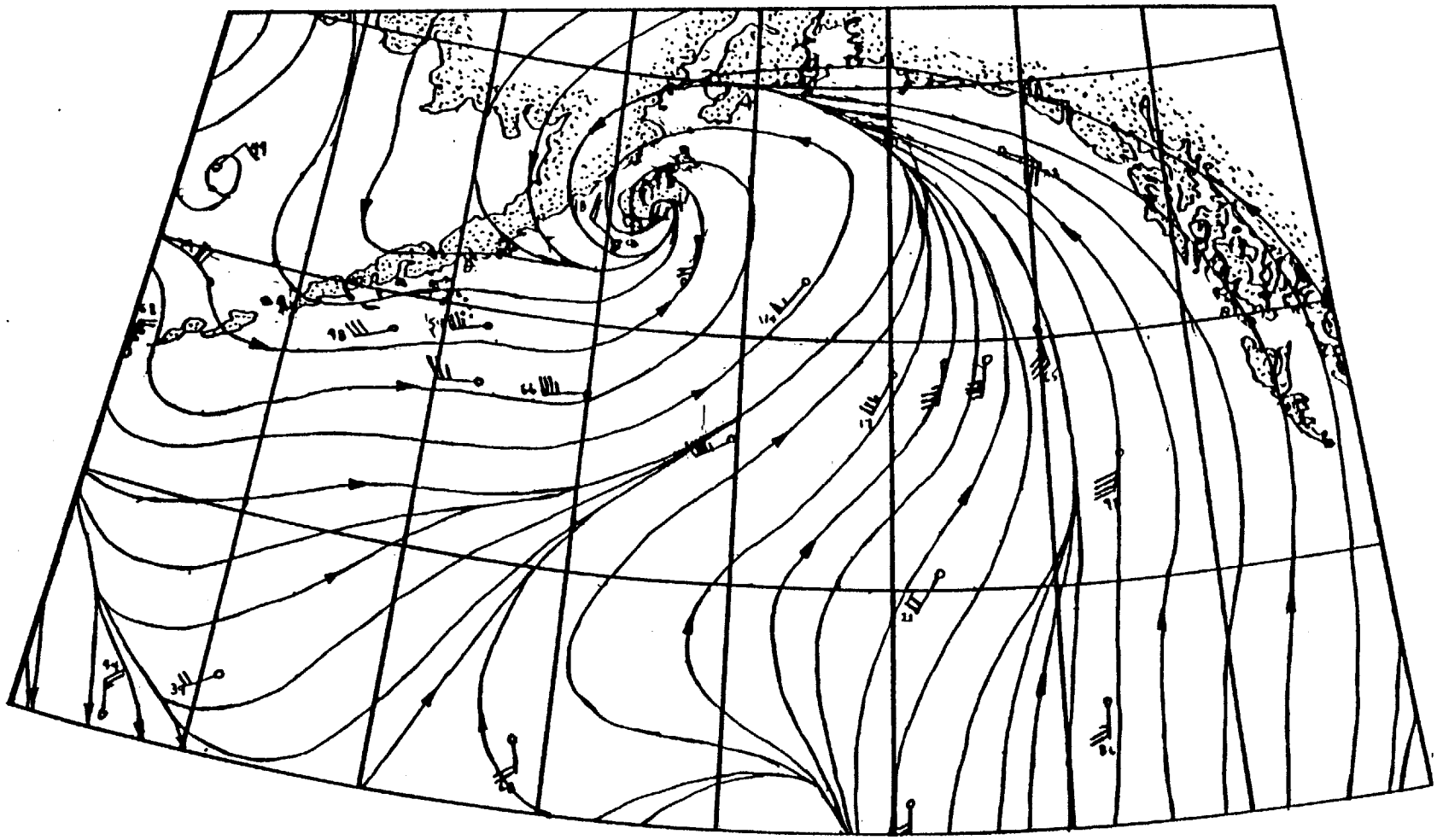


Fig. 5.1 Synoptic weather map of extratropical cyclone in the Gulf of Alaska for 0600 GMT, January 30, 1976. (From Overland and Cardone, 1980).

test the windsea-swell transition regime, because the high forward velocity of the storm could outrun swell and if stalled, the swell could catch up and interact again with the local windsea. The inclusion of directional relaxation should help to minimize the associated loss by radiation into swell, a fact that was evident in an earlier model version, where the mean wave direction was always assumed to align itself instantaneously with the local wind direction.

In addition to wave and wind observations from the EB03 NOAA data buoy, we have also available waverider and spectral data from five other locations which were part of the GAWWMP (Gulf of Alaska Wind and Wave Measurement Program) project. The GAWWMP study was an industry sponsored effort by a consortium of oil companies to measure winds and waves in the Gulf of Alaska (McLeod et al., 1975). Figure 5.2 shows the locations of waverider buoys and recording stations in the Gulf of Alaska. Except very close to the shore, the water depths within the model area can be considered infinitely deep. Refraction effects due to both slowly varying currents and bottom topography are neglected. No directional wave data was available from any of the stations.

The model grid is set up on a polar stereographic projection with grid points at constant spacings of approximately 150 km (Figure 5.3). The cartesian grid is defined by the latitude ϕ and longitude λ,

$$(1 + \sin\phi)^{-1} = 0.5 + \frac{1}{8R_E^2}(x^2 + y^2) \qquad (5.1.1)$$

$$\lambda - \lambda_o = \tan^{-1}\left(\frac{y}{x}\right) \qquad (5.1.2)$$

with the origin at the north pole and with the x-axis pointing along the longitude λ_o = 95°W. Here R_E (radius of the earth) = 6367 km

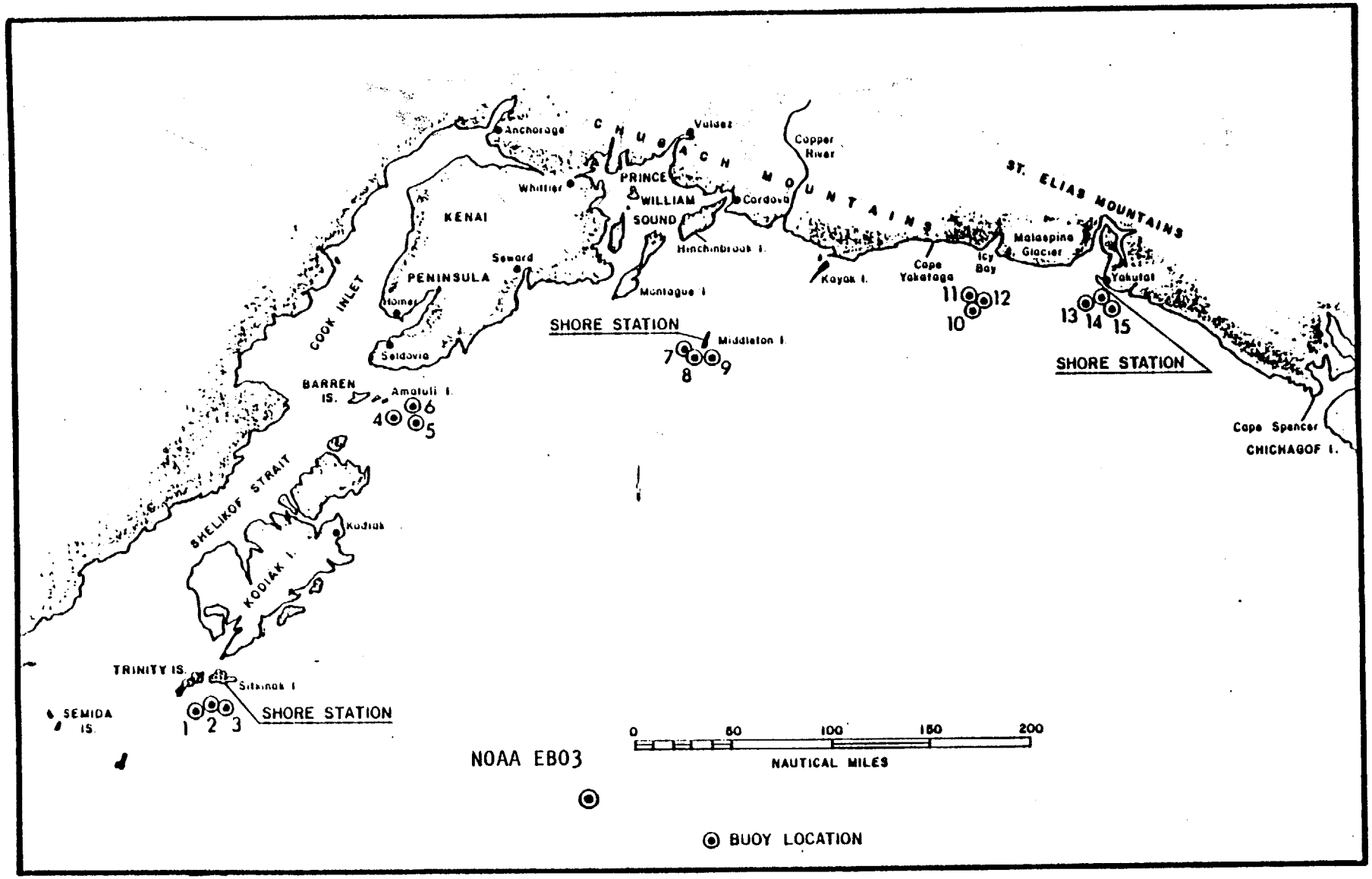


Fig. 5.2 Location map of measuring stations in the Gulf of Alaska. (From McLeod et al. 1975).

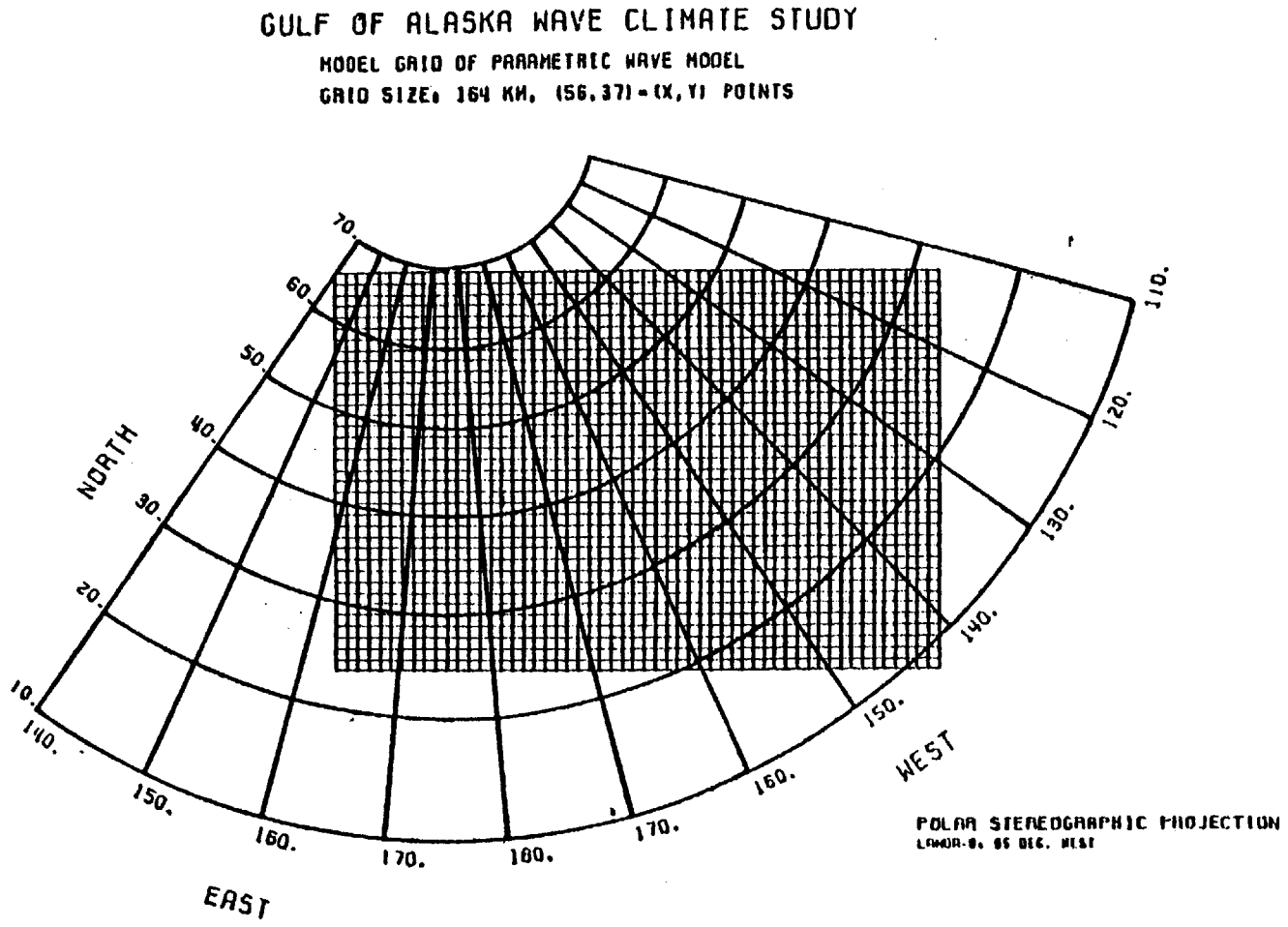


Fig. 5.3 Grid used in numerical wave model. Based on a polar stereographic projection, the average grid spacing is approximately 150 km.

5.1.1 Meteorological Conditions and Wind Fields

The extratropical storm selected for this study occurred during January 27-31, 1976. The initial development of this storm can be traced back to a weak depression in the outer circulation of an intense, northward-moving cyclone (964 mb) heading for the Aleutian Islands into the Bering Sea. At this time 0600 GMT January 28, our storm of interest just formed an enclosing isobar of 996 mb and showing only a slight eastward movement. However, at 1800 GMT January 28, our storm picked up in movement, turning northeastward and had deepened very rapidly (980 mb). Figure 5.4 depicts the model wind fields around the time of inception (1500 and 1800 GMT). By 0600 GMT January 29, the storm further intensified (973 mb) and commencing its track towards the northeast at over 70 km/h (this corresponds to the group velocity of a 25 s wave in deep water). The storm continued to deepen and turning more towards the north-northeast. By 0000 GMT January 30, the storm was fully matured and attained its lowest central pressure of 958 mb when the "eye" was about 200 miles south of the Trinity Islands. Figure 5.5 shows the track of the storm's low pressure center. The National Weather Service had sent out its first advisory for the Gulf of Alaska (January 29, 2345 GMT) warning of winds up to 23 m/s and seas in excess of 7 m. Furthermore, the fully developed extratropical storm now engulfed the entire eastern area within a semi-circle of 800 km where prevailing winds reached speeds up to 28 m/s. The National Weather Service issued its second warning (January 30, 1145 GMT), forecasting heavy rains, high winds and very high seas up to 10 m. The storm now took a course due north and within six hours, it had crossed

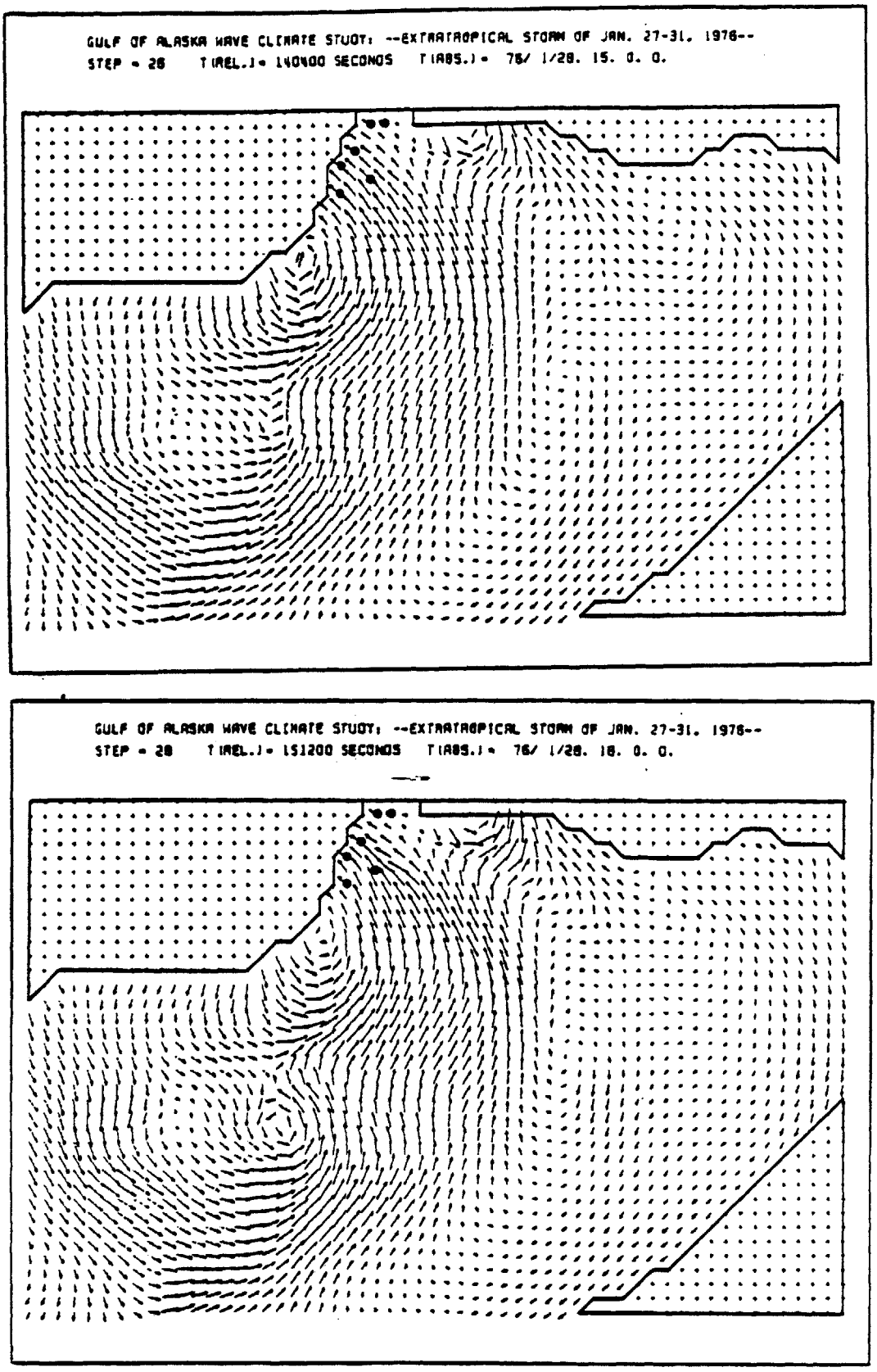


Fig. 5.4 Examples of wind field input to the numerical model for 1500 GMT and 1800 GMT, January 28, 1976. The vectors show speed and direction of the wind. Dots indicate stations where wave measurements have been made.

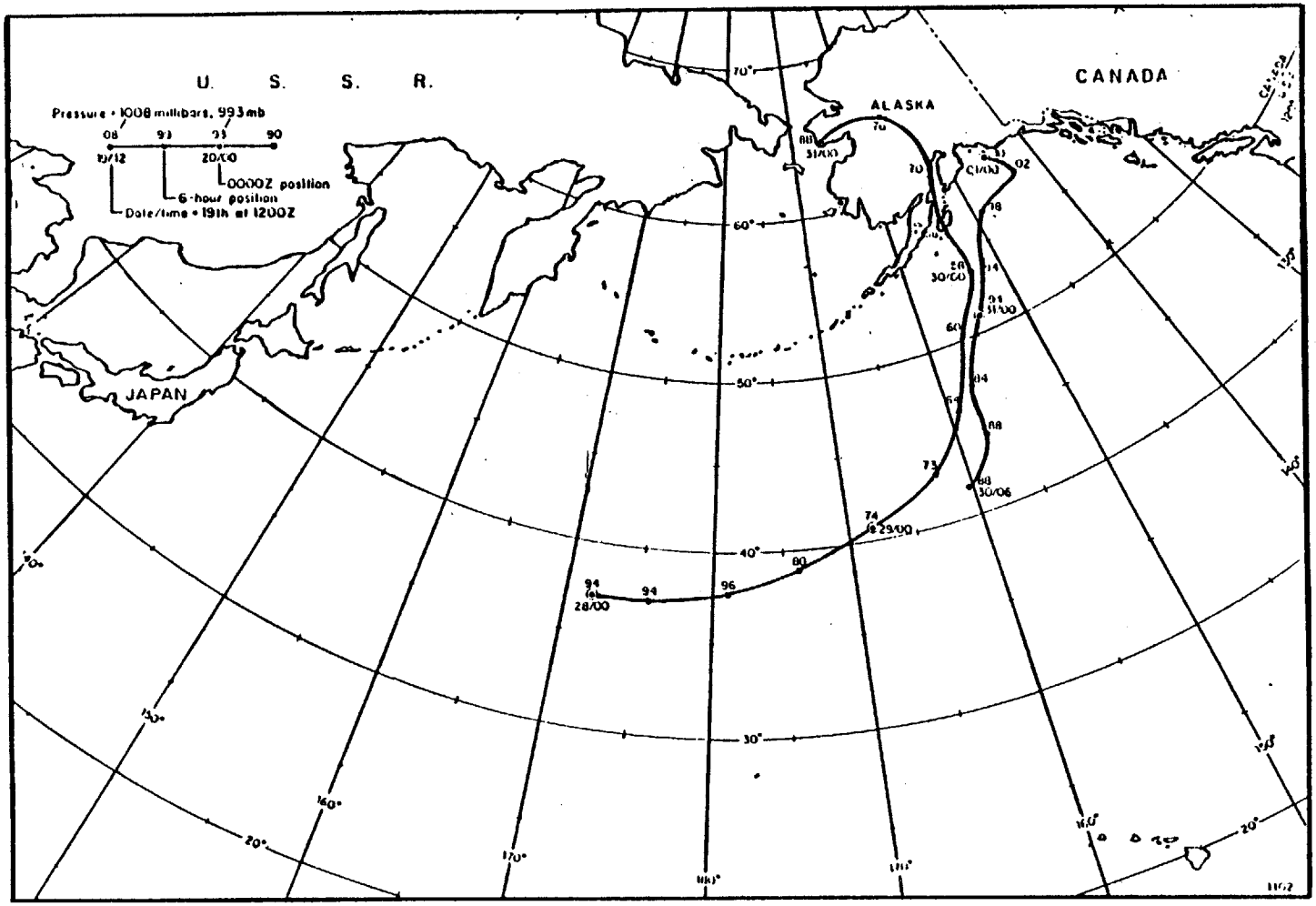


Fig. 5.5 Storm track of extratropical cyclone.

Sitkinak Island and the southern tip of Kodiak Island. Seemingly uninfluenced by the large land mass, the storm advanced with unchanged intensity towards Cook Inlet (0600 GMT, January 30) and slowly began to weaken over land, until it finally entered the Bering Sea on January 31, 1976.

While our storm was heading for land, a new system was developing in its wake roughly 900 miles south. At 0600 GMT January 30, it was classified as open cyclone with a central pressure of 988 mb. By early January 31, the now enclosed cyclone was moving north-northeastward and provided a sustained flow of moderately high winds over most of the Gulf of Alaska for the following day. The model wind fields corresponding to the times when our storm attained its lowest pressure and subsequently entered the Gulf are shown in Figure 5.6.

The original surface wind field, corresponding to a 10 m anemometer height, was specified on a Mercator projected grid and a discussion of the analysis can be found in Cardone et al. (1979). These winds were transposed onto the polar stereographic projected grid by means of linear interpolation. To retain the dynamics of the cyclone, the wind speed to the fourth power was used for interpolation and the directions were deduced from the Fourier components of the wind vectors. Interpolation in time is automatically performed by the wave model using a mixed radix FFT (Singleton, 1969).

5.1.2 Model Results

Three different versions of the deep water hybrid parametric (HYPA) model were tested against this storm: i. directional relaxation using an energy flux approach, ii. directional relaxation using a wave

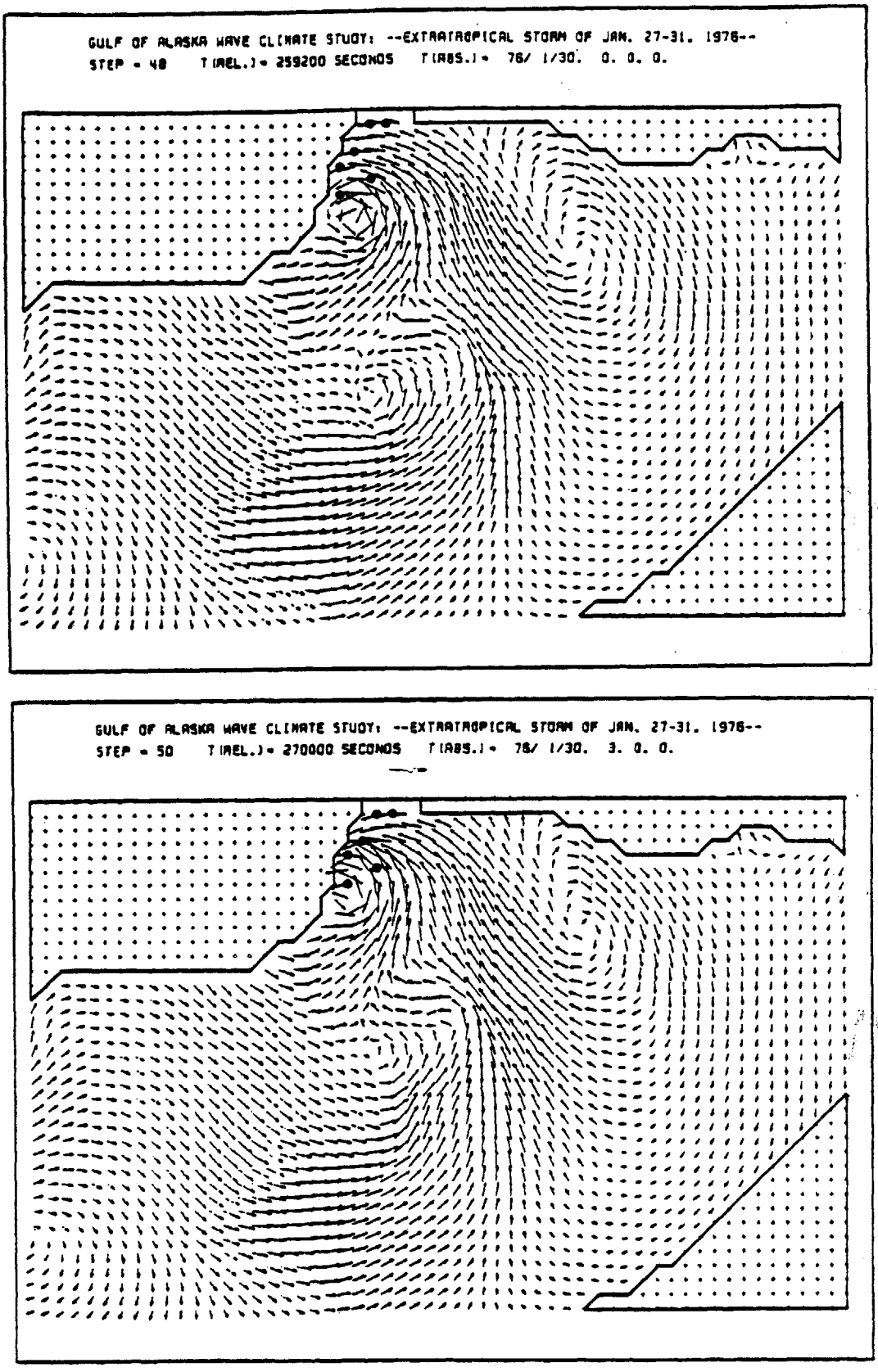


Fig. 5.6 Examples of wind field input to the numerical model for 0000 GMT and 0300 GMT, January 30, 1976. The vectors show speed and direction of the wind. Dots indicate stations where wave measurements have been made.

momentum approach and iii. no directional relaxation. The results of the approaches i. and ii. showed no discernible differences in either the mean wave direction or the wave height. These differences were limited to a few degrees for the mean windsea direction and to about 10 - 20 cm in wave height. The remaining JONSWAP parameters exhibited hardly any noticable differences. Therefore, all results concerning the directional aspect of the waves will be present in terms of the energy flux approach only.

The model results of the no directional relaxation version, i.e., the waves are instantaneously aligned with the local wind direction, differed considerably in all wave parameters from the directional results. As we discuss the results at the individual stations we shall point out these differences as deemed necessary. In Figures 5.7 to 5.9 the evolution of wave spectra at each of the six measuring locations (c.f. Figure 5.2) are depicted. Both locations EB03 and Middleton Island (Figure 5.7) attained relatively high spectral densities when compared to the other locations. It should also be noted that the structure of their spectral form is very similar, indicating that the storm's influence at both sites was approximately the same. It turned out that both these locations recorded the highest waves, of the order of 10 meters. Sitkinak Island (Figure 5.8) was exactly in the path of the extratropical storm. This is evident in the two pronounced peaks of a windsea and swell, but the waves never reached heights as high as at Middleton Island which was situated in the right front quadrant of the storm. Amatuli Island (Figure 5.8) appeared to be positioned in a somewhat sheltered location between the northern tip of Kodiak Island

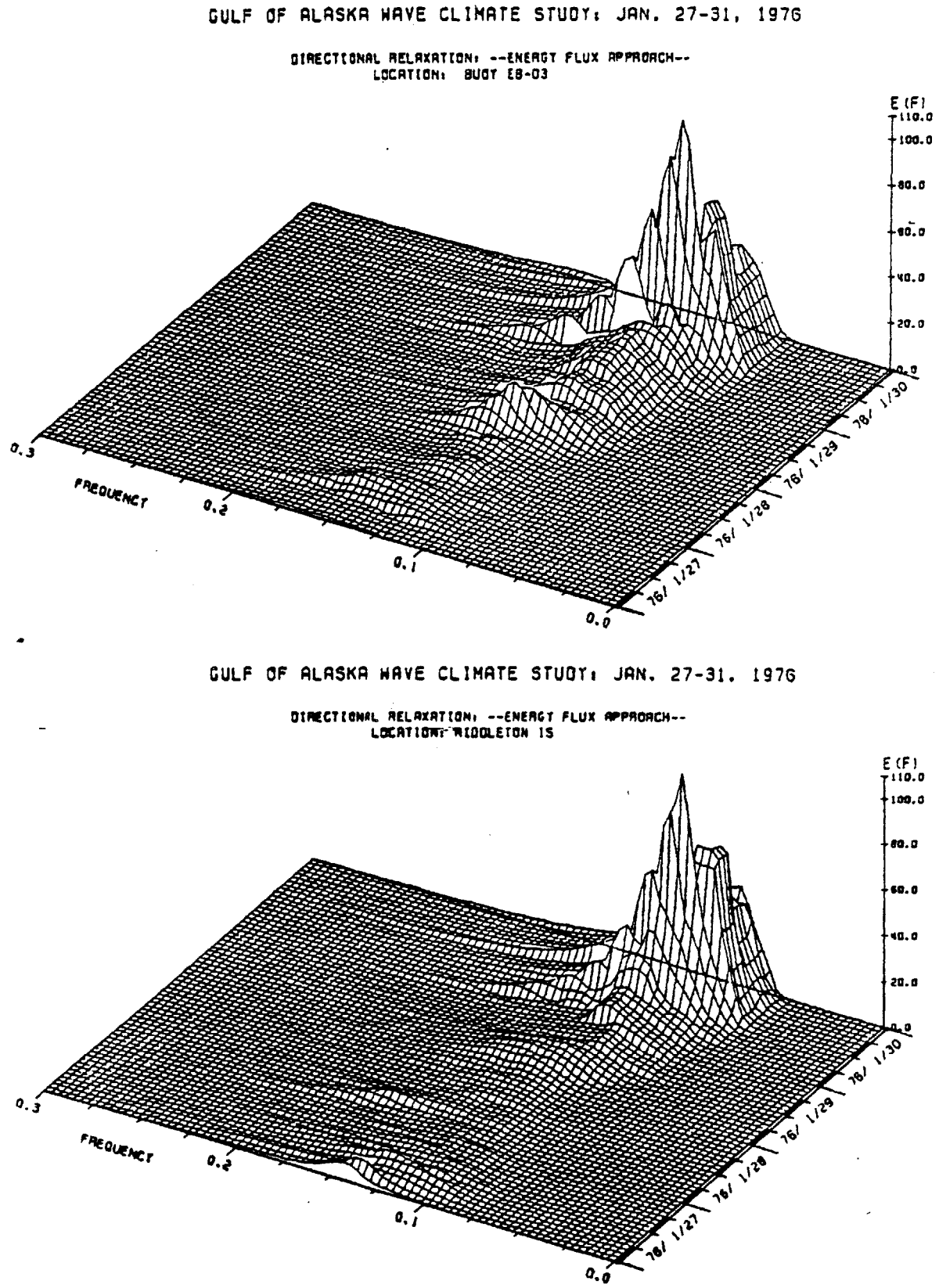


Fig. 5.7 Evolution of hindcasted wave spectra at station NOAA EB03 (top) and Middleton Island (bottom) for the extratropical cyclone of January 27-31, 1976.

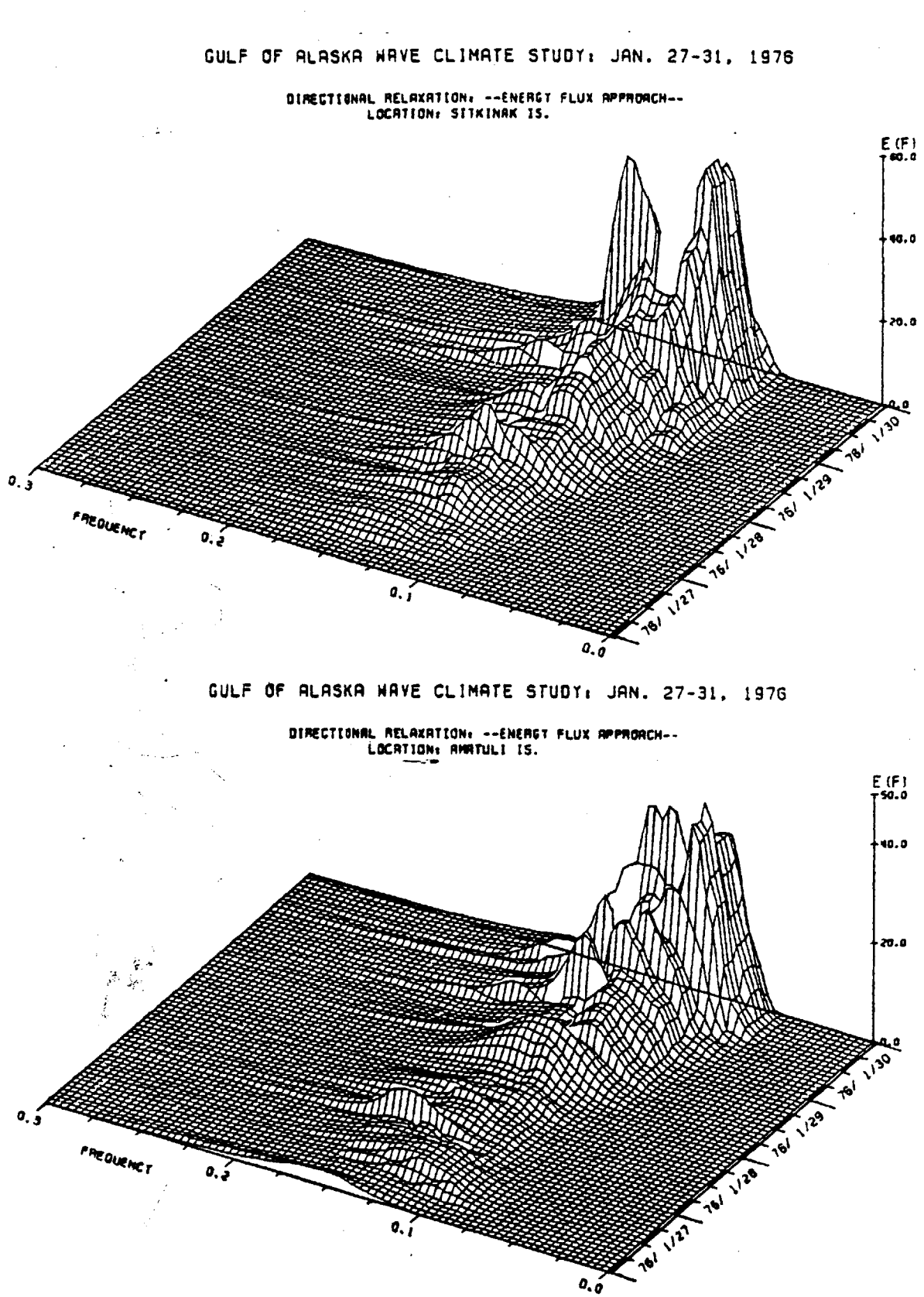


Fig. 5.8 Evolution of hindcasted wave spectra at station Sitkinak Island (top) and Amatuli Island (bottom) for the extratropical cyclone of January 27-31, 1976.

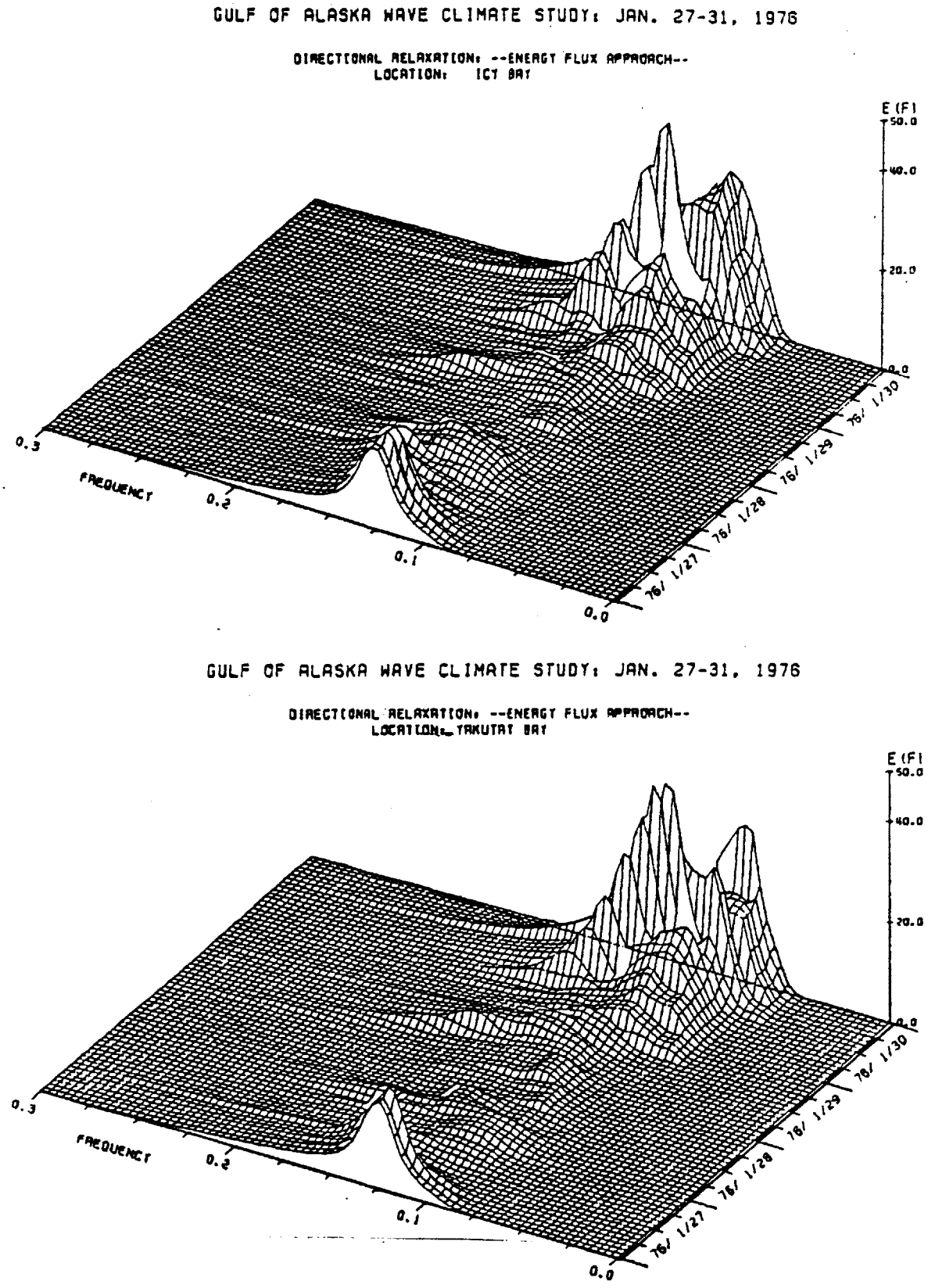


Fig. 5.9 Evolution of hindcasted wave spectra at station Icy Bay (top) and Yakutat Bay (bottom) for the extratropical cyclone of January 27-31, 1976.

and the southern part of Kenai Penisula. Although it experienced the full intensity of the storm's onshore blowing winds, the waves didn't develop as might be expected. Figure 5.9 shows the spectral evolution at Yakutat and Icy Bays. Both locations show very similar spectral developments, marked by an initial spectral peak at the beginning of the modeling period. In the following we will discuss the hindcasted results for the individual measuring locations and how they compare with observed data.

NOAA Buoy EB03:

For almost two days, EB03 was recording moderately strong winds from southerly directions and waves corresponding to an unlimited fetch. The time history for the grid point closest to EB03 is shown in Figure 5.10. The stick plot of the wind illustrates the temporal variation in speed and direction. The effect of the approaching extratropical storm was felt late on January 29, with winds initially decreasing in speed and shifted towards the east. As the storm came closer, the winds pick up in speed, reaching up to 25 m/s, and the direction continuously turned towards the south and southwest. The plot below shows the behavior of the windsea direction scaled by the windsea wave height. The mean windsea direction mimics with some delay the behavior of the local wind vector. The lag between wind and waves is depicted in the time history plot at the bottom left. The convention of the lag is as follows: if the wind vector rotates clockwise, the lag is indicated by a positive value and if the wind rotates counter-clockwise, the lag is given by a negative value. The presence of swell is indicated in the plot above. The direction of the

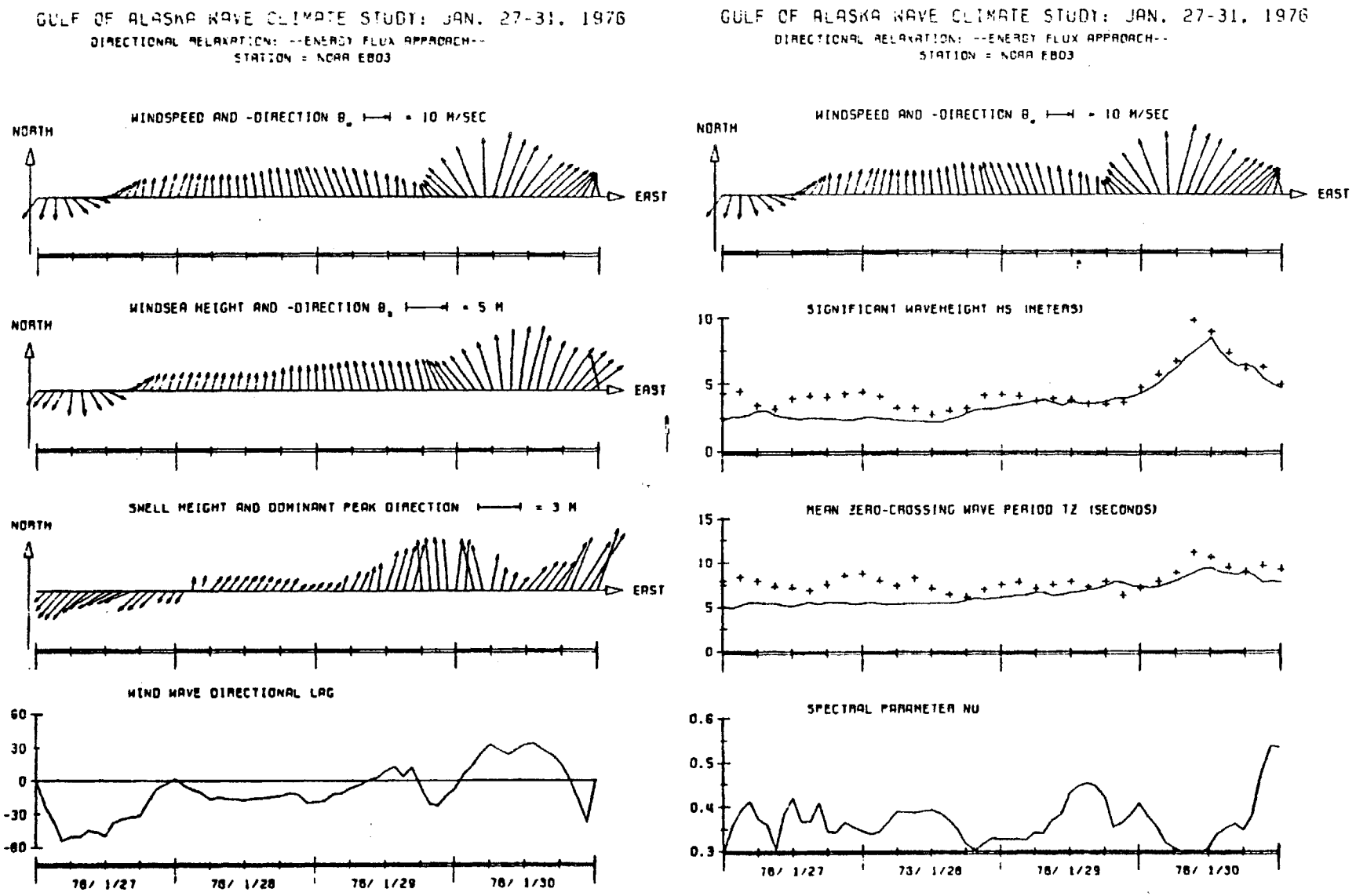


Fig. 5.10 Time series of hindcasted spectral wave parameters and measurements (+++) at station NOAA EB03 using a model with directional relaxation.

swell corresponds to the bin containing the most energy and the arrow is scaled with the total energy in the swell field. From this it is clear that the wave field always consisted of a relatively equal windsea and swell, except at the peak of the storm. At this time, the waves were almost all windsea with very little swell. After the storm had passed, swell waves were prevailing at EB03.

The right-hand side of Figure 5.10 shows the time series of significant wave height and mean zero-crossing wave period as compared with observations recorded at EB03. The overall agreement is considered good, particularly in the initial rise before and in the fall after the peak wave conditions. The reason for disagreement in the peak wave heights as predicted and measured, has several possible explanations. For one, wave growth of the model is proportional to $U \cdot \cos(\theta_w - \theta_o)$, the product of wind speed times the cosine of the difference angle between the local wind and mean wave direction. This effectively reduces wave growth for all situations except when wind and waves are parallel to one another. Two, the wind input occurs via the α parameter equation, by means of a source function which was derived from an equilibrium relationship between α and $\nu = fmU/g$. This empirical relationship was established for fetch-limited and less severe wind conditions. A third possibility is that the two recorded wave heights at the peak are questionable. This conjecture is supported by the fact that the observed spectral data showed a recording error entry for the times at 0600 GMT and 0900 GMT on January 30, 1976. According to D.B. Ross (personal communication), the recorded data was only scrambled and its spectral densities were manually re-analyzed.

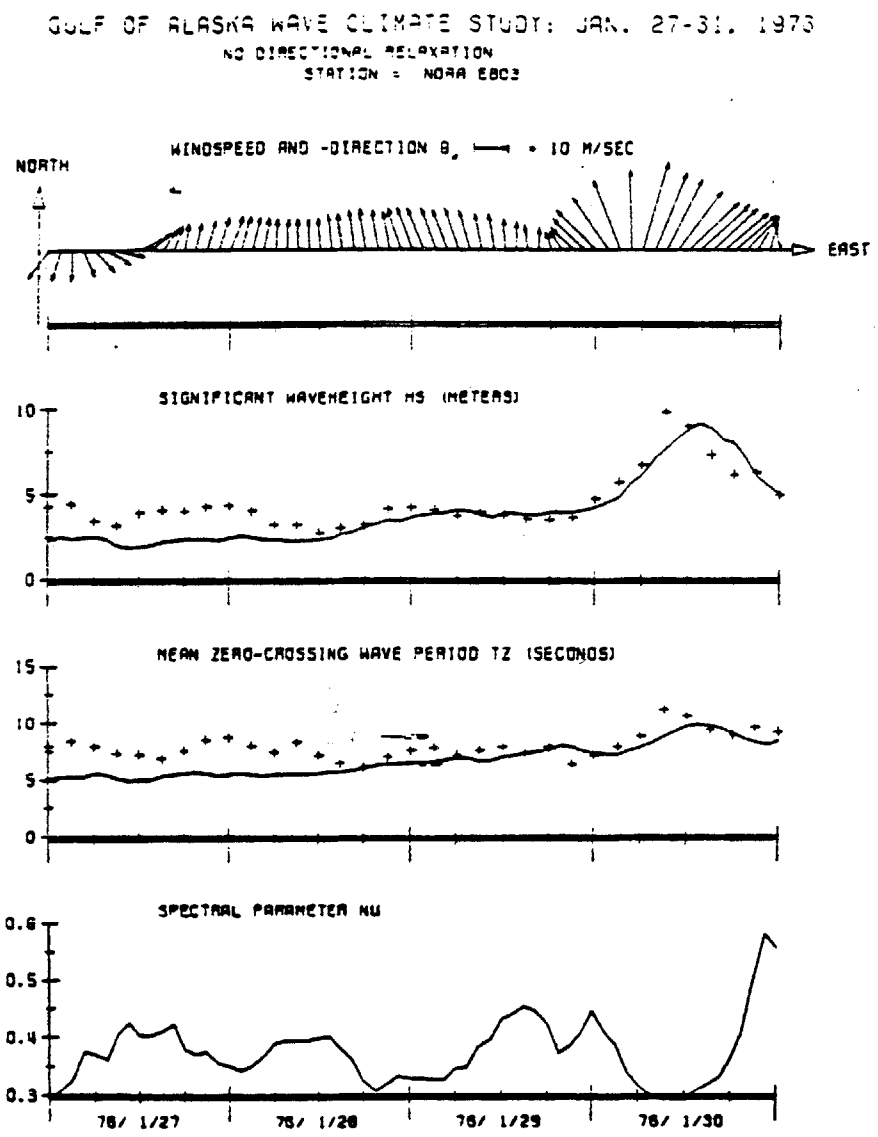


Fig. 5.11 Time series of hindcasted spectral wave parameters and measurements (+++) at station NOAA EB03 using a model without directional relaxation.

If the directional effect on spectral growth seems to be a major cause in reducing predicted wave heights, then the model run without the directional parameter should remedy this discrepancy. Figure 5.11 shows these results. The overall wave heights are somewhat increased, but still the model peak fails to concur with the peak of observations. The time history of the spectral parameter ν_s (cf. section 3.1.1) gives an indication of the narrowness of the wave spectrum, i.e., $\nu_s \to 0$. The results of H_s, T_z and ν_s together provide enough information to determine the joint statistics of waves as described in Shum (1984).

Figures 5.12, 5.13 and 5.14 illustrate hindcasted and observed wave spectra at 0600 GMT, 0900 GMT and 1200 GMT on January 30, respectively. Maximum.wave conditions occurr at 0900 GMT. Each figure presents hindcasted spectra from the models including and excluding the directional parameter, respectively. Generally the agreement is not too good, which may reflect on the one hand the capability of the model to respond to rapid growth and on the other hand may also point to a problem relating to the transition region between swell and windsea.

MIDDLETON ISLAND:

The wind history at the grid point simulating wave conditions for Middleton Island was essentially identical to one of EB03. The time series of wind and wave parameters are shown in Figure 5.15. Similarly, the hindcasted maximum wave height is well below the recorded maximum. However, in this case it appears that the model response regarding the rise and occurrence of maximum wave conditions are far better than EB03. The mean zero-crossing wave period is

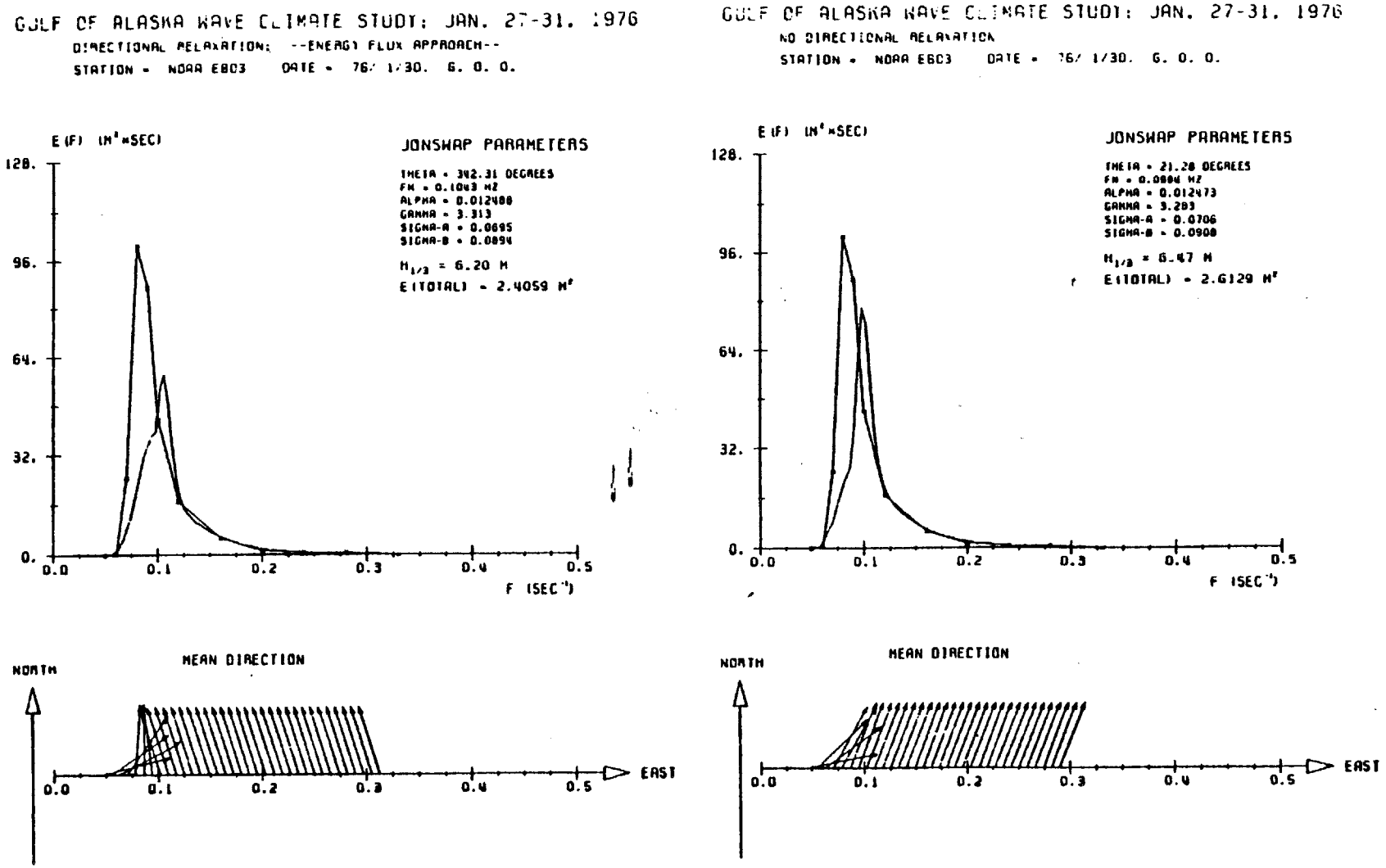


Fig. 5.12 Comparison between hindcasted (——) and measured (*—*) wave spectra at station NOAA EB03 for 0600 GMT, January 30, 1976. (Left: with directional relaxation; right: without directional relaxation).

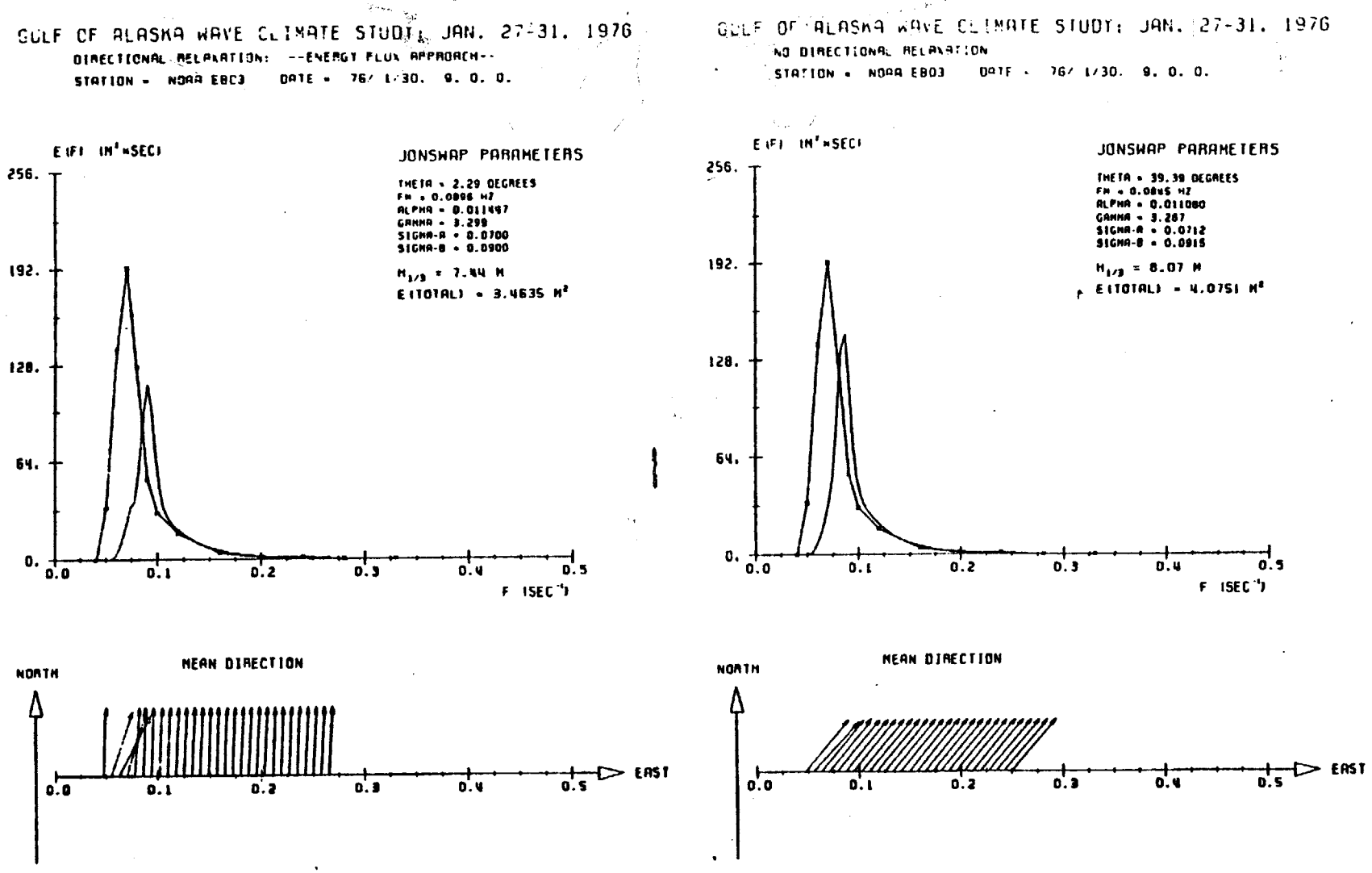


Fig. 5.13 Comparison between hindcasted (——) and measured (*–*) wave spectra at station NOAA EB03 for 0900 GMT, January 30, 1976. (Left: with directional relaxation; right: without directional relaxation).

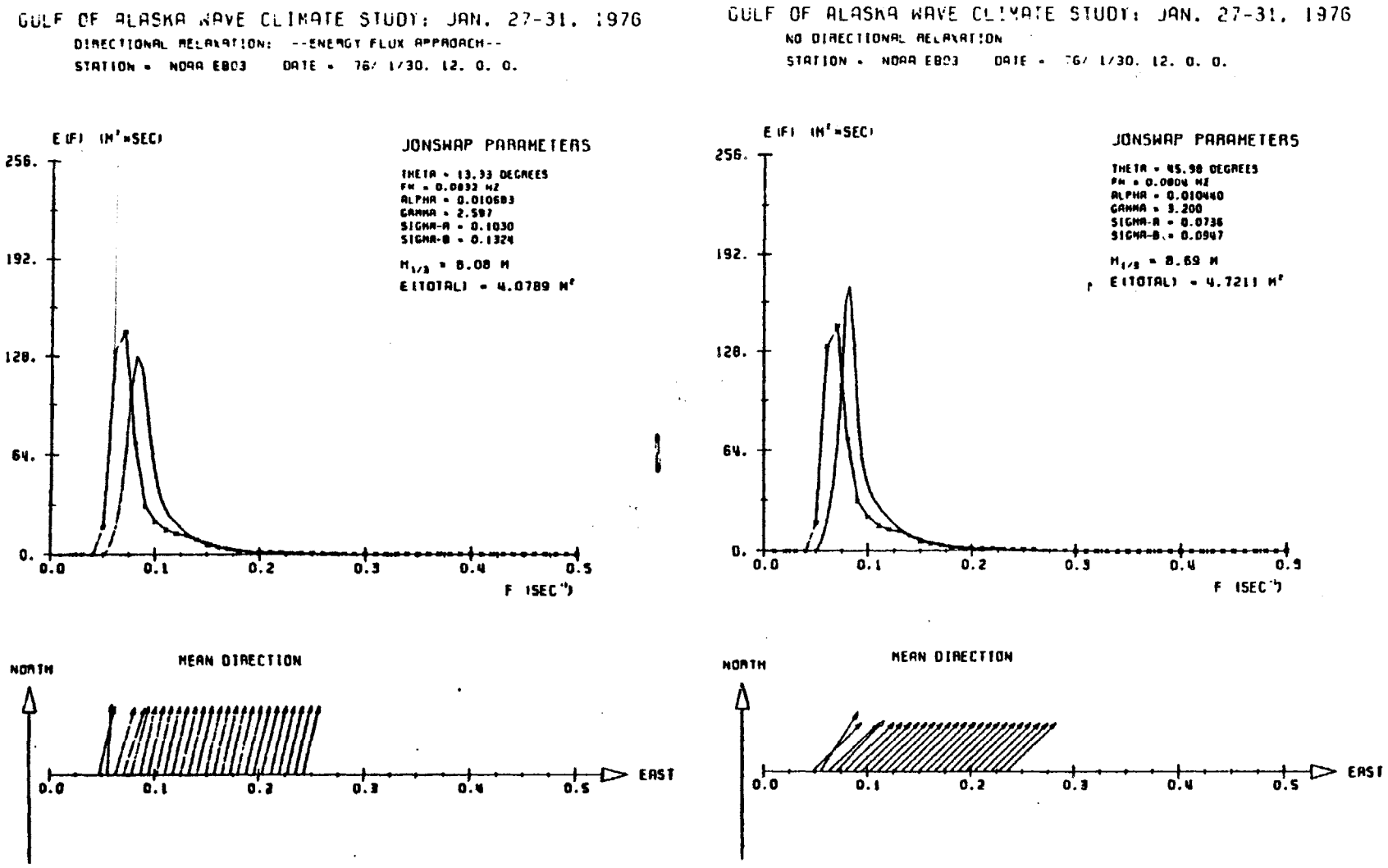


Fig. 5.14 Comparison between hindcasted (——) and measured (*—*) wave spectra at station NOAA EB03 for 1200 GMT, January 30, 1976. (Left: with directional relaxation; right: without directional relaxation).

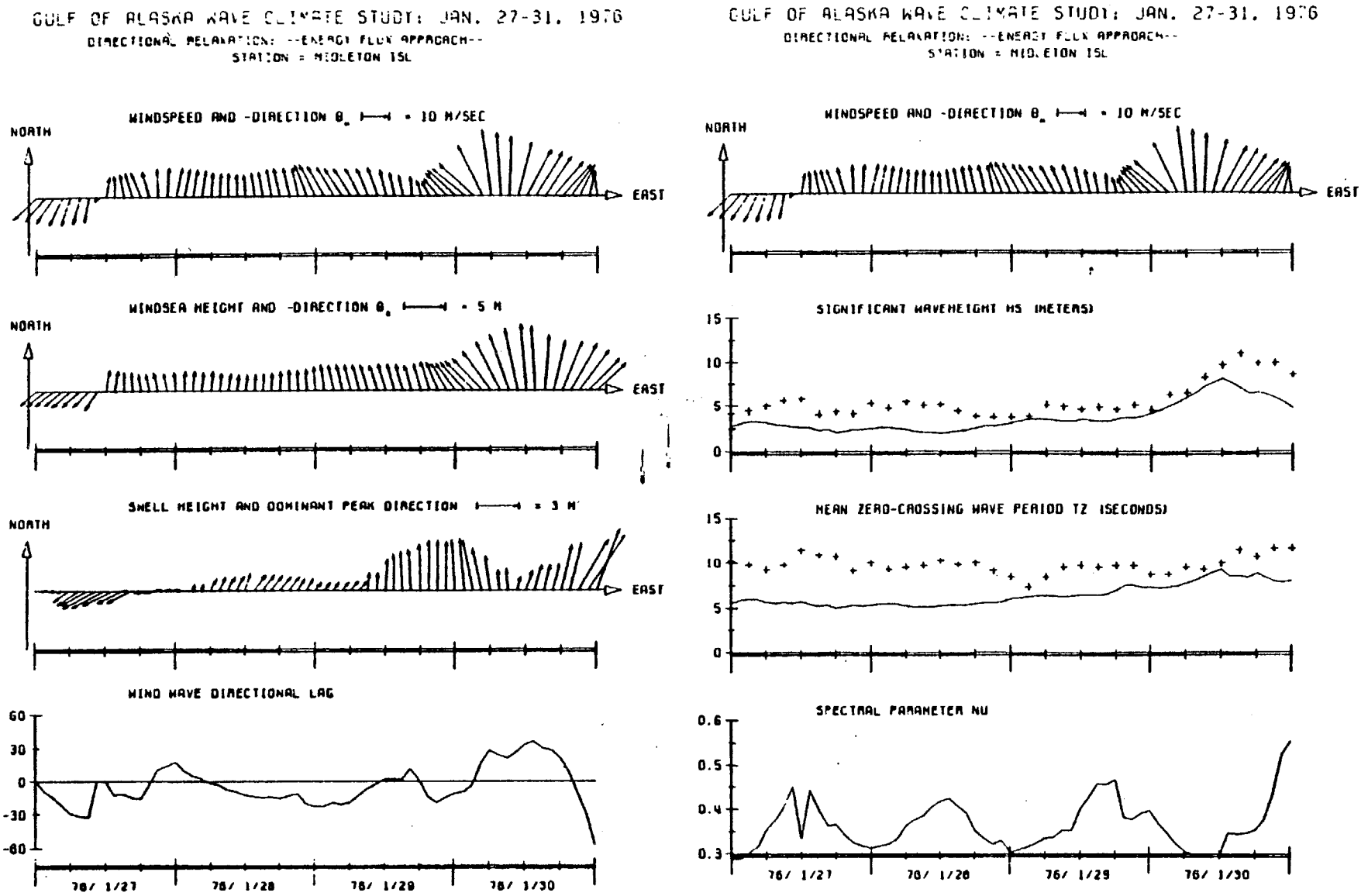


Fig. 5.15 Time series of hindcasted spectral wave parameters and measurements (+++) at station Middleton Island using a model with directional relaxation.

consistently underpredicted by the model. The data of T_z features an odd periodicity of one day, where the period T_z seems to dip and then pick up again. If this behavior is real then it must be of local origin, because on a synoptic scale there was no indication of this feature. Another possible source could be Doppler-shifted frequencies due to currents or long distance swell. The hindcasted results without the directional parameter (Figure 5.16) show an increased maximum wave height by more than one meter, although still lying below the observed wave height peak of over 11 meters. Nevertheless, there appears to be some discrepancy in the data. Reece and Cardone (1982) reported on the results of the calibrated GAPS model for the same storm. According to them, the maximum measured wave height was just over 10 meters which falls short by 1.5 meters of the data we compared to. The results of the GAPS model are depicted in Figure 5.17 with our hindcasted predictions for both model versions. It should be pointed out that no attempt was made to tune the parametric wave model. In order to demonstrate the model's sensitivity to the wind field, we made one run where all winds were categorically increased by 10%. This produced everywhere an increase of approximately 15% in H_s and is sufficient to provide a favorable agreement between our model results and data.

SITKINAK ISLAND:

This location was unique, since the storm's low pressure center passed right over it. This is evident in the very rapid change in the wind vector (Figure 5.18). Except for the beginning of the modeling period, this measuring site experienced winds blowing approximately from south until the second half of January 29. Then, within a very

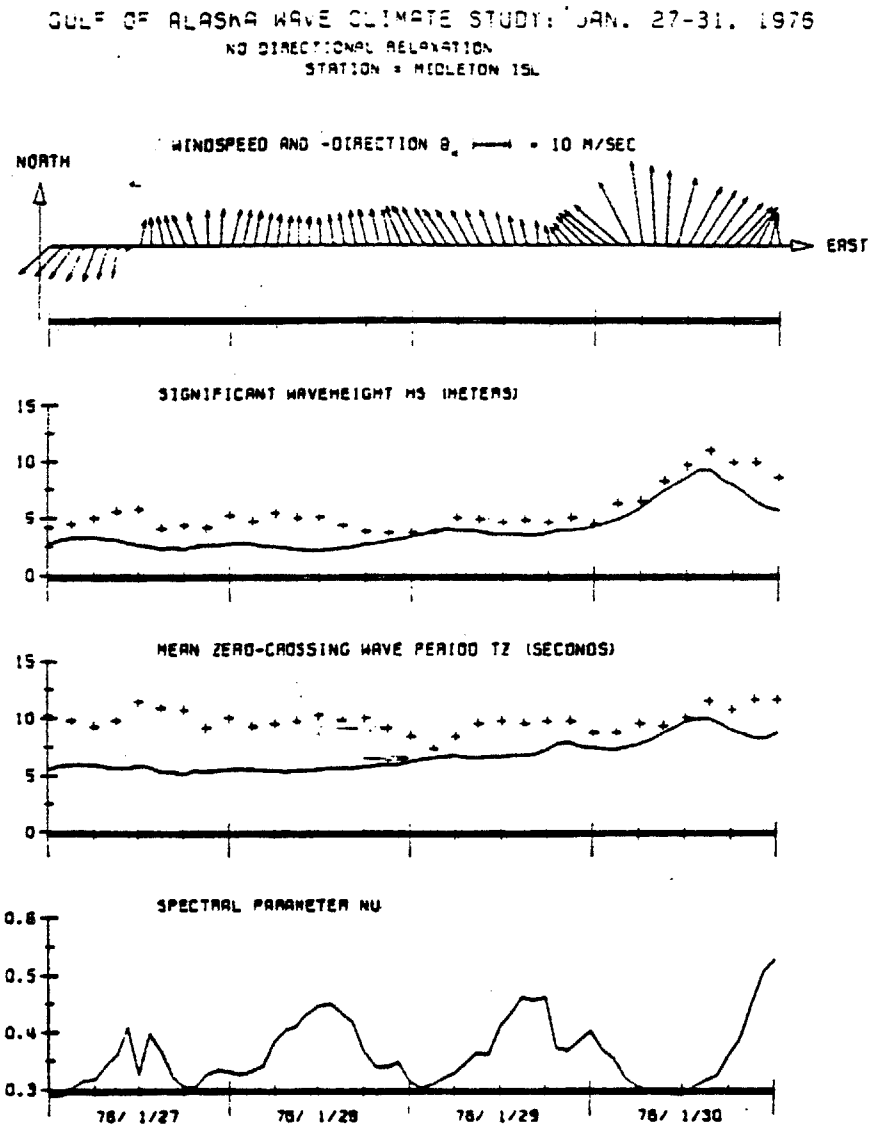


Fig. 5.16 Time series of hindcasted spectral wave parameters and measurements (+++) at station Middleton Island using am odel without directional relaxation.

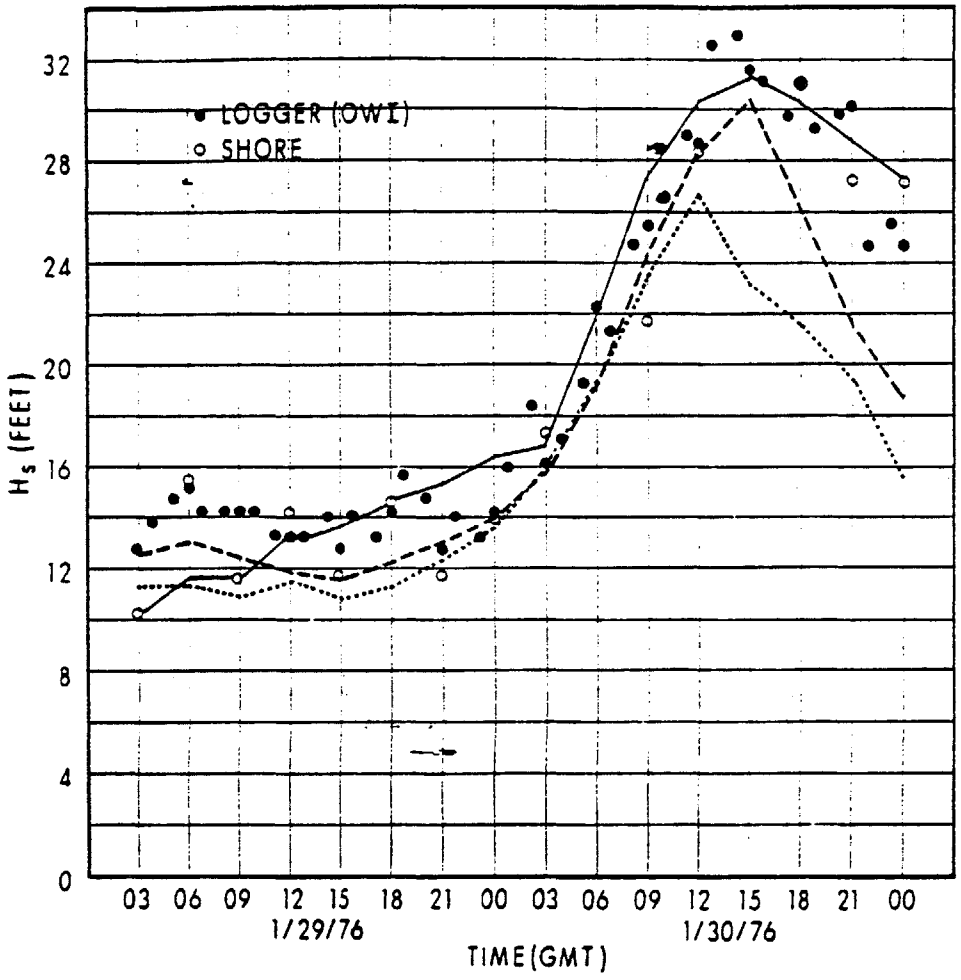


Fig. 5.17 Comparison of hindcasted significant wave heights from three wave models with data for Middleton Island. (——) GAPS model; (---) HYPA model, no directional relaxation; (.....) HYPA model, with directional relaxation. (From Reece and Cardone, 1982).

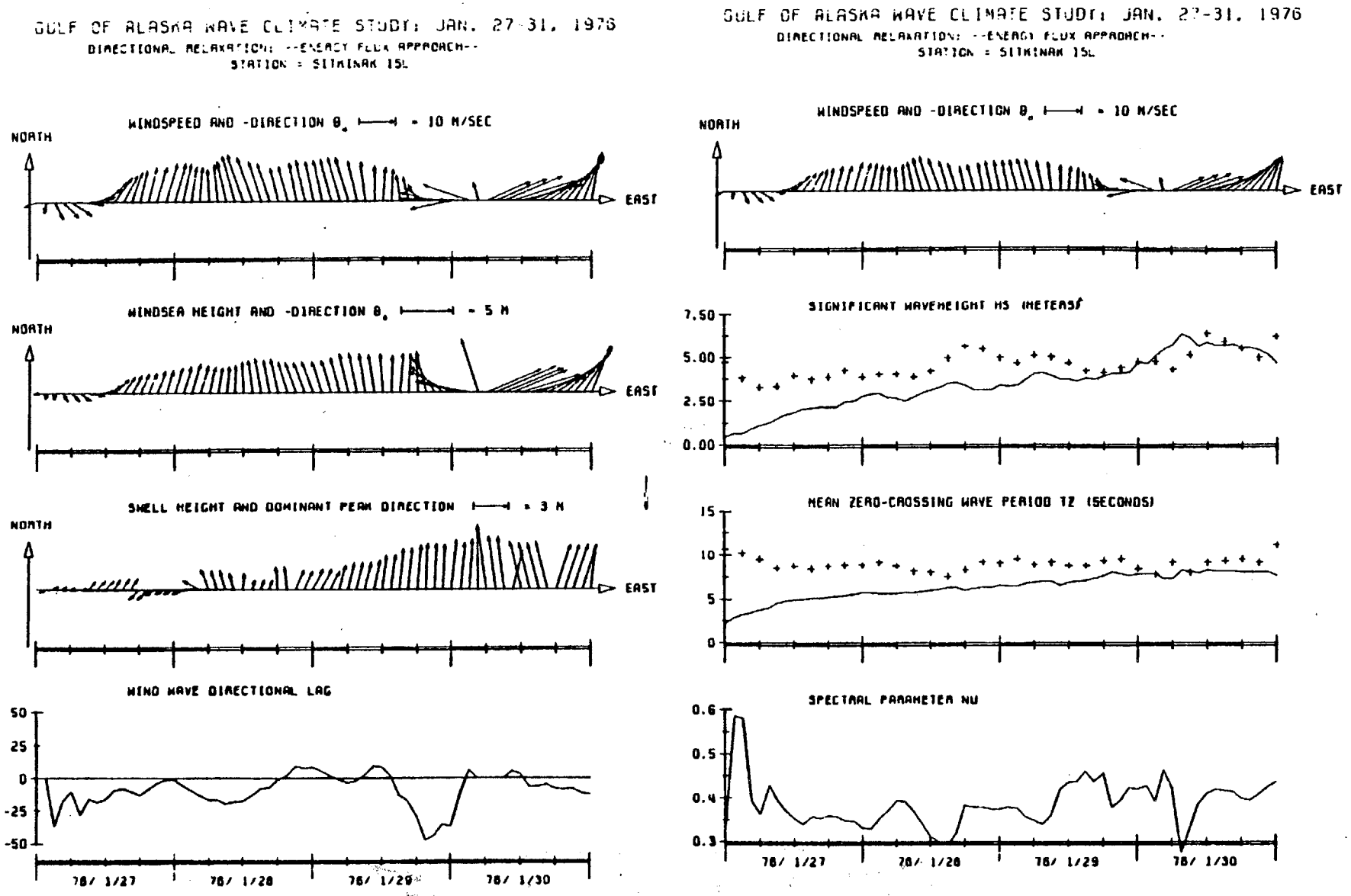


Fig. 5.18 Time series of hindcasted spectral wave parameters and measurements (+++) at station Sitkinak Island using a model with directional relaxation.

short time, the winds first blew from east at the storm's edge ahead of the center and rapidly changed to almost westerly winds behind the pressure low. The mean wave direction considerably lags the wind vector during the storm's passage. Hindcasted and observed wave heights are generally in good agreement for the later part of the hindcast period. The model seems sensitive enough to produce responses to the smaller secondary maxima prior to the storm. The lower levels in these secondary peaks may be attributed to the effect of model spin-up time for the model at this site, as can be seen in the very low starting wave height. The measured wave period T_z hardly varies over the entire time from an average value of approximately 9 seconds.

As might be expected, the model without directional relaxation performed poorly during the rapid shift in the wind direction. This is clearly demonstrated in Figure 5.19, where most of the energy in the windsea is lost by radiation into swell after the peak occurred.

AMATULI ISLAND:

It was anticipated that the proximity of land on either side at this measuring site (cf. Figure 5.2) would have some sheltering effect on the wave climate there. As can be seen in Figure 5.20, the changes in the wind history for this grid point seem to be more gradual. On the average the wave directions were lagging the wind just slightly up to the time when the cyclone passed over Sitkinak and Kodiak Islands. Then the difference increased to as much as 60°. This also shows up in the swell, where for a short period around 0900 GMT January 30, relatively little swell was present and then was followed by a sudden increase in swell energy. This is better explained on the significant

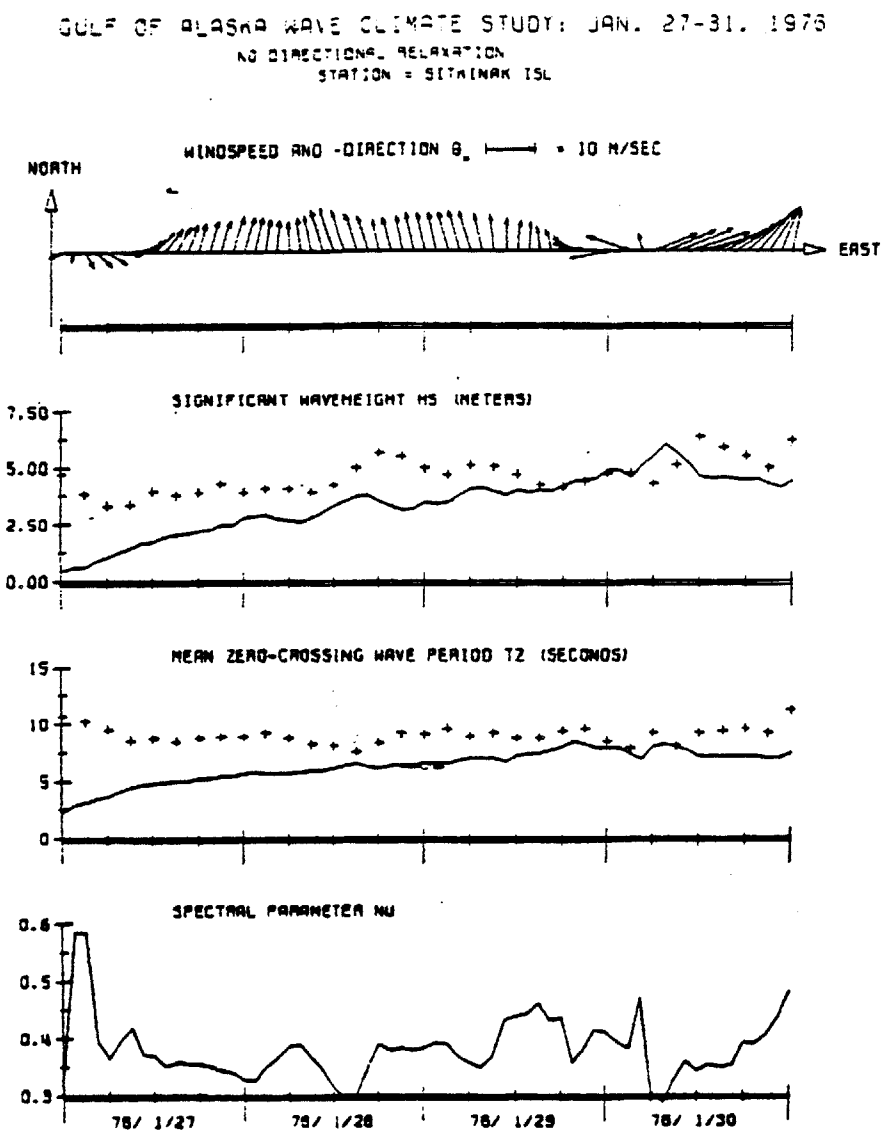


Fig. 5.19 Time series of hindcasted spectral wave parameters and measurements (+++) at station Sitkinak Island using a model without directional relaxation.

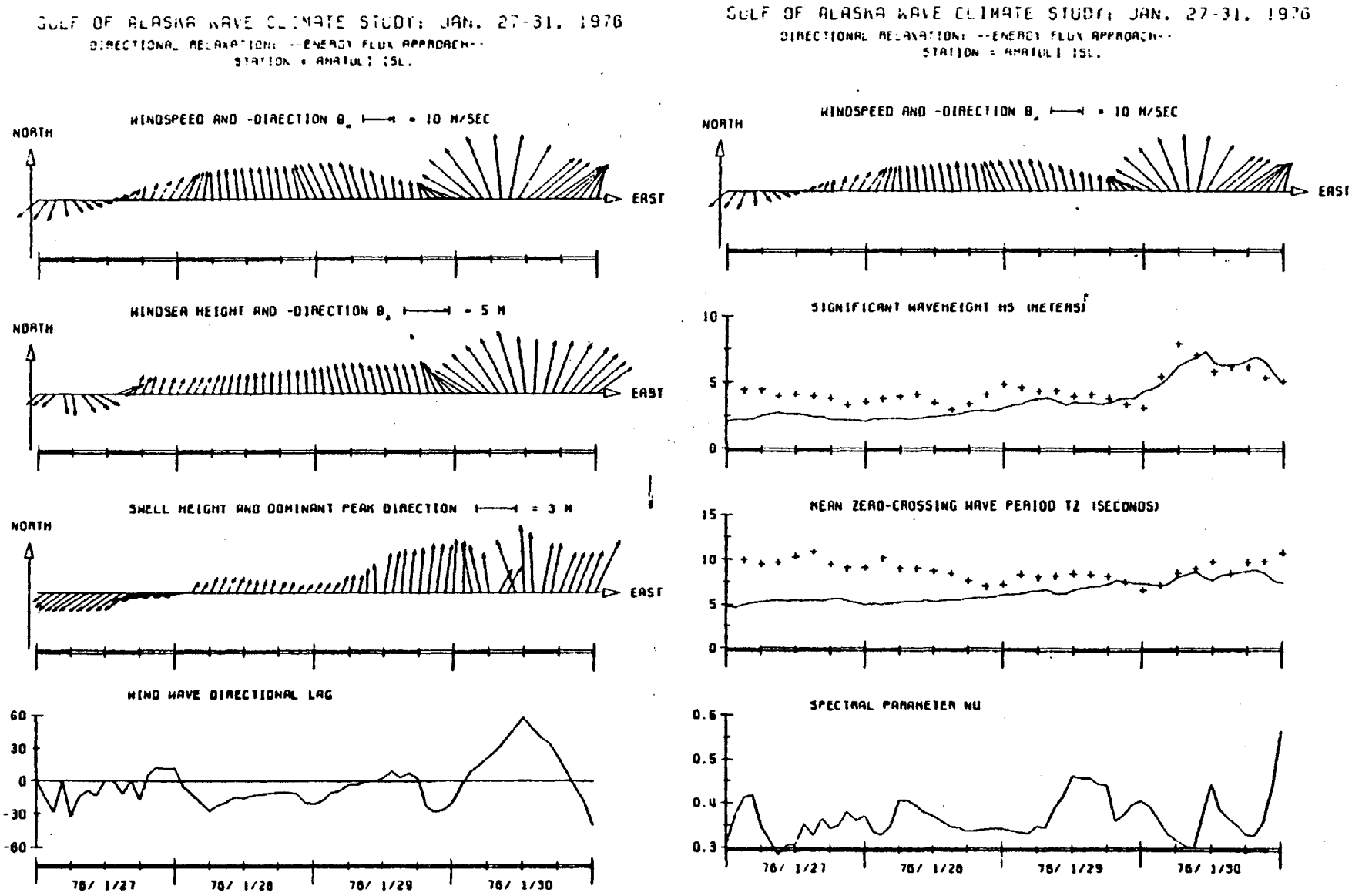


Fig. 5.20 Time series of hindcasted spectral wave parameters and measurements (+++) at station Amatuli Island using a model with directional relaxation.

wave height time series. Wave heights considerably dropped just before the arrival of the cyclone on midnight (0000 GMT) January 30. This was a consequence of the sheltering provided by Kodiak Island. Then within six hours, wave heights rose by 5 meters under the wind action of the approaching extratropical cyclone. By 0600 GMT January 30, the storm hit land at Sitkinak Island (cf. Figure 5.5), and the windsea wave height quickly diminished until swell waves arrived from further south to maintain a level of high waves. This history of events is also evident in the wave periods. The hindcasted wave periods show the same feature, but more gradually. Nevertheless, the model captures the fall and rise signature until the arrival of swell, although somewhat delayed. The geometrical obstruction of Kodiak Island causing the sheltering effect can hardly be resolved on a model grid of this scale. A finer grid system would be needed to perform better for this situation. It should be pointed out that the wave periods have the same underlying periodicity as previously mentioned for Middleton Island. The results without directional relaxation appear to be somewhat better, at least with respect to attained maximum wave height (Figure 5.21).

ICY BAY:

Similarly to Middleton Island, the measuring location at Icy Bay was completely exposed to the ocean side with the mountains along the coastline. The winds didn't shift too rapidly, because Icy Bay was situated more at the outer edge of the cyclonic circulation pattern. This shows up clearly in the continuously developing windsea as depicted on the left-hand side of Figure 5.22. At the time of peak

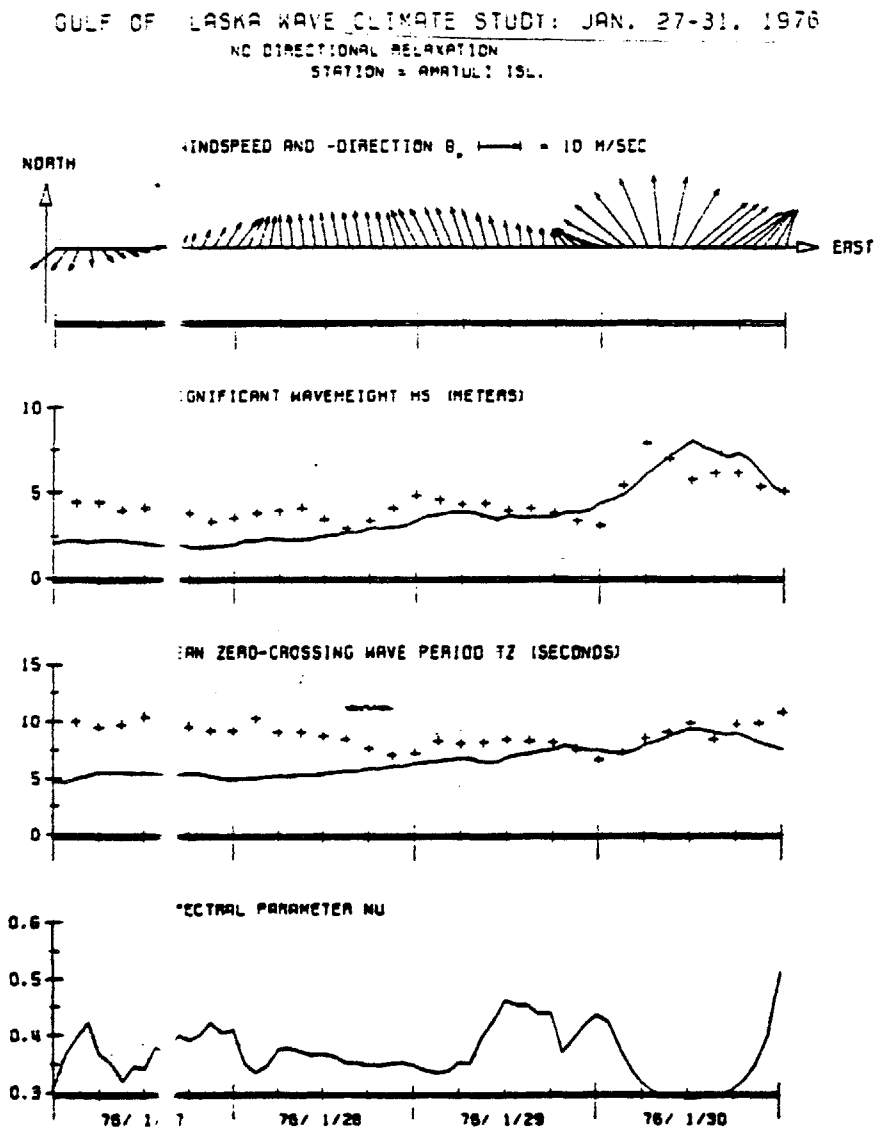


Fig. 5.21 Time series of hindcasted spectral wave parameters and measurements (+++) at station Amatuli Island using a model without directional relaxation.

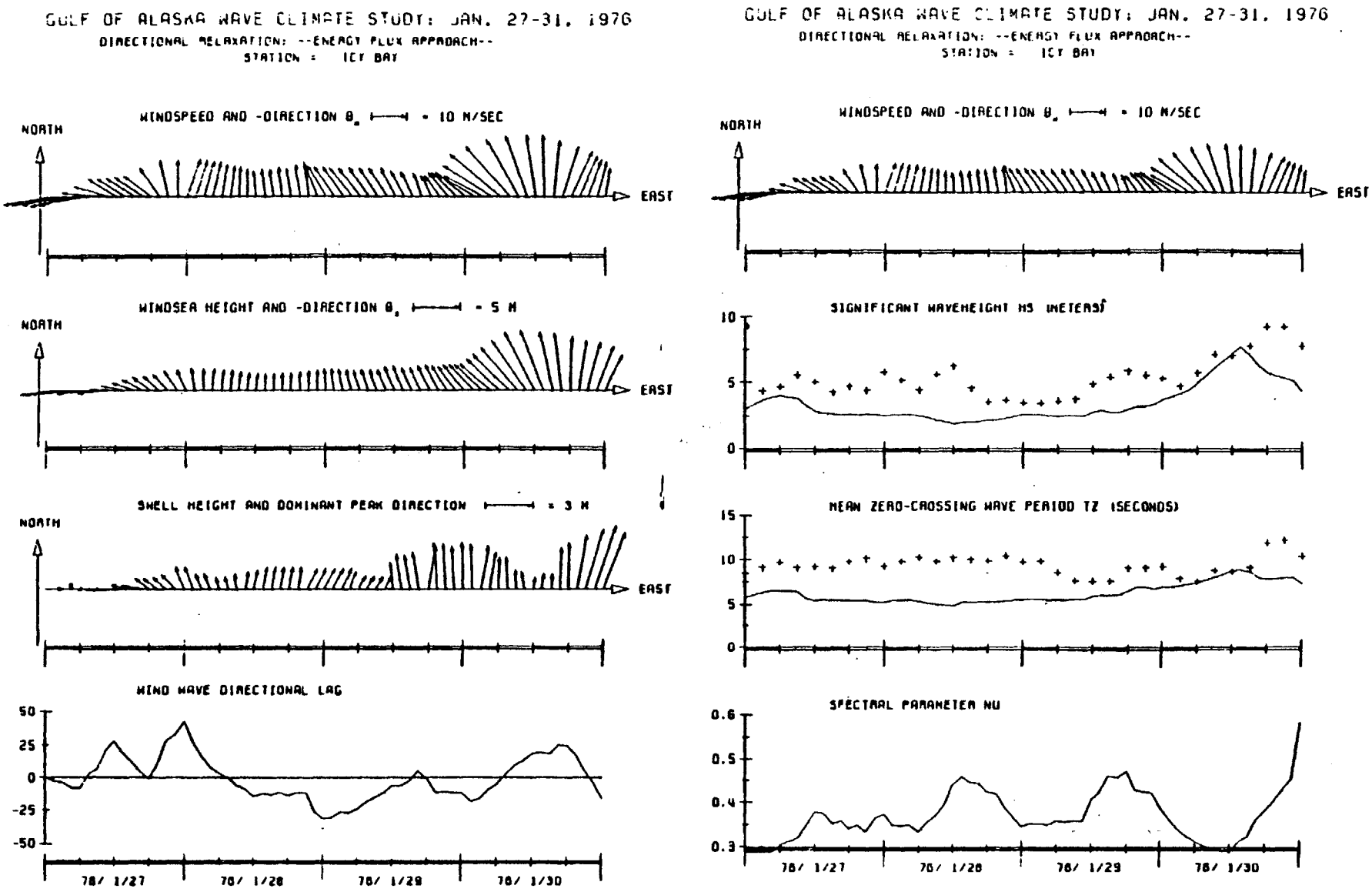


Fig. 5.22 Time series of hindcasted spectral wave parameters and measurements (+++) at station Icy Bay using a model with directional relaxation.

winds (0900 GMT, January 30) the wave field was almost pure windsea. Within six hours, swell from the open ocean arrived, dominating the diminishing windsea. However, a closer look at the time series of H_s reveals a quite different picture. For one, the observed maximum waves occured near the end of the day, reaching up to 10 meters as reported by Reece and Cardone (1982). Maximum winds were present in the early morning of January 30 (≈ 21 m/s), and steadily decreased thereafter. This implies that at this site the highest waves were swell. This fact is also indicated by the observed wave periods of the order 13 seconds and more. For two, there was an initial relative peak in wave height and period prior to the storm (1800 GMT, January 29). We were not able to attribute the origin of this relative maxima to any local generation. The synoptic weather maps for this time showed no small-scale disturbance, which could be the source for this increase. Generally, the prevailing winds before the arrival of the storm were well below 15 m/s, which is not sufficient to generate waves of this height (≈ 6 m). Finite depth effects were also excluded as a possible generation mechanism, since the water depth for this area was at least 200 m deep. Long distance swell was another possible source, but was considered unlikely, since a similar signature should have been present in the records of EB03 and Middleton Island. This leaves the possibility that these waves could be swell radiated from the storm while it was still in the open ocean. However, even this seems to be unlikely, since a similar effect should certainly register at the measuring sites of EB03 and Middleton Island. For this site, the hindcasted model results were quite poor when compared with observations. Even the model without directional relaxation did not perform much better (Figure 5.23).

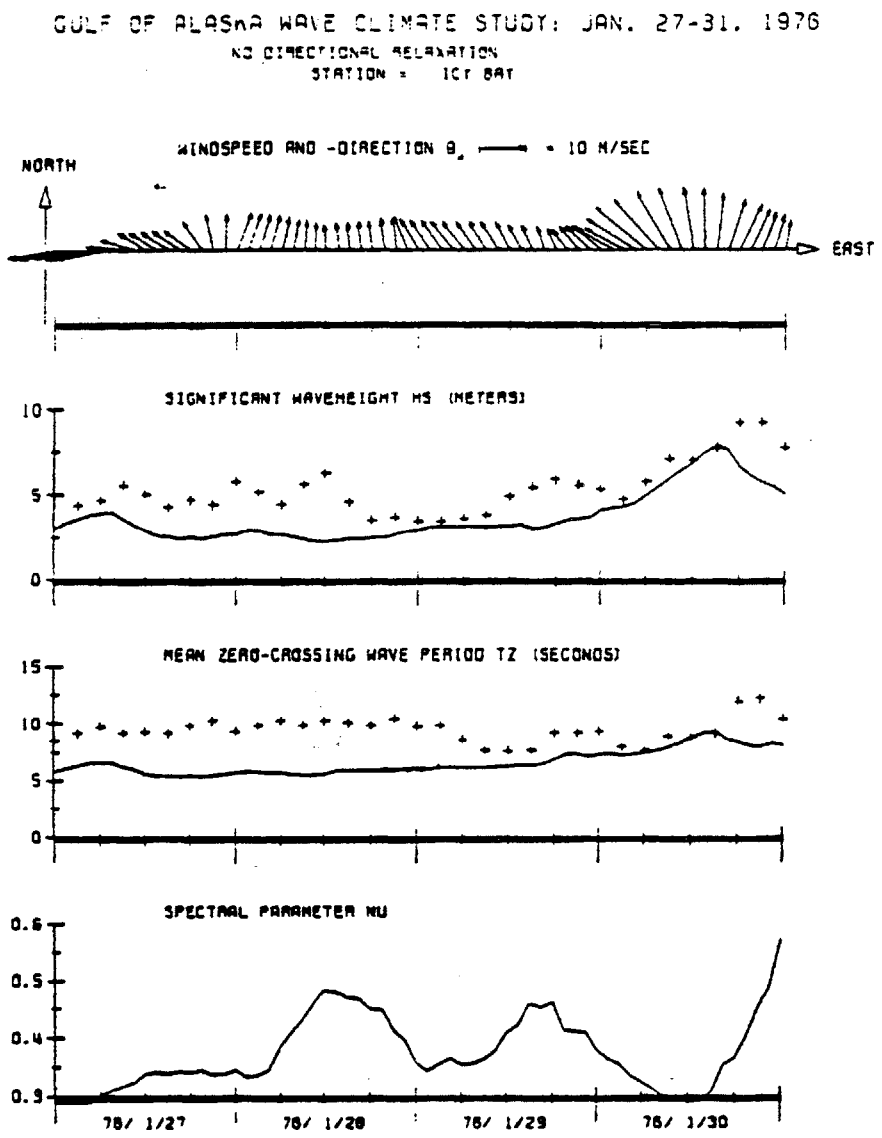


Fig. 5.23 Time series of hindcasted spectral wave parameters and measurements (+++) at station Icy Bay using a model without directional relaxation.

YAKUTAT BAY:

Similarly to the events taking place at the site Icy Bay, Yakutat Bay also recorded three maxima in wave height (Figure 5.24). The first one around 1800 GMT, January 29, is again of mysterious origin. The model predictions do not resolve this feature at all. A second peak, coinciding with the hindcasted maximum H_s at approximately 1200 GMT, January 30, appears to be the windsea peak, since winds attained their highest speed (≈ 20 m/s) and very little swell was present around this time (cf. left-hand side of Figure 5.24). The last peak, with a measured maximum of $H_s \approx 9$ m occurred at the end of the day. At this time wind speeds were less than 10 m/s. This implies that most of the energy was contained in the swell field. There are two possible explanations, why the model results are in disagreement with the measured data. As we have already mentioned, a trouble spot of the hybrid parametric model is its ability to treat the transition region windsea-swell. The other cause could lie within the assumption that the earth is flat over the extent of the model area. A more realistic representation should account for curvature effects of the earth. Neglecting this could yield a retardation or a speeding up of the swell movement in the model. Some indication of this can be seen in Figure 5.25, where hindcasted wave heights and periods for the model excluding directional relaxation show a rise just at the end of the hindcast period.

Finally, Figure 5.26 gives an impression of the spatial distribution of significant wave heights, corresonding to the time when the extratropical cyclone started to intensify and took course towards the Gulf of Alaska.

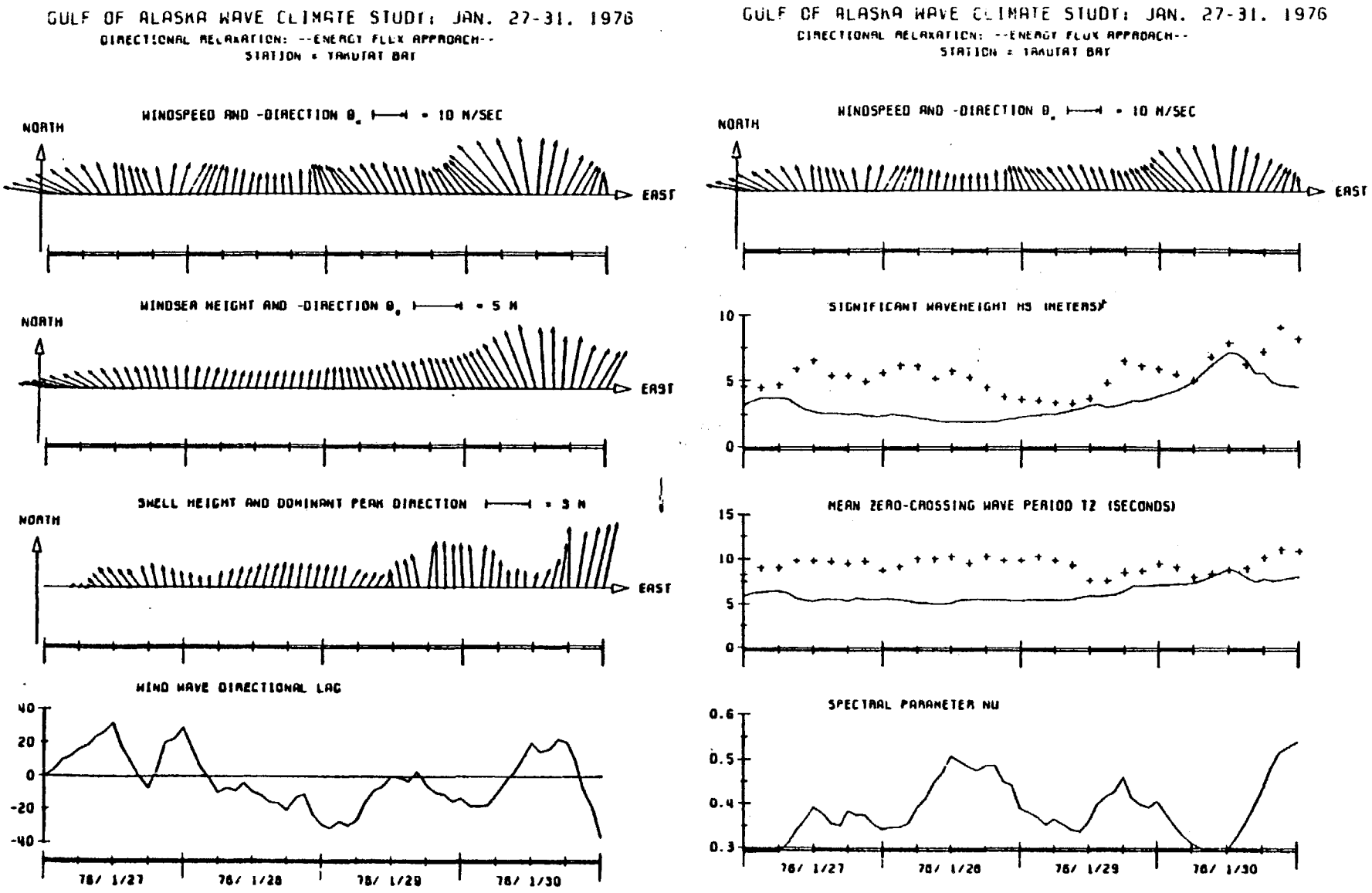


Fig. 5.24 Time series of hindcasted spectral wave parameters and measurements (+++) at station Yakutat Bay using a model with directional relaxation.

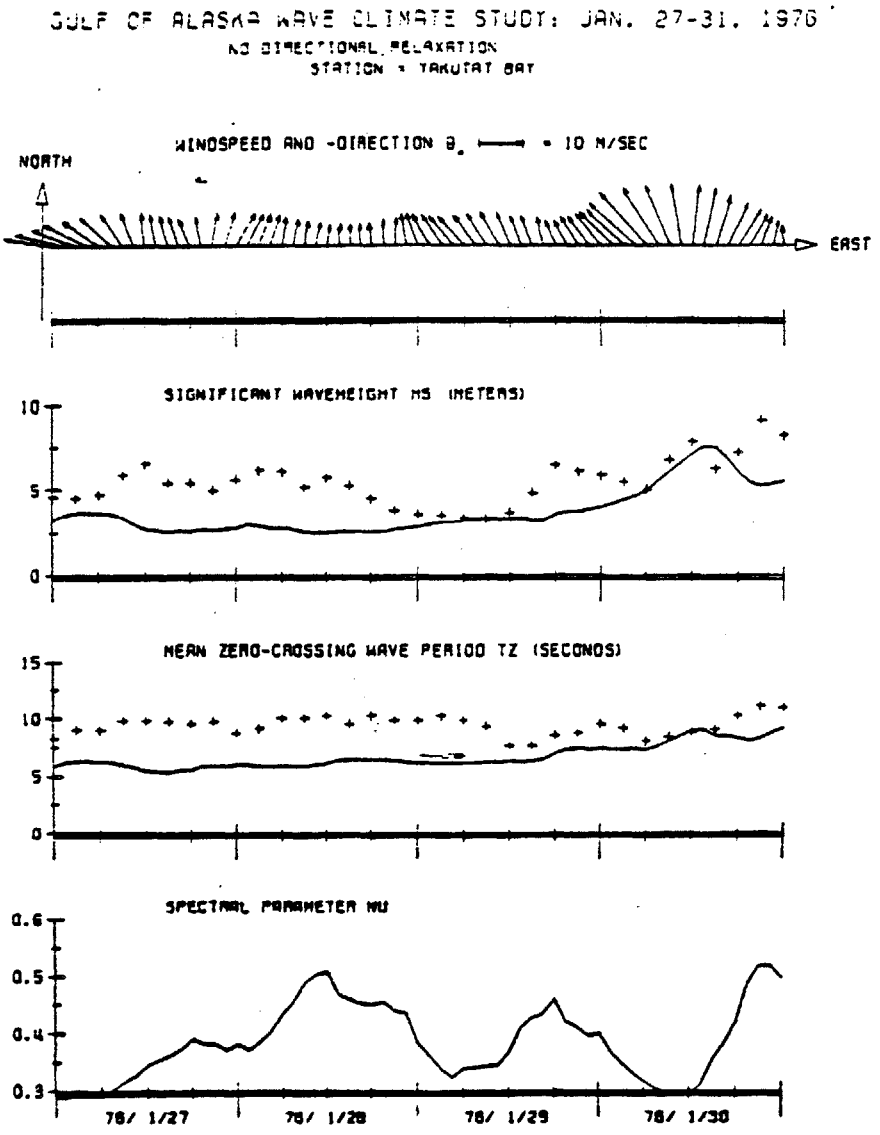


Fig. 5.25 Time series of hindcasted spectral wave parameters and measurements (+++) at station Yakutat Bay using a model without directional relaxation.

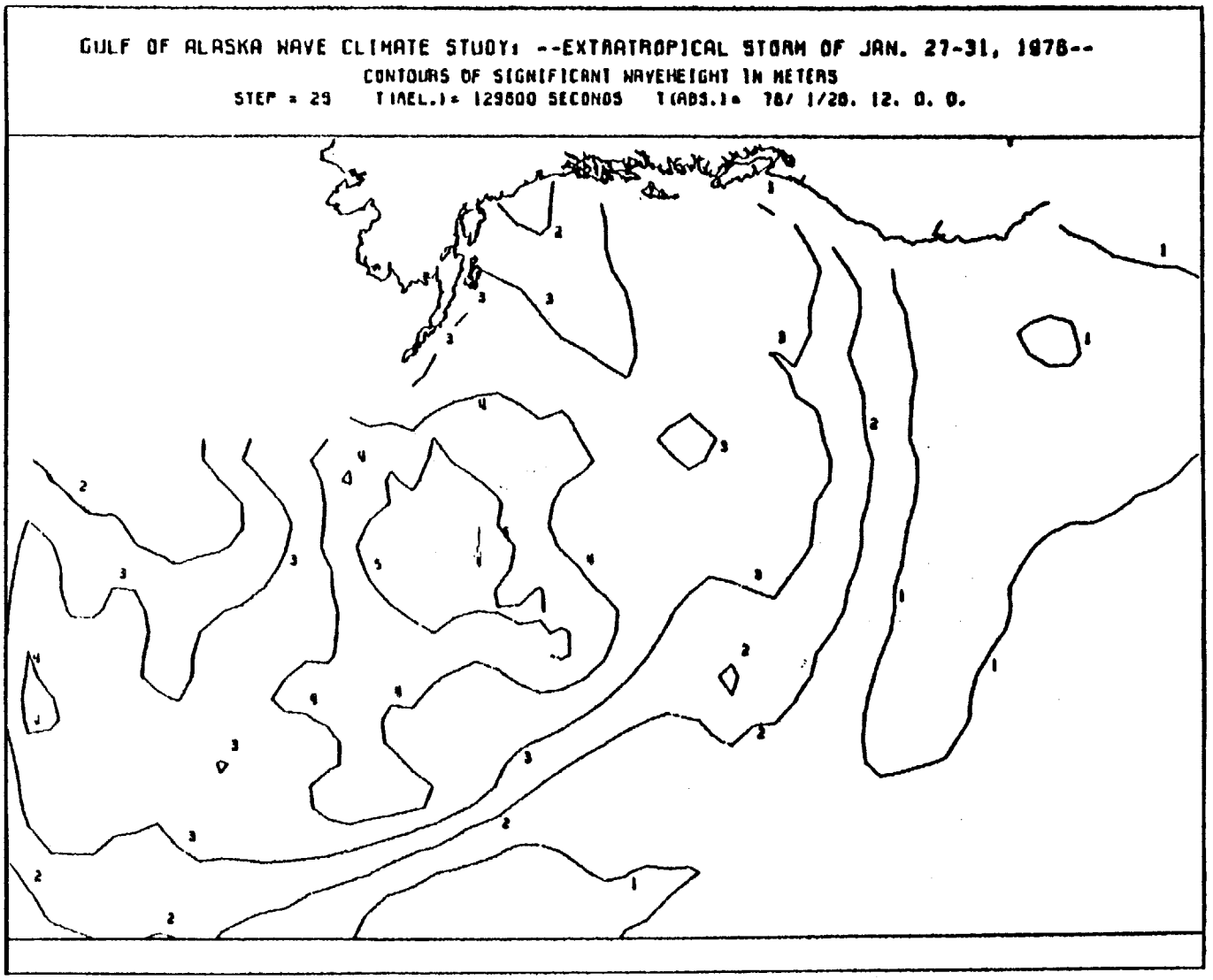


Fig. 5.26 Contours of hindcasted significant wave heights in the Gulf of Alaska for the extratropical cyclone on 1200 GMT January 28, 1976.

5.2 ARSLOE (Finite Depth Case)

One of the objectives of ARSLOE (Atlantic Remote Sensing Land Ocean Experiment) was to obtain basic information on wave transformation in waters of finite depth and provide a testing ground for shallow water wave models. Along a cross-shaped array, a variety of measurement devices such as waveriders, wave staffs and directional sensors were deployed to measure the influence of wave transformation on the spectral shape and wave directions. The outer most XERB buoy was located 35 km offshore in waters approximately 36 m deep. Spectral wave data were recorded as close as 3 km from the shore in a water depth of 17 m (Figure 5.27).

During the time period of ARSLOE a sharp frontal system made its passage over the ARSLOE site on October 25, 1980. Winds during the ARSLOE storm reached gale force and were accompanied with the generation of relatively high waves. The interesting feature of this storm was a pronounced flow of onshore winds ahead of the front, which changed within a few hours to equally strong offshore winds after the front had passed. Thus, within a three hour period the winds essentially changed direction by as much as 180°. The synoptic weather map of the frontal system is depicted in Figure 5.28. Examination of the data confirmed the appearance of multi-peaked spectra as well as directional cross-seas with swells propagating in an onshore direction and the newly generated windsea moving out towards deeper water. This situation provided an excellent case to test for one, the sensitivity of the directional parameter to a 180° switch in the wind direction, and for two, the verification of the finite depth version of the model.

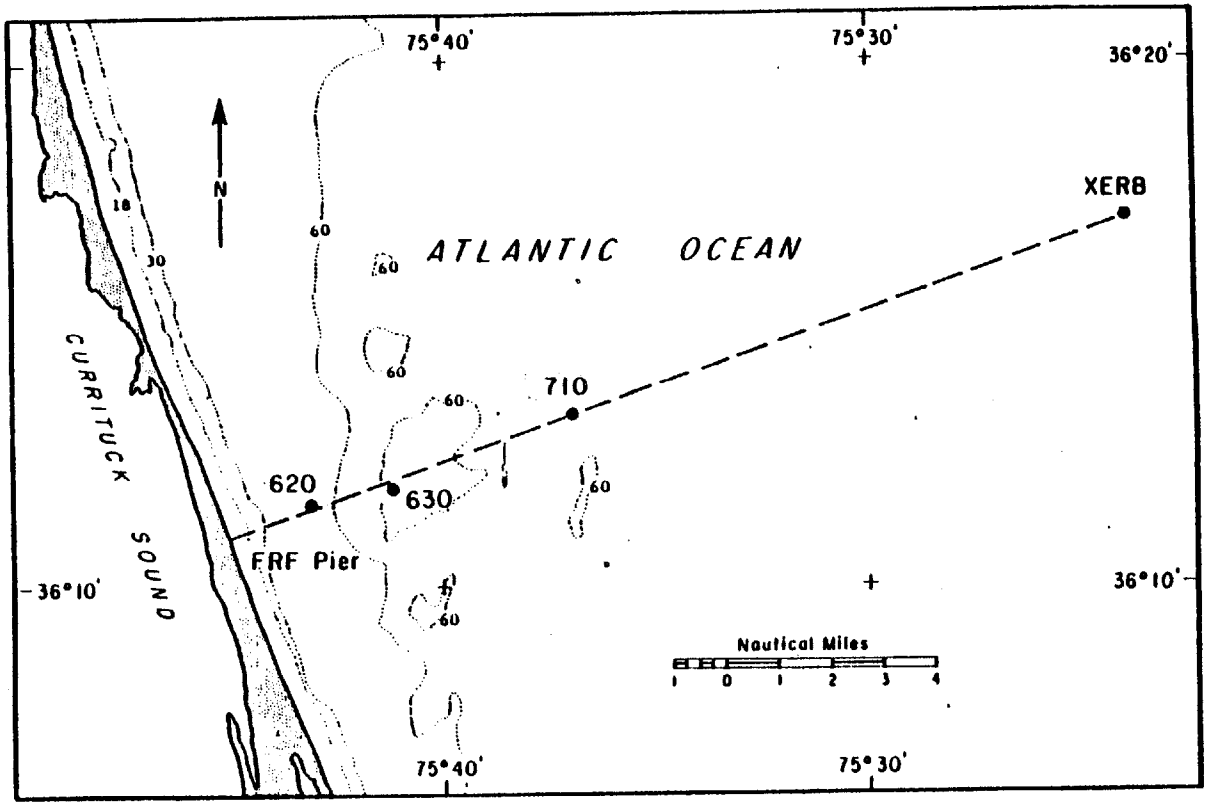


Fig. 5.27 Location map of ARSLOE experimental area off the North Carolina coast. (From Grosskopf et al. 1982).

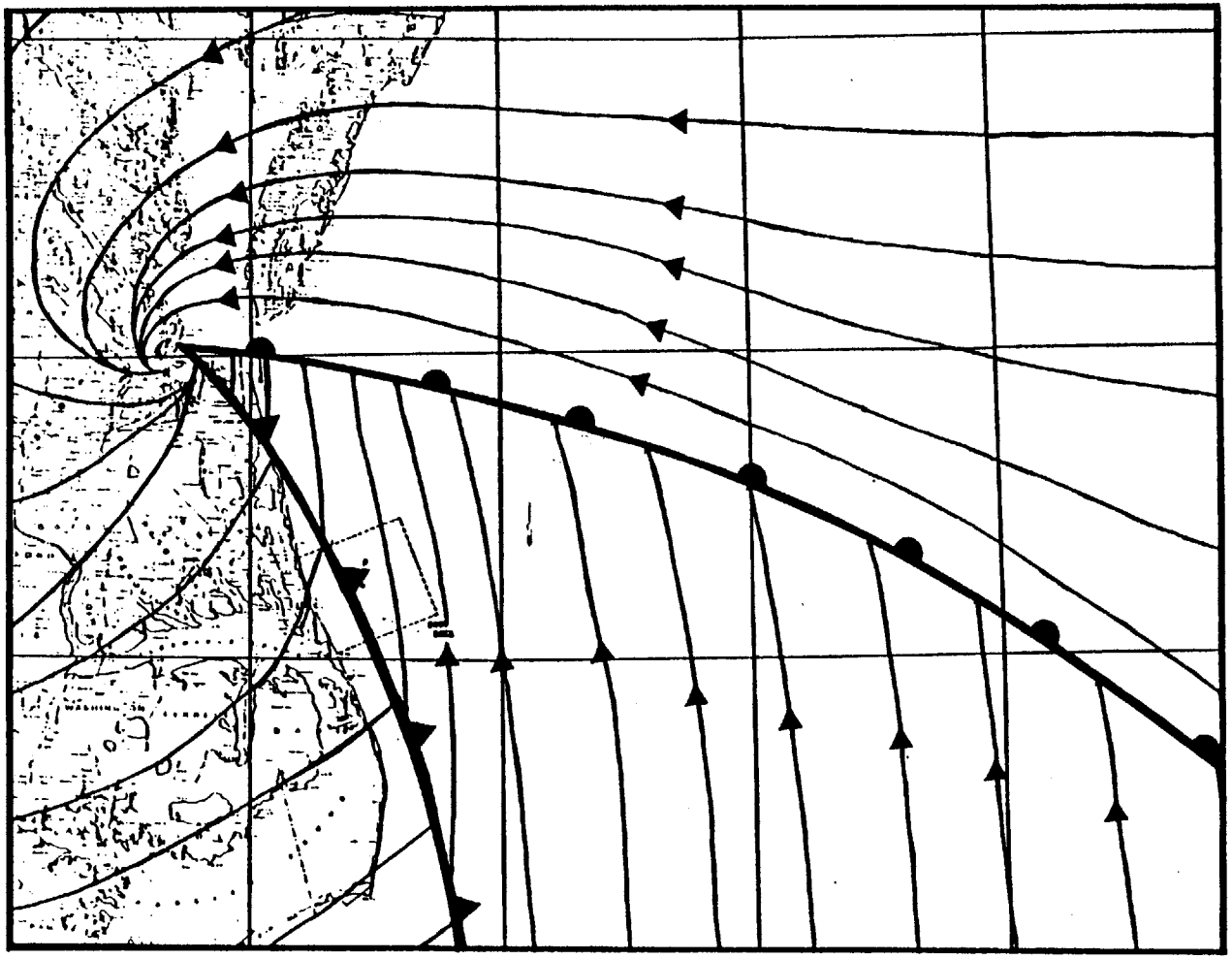


Fig. 5.28 Synoptic weather map of frontal system over the ARSLOE site showing the streamline pattern at 1200 GMT, October 25, 1980. (From Burroughs, 1982).

The model grid for ARSLOE was also established on a polar stereographic projection as defined in (5.1.1) and (5.1.2) but using a constant grid spacing of approximately 80 km. Here, the x-axis was pointing along the longitude λ_o = 15°E.

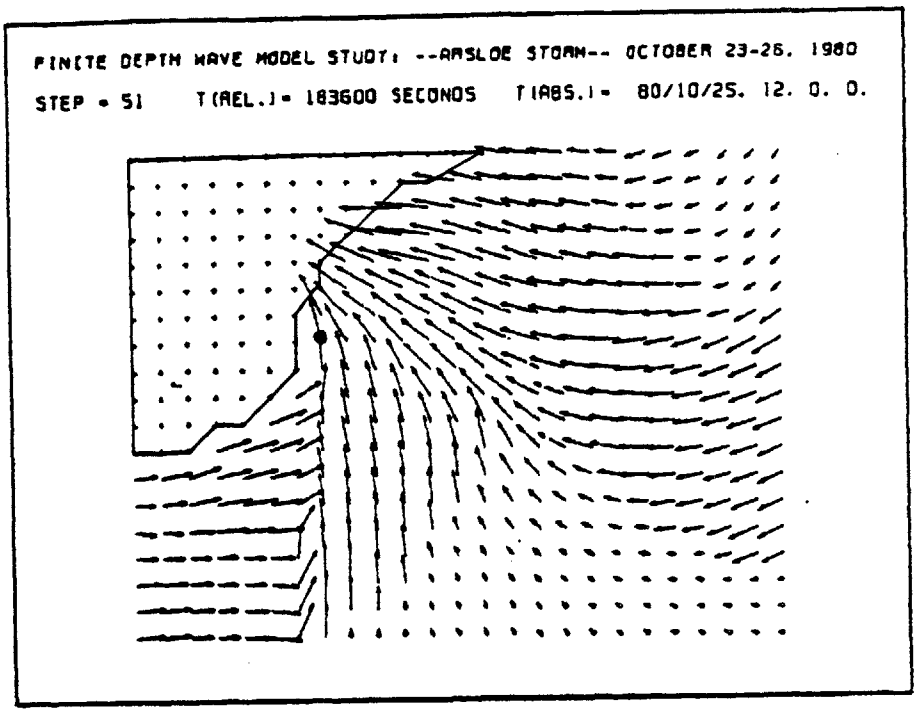
5.2.1 Meteorological Conditions and Wind Fields

On October 24, 1980 a low pressure center developed off the northern Florida coastline and slowly advanced northward. By the following morning, October 25, the frontal system had moved to the vicinity of the ARSLOE site, subjecting the area to strong onshore winds from the east and northeast with wind speeds up to 15 m/s ahead of the warm front. For the next three hours, southernly winds within the warm sector dominated the area until the arrival of the cold front (cf. 5.28). With the passage of the cold front, the winds were blowing offshore up to 20 m/s, generating fetch-limited wave conditions. In Figure 5.29 the model winds during the frontal passage are shown. Thus within three hours the wave conditions in the ARSLOE area changed from northeasterly windseas of unlimited fetch to fetch-limited windseas propagating against the arriving swell of the earlier windsea.

The wind fields were manually constructed from three hourly synoptic surface weather maps. Interpolation in time is automatically performed by the wave model using a mixed-radix FFT (Singleton, 1969).

5.2.2 Model Results

The arbitrary depth version of the HYPA model was applied to this frontal system during the ARSLOE experiment. The continental shelf



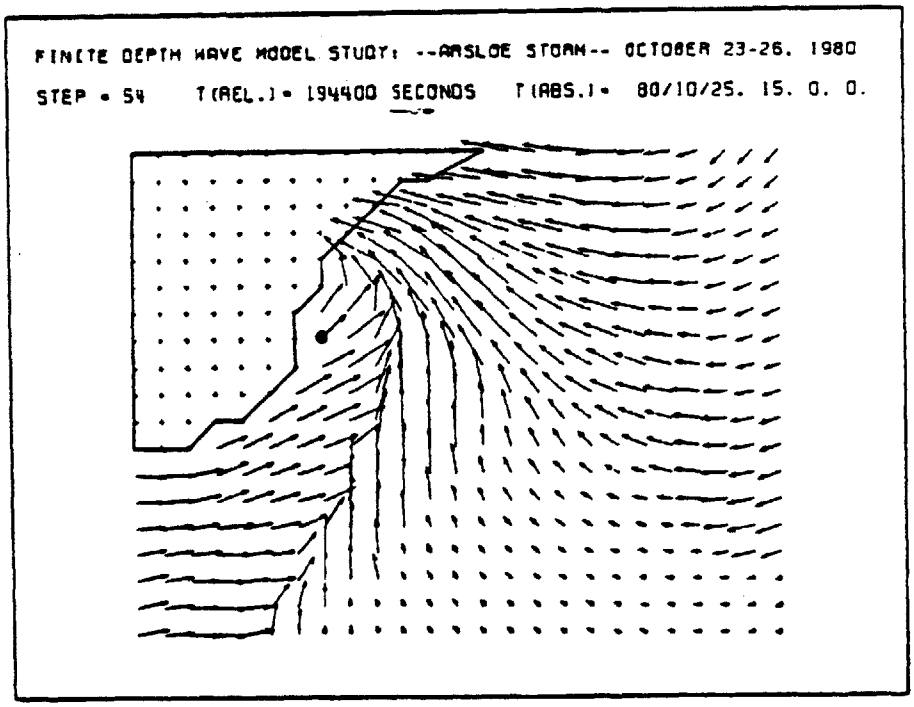
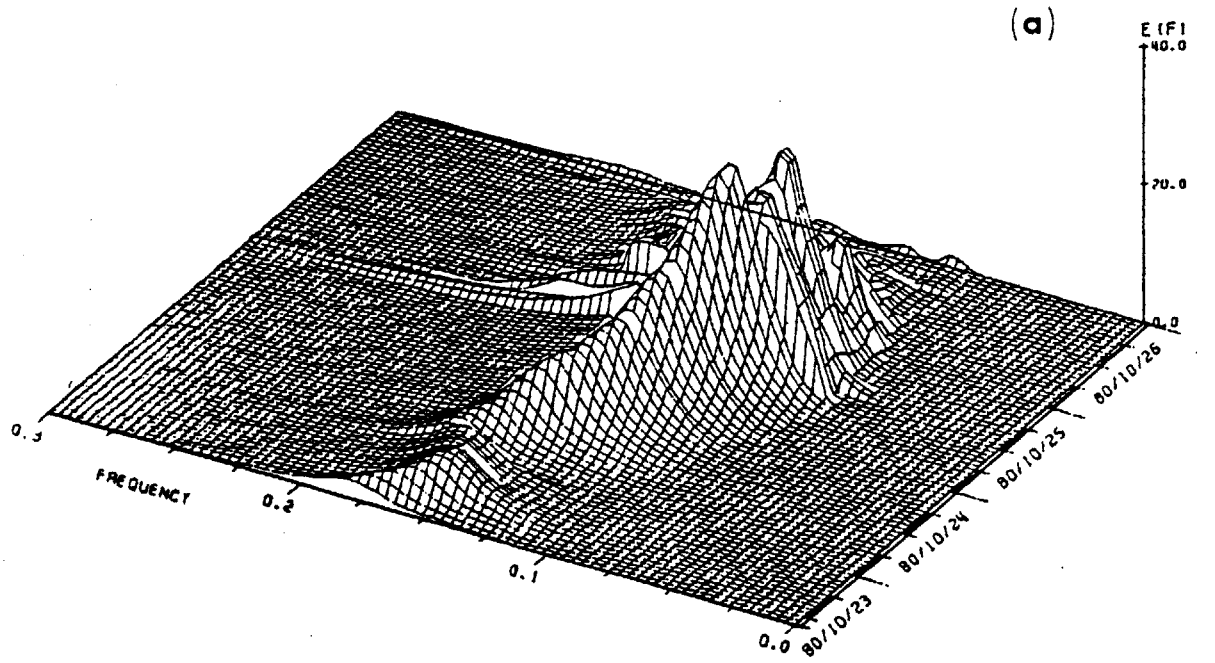


Fig. 5.29 Examples of wind field input to the numerical wave model for the ARSLOE storm at 1200 GMT and 1500 GMT, October 25, 1980. The vectors show speed and direction of the wind. The dot indicates location of XERB buoys.

along the east coast of the United States is generally a few hundred kilometers wide, which means that finite depth effects for this wave hindcast will show up only at a few grid points. The bathymetry along the shelf consisted of approximately parallel contours, with an average 10° bearing to the east from the North-South axis. Figure 5.30a provides an impression of the evolution of wave spectra at the grid point closest to the location of the XERB buoy. It clearly demonstrates the migration of the spectral peak to lower frequencies. The two days prior the frontal passage was governed by slowly changing, onshore blowing winds of increasing speed. The spectral evolution shows quite well the developing windsea until the front passed over the site. The wave conditions after the front had passed was that of a cross-sea with multiple spectral peaks due to a strong swell field refracted towards the shore and a new, opposing windsea developing under fetch-limited conditions. The post-peak development is depicted in the spectral evolution shown in Figure 5.30b. Several swell peaks can be recognized as well as the newly developing windsea located around frquencies ≈ 0.16 Hz and higher.

The model was run for a minimum dissipation case corresponding to a friction factor $f_w = 0.025$. Both windsea and swell were attenuated. The hindcasted time series are shown in Figure 5.31. The uniform, onshore flow governing the ARSLOE site for the two days ahead of the advancing front is reflected in the stick plot for the wind history. This pattern is closely described by the windsea for the same period, and is also evident in the wind-wave directional lag. The duration-limited windsea dominated the wave field at the XERB buoy. During this time, swell was either entirely absent or only present in



FINITE DEPTH WAVE STUDY: --ARSLOE STORM-- OCTOBER 23-26, 1980

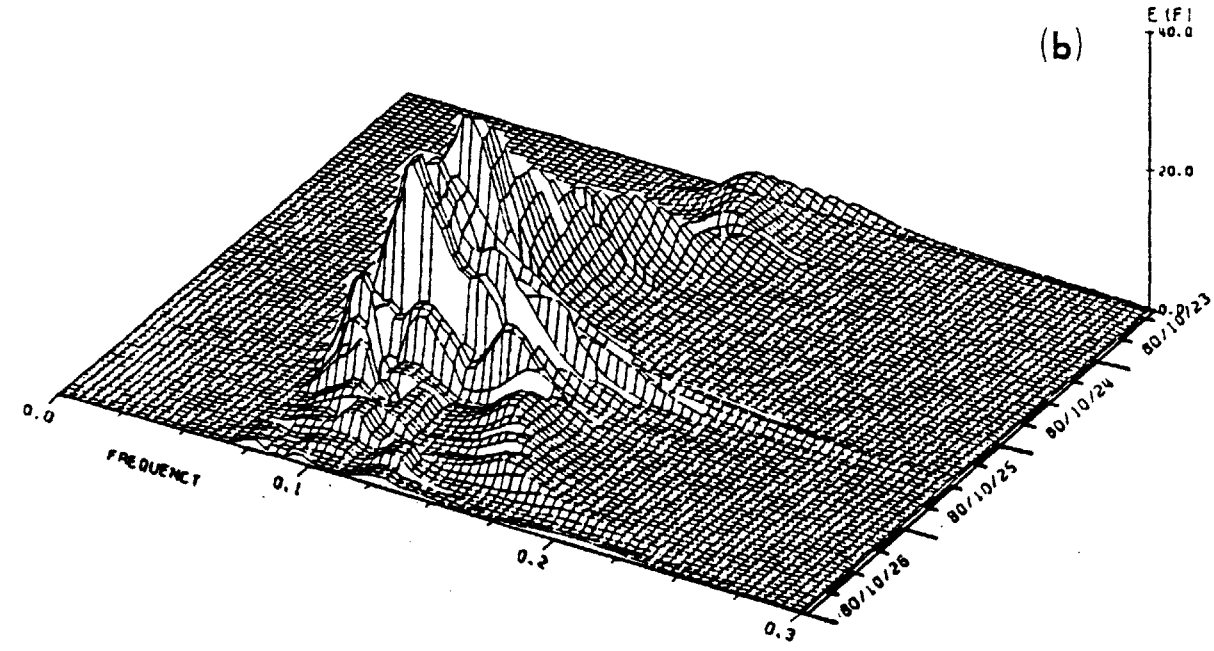


Fig. 5.30 Evolution of hindcasted wave spectral at station XERB for the ARSLOE storm of October 23-26, 1980. (a) pre-storm development; (b) post-storm development.

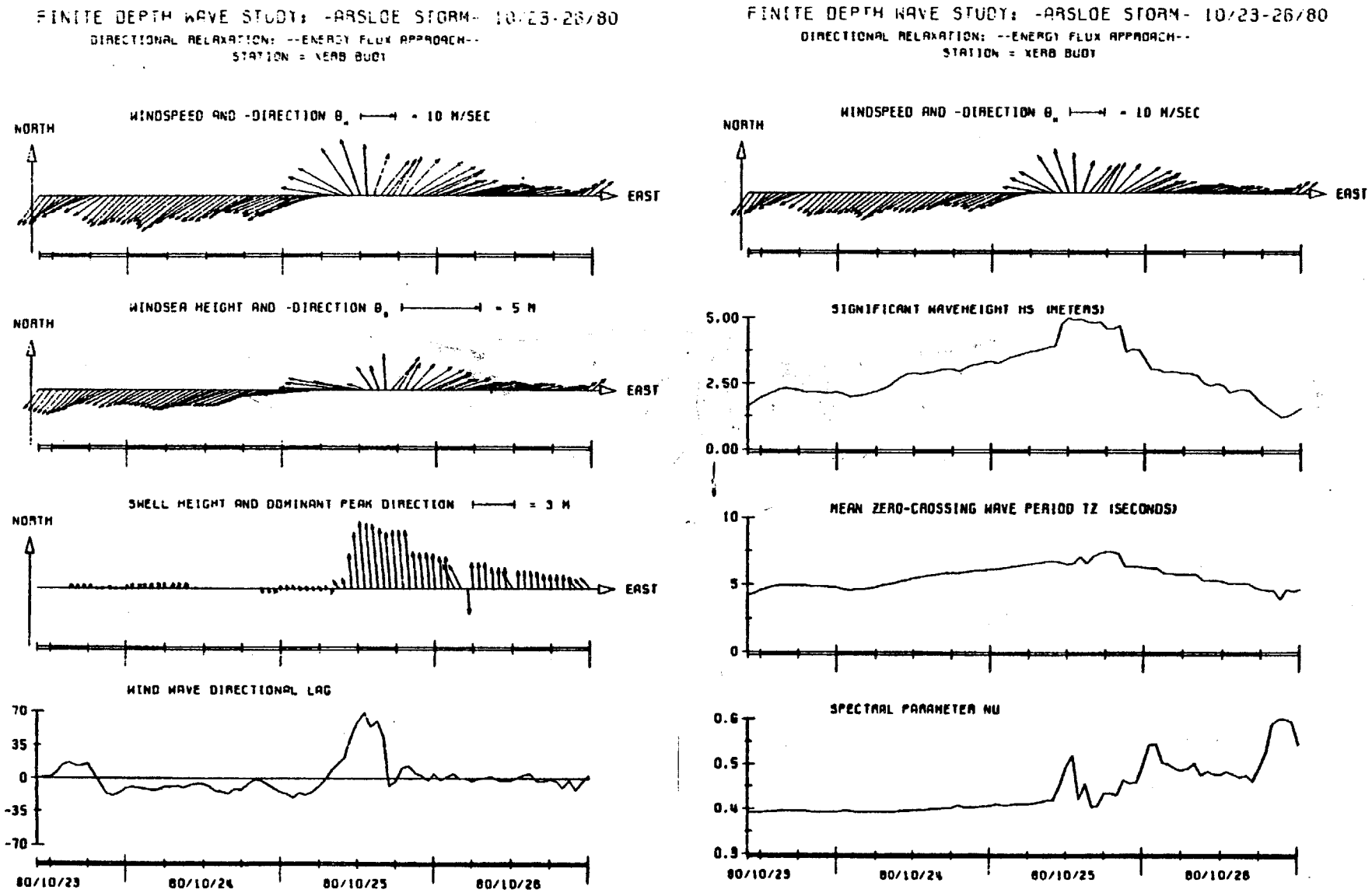


Fig. 5.31 Time series of hindcasted spectra wave parameters at station XERB for the ARSLOE storm.

negligible amounts as is easily seen in the swell plot.

Once the front arrived, the winds rapidly turned from the northeast to southwest, but maintaining roughly the same speed. The response of the mean windsea direction was initially slow, lagging the wind by as much as 70°. The large change in direction forced the windsea to transfer most of its energy to swell as is clearly visible in the sudden increase of swell at the XERB buoy. For the next 12 hours a strong swell field from the south dominated the new windsea which now developed under fetch-limited conditions. By the evening of October 25, the swell waves had substantially diminished in height and by morning of the next day, swell was comparable to the windsea in terms of total energy. The uniform, offshore wind and wave conditions in the post-period of the front is well described by a nearly vanishing wind-wave directional lag.

The right-hand side of Figure 5.31 shows the model results for the wave height and wave period. The predicted maximum wave height is 5 m at 1200 GMT, October 25, which coincides with the measured peak. Predicted wave periods T_z peaked at 7.5 seconds during the time of strong swell from the south.

Since the initial period of wave generation was entirely dominated by a developing windsea, the plot of the spectral parameter ν_s represents the feature nicely. At the start of the modeling period the windsea corresponded to a mean JONSWAP spectrum for which $\nu_s \approx 0.39$. As the spectrum developed ν_s gradually increased, reaching a value $\nu_s \approx 0.425$, corresponding to a Pierson-Moskowitz spectrum, just before the storm hit. The large values afterwards indicate the presence of multi-peaked spectra as is the case for wave fields

consisting of swell and windsea.

Figure 5.32 shows the hindcasted wave parameters for significant wave height, frequency of spectral peak and mean wave direction corresponding to the frequency of the spectral peak superposed on the ARSLOE data set. The overall agreement for all wave parameters can be considered extremely good. The wave height is presented in Figure 5.32a. The solid line is the model results. As previously mentioned, the wave field was purely windsea up to the arrival of the front (1200 GMT, October 25). The hindcasted wave heights just hug the upper side of the data, and follows quite accurately the trend leading up to the maximum wave height. On the backside of the storm, the predicted H_s values are generally too high. During this time swell was prominent everywhere and the windsea was of secondary importance. The level of windsea energy is approximately given by the square symbols, representing measurements from wave riders which were located closer to shore. Although refraction is included in the windsea description of the wave model, this is not the case in the swell model. Regardless of depth, swell is propagated along straight characteristics. The neglect of swell refraction can lead not only to an overestimate in total wave height, but also represent a false distribution of energy in terms of wave spectra. A closer look at the surrounding grid points revealed that swell was approximately the same everywhere in magnitude and direction. Therefore, a simple analysis by refracting each swell component separately was thought to be adequate to remedy this problem. The total wave height with swell corrected for refraction effects is shown by the dashed line. Several things can be observed. One, the maximum wave height is reduced by ≈ 50 cm. The overall

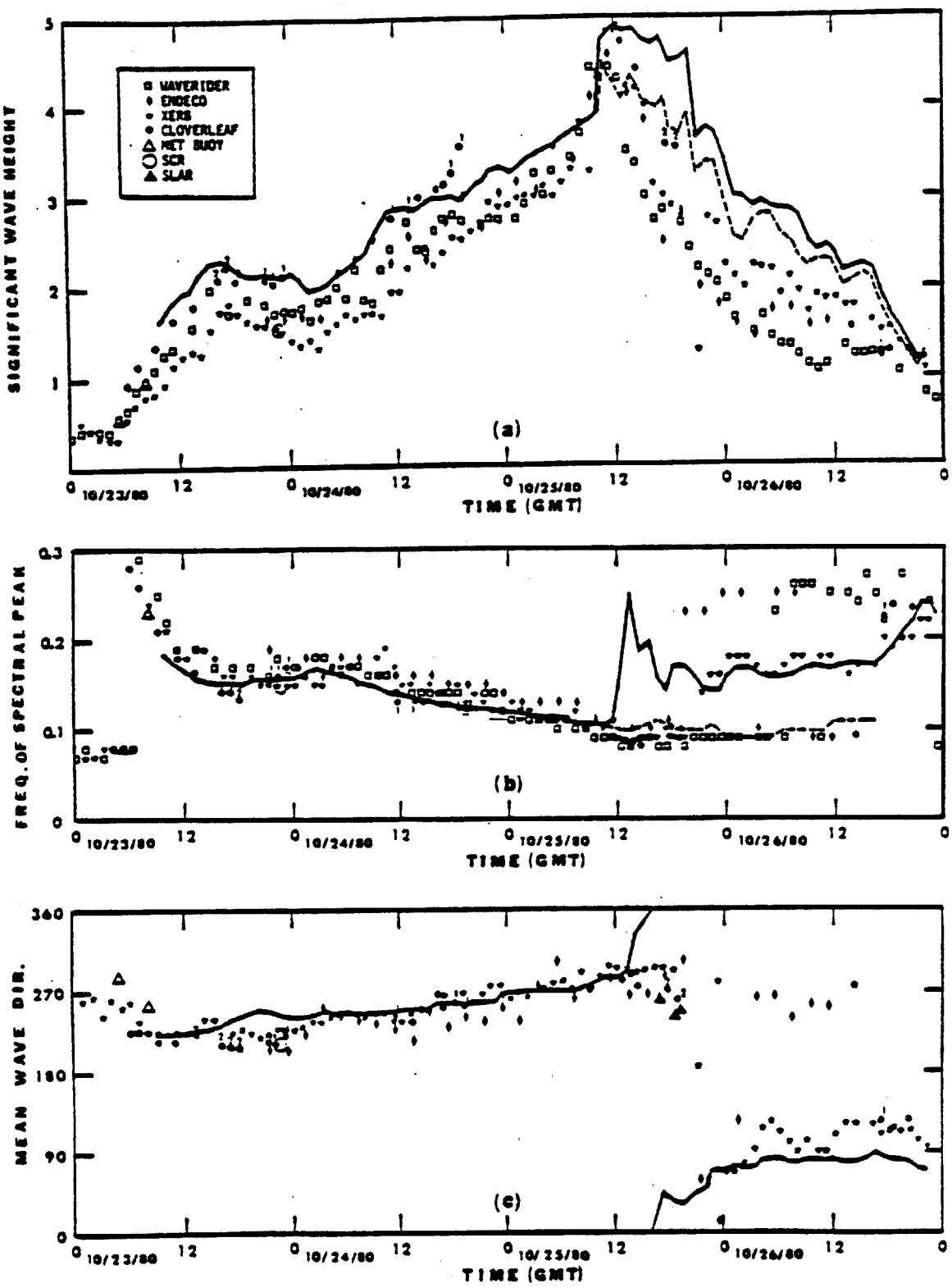


Fig. 5.32 Comparison of measured and hindcasted significant wave height, spectral peak frequency and mean wave direction at station XERB. (From Szabados, 1982).

agreement is improved, which indicates that swell refraction is significant to predict wave heights in coastal waters. The remaining discrepancies between predicted and observed H_s values can be primarily attributed to the resolution of the swell field. This can be seen in the predicted results on October 26, where most swell energy was contained in higher frequencies for which refraction effects are of diminishing significance.

A comparison of hindcasted and observed spectral peak frequencies is depicted in Figure 5.32b. Here the solid line corresponds to the windsea peak frequency parameter fm. Again, for the period before the storm, this fm parameter describes quite accurately the spectral peak. As soon as the windsea energy is transfered to swell, indicating the presence of multi-peaked spectra, the fm parameter can no longer be used without inspection of the actual wave spectra. This explains the spike in fm right at the time when the front made its passage. For this time we also plotted the frequency of the swell peak (dashed line). This frequency seems to be appropriate, since all the measuring stations recorded a spectral peak frequency ≈ 0.1 Hz. By the evening of October 25, three distinct sets of observed peak frequencies are shown. The top set at ≈ 0.25 Hz corresponds to waveriders very close to shore which measured the peak frequency of the newly developing windsea (fetch-limited conditions). The lower set also corresponds to waveriders which were located at a distance halfway between the XERB buoy and the shoreline (cf. Figure 5.27). At this site the swell peak (≈ 0.1 Hz) was still larger relative to the offshore propagating windsea peak. The data points (stars) in the center correspond to the XERB buoy. Here the fetch was long enough so that the windsea could

sufficiently develop and dominate the wave field again. Hence, the parameter fm appears to be the appropriate one to characterize the frequency of the spectral peak there.

At this point we should mention that the deep water model version was also applied to this complex frontal system using the same wind field and model grid. Both the deep water and finite depth model predicted identical results in H_s up to the evening of October 24. Then, the deep water results significantly deviated from data and the finite depth predictions by shooting up in a linear manner to a peak wave height of ≈ 5.5 m at 1100 GMT, October 25. This demonstrates the importance of including finite depth effects, because by noon of October 24, the peak frequency fm has migrated towards frequencies low enough where the deep water assumption is no longer valid in a water depth of 35 m. For example, the presence of the bottom in waters 35 m deep is felt by all spectral components corresponding to frequencies 0.15 Hz or lower.

Finally, we focus our attention on the mean wave direction which is shown in Figure 5.32c. Here the solid line represents the hindcasted values of the directional parameter θ_o. This parameter characterizes the mean direciton of the windsea only. As could be anticipated, the agreement of θ_o between data and prediction are excellent for the pre-storm period where the windsea dominated the wave field. Once the frontal system arrived and had passed, the parameter θ_o eventually responds to the changing wind vector. Thus for the time from noon to midnight of October 25, the mean windsea direction, θ_o, cannot be used to describe the mean wave direction. The data shows no consistent trend in the wave direction after the frontal

passage. Although θ_o has approximately the same trend in the mean wave direction during post-storm period, the data exhibits considerably more variability. Nevertheless, these results are encouraging and give some indication that the approach used to derive the directional relaxation parameter θ_o is correct.

Finally, we show some examples of wave spectra. Figure 5.33 depicts a comparison between a hindcasted and observed wave spectrum for 1800 GMT, October 24. It should be noted that not only the location of the spectral peak but also the energy density at the peak of the predicted energy spectrum almost coincides with the measured spectrum. From this, one can conclude that the JONSWAP shape can also describe quite adequately windsea spectra in finite depth. The arrows show the direction of propagation for the wave components. Since this is a windsea spectrum, all spectral components propagate in the same direction as predicted by the directional parameter θ_o. Figure 5.34 shows the wave spectrum one hour after the front had arrived. Here the arrows depict visibly the prominent swell field from the south with a windsea propagating approximately northwest. In this spectral plot the swell directions have not been corrected for refraction. The agreement of the observed and predicted spectral shape is remarkably good, in particular the energy density at the peak. The discrepancy in the location of the peak can be attributed to the resolution of the swell bins. The model uses a bin size of 0.1 Hz.

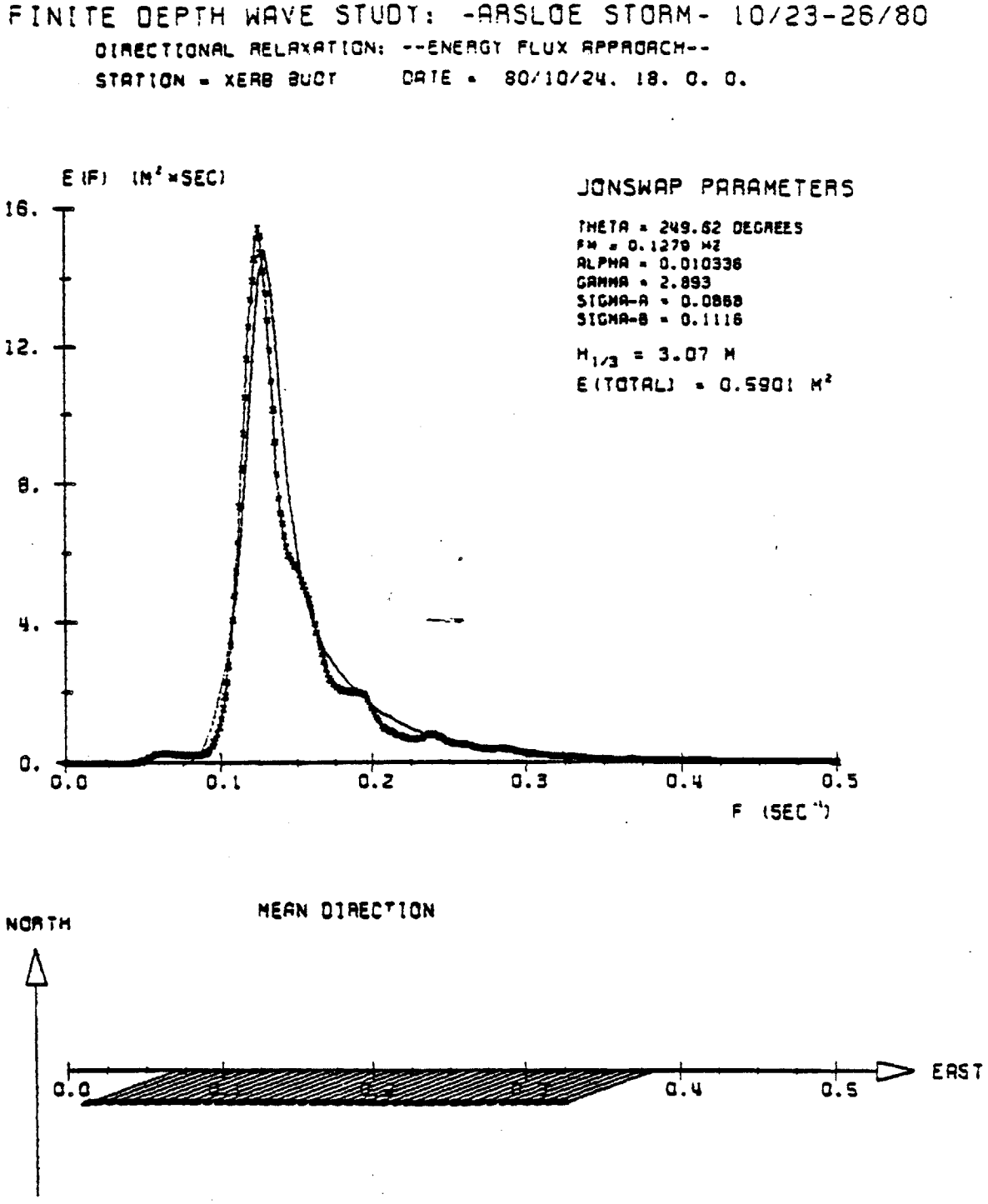


Fig. 5.33 Comparison of measured and hindcasted wave spectrum at station XERB for the ARSLOE storm at 1800 GMT, October 24, 1980.

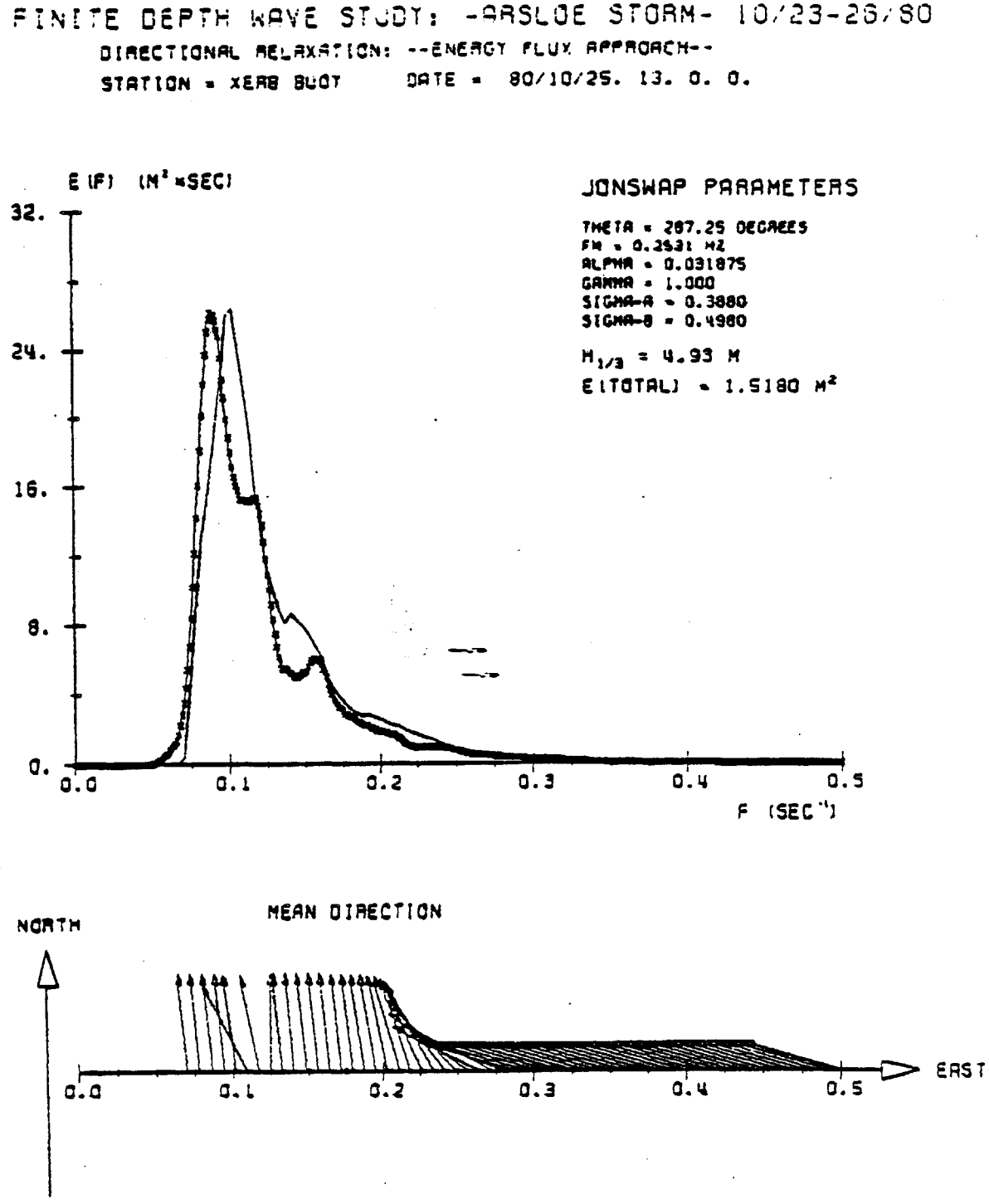


Fig. 5.34 Comparison of measured and hindcasted wave spectrum at station XERB for the ARSLOE storm at 1300 GMT, October 25, 1980.

CHAPTER 6

CONCLUSIONS AND RECOMMENDATIONS

Wer Wunder hofft.
Der starke seinen Glauben.

Who hopes for miracles.
Should strengthen his faith.

(Astrologe)

--FAUST II, Saal des Thrones
Johann Wolfgang von Goethe

A hybrid parametric wind-wave model has been developed for general use in waters of arbitrary depth. This model differs from other parametric models in two specifc areas. One, the directional parameter controlling the relaxation of the mean windsea direction has been rederived based on more general energy flux arguments. Two, the wave model is capable of predicting wave spectra and other spectral parameters not only in deep water, but also in finite water depths.

The wave model was applied to two test situations. One case study is a hindcast of deep water wave conditions in the Gulf of Alaska due to an intense extratropical cyclone. Predicted wave parameters were compared with measurements from six locations in the Gulf of Alaska. Generally, the overall agreement of model results with observations at these sites can be considered good. This study also helped to identify some weaknesses of the parametric approach. These shortcomings will be addressed in the following paragraphs of this chapter and suggestions are made to remedy some of the problems.

The second test case dealt with a frontal passage over coastal waters on the continental shelf off the North Carolina coast where depths ranged from infinitely deep water to shallow water of the order 20 m deep. The significance of hindcasting this storm was twofold. Firstly, the model's capability was tested in predicting transformed

windsea spectra in shoaling waters. Secondly, since the passage of this front was associated with a 180° shift in the wind direction, this provided an ideal situation to examine the response of the directional relaxation parameter to such extreme changes. In summary, the model predictions of significant wave height, spectral peak frequency and mean wave direction compared exceptionally well with measurements at the hindcasted location. Some minor shortcomings in the modeling of swell have been identified and will be discussed in the paragraphs below.

From the Gulf of Alaska wave study the major conclusion was that model wave growth was too sluggish in rapidly turning wind fields with moderately high to very high wind speeds. A possible explanation of this shortcoming is given here as follows. Energy input from the wind is introduced in the model as a source function in the α parameter equation, where α characterizes the energy level in the high-frequency equilibrium range. The functional form of this source function is based on the empirical α-ν relation originally presented by Hasselmann et al. (1976), in which α has a standard deviation of 38%. Since the wave height H_s is proportional to $\sqrt{\alpha}$, this implies an error in H_s of at least 19% due to the uncertainty in this relation. Additional errors are introduced in determining the model wind fields, which may be of the order of 15% or more depending on the method used to calculate surface winds (Cardone et al., 1979). The uncertainty in the wind speed also enters the α-ν relation through the ν parameter. It stands to reason that to some extent the error in the wind speed could have a cancelling effect on the uncertainty in α, but in the worst case, could also amplify the total error. Nevertheless, the error

associated with the α-ν relation is inherent to the model regardless of wind speed accurac. This means that a prediction of a 10 m significant wave height could be off by approximately 2 m. In order to minimize this source of error, a new α-ν relation is warranted. A subsequent analysis of this relation should focus especially on extreme wind situations such as extratropical cyclones and hurricanes.

The effective wave growth is further reduced due to the incorporation of directional relaxation, since only the wind component parallel to the mean wave direction causes waves to grow in the model. The wind component normal to the mean wave direction prescribes the rate at which the waves are turned into the direction of the wind. Hence, the effect of directional relaxation shows up as a reduction in the wave height and a slower migration of the spectral peak to lower frequencies. This is particularly noticed in the different results one obtains for the Gulf of Alaska study when using a model with directional relaxation and another model version without the directional parameter. However, it is unfortunate that the Gulf of Alaska data did not provide any information on wave directions. Such data could have aided in clarifying the specific cause for the generally low model wave heights for this study.

The inclusion of directional relaxation and the α-ν relation did not adversely affect the predictions in the ARSLOE wave study. On the contrary, as already mentioned, the final answers compared favorably with measurements. One possible reason for this success is due to the fact that before the arrival of the storm, which consisted of three sharp fronts, the wind field was relatively uniform over the entire model area providing duration-limited onshore winds. In addition, wind

speeds were not much in excess of 15 m/s, which was approximately the upper limit in determining the empirical α-ν relation from the JONSWAP results.

The transition region between windsea and swell still presents a difficulty for hybrid parametric wave model. The simple exchange criteria controlling the transfer of energy between the two wave domains requires more research and empirical evidence. The inclusion of directional relaxation provides a physical means by which hybrid parametric models can simulate more effectively radiation of windsea energy into swell for a continuously revolving wind field. The treatment of swell in the hybrid parametric model takes up most of the time. The ARSLOE results have clearly demonstrated that neglecting refraction effects in the swell can lead to overprediction of the total wave energy and to incorrect results in the wave direcions. A simple post-analysis of swell refraction as performed for the ARSLOE case, cannot always be applied to more general situations. Therefore, a new algorithm should be developed for the swell part of the hybrid wave model which includes refraction but is efficient enough so that the overall model computational efficiency is not reduced.

Similarly, the swell field was not adequately reproduced by either model version for the Gulf of Alaska, but for different reasons. To isolate the exact cause for this discrepancy is very difficult, since several processes take effect at the same time in rapidly turning winds. Nevertheless, some explanations can be inferred and additional investigations may lead to more conclusive answers. As already discussed, a primary source of error is associated with the α-ν relation. The reasoning is as follows. The ν parameter controls when

a transfer of windsea energy to swell takes place. A smaller α value indicates less energy input into the high-frequency portion of the spectrum. At the same time this means a reduced rate of energy transfer to lower frequencies by nonlinear wave-wave interactions. This in turn implies a slower migration of the windsea peak to lower frequencies, which indicates the state of wave development. If a fully-developed state is never reached, i.e., $\nu = 0.13$, no energy is transfered to swell. A revised α-ν relation derived from extreme wind conditions may provide some answers. In addition, the fact that we approximate the earth as a plane within our model area, is certainly not realistic for the Gulf of Alaska study. The neglect of the earth's curvature may significantly affect swell propagation. This could lead to a delay in moving swell or conversely, swell could propagate too fast. In both cases the timing when swell should actually arrive at a certain location would considerably deviate from the correct one. Thus, a future modification of the model should incorporate the flexibility to handle uneven grid spacings and nesting to allow for a finer resolution in areas of interest.

An important aspect in finite depth wave modeling pertains to the question of the existence of equilibrium spectra, i.e., the condition when the net source function vanishes. This calls for more research elucidating the interplay of the various source functions in shallow seas. The lack of empirical evidence regarding shallow water wave generation makes this task more cumbersome to solve. For example, most data on bottom friction is for monochromatic waves. The bottom friction mechanism for a monochromatic wave cannot simply be translated into the spectral space since it is unknown a priori which wave mode,

e.g., the peak frequency, can be considered representative for the total frictional effect on the wave spectrum.

The final conclusion of this dissertation can be stated as follows. The arbitrary depth wave model using a hybrid-parametric approach demonstrated its capability to predict wave conditions not only in deep, but also in fairly shallow water. It should also be realized that the resulting wave predictions are only at best of synoptic quality, since the winds entered into the wave model are derived from synoptic weather maps. This leaves still the urgent need for more accurate and objective methods to calcuate model wind fields from meteorological data.

REFERENCES

Nicht Kunst und Wissenschaft allein,
Geduld will bei dem Werke sein.

Science is not enough, nor art;
In this work patience plays a part.

(Mephistopheles)

--FAUST I, Hexenkuche
Johann Wolfgang von Goethe

Abernethy, C.L. and G. Gilbert, 1975: Refraction of wave spectra. Hydraulics Research Station, Report INT 117.

Allender, J.H, J. Albrecht and G. Hamilton, 1983: Observations of directional relaxation of wind sea spectra. J. Phys. Oceanogr., Vol. 13, 1519-1525.

Backus, G.E., 1962: The effect of the earth's rotation on the propagation of ocean waves over long distances. Deep-Sea Res., Vol. 9, 185-197.

Banner, M.L. and O.M. Phillips, 1974: On the incipient breaking of small scale waves. J. Fluid Mech., Vol. 65, 647-656.

Barnett, T.P., 1966: On the generation, dissipation, and prediction of ocean wind waves. Ph.D. Dissertation, University of California, San Diego, California.

Barnett, T.P., 1968: On the generation, dissipation, and prediction of ocean wind waves. J. Geophys. Res., Vol. 73, No. 2, 513-529.

Barnett, T.P. and J.C. Wilkerson, 1967: On the generation of ocean wind waves as inferred from airborne radar measurements of fetch-limited spectra. J. Marine Res., Vol. 25, 292-328.

Barnett, T.P. and A.J. Sutherland, 1968: A note on an overshoot effect in wind-generated waves. J. Geophys. Res., Vol. 73, 6879-6885.

Barnett, T.P., H. Holland, Jr. and P. Yager, 1969: A general technique for wind wave prediction, with application to the South China Sea. Final Report, U.S. Naval Oceanogr. Office, Washington, D.C.

Barnett, T.P. and K.E. Kenyon, 1975: Recent advances in the study of wind waves. Rep. Prog. Phys., Vol. 38, 667-729.

Bea, R.G., 1974: Gulf of Mexico hurricane wave heights. Offshore Technology Conference, OTC 2110, 791-810.

Benilov, A.Yu., M.M. Zaslavskii, and S.A. Kitaigorodskii, 1978a: Construction of small-parameter models of wind wave generation. Oceanology, Vol. 18, 387-390.

Benilov, A.Yu., A.I. Gumbatov, M.M. Zaslavskii and S.A. Kitaigorodskii, 1978b: A nonstationary model of development of the turbulent boundary layer over the sea with generation of surface waves. Izv. Akad. Nauk. SSSR, Atmos. Ocean. Phys., Vol. 14, 830-836.

Biot, M.A., 1962: Mechanics of deformation and acoustic propagation in porous media. J. Appl. Physics, Vol. 33, 1482-1498.

Bole, J.B. and E.Y. Hsu, 1969: Response of gravity water waves to wind exitation. J. Fluid Mech., Vol. 35, 657-675.

Bouws, E., 1980: Spectra of extreme wave conditions in the Southern North Sea considering the influence of water depth. Proc. Int. Conf. Sea Climatology, Paris, October 1979, Collection Collogues et Seminaires, No. 34, Technip. Paris, 51-71.

Bouws, E. and G.J. Komen, 1983: On the balance between growth and dissipation in an extreme depth-limited wind-sea in the Southern North Sea. J. Phys. Oceanogr., Vol. 13, 1653-1658.

Bouws, E., H. Günther, W. Rosenthal and C.L. Vincent: 1984. Similarity of the wind wave spectrum in finite depth water. Submitted for publication.

Bretheron, F.P. and C.J.R. Garrett, 1969. Wave trains in inhomogeneous moving media. Proc. Roy. Soc. Lond., Ser. A, Vol. 302, 529-554.

Bretschneider, C.L., 1952: Revised wave forecasting relationships. Proc. Second Conf. Coastal Engineering, 1-5.

Bretschneider, C.L., 1958: Revision in wave forecasting, deep and shallow water. Proc. Sixth Conf. Coastal Engineering, 30-67.

Bretschneider, C.L., 1973: see Coastal Engineering Research Center (CERC), 1975.

Bretschneider, C.L. and E.E. Tamaye, 1976: Hurricane wind and wave forcasting techniques. Proc. Fifteenth Conf. Coastal Engineering, 202-237.

Bunting, D.C., 1970: Evaluating forecasts of ocean-wave spectra. J. Geophys. Res., Vol. 75, 4131-4143.

Burroughs, L.D., 1982: Analyses of elements of the marine environment for the Atlantic Remote Sensing Land Ocean Experiment (ARSLOE). An atlas for October 22-27, 1980. NOAA Tech. Rep. NWS 29.

Bye, J.A.T., 1967: The wave-drift current. J. Marine Res., Vol. 25, 95-102.

Cardone, V.J., W.J. Pierson and E.G. Ward, 1976: Hindcasting the directional spectra of hurricane generated waves. J. Petroleum Techn., Vol. 28, 385-394.

Cardone, V.J., A.J. Broccoli, C.V. Greenwood and J.A. Greenwood, 1979: Error characteristics of extratropical storm windfields specified from historical data. Offshore Technology Conf., OTC 3598, 2103-2111.

Cardone, V.J., H. Carlson, J.A. Ewing, K. Hasselmann, S. Lazanoff, W. McLeish and D. Ross, 1981: The surface wave environment in the GATE B/C Scale - Phase III. J. Phys. Oceanogr., Vol. 11, 1280-1293.

Carter, D.J.T., 1982: Prediction of wave height and period for a constant wind velocity using the JONSWAP results. Ocean Engng., Vol. 9, No. 1, 17-33.

Cartwright, D.E. and M.S. Longuet-Higgins, 1956: The statistical distribution of the maxima of a random function. Proc. Roy. Soc. Lond., Ser. A, Vol. 237, 212-232.

Cavaleri, L. and P. Malanotte-Rizzoli, 1977: A wind-wave prediction model in the Adriatic Sea. NATO Conf. Series: V, Air-Sea Interactions, Vol. 1, 629-646, Plenum Press.

Chao, Y.Y., 1971: An asymptotic evaluation of the wave field near a smooth caustic. J. Geophys. Res., Vol. 76, 7401-7408.

Chao, Y.Y. and W.J. Pierson, 1972: Experimental studies of the refraction of uniform wave trains and transient wave groups near a straight caustic. J. Geophys. Res., Vol. 77, 4545-4554.

Chase, J., L.J. Côte, W. Marks, E. Mehr, W.J. Pierson, Jr., F.G. Rönne, G. Stephenson, R.C. Vetter and R.G. Walden, 1957: The directional spectrum of a wind generated sea as determined from data obtained by the Stereo Wave Observation Project. N.Y.U., Coll. of Eng., Dept. of Meteorolog. & Oceanogr., Tech. Rep. for ONR, Nonr 285(03).

Coastal Engineering Research Center (CERC), 1975: Shore Protection Manual, Vol. 1, U.S. Army Coastal Eng. Res. Center, Corps. of Engineers.

Collatz, L., 1964: FUNKTIONANALYSIS UND NUMERISCHE MATHEMATIK, Springer-Verlag, Berlin-Heidelberg, New York, pp. 371.

Collins, J.I., 1972: Prediction of shallow-water spectra. J. Geophys. Res., Vol. 77, 2693-2707.

Courant, R. and D. Hilbert, 1968: METHODEN DER MATHEMATISCHEN PHYSIK, Vol. II. Heidelberger Taschenbücher Band 31, Springer-Verlag, Berlin, 549 pp.

Darbyshire, J. 1952: The generation of waves by wind. Proc. Roy. Soc. Lond., Ser. A, Vol. 215, 299-328.

DeLeonibus, P.S., L.S. Simpson and M.G. Mattie, 1974: Equilibrium range in wave spectra observed at an open-ocean tower. J. Geophys. Res., Vol. 79, 3041-3053.

Dingemans, M.W., 1978: Refraction and diffraction of irregular waves: a literature survey. Delft Hydraulics Laboratory, Report W301-I.

Dobson, F.W., 1969: Observations of normal pressure on wind-generated sea waves. Part I. Ph.D. Thesis, Inst. of Oceanography, University of British Columbia, Vancouver.

Dobson, F.W., 1971: Measurements of atmospheric pressure on wind-generated sea waves. J. Fluid Mech., Vol. 48, 91-127.

Dobson, F.W. and J.A. Elliot, 1978: Wave-pressure correlation measurements over growing sea waves with a wave follower and fixed-height pressure sensors. NATO Conf. Series: V, Air-Sea Interactions, Vol. 1, 421-432, Plenum Press.

Donelan, M.A., J. Hamilton and W.H. Hui, 1982: Directional spectra of wind-generated waves. Unpublished manuscript.

Donelan, M.A., M.S. Longuet-Higgins and J.S. Turner, 1972: Periodicity in whitecaps. Nature, Vol. 239, 449-451.

Dorrestein, R., 1960: Simplified method of determining refraction coefficients for sea waves. J. Geophys. Res., Vol. 65, 637-642.

Dreyer, A.A., 1973: Study of wind-generated seawaves in shallow seas. Thesis, USSR Academy of Sciences, Shirshov Institute of Oceanology.

Dungey, J.C. and W.H. Hui, 1979: Nonlinear energy transfer in a narrow gravity-wave spectrum. Proc. Roy. Soc. Lond., Ser. A, Vol. 348, 467-483.

Earle, M.D., 1978: Practical determinations of design wave condtions. In: OCEAN WAVE CLIMATE, Eds.: M.D. Earle and A. Malahoff, Plenum Press, 39-60.

Eckart, C., 1953: The generation of wind waves over a water surface. J. Appl. Phys., Vol. 24, 1485-1494.

Elliot, J.A., 1972: Microscale pressure fluctuations near waves being generated by wind. J. Fluid Mech., Vol. 54, 427-448.

Ellison, T.H., 1956: Atmopsheric Turbulence. In: SURVEYS IN MECHANICS (Ed. G.K. Batchelor and R.M. Davis), Cambridge University Press.

Ewing, J.A., 1971: A numerical wave prediction method for the North Atlantic Ocean. Deutsche Hydrographische Zeitschrift, Vol. 24, 241-261.

Ewing, J.A., T.J. Weare and B.A. Worthington, 1979: A hindcast study of extreme wave conditions in the North Sea. J. Geophys. Res., Vol. 84, 5739-5747.

Forristall, G.Z., E.G. Ward, V.J. Cardone, and L.E. Borgmann, 1978: The directional spectra and kinematics of surface gravity waves in tropical storm DELIA. J. Phys. Oceanogr., Vol. 8, 888-908.

Forristall, G.Z., 1981: Measurements of a saturated range of ocean wave spectra. J. Geophys. Res., Vol. 86, 8075-8084.

Fox, M.J.H., 1976: On the non-linear transfer of energy in the peak of a gravity-wave spectrum - II. Proc. Roy. Soc. Lond., Ser. A 348, 467-483.

Gadzhiyev, Y.Z. and B.P. Krasitskiy, 1978: The equilibrium range of the frequency spectra of wind-generated waves in a sea of finite depth. Izv. Akad. Nauk. SSSR, Atmos. Ocean. Phys., Vol. 14, 238-241.

Garratt, J., 1977: Review of drag coefficients over oceans and continents. Mon. Weather Rev., Vol. 105, 915-929.

Gelci, R., H. Cazale and J. Vassal, 1956: Utilization des diagrammes de propagation a la prévision énergétique de la houle. Bull. Inform. Comité Central Océanogr. d'Études Côtes, Vol. 8, No. 4, 169-197.

Gelci, R., H. Cazale and J. Vassal, 1957: Prévision de la houle. La methode des densites spectroangulaires. Bull. Inform. Comité Central Océanogr. d'Étude Côtes, No. 9, 416 pp.

Goda, Y., 1970: Numerical experiments on wave statistics with spectral simulation. Rep. of Port and Harbor Res. Inst., Vol. 9, No. 3, Japan.

Goda, Y., 1975: Irregular wave deformation in the surf zone. Coastal Engineering in Japan, Vol. 18, 13-26.

Golding, B.W., 1978: A depth dependent wave model for operational forecasting. NATO Conf. Series: V, Air-Sea Interactions, Vol. 1, 593-606, Plenum Press.

Graber, H.C., 1979: A hybrid wind-wave model, S.M. Thesis, R.M. Parsons Laboratory, Massachusetts Institute of Technology.

Graber, H.C., H. Günther, O.S. Madsen, K. Richter and R. Spanhoff, 1981: Propagation of swell energy in the North Sea. Poster presentation at IUCRM Sym. on Wave Dynamics, Miami, Florida.

Grant, W., 1977: Bottom friction under waves in the presence of a weak current: its relationship to sediment transport. Sc.D. Thesis, Massachusetts Institute of Technology, 275 pp.

Grant, W. and O.S. Madsen, 1979: Combined wave and current interaction with a rough bottom. J. Geophys. Res., Vol. 84, 1797-1808.

Grant, W. and O.S. Madsen, 1982: Movable bed roughness in unsteady oscillatory flow. J. Geophys. Res., Vol. 87, 469-481.

Groves, G.W. and J. Melcer, 1961: On the propagation of ocean waves on a sphere. Geofis. Intern. Mexico, Vol. 1, 77-93.

Günther, H., 1981: A parametric surface wave model and the statistics of the prediction parameters. Ph.D. dissertation, Institut für Geophysik, Universität Hamburg, Hamburg.

Günther, H. and W. Rosenthal, 1979: A hybrid parametrical surface wave model applied to North-Sea sea state prediction. In: MARINE FORECASTING; Ed. J.C.J. Nihoul, Elsevier Scientific, 127-139.

Günther, H., W. Rosenthal and K. Richter, 1978: Parametrical numerical wave prediction tested in wind situations varying in space and time. Nato Conf. Series: V, Air-Sea Interactions, Vol. 1, 607-616, Plenum Press.

Günther, H., W. Rosenthal and K. Richter, 1979a: Application of the parametrical surface wave prediction model to rapidly varying wind fields during JONSWAP 1973. J. Geophys. Res., Vol. 84, 4855-4864.

Günther, H., W. Rosenthal, T.J. Weare, B.A. Worthington, K. Hasselmann, and J.A. Ewing, 1979b: A hybrid parametrical wave prediction model. J. Geophys. Res., Vol. 84, 5727-5738.

Günther, H., W. Rosenthal and M. Dunckel, 1981: Response of surface gravity waves to changing wind direction. J. Phys. Oceanogr., Vol. 11, 718-728.

Hasselmann, D.E., M. Dunckel and J.A. Ewing, 1980: Directional wave spectra observed during JONSWAP 1973. J. Phys. Oceanogr., Vol. 10, 1264-1280.

Hasselmann, K., 1960: Grundgleichungen der Seegangsvorhersage. Schiffstechnik, Vol. 7, Nr. 39, 191-195.

Hasselmann, K., 1962: On the non-linear energy transfer in a gravity wave spectrum, 1. General theory. J. Fluid Mech., Vol. 12, 481-500.

Hasselmann, K., 1963a: On the non-linear energy transfer in a gravity wave spectrum, 2. Conservation Theorems; Wave particle analogy; Irreversibility. J. Fluid Mech., Vol. 15, 273-281.

Hasselmann, K., 1963b: On the non-linear energy transfer in a gravity wave spectrum, 3. Evaluation of the energy flux and swell-sea interaction for a Neumann spectrum. J. Fluid Mech., Vol. 15, 385-398.

Hasselmann, K., 1963c: A statistical analysis of the generation of microseism. Rev. Geophys., Vol. 1, 177-210.

Hasselmann, K., 1967: Non-linear interactions treated by the methods of theoretical physics (with application to the generation of waves by wind). Proc. Roy. Soc. Lond., Ser. A, Vol. 229, 77-100.

Hasselmann, K., 1968: Weak-interaction theory of ocean waves. In: BASIC DEVELOPMENTS IN FLUID DYNAMICS, Vol. 2, Ed. by M. Holt, Academic Press, New York, 117-181.

Hasselmann, K., 1970: Wave-driven inertial oscillations. Geophys. Fluid Dyn., Vol. 1, 463-502.

Hasselmann, K., 1974: On the spectral dissipation of ocean waves due to white-capping. Boundary-Layer Meteorology, Vol. 6, 107-127.

Hasselmann, K., 1978: On the spectral energy balance and numerical prediction of ocean waves. NATO Conf. Series: V, Air-Sea Interactions, Vol. 1, 531-545, Plenum Press.

Hasselmann, K., T.P. Barnett, E. Bouws, H. Carlson, D.E. Cartwright, K. Enke, J.A. Ewing, H. Gienapp, D.E. Hasselmann, P. Krusemann, A. Meerburg, P. Muller, D.J. Olbers, K. Richter, W. Sell and H. Walden, 1973: Measurements of wind-wave growth and swell decay during the Joint North Sea Wave Project (JONSWAP). Deutsche Hydrographische Zeitschrift, Ergänzungsheft Reihe A(8°), Nr. 12, 1-95.

Hasselmann, K. and J.I. Collins, 1968: Spectral dissipation of finite-depth gravity waves due to turbulent bottom friction. J. Marine Res., Vol. 26, 1-12.

Hasselmann, K., D.B. Ross, P. Müller and W. Sell, 1976: A parametric wave prediction model. J. Phys. Oceanogr., Vol. 6, 200-228.

Hasselmann, S. and K. Hasselmann, 1981: A symmetrical method of computing the nonlinear transfer in a gravity wave spectrum. Hamburger Geophysikalische Einzelschriften, Heft 52.

Hasselmann, S. and K. Hasselmann, 1984: The wave model Exact-NL. In: Proc. IUCRM Symp. on Wave Dynamics and Radio Probing of the Ocean Surface, Miami, 1981, Plenum Press.

Helmholtz, H., 1888: Über atmosphärische Bewegungen. S. Ber. Preuss. Akad. Wiss., Berlin, Mathem.-Physik. Kl.

Herterich, K. and K. Hasselmann, 1980: A similarity relation for the nonlinear energy transfer in a finite-depth gravity-wave spectrum. J. Fluid Mech., Vol. 97, 215-224.

Houmb, O.G. and T. Øyan, 1981: Fits between empirical spectra and the JONSWAP model. Report No. 5, Div. of Port and Ocean Eng., The Norwegian Inst. of Tech., Trondheim, December 1980.

Hsiao, S.V. and O.H. Shemdin, 1980: Interaction of ocean waves with a soft bottom. J. Phys. Oceanogr., Vol. 10, 607-610.

Hubert, W.E., 1964: Operational forecasts of sea and swell. Proc. First U.S. Navy Symposium on Military Oceanography, 113-124.

Hydraulics Research Station, 1977a: Numerical wave climate study for the North Sea (NORSWAM). Report EX 775, Wallingford, England.

Hydraulics Research Station, 1977b: Numerical wave climate study for the North Sea (User manual). Report EX 776, Wallingford, England.

Inoue, T., 1967: On the growth of the spectrum of a wind generated sea according to a modified Miles-Phillips mechanism. Geophys. Lab. Rep. No. TR66-6, Dept. Meteorology and Oceanography, New York University, 64 pp.

Isozaki, I. and T. Uji, 1973: Numerical prediction of ocean wind waves. Papers in Meteorology and Oceanography, Vol. 24, 207-231.

Janssen, P.A.E.M., 1982: Quasilinear approximation for the spectrum of wind-generated water waves. J. Fluid. Mech., Vol. 117, 493-506.

Jeffreys, H., 1924: On the formation of waves by wind. Proc. Roy. Soc. Lond., Ser. A, Vol. 107, 189-206.

Jeffreys, H., 1925: On the formation of waves by wind. II. Proc. Roy. Soc. Lond., Ser. A., Vol. 110, 341-347.

Jonsson, I.G., 1966: Wave boundary layers and friction factors. Proc. Tenth Conf. Coastal Engineering, Vol. I, 127-148.

Jonsson, I.G. and N.A. Carlsen, 1976: Experimental and theoretical investigations in an oscillatory turbulent boundary layer. J. Hydraul. Res., Vol. 14, 45-60.

Kahma, K.K., 1981: A study of the growth of the wave spectrum with fetch. J. Phys. Oceanogr., Vol. 11, 1503-1515.

Kajiura, K., 1964: On the bottom friction in an oscillatory current. Bull. Earthquake Res. Inst., Vol. 42, 147-174.

Kajiura, K., 1968: A model of the bottom boundary layer in water waves. Bull. Earthquake Res. Inst., Vol. 46, 75-123.

Kamphuis, J.W., 1975: Friction factor under oscillatory waves. J. Waterways, Harbors, Coastal Eng. Div., ASCE, Vol. 101, WW2, 135-144.

Karlsson, T., 1969: Refraction of continuous ocean wave spectra. J. Waterways and Harbors Div., ASCE, Vol. 95, WW4, 437-447.

Kawai, S., P.S. Joseph and Y. Toba, 1979: Prediction of ocean waves based on the single-parameter growth equation of wind waves. J. Oceanogr. Soc. of Japan, Vol. 35, No. 3-4, 151-167.

Keller, J.B., 1958: Surface waves on water of non-uniform depth. J. Fluid Mech., Vol. 4, 607-614.

Kelvin, Lord, 1887: On the waves produced by a single impulse in water of any depth, or in a dispersive medium. Mathematical and Physical Papers, Vol. IV, London, Cambridge University Press, 1910, 303-306.

Kenyon, K.E., 1969: Stokes drift for random gravity waves. J. Geophys. Res., Vol. 74, 6991-6994.

Kinsman, B., 1960: Surface waves at short fetch and low wind speed - a field study. Tech. Rep. 19, Chesapeake Bay Institute, John Hopkins University.

Kinsman, B., 1965: WIND WAVES: THEIR GENERATION AND PROPAGATION ON THE OCEAN SURFACE. Englewood Cliffs, N.J., Prentice-Hall Inc., 676 pp.

Kitaigorodskii, S.A., 1962: Applications of the theory to the analysis of wind-generated wave motion as a stochastic process. Academy of Sciences USSR Bulletin, Series Geophysics, 73-80.

Kitaigorodskii, S.A., 1983: On the theory of the equilibrium range in the spectrum of wind-generated gravity waves. J. Phys. Oceanogr., Vol. 13, 816-827.

Kitaigorodskii, S.A., V.P. Krasitskii and M.M. Zaslavskii, 1975: On Phillip's theory of equilibrium range in the spectra of wind-generated gravity waves. J. Phys. Oceanogr., Vol. 5, 410-420.

Knowles, C.E., 1982: On the effects of finite depth on wind-wave spectra: 1. A comparison with deep-water equilibrium-range slope and other spectral parameters. J. Phys. Oceanogr., Vol. 12, 556-568.

Komen, G.J., S. Hasselmann and K. Hasselmann, 1984: On the existence of a fully developed wind-sea spectrum. To be published.

Krasitskiy, V.P., 1974: Toward a theory of tranformation of the spectrum on refraction of wind waves. Izv., Atmospheric and Ocean Physics, Vol. 10, No. 1, 72-82.

Lamb, H., 1932: HYDRODYNAMICS, 6th Edition, Dover Publications, New York, 738 pp.

Lazanoff, S.M. and N. Stevenson, 1975: An evaluation of a hemisphere operational wave spectral model. Fleet Numerical Weather Control, Tech. Note 75-3, Monterey, California.

LeBlond, P.H. and L.A. Mysak, 1981: WAVES IN THE OCEAN. Elsevier Oceanography Series 20, Elsevier Scientific Publ., Amsterdam.

Lighthill, M.J., 1962: Physical interpretation of the mathematical theory of wave generation by wind. J. Fluid Mech., Vol. 14, 385-398.

Lighthill, M.J., 1965: Group velocity. J. Inst. Maths Applics., Vol. 1, 1-28.

Lighthill, M.J., 1978: WAVES IN FLUIDS. Cambridge University Press, Cambridge.

Liu, P.C. and D.B. Ross, 1980: Airborne measurements of wave growth for stable and unstable atmospheres in Lake Michigan. J. Phys. Oceanogr., Vol. 10, 1842-1853.

Lock, R.C., 1954: Hydrodynamic stability of the flow in the laminar boundary layer between parallel streams. Proc. Camb. Phil. Soc., Vol. 50, 105-124.

Long, R.B., 1973: Scattering of surface waves by an irregular bottom. J. Geophys. Res., Vol. 78, 7861-7870.

Longuet-Higgins, M.S., 1950: A theory of the origin of microseisms. Philos. Trans. R. Soc. London, Ser. A, Vol. 243, 1-35.

Longuet-Higgins, M.S., 1957: On the transformation of a continuous spectrum by refraction. Proc. Camb. Phil. Soc., Ser. A 53, 226-229.

Longuet-Higgins, M.S., 1962: The directional spectrum of ocean waves, and processes of wave generation. Proc. Roy. Soc. Lond., Ser. A, Vol. 265, 286-315.

Longuet-Higgins, M.S., 1969: On wave breaking and the equilibrium spectrum of wind-generating waves. Proc. Roy. Soc. Lond., Ser. A, Vol. 310, 151-159.

Longuet-Higgins, M.S., 1975: On the joint distribution of the periods and amplitudes of sea waves. J. Geophys. Res., Vol. 80, 2688-2694.

Longuet-Higgins, M.S., 1976: On the nonlinear transfer of energy in the peak of a gravity wave spectrum; A simplified model. Proc. Roy. Soc. Lond., Ser. A, Vol. 347, 314-328.

Longuet-Higgins, M.S., 1983: On the joint distribution of wave periods and amplitudes in a random wave field. Proc. Roy. Soc. Lond., Ser. A, Vol. 389, 241-258.

Longuet-Higgins, M.S., D.E. Cartwright and N.D. Smith, 1963: Observations of the directional spectrum of sea waves using the motions of a floating buoy. In: OCEAN WAVE SPECTRA, Prentice Hall, 111-136.

Longuet-Higgins, M.S. and N.D. Smith, 1966: An experiment on third order resonant wave interactions. J. Fluid Mech., Vol. 25, 417-435.

Madsen, O.S., 1978: Wave induced pore pressures and effective stresses in a porous sea bed. Geotechnique, Vol. 28, 377-393.

Madsen, O.S. and W.D. Grant, 1976: Sediment transport in the coastal environment. TR 209, R.M. Parsons Laboratory, Massachusetts Institute of Technology.

Masuda, A., 1981: Nonlinear energy transfer between wind waves. J. Phys. Oceanogr., Vol. 10, 2082-2093.

McGoldrick, L.F., O.M. Phillips, N. Huang, and T. Hodgson, 1966: Measurements on resonant wave interactions, J. Fluid Mech., Vol. 25, 437-456.

McIntyre, M.E., 1981: On the 'wave momentum' myth. J. Fluid Mech., Vol. 106, 331-347.

McLeod, W.R., L.C. Adamo, and R.C. Hamilton, 1975: A unique strategy for obtaining wave and wind data in the Gulf of Alaska. Offshore Technology Conf., OTC 2297.

Mei, C.C., 1983: THE APPLIED DYNAMICS OF OCEAN SURFACE WAVES. Wiley-Interscience Publications, pp. 740.

Melville, W.K., 1983: The instability and breaking of deep-water waves. J. Fluid Mech., Vol. 115, 165-185.

Miles, J.W., 1957: On the generation of surface waves by shear flows. J. Fluid Mech., Vol. 3, 185-204.

Miles, J.W., 1959a: On the generation of surface waves by shear flows. Part 2. J. Fluid Mech., Vol. 6, 568-582.

Miles, J.W., 1959b: On the generation of surface waves by shear flows. Part 3. J. Fluid Mech., Vol. 6, 583-598.

Miles, J.W., 1960: On the generation of surface waves by turbulent shear flows. J. Fluid Mech., Vol. 7, 469-478.

Miles, J.W., 1962: On the generation of surface waves by shear flows. Part 4. J. Fluid Mech., Vol. 13, 433-448.

Mitsuyasu, H., 1968: On the growth of the spectrum of wind-generated waves. Part 1. Reports of Research Institute for Applied Mechanics, Vol. XVI, No. 55, 459-465, Kyushu University.

Mitsuyasu, H., 1969: On the growth of the spectrum of wind-generated waves. Part 2. Reports of Research Institute for Applied Mechanics, Vol. XVII, No. 59, 235-243, Kyushu University.

Mitsuyasu, H., 1973: The one-dimensional wave spectra at limited fetch. Reports of Research Institute for Applied Mechanics, Vol. XX, No. 66, 37-53, Kyushu University.

Mitsuyasu, H., and K. Rikiishi, 1978: The growth of duration-limited wind waves. J. Fluid Mech., Vol. 85, No. 4, 705-730.

Mitsuyasu, H., F. Tasai, T. Sukara, S. Mizuno, M. Ohkuso, T. Honda and K. Rikiishi, 1975: Observations of the directional spectrum of ocean waves using a cloverleaf buoy. J. Phys. Oceanogr., Vol. 5, 750-760.

Müller, P., 1976: Parameterization of one-dimensional wind wave spectra and their dependence on the state of development. Hamburger Geophysikalische Einzelschriften, Heft 31, pp. 177.

Nikuradse, J., 1933: Strömungsgesetze in rauhen Rohren. Forschungshefte 361, VDI.

Osborne, A.R., 1982: The simulation and measurement of random ocean wave statistics. Proc. Intern. School of Physics, Course LXXX, Topics in Ocean Physics, A.R. Osborne and P. Malanotte-Rizzoli, Eds., North Holland Pub., 515-550.

Ou, S.H., 1980: The equilibrium range in frequency spectra of the wind-generated gravity waves. Proc. 4th Conf. on Ocean Engineering in the Republic of China, Taiwan.

Ou, S.H., and F.L.W. Tang, 1974: Wave characterisitcs in the Taiwan Straits. Proc. Int. Symp. on Ocean Wave Measurements and Analysis, ASCE,Vol. 2, 139-158.

Overland, J.E., and V.J. Cardone, 1980: Case studies of four severe Gulf of Alaska storms. NOAA Tech. Memo., ERL PMEL-19.

Patterson, M.M., 1972: Hindcasting hurricane waves in the Gulf of Mexico. Soc. Petroleum Eng. J., Vol. 12, 321-328.

Patterson, M.M., 1974: Oceanograhic data from hurricane Camille. Proc. Sixth Offshore Technology Conf., OTC 2109, 781-790.

Phillips, O.M., 1957: On the generation of waves by turbulent wind. J. Fluid Mech., Vol. 2, 417-445.

Phillips, O.M., 1958: The equilibrium range in the spectrum of wind generated waves. J. Fluid Mech., Vol. 4, 426-434.

Phillips, O.M., 1960: On the dynamics of unsteady gravity waves of finite amplitude. Part 1. J. Fluid Mech., Vol. 9, 193-217.

Phillips, O.M., 1977: THE DYNAMICS OF THE UPPER OCEAN, 2nd Edition, Cambridge University Press, Cambridge, 336 pp.

Phillips, O.M., 1981: Wave interactions - the evolution of an idea. J. Fluid Mech., Vol. 106, 215-227.

Pierson, W.J., 1964: The interpretation of wave spectrums in terms of the wind profile instead of the wind measured at a constant height. J. Geophys. Res., Vol. 69, 5191-5203.

Pierson, W.J., 1977: Comments on "A parametric wave prediction model". J. Phys. Oceanogr., Vol. 7, 127-134.

Pierson, W.J., G. Neumann, and R.W. James, 1955: Practical methods for observing and forecasting ocean waves by means of wave spectra and statistics. H.O. Pub. No. 603, U.S. Navy Hydrographic Office, Washington, D.C.

Pierson, W.J., and L. Moskowitz, 1964: A proposed spectral form for fully-developed wind seas based on the similarity theory of S.A. Kitaigorodskii. J. Geophys. Res., Vol. 69, 5181-5190.

Pierson, W.J., L.J. Tick, and L. Baer, 1966: Computed-based procedures for preparing global wave forecasts and wind field analysis capable of using data obtained by a spacecraft. Proc. Sixth Naval Hydrodynamics Conference, 449-532.

Pierson, W.J., and R.A. Stacy, 1973: The elevation, slope and curvature spectra of a wind roughened sea surface. Final Report, NASA-CR-2247, December 1973, pp. 129.

Pore, N.A., and W.S. Richardson, 1969: Second interim report on sea and swell forecasting. ESSA Tech. Memo, WBTM TDL 17, 17 pp.

Priestly, J.T., 1965: Correlation studies of pressure fluctuations on the ground beneath a turbulent boundary layer. U.S. National Bureau of Standards, NBS Report 8942, 92 pp.

Putnam, J.A., 1949: Loss of wave energy due to percolation in a permeable sea bottom. Trans. A.G.U., Vol. 30, No. 3, 349-356.

Reece, A., and V.J. Cardone, 1982: Test of wave hindcast model results against measurements during four different meteorological systems. Offshore Technology Conf., OTC 4323, 269-293.

Reid, R.O., and K. Kajiura, 1957: On the damping of gravity waves over a permeable sea bed. Trans. A.G.U., Vol. 38, No. 5, 662-666.

Resio, D.T., 1981: The estimation of wind-wave generation in a discrete spectral model. J. Phys. Oceanogr., Vol. 11, 510-525.

Richter, K., H. Günther, and W. Rosenthal, 1982: Anwendung eines numerischen Seegangsmodells für die Rekonstruktion der Seegangsverhältnisse während der Schiffskatastrophen der "München" und des Fastnet-Rennens. Proc. INTERMARITEC 82 Conf., IMT 82-506/01, 814-828.

Rosenthal, W., 1978: Energy exchange between surface waves and motion of sediment. J. Geophys. Res., Vol. 83, 1980-1982.

Ross, D.B., 1976: A simplified model for forecasting hurricane generated waves. (Abstract). Bull. Amer. Meteorol. Soc., January, 113.

Ross, D.B., 1978: On the use of aircraft in the observation of one- and two-dimensional ocean wave spectra. In: OCEAN WAVE CLIMATE; Eds. M.D. Earle and A. Malahoff, Plenum Press, 253-267.

Ross, D.B., and V.J. Cardone, 1974: Observations of oceanic white caps and their relations to remote measurements of surface wind speed. J. Geophys. Res., Vol. 79, 444-452.

Ross, D.B., and V.J. Cardone, 1978: A comparison of parametric and spectral huricane wave prediction products. NATO Conf. Serives: V, Air-Sea Interactions, Vol. 1, 647-665, Plenum Press.

Ross, D.B., V.J. Cardone and J.W. Conaway, 1971: Laser and microwave observations of sea-surface conditions for fetch-limited 17 to 25 m/s winds. IEEE Trans. on Geosciences Electronics, GE-8, 326-335.

Rottier, J.R., and C.L. Vincent, 1982: Fetch-limited wave growth observed during ARSLOE. Proc. OCEANS 82 Conf., 914-919.

Rye, H., R.C. Byrd, and A. Tørum, 1974: Sharply peaked wave energy spectra in the North Sea. Proc. Offshore Technology Conf., OTC 2107, 739-747.

Rye, H., and R. Svee, 1976: Parametric representation of a wind-wave field. Proc. Coastal Engineering Conf., 183-201.

Schule, J.J., L.S. Simpson, P.S. DeLeonibus, 1971: A study of fetch-limited wave spectra with an airborne laser. J. Geophys. Res., Vol. 76, 4160-4171.

Sell, W., and K. Hasselmann, 1972: Computations of non-linear energy transfer for JONSWAP and empirical wind wave spectra. Unpublished M.S. Thesis, Universität Hamburg.

Shemdin, O.H., and E.Y. Hsu, 1967: The dynamics of wind in the vicinity of progressive water waves. J. Fluid Mech., Vol. 30: 403-416.

Shemdin, O.H., S.V. Hsiao, H.E. Carlson, K. Hasselmann, and K. Schulze, 1980: Mechanisms of wave transformation in finite-depth water. J. Geophys. Res., Vol. 85, 5012-5018.

Shum, K.T., 1984: Joint statistics of water waves. M.S. Thesis, R.M. Parsons Laboratory, Massachusetts Institute of Technology.

Singleton, R.C., 1969: An algorithm for computing the mixed radix Fast Fourier Transform. IEEE Trans. Audio Electroacoustics, Vol. AU-17, 93-103.

Sleath, J.F.A., 1970: Wave-induced pressures in beds of sand. J. Hydraulics Div., ASCE, HY2, 367-378.

Snyder, R.L., 1974: A field study of wave-induced pressure fluctuations above surface gravity-waves. J. Marine Res., Vol. 32, 497-531.

Snyder, R.L., and C.S. Cox, 1966: A field study of the wind generation of ocean waves. J. Marine Res., Vol. 24, 141-178.

Snyder, R.L., F.W. Dobson, J.A. Elliot, R.B. Long, 1981: Array measurements of atmospheric pressure fluctuations above surface gravity waves. J. Fluid Mech., Vol. 120, 2-59.

Stacy, R.A., 1974: Spectral analysis of high-frequency gravity waves generated by a hurricane. Ph.D. Dissertation, The School of Engineering and Science, New York University, 63 pp.

Starr, V.P., 1959: Hydrodynamical analogy to $E = mc^2$. Tellus, Vol. 11, 135-138.

Stokes, G.G., 1847: On the theory of oscillatory waves. Trans. Cambridge Philos. Soc., Vol. 8, 441-455.

Sverdrup, H.U., and W.H. Munk, 1947: Wind, sea, and swell: Theory of relations for forecasting. H.O. Pub. No. 601, United States Navy Department, Hydrographic Office, Washington, D.C., 44 pp.

SWAMP, 1982: Sea wave modeling project, Part 1: Principal results and conclusions. In: WAVE DYNAMICS AND RADIO PROBING OF THE OCEAN SURFACE; Eds. K. Hasselmann and O.M. Phillips, Plenum Press.

Synge, J.L., 1963: The Hamiltonian method and its application to water waves. Proc. Roy. Irish Acad., Vol. 63, Sect. A, No. 1, 1-34.

Szabados, M.W., 1982: Intercomparison of the offshore wave measurements during ARSLOE. Proc. OCEANS 82 Conf., 876-881.

Thornton, E.B., 1977: Rederivation of the saturation range in the frequency spectrum of wind-generated gravity waves. J. Phys. Oceanogr., Vol. 7, 137-140.

Tick, L.J., 1959: A non-linear random model of gravity waves, part I. J. Math. Mech., Vol. 8, 643-652.

Toba, Y., 1978: Stochastic form of the growth of wind waves in a single-parameter representation with physical implications. J. Phys. Oceanogr., Vol. 8, 494-507.

Tyler, G.L., C.C. Teague, R.H. Steward, A.M. Peterson, W.H. Munk, and J.W. Joy, 1974: Wave directional spectra from synthetic aperture observations of radio scatter. Deep-Sea Res., Vol. 21, 989-1016.

Uji, T., 1975: Numerical estimation of the sea wave in a typhoon area. Papers in Meteorology and Geophysics, Vol. 26, 199-217.

Ursell, F., 1950: On the theoretical form of ocean swell on a rotating earth. Mon. Not. R. Astr. Soc., Geophys. Suppl., Vol. 6, 1-8.

Ursell, F., 1956: Wave generation by wind. In: SURVEYS IN MECHANICS; Ed. G.K. Batchelor, Cambridge University Press, 216-249.

Van Dorn, W.G., and S.E. Pazan, 1975: Laboratory investigation of wave breaking II, Deep water waves. Ref. 75-21, Rep. 71, Advan. Ocean Eng. Lab., Scripps Inst. of Oceanogr., La Jolla, California.

Vincent, C.L., W.G. Grosskopf, and J.M. McTamany: Transformation of storm wave spectra in shallow water observed during the ARSLOE storm. Proc. OCEANS 82 Conf., 920-925.

Ward, E.G., D.J. Evans, and J.A. Pompa, 1977: Extreme wave heights along the Atlantic coast of the United States. Offshore Technology Conf., OTC 2846: 315-324.

Weare, T.J., and B.A. Worthington, 1978: A numerical model hindcast of severe wave conditions for the North Sea. NATO Conf. Series: V, Air-Sea Interactions, Vol. 1, 617-628, Plenum Press.

Webb, D.J., 1978: Non-linear transfers between sea waves. Deep-Sea Res., Vol. 25, 279-298.

West, B.J., 1981: On the simpler aspects of nonlinear fluctuating deep water gravity waves (weak interaction theory). Lecture Notes in Physics, 146, Springer Verlag, pp. 341.

West, B.J. and V. Seshadri, 1981: Model of gravity wave growth due to fluctuations in the air-sea coupling parameter. J. Geophys. Res., Vol. 86, 4293-4298.

Whitham, G.B., 1960: A note on group velocity. J. Fluid Mech., Vol. 9, 347-352.

Willebrand, J., 1975: Energy transport in a nonlinear and inhomogeneous random gravity wave field. J. Fluid Mech., Vol. 70, 113-126.

Wilson, B.W., 1955: Graphical approach to the forecasting of waves in moving fetches. U.S. Army Corps of Engineers, Beach Erosion Board, Tech. Memo. 73.

WMO, 1976: Handbook on wave analysis and forecasting. World Meteorological Organization, Geneve, WHO - No. 446.

Wu, J., 1975: Wind-induced drift currents. J. Fluid Mech., Vol. 68, 49-70.

Wu, H.-Y., E.Y. Hsu, and R.L. Street, 1977: The energy transfer due to air-input, non-linear wave-wave interaction and white-cap dissipation associated with wind-generated waves. Tech. Rep. 207, Stanford University, Stanford, California.

Wuest, W., 1949: Beitrag zur Entstehung von Wasserwellen durch Wind. Z. angew. Math. Mech., Vol. 29, 239-252.

Yamamoto, T., 1981: Ocean wave spectrum transformation due to sea-seabed interactions. Proc. Offshore Technology Conference, OTC 3977, 249-258.

APPENDIX A

Propagation Coefficients For The JONSWAP Parameters In Finite Depth

The general form of the finite depth propagation matrix is defined in (4.1.13). Here, we have

$$D_{ijk} = \phi_i' \left\{ c_{g_k}(f,h) \frac{\partial \underline{F}(f,\theta,h)}{\partial a_j} \right\} \qquad \begin{matrix} i = 1,\ldots,6 \\ j = 1,\ldots,6 \\ k = 1,2 \end{matrix} \qquad (A.1)$$

where the depth-dependent group velocity is calculated in (3.1.37) as:

$$c_g(f,h) = \frac{1}{2}\frac{\omega}{k}\left(1 + \frac{2kh}{\sinh 2kh}\right) = \frac{g}{2\omega\chi}\left[1 + \omega_h^2(\chi^2 - 1)\right] \qquad (A.2)$$

and the partial derivative is given by (4.3.1)

$$\frac{\partial \underline{F}}{\partial a_j} = \frac{g}{2\omega\chi^3}\frac{\partial E}{\partial a_j}\frac{2}{\pi}\cos^2(\theta - \theta_o)\begin{bmatrix}\sin\theta \\ \cos\theta\end{bmatrix} \qquad (A.3)$$

Because the functionals are linear in their arguments, the angular dependence can be integrated out according to (4.2.3) which yields

$$D_{ijx} = \frac{8}{3\pi}\sin\theta_o\, D_{ij} \quad ; \quad D_{ijy} = \frac{8}{3\pi}\cos\theta_o\, D_{ij} \qquad (A.4)$$

and leaves the determination of D_{ij}, where

$$D_{ij} = \phi_i' \left\{ c_g(f,h) \frac{\partial E}{\partial a_j} \right\} \qquad (A.5)$$

Thus for i = j = 1, we have specifically by (4.2.15)

$$D_{11} = \phi_1' \left\{ c_g(f,h) \frac{\partial E}{\partial fm} \right\} = -\frac{1}{E''(fm)} \int_{-\infty}^{\infty} \delta(f-fm) \frac{d}{df}\left(c_g \frac{\partial E}{\partial fm}\right) df \qquad (A.6)$$

where $\partial E/\partial fm$ is the partial derivative of the JONSWAP spectrum (3.1.45) with respect to the peak frequency parameter fm,

$$\frac{\partial E}{\partial fm} = \alpha g^2 (2\pi)^{-4} f^{-5} \exp[A]\{-\frac{5}{fm}(\frac{f}{fm})^{-4} + \ell m\gamma \exp[B](\frac{f(\frac{f}{fm} - 1)}{\sigma^2 fm^2})\} \quad (A.7)$$

with $A = -\frac{5}{4}(\frac{f}{fm})^{-4} + \ell m\gamma \exp[B]$

and $B = -\frac{(\frac{f}{fm} - 1)^2}{2\sigma^2}$

Here, $E''(fm) \equiv \left.\frac{\partial^2 E}{\partial f^2}\right|_{f=fm}$. It remains now to show that

$$\frac{d}{df}(c_g \frac{\partial E}{\partial fm}) = \frac{dc_g}{df}\frac{\partial E}{\partial fm} + c_g \frac{\partial^2 E}{\partial fm\, \partial f} \quad (A.8)$$

where, according to (A.2) we have

$$\frac{dc_g}{df} = \frac{\partial c_g}{\partial f} + \frac{\partial c_g}{\partial \chi}\frac{\partial \chi}{\partial f} \quad (A.9)$$

One finds,

$$\frac{\partial c_g}{\partial f} = c_g\left(\frac{4\pi\omega_h(\chi^2 - 1) + \omega_h^2 2\chi \frac{\partial \chi}{\partial f}}{1 + \omega_h^2(\chi^2 - 1)} - \frac{1}{f} - \frac{1}{\chi}\frac{\partial \chi}{\partial f}\right) \quad (A.10)$$

and $$\frac{\partial c_g}{\partial \chi} = c_g\left(\frac{2 + \omega_h^2}{1 + \omega_h^2(\chi^2 - 1)} - \frac{1}{\chi}\right) \quad . \quad (A.11)$$

From (3.1.41) we have

$$\frac{\partial \chi}{\partial f} = -\frac{2\omega_h^2(\chi^2 - 1)}{[1 + \omega_h^2(\chi^2 - 1)]}\frac{\chi}{f} \quad (A.12)$$

Combining (A.10) - (A.12) and evaluating (A.9) yields

$$\frac{dc_g}{df} = -\frac{c_g}{f}\left[1 - 4\frac{\omega_h^2(\chi^2 - 1)(1 - \omega_h^2)}{\left(1 + \omega_h^2(\chi^2 - 1)\right)^2}\right] = \frac{c_g}{f}[1 - 4\Omega_1] \quad (A.13)$$

Substitution of (A.13), (A.7) and (A.8) into (A.6) gives after evaluation of the integral

$$D_{11} = -\frac{1}{E''(fm)}\left[-\frac{c_g(fm,h)}{fm}(1 - 4\Omega_1)(-\frac{5}{fm}) + c_g(fm,h)\left(\frac{20}{fm^2} + \frac{\ell m\gamma}{\sigma^2 fm^2}\right)\right] E(fm) \tag{A.14}$$

in which

$$E(fm) = \alpha g^2 (2\pi)^{-4}\ fm^{-5}\ \exp\left[-\frac{5}{4} + \ell m\gamma\right] \tag{A.15}$$

and

$$E''(fm) = E(fm)\left(\frac{20}{fm^2} + \frac{\ell m\gamma}{\sigma^2 fm^2}\right) \tag{A.16}$$

Introducing (A.15) and (A.16) in (A.14) finally yields after some algebraic manipulations

$$D_{11} = c_g(fm,h)\ [1 + \underline{5\Delta}_1] \tag{A.17}$$

where Δ_1 is given in (4.3.7).

For the case i = 1 and j = 6 we must use $\partial \underline{F}/\partial\theta_o$ instead of (A.3), which is given by (4.3.24) as

$$\frac{\partial \underline{F}}{\partial \theta_o} = \frac{g}{2\omega\chi^2} E(f) \frac{2}{\pi} \sin 2(\theta - \theta_o)\begin{bmatrix}\sin\theta \\ \cos\theta\end{bmatrix} \tag{A.18}$$

Because α is not affected by the operation in (A.6), we can write

$$\frac{\partial E}{\partial \alpha} = \frac{1}{\alpha} E \tag{A.19}$$

Making use of (A.19) in (A.18) and introducing the result in (A.6) we get

$$D_{16} = \phi_1'\left\{\alpha c_g(f,h)\frac{\partial E}{\partial \alpha}\right\} = -\frac{\alpha}{E''(fm)} \int_{-\infty}^{\infty} \delta(f - fm)\frac{d}{df}\left(c_g \frac{\partial E}{\partial \alpha}\right) df \tag{A.20}$$

We recognize that (A.20) is related to the advection coefficient D_{12}. Thus, we obtain

$$D_{16} = \alpha D_{12} \tag{A.21}$$

For the sake of completeness we list the remaining advection coefficients involving the parameters σ_a and σ_b. The derivation of these terms is quite lengthy and tedious. Using the functional ϕ_4' as defined in (4.2.18) one obtains the following propagation terms for σ_a:

$$D_{41} = \frac{c_g(fm,h)}{fm}\{5\Delta_1(1-\sigma_a) - \sigma_a(1 + \frac{8.24}{\ell m\gamma}[\sigma_a - \Delta_1(1.7 + 2.0\sigma_a + 0.08\Delta_2 1)\} \tag{A.22}$$

$$D_{42} = \frac{c_g(fm,h)}{\alpha}\{\Delta_1(\sigma_a - 1) + \frac{0.65\sigma_a}{\ell m\gamma}[1 - \Delta_3 + 2.5\sigma_a - 4.3\Delta_1(1 + 11.9\sigma_a)1\} \tag{A.23}$$

$$D_{43} = \frac{c_g(fm,h)}{\gamma}\{\Delta_1(\sigma_a - 1) + \frac{\sigma_a}{\ell m\gamma}[\sigma_a - \Delta_1(33\sigma_a + 2.8)1\} \tag{A.24}$$

$$D_{44} = c_g(fm,h)(1 + \sigma_a) \tag{A.25}$$

Similarly, using ϕ_5' as defined in (4.2.19), the following coupling coefficients for σ_b are obtained:

$$D_{51} = -\frac{c_g(fm,h)}{fm}\{5\Delta_1(1 + \sigma_b) + \sigma_b(1 - \frac{8.24}{\ell m\gamma}[\sigma_b - \Delta_1(20\sigma_b - 1.7) - 0.08\Delta_2 1)\} \tag{A.26}$$

$$D_{52} = \frac{c_g(fm,h)}{\alpha}\{\Delta_1(1 + \sigma_b) + \frac{0.65\sigma_b}{\ell m\gamma}[\Delta_3 - 1 - 2.5\sigma_b + 4.3\Delta_1(11.95\sigma_b - 1)]\} \tag{A.27}$$

$$D_{53} = \frac{c_g(fm,h)}{\gamma}\{\Delta_1(1 + \sigma_b) - \frac{\sigma_b}{\ell m\gamma}[\sigma_b - \Delta_1(33\sigma_a - 2.8)]\} \tag{A.28}$$

$$D_{55} = c_g(fm,h)\ (1 - \sigma_b) \tag{A.29}$$

Here Δ_1, Δ_2 and Δ_3 have been previously given in (4.3.7), (4.3.19) and (4.3.20), respectively. All other coupling coefficients not explicitly shown are by definition zero.

APPENDIX B

Propagation Coefficients for the Directional Parameter θ_o in Finite Depth

The functional ϕ_6' is defined in (4.4.8) as

$$\phi_6'\{\delta\underline{F}\} = \frac{3\pi}{8} \frac{\iint |\cos\theta_o \, \delta F_y - \sin\theta_o \delta F_x| df d\theta}{\int c_g \cdot \Phi \cdot E(f) \, df} \tag{B.1}$$

where the energy flux spectrum $\underline{F}$ is specified in (4.1.4). Applying the functional ϕ_6' to the definition of the D_{ij}'s in (4.1.13), we can write the x and y components for the D_{6j} term, respectively, as

$$D_{6jx} = \phi_6' \{\sin\theta \; c_g(f,h) \frac{\partial \underline{F}}{\partial a_j}\}$$

$$= \frac{3\pi}{8} \frac{\int c_g^2 \Phi \frac{\partial E}{\partial a_j} df}{\int c_g \Phi E \, df} \frac{2}{\pi} \int \cos^2(\theta - \theta_o)(\cos\theta_o \sin\theta - \sin\theta_o \cos\theta) \sin\theta \, d\theta \tag{B.2}$$

$$D_{6jy} = \phi_6' \{\cos\theta \; c_g(f,h) \frac{\partial \underline{F}}{\partial a_j}\}$$

$$= \frac{3\pi}{8} \frac{\int c_g^2 \Phi \frac{\partial E}{\partial a_j} df}{\int c_g \Phi E \, df} \frac{2}{\pi} \int \cos^2(\theta - \theta_o)(\cos\theta_o \sin\theta - \sin\theta_o \cos\theta) \cos\theta \, d\theta \tag{B.3}$$

Carrying out the integration over the direction θ in (B.2) and (B.3) yields

$$D_{6jx} = -\frac{3\pi}{32} \sin\theta_o \, D_{6j} \tag{B.4}$$

$$D_{6jy} = \frac{3\pi}{32} \cos\theta_o \, D_{6j} \tag{B.5}$$

where

$$D_{6j} = \frac{\int c_g^{\,2} \Phi \frac{\partial E}{\partial a_j} \, df}{\int c_g \Phi \, E \, df} \tag{B.6}$$

remains to be evaluated. The integral in the demominator of (B.6) is approximated by

$$\int c_g \Phi \, E \, df = \frac{\alpha g^3}{2(2\pi)^5} \, fm^{-5} \, J_1(\omega_h, \gamma) \tag{B.7}$$

with J_1 given in (4.4.14), which must be numerically integrated. The integral in the numerator of (B.6) can be written as

$$\int c_g^{\,2} \Phi \frac{\partial E}{\partial a_j} \, df = \frac{\partial}{\partial a_j} \int c_g^{\,2} \Phi \, E \, df \tag{B.8}$$

since the differentiation does not depend on the integrand. Hence, the integral is readily evaluated and we get

$$\int c_g^{\,2} \Phi \, E \, df = \frac{\alpha g^4}{4(2\pi)^6} \, fm^{-6} \, J_2(\omega_h, \gamma) \tag{B.9}$$

with J_2 given in (4.4.15). Then for $j = 1$, we obtain from (B.6)

$$D_{61} = \frac{\alpha g^4 \, 2(2\pi)^5}{4(2\pi)^6 \, \alpha g^3 \, fm^{-5}} \frac{\partial \, fm^{-6}}{\partial \, fm} \frac{J_2}{J_1} = -\frac{g}{4\pi} \, 6 \, fm^{-2} \frac{J_2}{J_1} \tag{B.10}$$

Combining (B.10) with (B.4) and (B.5), then finally gives

$$D_{61x} = \frac{3g}{128} \sin\theta_o \, 6 \, fm^{-2} \frac{J_2}{J_1} \tag{B.11}$$

$$D_{61y} = -\frac{3g}{128}\cos\theta_o \; 6 \; fm^{-2} \; \frac{J_2}{J_1} \qquad (B.12)$$

The remaining coupling terms can be derived following this procedure.